Contributions from the Department of Meteorology and Wind Energy to the EUWEC '96 conference in Göteborg, Sweden

Larsen, Gunner Chr.

Publication date:
1996

Document Version
Publisher's PDF, also known as Version of record

Contributions from the Department of Meteorology and Wind Energy to the EUWEC'96 Conference in Göteborg, Sweden

Risø-R-909(EN)

Edited by Gunner C. Larsen

Risø National Laboratory, Roskilde, Denmark
August 1996

Abstract The 5'th European Union Wind Energy Conference and Exhibition – EUWEC'96 – was held in Göteborg, Sweden during the period 20–24 May 1996. 520 delegates, mainly from Europe but also from other parts of the world, attended the conference. The conference contributions included roughly 70 oral presentations and 200 posters.

The Department of Meteorology and Wind Energy contributed with 17 oral presentations and 15 posters with members of the department as authors or co–authors. The present report contains the full set of these papers, covering a wide spectrum of subjects including research strategy, wind resources, power quality, grid connection, wind–diesel systems, aerodynamics, load assessment and reliability, and certification.

In the table of content, reference is made to the session where a particular paper was presented. ORv.x denotes oral session v, paper no. x. Py.z denotes poster session y, paper no. z.

ISBN 87–550–2206–5
ISSN 0106–2840

Grafisk Service · Risø · 1996

Contents

A EUROPEAN STRATEGY FOR WIND ENERGY R&D

P. D. Andersen, P. H. Jensen, E. L. Petersen
Risø National Laboratory, Postboks 49, DK-4000 Roskilde, Denmark
J. Beurskens
Netherlands Energy Research Foundation ECN, Postbus 1, NL-1755 ZG Petten, the Netherlands
G. Elliot
National Engineering Laboratory, East Kilbride, Glasgow G75 0QU, U.K.
J. P. Molly
Deutsches Windenergie-Institut, Ebertstrasse 96, D-26382 Wilhelmshaven, Germany

ABSTRACT: The aim of this paper is to suggest a strategy for research, development and demonstration (R,D&D) activities on a European Union level the next 3 to 5 years. The strategy is goal (or problem) oriented where overall political goals leads to the goals for the R,D&D effort. The paper is based on a position paper on wind energy R,D&D by the European Renewable Energy Centres Agency (EUREC-Agency), a European Economic Interest Grouping.

KEYWORDS: Energy Policies; R&D; Strategies; Wind Energy.

1. INTRODUCTION

This paper is based on a position paper on wind energy research, development and demonstration (R,D&D) by the European Renewable Energy Centres Agency (EUREC-Agency), a European Economic Interest Grouping founded in 1991 [1]. EUREC Agency has now 35 member institutions.

The position paper was primarily written for European policy makers and not for the European wind energy community. Our goal was to link recommended initiatives on wind energy R,D&D to overall European policies and objectives. Therefore, the paper is goal (or problem) oriented, and the structure of the paper does not follow technical issues or scientific disciplines.

The process leading up to this paper consisted of six steps:

Step one: Relevant European policies which establish the context of this strategy: European energy policy [2], European policy on growth, competitiveness and employment [3], and European policy on innovation [4]. The questions was: What is EU's interest in windpower utilization? Why should EU fund R,D&D activities in this area? (paragraph 2).

Step two: Adaptation of overall, strategic goals for the European Union's activities on wind energy (paragraph 3).

Step three: Identification of the most important constrains for achieving the overall goals (paragraph 4).

Step four: Identification and recommendation of activities by which the scientific community can contribute to overcome the constrains (paragraph 4).

Step five: Realistic targets for each area (paragraph 4).

Step six: Recommendations for European level responsibilities and program management (paragraph 5).

The work leading to this strategy has been financed solely by the participating institutions.

2. WHY WINDPOWER ?

2.1 Status of the Technology

The technology related to grid-connected wind turbine generators (WTGs) is becoming mature. The size of commercially available grid connected WTGs has evolved from 50 kW in the early 1980'ies to 500 to 800 kW today. The next generation of commercial WTGs in the 1000 - 1500 kW size is expected to reach the market in 1996.

At the end of 1995 global installed capacity of modern grid connected WTGs was some 4900 MW, of which 2500 MW was in Europe. The world-wide annually added capacity of WTGs (the World market) is rapidly increasing; and is expected to increase to 2000 MW/year by year 2000.

2.2 Energy Policy Aspects

Europe has a very large untapped source of wind energy. The total exploitable wind energy potential of Europe equates to approximately half of the total electricity consumption of the countries in the European Union.

Wind energy is a European domestic source of energy. As 50% of all energy consumed in the European Union is imported, wind energy can improve Europe's degree of self-sufficiency.

Wind energy is clean and safe. Wind turbines do not produce green house gases. Wind energy has very low external and social costs. Wind energy has no liabilities related to decommissioning of obsolete plants. The energy invested in the production of a typical wind turbine has a "pay back" time (energy balance) of less than half a year of operation.

Wind energy today is competitive at specific sites with favourable conditions, as remarked in the Commission's Green Paper "For a European Union Energy Policy". International organisations expect wind energy within the timeframe of 2005 to 2010 to be economically fully competitive to fossil fuel and nuclear based power production.

Wind energy is a popular source of energy. Opinion surveys indicate, that the majority of citizens in most European countries in general favour renewable energy sources such as windpower. Opinion surveys in areas of Denmark and UK with wind farms indicate that 70 to 80 % of the population is "general supportive" or "unconcerned" with respect to the turbines.

Windpower generating capacity can be installed fast. Windpower plants of, for example, 50 MW can be in operation within less than a year from a decision is taken.

Wind is a reliable source, which can now be predicted with a high degree of precision.

Wind turbines can be used competitively as a dispersed energy production technology in areas with dispersed electricity consumption.

2.3 Industry and Innovation Policy Aspects

European growth. European wind industry is one of the fastest growing industries with annual growth rates of 50% during recent years.

European competitiveness. European wind industry (consisting of rapidly growing SMEs) is very competitive with a ca. 70% share of the World market in 1995.

European employment. In 1995 20,000 Europeans were estimated to be employed in relation to European wind energy activities; primarily in the wind turbine industry and its supporting industries [3] [4].

3. STRATEGIC GOALS FOR EUROPEAN WIND ENERGY R&D

Taking the above factors into account windpower is the most competitive and promising new renewable source of energy. However, scientific research is able to give a significant contribution to the further development of wind energy technology and to the European windpower industry's international competitiveness.

The European Renewable Energy Centres' Agency has agreed on recommending two strategic goals for an European wind energy policy:

3.1 Windpower in Europe

The first strategic goal for windpower R,D&D activities in the EU should be to achieve an installed capacity of 100,000 MW by 2030 as suggested by European Wind Energy Association. 100,000 MW of windpower in 2030 (equal to ten percent of the Union's electricity demand in 1990). The area needed for this is less than 0.3% of the territory covered by the European Union. Onshore wind farms have the advantage of dual land use. 99% of the area occupied by a wind farm can be used for agriculture or remain as natural habitat. Furthermore, a part of the installations can be made offshore. Consequently, limited area of land is not a physical constrain for windpower utilisation.

3.2 Windpower outside Europe

The second strategic goal for windpower R,D&D in general should be to provide developing countries and areas with sustainable energy at a competitive cost.

4. GOALS FOR EUROPEAN WIND ENERGY R&D

Based on this, the following six sets of goals and means are recommended for a European R,D&D strategy on wind energy. For each set of goals realistic targets or "deliverables" are indicated.

4.1 Generation Costs

Compared with traditional energy sources wind energy today is competitive at specific sites with favourable conditions. However, to install 100,000 MW of windpower in EU economically fully competitive to fossil fuel and nuclear based power production requires further cost reduction of windpower.

If the goal for windpower in Europe is realised, Europe will be one of the world's largest markets for wind turbines. European windpower industry must be competitive at this market as well as on the other international markets for wind turbines. European windpower industry competes on a range of parameters, but production cost is - and will be - the most important parameter.

Recommended R,D&D activities during the next 3 to 5 years: Basic aerodynamic and aeroelastic research including numerical and empirical investigations, modelling and experimental verification. Development of WTGs specialised to match wind conditions on specific sites. R,D&D on lowering uncertainties on loads, material properties, and partial coefficients. Basic R,D&D in new concepts and components, proof of concepts by means of development, construction, and field testing of components and complete wind turbine systems. Parallel with concept development, aeroelastic models need to be extended and verified in order to be able to scale up and design cost effective machines for both onshore and offshore use. New materials, including recycling and integration of recycling already in the design phase. Analysis and mitigation of lightning damage and definition of the lightning risk. Further improvement of tools for micrositing in mountains.

Recommended demonstration activities during the next 3 to 5 years: Demonstration of new concepts, offshore MW size WTGs, and WTGs in mountains and offshore.

Realistic targets: Reduction of kWh cost with 30% within 2000, 40% within 2005, and 50% within 2030.

4.2 Market issues

The European Commission mentions that the free operation of the market has to be the principal instrument of any policy [2]. A separate goal for a European policy on wind energy utilisation must be the free operation of the markets for wind turbines and windpower. Also non-EU based actors must have access to this market.

The key role of the European Commission, as well as national authorities, is to ensure that these markets function to satisfy the general interest. The means are harmonised European standards, legal structures and institutional frameworks.

Recommended R,D&D activities during the next 3 to 5 years: R,D&D leading to European standards for performance, tests, measurements, and energy prediction methods. Accurate measurement and modelling of wind resources offshore and in mountainous terrain.

Recommended demonstration and support activities during the next 3 to 5 years: Investigation of financial cost/benefits and legal issues concerning transmitting substantial amounts of wind-generated electricity across national boundaries within Europe. European planning procedures suggesting and ranking sites for 100,000 MW both offshore and onshore, including mountainous terrain. Conceive and implement European quality assurance systems. Continuous upgrading and harmonisation of measurement methods and procedures throughout the EU. Harmonisation and updating of European technical basis for certification

Realistic targets: European planning procedures suggesting and ranking feasible sites (on-, offshore, mountains) for 10,000 MW in year 2000 and 100,000 MW in 2005. A European certification system facilitating a free

market for windpower technology within 2005. A European standard for performance (test and measurement) within 2000. European standard for risk assesment for investment renewable energy within 2000. A transparent, harmonized transmission, cost and tariffs system facilitating free market for windpower within 2005.

4.3 Cost uncertainty

Wind is a reliable source, which can be predicted with a defined degree of uncertainty. Financial and insurance institutions increasingly consider windpower as a reliable source of energy and has increased confidence in the economical performance of the industry. However, the pattern and economics differ significantly between the European countries depending on the track record of windpower in the specific country. If windpower is to be utilised widely, the technology's credibility from the perspective of the financial and insurance institutions must be increased. To obtain this the financial, and consequently the technical, uncertainties of windpower must be minimised. Better prediction of wind resource and wind turbine performance. Especially better prediction of the wind resource offshore and in mountainous terrain is needed.

Recommended R,D&D activities during the next 3 to 5 years: Improved prediction of turbulence, gust and extreme levels for different types of terrain; including mountainous terrain and offshore sites. Improved 3D turbulence modelling and meso-scale models. Improved measurement techniques, reference procedures, and reference anemometer calibration facilities. Analysis and mitigation of the lightning damages and definition of lightning risk

Recommended demonstration and support activities during the next 3 to 5 years: Credible, harmonised production prediction systems must be established. Make existing meteorological databases exchangeable.

Realistic targets: For flat terrain uncertainty of generation cost for flat terrain should be reduced to 10 - 15% by 2000 and to 5 - 10 % by 2010. For mountainous terrain uncertainty should be reduced to 20 - 30 % by 2000 and to 10 - 15% by 2010.

4.4 Grid Issues

European power utilities increasingly consider windpower as a new viable and reliable source of energy their supply portfolio. However, in countries with no experience in windpower utilities are reluctant to accept windpower. This is often rooted in concern for technical issues such as power quality, power predictability, and grid integration. Furthermore, Europe's power utility sector is facing a significant restructuring process, leaving less attention to the introduction of windpower and other renewable energy sources.

As widespread use of windpower in Europe demands an active participation by European utilities, windpower's credibility from the perspective of the utilities must be increased. The most important means for this end are 1) ensuring power quality and predictability of wind energy and 2) reduction of windpower's transmission costs and grid costs.

Recommended R,D&D activities during the next 3 to 5 years: R,D&D in better local physical models and numerical weather prediction models. Make existing databases (which can provide the input to the models) exchangeable. R,D&D on further improvement of controlling power quality in order to minimise grid connection cost and optimise wind capacity to the grid (micro scale). R,D&D on methods to meet grid connection requirements: controllability of output, reduction of higher harmonics, etc.

Recommended demonstration activities during the next 3 to 5 years: Demonstration and verification of short term prediction models in utility planning tools. Implementation of planning tools at utility dispatch centres.

Realistic targets: An electrical output prediction 24 hours in advance for wind farms with at standard deviation of 10 - 15 % by 2000 and 5 - 10 % by 2010. Within 2010 a technical and economical optimal solution for and planning of integration of 100.000 MW of windpower in the European grid.

4.5 Public acceptance

Opinion surveys indicate, that the majority of citizens in most European countries in general favours renewable energy sources such as windpower. However, the benefits of wind energy is on a global or national level, whereas, the costs are often carried by local communities with large windfarm installations. If not dealt with properly, this can cause a Not-In-My-Back-Yard dilemma.

If 100,000 MW of windpower is to be installed in Europe over the next 35 years, it is essential to maintain and increase the public's acceptance of windpower. The means for this are primarily of a political nature and therefore outside the scope of this paper. However, means for minimising environmental and social consequences of wind turbine deployment and operation are partly based on scientific research and development.

Recommended R,D&D activities during the next 3 to 5 years: Fundamental research on aeroacoustical noise emission (suited for a concerted action). Development of better models of noise propagation, incorporating topographic and meteorological variables. More accurate assessment of the comparative advantage of windpower concerning external and social costs. Evaluation of the value windpower for society.

Recommended demonstration and support activities during the next 3 to 5 years: Research on the publics attitudes to windpower, in particular with respect to measures ensuring local acceptance (such as local ownership and control).

Realistic target: European Standards for noise, siting and stealthing within 2005.

4.6 Other applications

Applications other than large grid connected wind turbines are relevant for both areas within EU and especially in developing areas and countries. The technology and components, by and large, exist, with potentially a very large market.

It is generally believed, that the largest impediment for a more widespread use of windpower in hybrid systems and for special applications is rooted in potential customer groups' (aid organisations, the World Bank, local utilities and industries, etc.) hesitating attitude towards the technology due to the lack of a solid track record.

Therefore, we recommend a programme that build up confidence in the technology by short term focusing on exploration, development and demonstration of ample and reliable technologies of hybrid systems, battery charters and windpumps.

Recommended R,D&D activities during the next 3 to 5 years: Further development of simple and reliable systems and technologies. Development of ample applied technology such as batteries, pumps, desalination systems, etc.

Recommended demonstration activities during the next 3 to 5 years: Verification of the technology through demonstration projects. Establishment of an EU programme for demonstration and installation of wind turbines (grid connected, stand alone, and hybrid systems) in developing countries.

Realistic targets: A proven, mature and competitive application of windpower in remote hybrid systems and as battery chargers and windpumps within 2005.

5. RECOMMENDATIONS ON EUROPEAN LEVEL RESPONSIBILITIES AND PROGRAM MANAGEMENT

Many governments and international organisations have initiated programmes for research, development, and demonstration in the area of windpower. However, on a European level we find that the European Union has an important role.

5.1 European Level Responsibilities

Wind energy technology and the industry, institutions, organisations affiliated with this technology are still young and small compared with the established, powerful energy sectors (coal, oil, gas and nuclear). It is the Commission's responsibility to ensure, that the interests of the wind energy sector are included in policy making processes on European level in the same way as that more established energy sectors.

It is our position that the Commission in its strategy and program formulation should include the point of view of the European windpower industry and power utilities as well as research institutions and national authorities. Wind energy research must be defined and carried out in close co-operation with industry, utilities and other "users" of the results of this research. This is the most efficient instrument for defining the activities needed, for successful achievement of the goals and for implementation of the results.

Europe has a build up a "critical mass" of knowledge, human resources and industrial competence in the area of windpower research and development; both within research institutions and within industry. It is a European level task to facilitate co-operation between this "critical mass" on wind technology and related areas of competence, such as aerodynamical or materials research.

5.2 Types of R,D&D Activities

European actions should address common problems and potentials faced by industry, utilities, energy planners, European and national authorities.

Activities requiring an effort exceeding the potential and capability of an individual country should be preferred.

European R,D&D programmes should not "pick-the-winner" among WTG concepts or technologies, but let the industry and its customers on the basis of the free operation of the market make the necessary choices and set the speed of which new concepts are introduced. Consequently, the Commission should support R,D&D on well-known concepts as well as on new ones.

5.3 Key Players

On program level the actions should not distort the market competition. However, to secure impact of the activities, it is important that programmes on project level are facilitating close co-operation between research organisations and individual companies.

The Commission does not operate any wind energy research institute of its own, nor is the Commission's R,D&D programmes able to provide "basic funding" for any existing European wind energy research institution. We find this fact an advantage. The Commission can draw on the experience in existing institutions.

Contractors on the research (Joule) part should primarily be found among industrial enterprises, universities, national research centres, etc. with a basic funding of its own and with a track record of high class research. Whereas, contractors on the demonstration (Thermie) part should primarily be found among the end-users of the technology; such as industrial enterprises, utilities, governmental bodies, finance & insurance community, etc. See Table 1.

EU funded R,D&D programmes should also in the future facilitate cross-national and cross-sectorial co-operation by demanding project partners from several member countries and from typical user groups such as industry, utilities, governmental institutions, etc. On the other hand we are worried about mega-projects including too many project partners, so that project administration paralyses the scientific process and devaluates the useful results of the projects. The Commission's legitimate interest in cross-national and cross-sectorial co-operation must not become a hindrance for efficient research and implementation of results.

6. REFERENCES

[1] Eurec Agency, *Renewable Energy for Europe*, James & James, London, to be published in 1996.

[2] European Commission, *For a European Union Energy Policy - Green Paper*, ECSC-EC-EAEC, Brussel/Luxembourg, 1995.

[3] European Commission, *Growth, Competitiveness, Employment. The Challenges and Ways Forward into the 21st Century. - White Paper*, ECSC-EC-EAEC, Brussel/Luxembourg, 1993.

[4] European Commission, *Green Paper on Innovation*, ECSC-EC-EAEC, Brussel/Luxembourg, 1996.

THE NEW EUROPEAN WIND ATLAS METHOD

Erik Lundtang Petersen
Meteorology and Wind Energy Dept., Risø National Laboratory, Roskilde, Denmark

ABSTRACT: The New European Wind Atlas Method which has been developed since 1990 is based on a combination of the Karlsruhe Atmospheric Meso-scale Model and the Wind Atlas Analysis and Application Model, and the use of the databases of ECMWF (geostrophic winds) and the CORINE (land use data). Several papers at this conference deal with details of this new methodology, hence the current paper deals only with the general features.
Keywords: Resources, complex terrain, models , siting.

1. INTRODUCTION

Proper siting and reliable power production prediction for the widespread deployment of windfarms on a global scale call for a continuing effort on model improvements and database building. Models for precise prediction of the wind speed at the exact location of the wind turbines are essential because for aerodynamic reasons the power output of a wind turbine is proportional to the third power of the wind speed. Hence, even small errors in prediction of wind speed may result in large deviations in the anticipated power production and thereby lead to considerable uncertainty in the assessment of the economic benefits of installing wind power. In addition to micro-siting models it is also necessary to have models that can provide reliable estimates of the wind climate over areas of dimensions 10 to 100 km. Such models are termed meso-scale models. Both types of models require accurate input of topographical and meteorological information in order to produce accurate results.

2. WIND RESOURCES ASSESSMENT AND MICRO-SITING

The wind speed experienced by a wind turbine in a wind farm is determined mainly by three factors:

a) the overall weather systems, which usually have an extent of several hundred kilometres,
b) the nearby topography out to a few tens of kilometres from the turbine, and
c) the wakes from the other wind turbines in the wind farm.

The now well known methodology laid down in the European Wind Atlas [1]and the Wind Atlas Analysis and Application Program (WAsP) [3] was essentially constructed to emphasise and handle the two first factors. Through a Wind Atlas Analysis meteorological data is cleaned from topographical effects and made regional representative and through a Wind Atlas Application the regional statistics is used for micro-siting. Since 1989, when the European Wind Atlas was published, a huge amount of experience on the practical use of the methodology has bee accumulated. Many papers in this volume reports on such experience.

The theories that have been used to construct the Wind Atlas methods predict a deteoriation of accuracy and reliability of calculated wind statistics or wind turbine productions when topography and local climate exceed certain levels of complexity. Experience generally shows this to be true. Especial difficult areas are found in highly mountainous region. This is unfortunate because these regions are the most promising for large scale wind farm deployments.

We are faced with a number of general problems for siting in mountainous regions: First, the overall wind climate which in flat terrain changes gradually over hundreds of kilometres can change markedly from one mountain valley to another. When further thermal effects begin to play an important role as is the case in many Mediterranean regions, the information necessary for precise siting becomes excessive and difficult to obtain. Then, taking flat terrain again, it is now well known that even in relatively uncomplicated terrain any shifts in the topography such as changes in surface properties and height changes have a profound influence on the wind speed in the lowest 100 metres of the atmosphere. For mountainous terrain the wind speed dependence on topography is so strong that it is crucial to have models which are able to model this dependence very accurately. This in turn calls for very detailed topography information to be feed into the micro-siting models.

The two inescapable requirements to proper wind energy assessments and micro-siting: Accurate and detailed wind climatologies and topography information, has lead to the formulation of the New (European) Wind Atlas Methodology [2].

3. THE NEW EUROPEAN WIND ATLAS METHODOLOGY

The methodology can be said to apply a telescoping principle: Global model → Meso-scale model → Micro-scale model.

Global model. At a number of large meteorological centres the weather is modelled on a global scale for the purpose of weather prediction. A huge number of observations is reported to the centres several times a day. The observations are analyses into homogeneous distributed fields before they are feed into the models. It is the climatological statistics of these fields that are of

interest for wind energy assessments. Particular the field of geostrophics winds. At the European Centre for Medium Weather forecast the so called Reanalyses Project has recently produced a homogeneous dataset of the last 15 years of global atmospheric observations. It is this dataset which provides the input to the meso-scale model.

Meso-scale model. These models are full atmospheric models that can utilise the large-scale climatological forcing described above to calculate the wind fields over regions of very complex topography. An example is given in this volume by Frank and Landberg: "Modelling the Wind Climate over Ireland" [5]. The model used is the Karlsruhe Atmospheric Meso-scale Model (KAMM). It is a three-dimensional, non-hydrostatic atmospheric meso-scale model which assumes non-divergent wind fields to filter sound waves. Subgrid scale fluxes are parameterized using stability dependent turbulent diffusivites. It employs centred differences on a terrain following co-ordinate system with variable resolution in vertical direction. The model is initialised from hydrostatic and geostrophic basis state. This large-scale pressure gradient and the daily cycle of radiation represent the external forcing of the model. In the simulation for Ireland an area of 500 x 600 km was covered with a resolution of 10 km.

Running a meso-scale model is extremely computer time consuming, therefore it is not possible to run the simulations for a climatological period. Instead, a cluster analysis is performed on the external forcing, i.e. the geostrophic wind. In the Ireland case, the cluster analysis of the geostrophic wind was made for 60 clusters (12 wind directions times 5 wind speed classes). For the 60 cases 6 hours of real time were simulated and the resulting wind climate for each of the 10 km square was constructed from the different simulations by calculating the weighted mean of the simulated wind at each grid point. The weights are the frequencies assigned to each class of geostrophic wind. The wind climate statistics for the 10 km squares are then the input to the micro-siting model.

Micro-siting model. Currently the most applied models are the linerized models, which are known to produce reliable and accurate results as long as the rather restricting assumptions of gently sloping terrain and not too high hills are observed approximately. The Wind Atlas Analysis and Application model (WAsP) has a special feature that fits well with the "telescoping principle": The expanding polar grid of its orographic module [4]. Because the terrain elevations closest to the actual locations exert the strongest influence, this type of grid enables a very detailed description of the close-by terrain, whereas the terrain far away is given less weight. In the new wind atlas methodology the output from the KAMM model is in the form of so called wind atlas data especially suited as input to WAsP.

Topographic information. As argued above, detailed topographic information is essential for reliable and accurate wind resource assessment and micro-siting. For the new wind atlas methodology we rely on the availability of data bases of high-resolution land cover data. Such data bases are being produced these years. For example the CORINE Land Cover Project (EU) has provided data for a number of countries. In the Ireland case, the landuse categories given by CORINE were assigned roughness values and then further use as input to the models.

Obtaining the right height description of a particular terrain, say a prospective wind farm site, can be rather difficult. Often the usual 10 metres resolution of the contours is not sufficient. The reason is quite simple, the uncertainty of the contours goes directly into the uncertainty of the predicted wind speed statistics which at the third power adds to the uncertainty of the wind farm production estimate.

4. CONCLUSION

The two inescapable requirements to proper wind energy assessments and micro-siting: Accurate and detailed wind climatologies and topography information, has lead to the formulation of the New (European) Wind Atlas Methodology. The application of the methodology is reported by several papers in this volume. It still requires final adjustments, but it is believed it will be available by the end of 1996.

5. ACKNOWLEDGEMENTS

The work by Risø National Laboratory on wind energy resources has - since 1981 - been supported by the Commission of the European Union, Directorate-General for Science, Research and Development (DG XII). The present work was supported under contract JOUR-CT90-0067.

6. REFERENCES

[1] Troen, I. and Petersen, E.L. European Wind Atlas. Published by Risø National Laboratory, Roskilde, Denmark, ISBN 87-550-1482-8 (1989) 656p.

[2] Petersen, E.L., Landberg, L. and Mortensen, N.G., European Wind Atlas, Vol. II: Measurements and modelling in complex terrain. To be published. Risø National Laboratory, Denmark (1996) 361p.

[3] Mortensen, N.G., Landberg, L., Troen, I. and Petersen, E.L. Wind Atlas Analysis and Application Program (WAsP), Vol.1: Getting Started. Vol.2: User's Guide. Risø National Laboratory, Roskilde, Denmark (1993) 126p.

[4] Troen, I. A high resolution spectral model for flow in complex terrain. Ninth Symposium on Turbulence and Diffusion. American Meteorological Soc., Risø National Laboratory, Denmark (1990) 417-20.

[5] Frank,H.P. and Landberg,L. Modeling the Wind Climate over Ireland. This volume.

MEASUREMENTS AND MODELLING IN COMPLEX TERRAIN

Erik L. Petersen, Niels G. Mortensen and Lars Landberg
Department of Meteorology and Wind Energy
Risø National Laboratory
Roskilde, Denmark

ABSTRACT: The main results of the EU-project "Measurements and Modelling in Complex Terrain" are presented. These include the preparation of the second volume of the European Wind Atlas – specifically directed towards wind resource assessment and siting issues in mountainous terrain – as well as the establishment of a comprehensive, CD-ROM-based database containing new, high-quality wind data from several topographically and climatologically complex regions of Europe. In the course of the project the limitations of the current Wind Atlas methodology has been identified and quantified, a novel concept of nested meso- and micro-scale models for wind resource assessment has been established, and a new model for the estimation of turbulence in complex terrain has been constructed.
Keywords: Wind Atlas, Mountains/High Terrain, Data Bases, Siting.

1 INTRODUCTION

The next volume of the European Wind Atlas – Volume II: Measurements and Modelling in Complex Terrain – is now being processed [9]. The new Atlas contains in condensed form the results of a comprehensive, multinational six-year EU-JOULE project with participants from 12 European countries.

The project itself has had four distinct tasks: 1) New wind measurements in mountainous terrain, 2) Meso-scale modelling, 3) Regional wind resource maps, and 4) Improvement of site-specific modelling. The work had several purposes: 1) To improve the knowledge of the European wind resources, 2) To improve the understanding of the existence and variability of the wind resources in mountainous terrain, 3) To improve the models for calculation of the wind resources and siting of wind farms in mountainous terrain, 4) To establish a database of the time-series of wind speeds and -directions measured during the project and a database of the turbulence data measured during experimental campaigns in Greece, France, Sweden and Denmark.

2 WIND MEASUREMENTS

Wind measurements have been carried out in Northern Portugal, in Galicia and the Ebro Valley in Spain, in Central Italy, in Ireland, on the Greek islands of Crete and Andros, in the Finnish Archipelago and Finnish Lapland, in Northern Sweden, and in Southern France. The measuring periods range from one to four years and the measuring heights from ten to thirty meters above ground level. Approximately 70 masts were operated.

The data are summarized for each station following an extended version of the layout in the European Wind Atlas [8]. An example of the new four-page station presentation is given in Fig. 1: Each station summary is printed on two pairs of facing pages. The first opening (upper panel) contains the station description, the station topography, the topographical model corrections employed, and several raw data summaries. The second opening (lower panel) provides the wind climatological fingerprint, the seasonal and inter-annual variation of wind speed, the calculated regional Weibull parameters, and the calculated regional mean wind speeds and energy densities.

All the raw data and derived statistics are furthermore collected in a database which will be made publicly available on a non-commercial basis.

2.1 Measurement recommendations

While a main purpose of the present project has been to provide wind data and wind atlas climatologies for several topographically complex regions of Europe – where the data coverage until now has been scarce or non-existent – much effort has also gone into securing the quality of the wind measurements. As atmospheric models and flow modelling becomes more sophisticated and accurate, the need for long-term, high-quality wind measurements becomes more and more apparent.

The accuracy of wind speed and direction measurements, as well as the applicability of these to wind energy studies, depend on a number of factors which were recently summarized by Mortensen [5]. These include:

- Tower shadow and other effects
- Boom and clamp effects
- Anemometer design (ℓ_0)
- Turbulent biases for cup anemometers [4]:
  - Overspeeding: u-bias $\propto (\sigma_u/U)^2$
  - DP-error: v-bias $\propto (\sigma_v/U)^2$
  - Angular response: w-bias $\propto (\sigma_w/U)^2$
  - Stress-bias $\propto \langle uw \rangle/U^2$
- Calibration procedures:
  - Wind tunnel studies
  - Atmospheric (in situ)
- Anemometer maintenance
- Siting of anemometers
- Documentation of wind measurements and measurement conditions

Careful attention to each of these factors and comprehensive documentation of the measurement conditions are prerequisites to obtaining high-quality wind data suitable for wind energy applications and/or testing of models. Given the importance of this, a series of measurements recommendations have been worked out during the project and included in the Atlas.

Station 07 (Drave) — Portugal

40° 51' 17" N 08° 06' 11" W	E 575 598 m N 4 523 085 m	982 m

The mast is situated in the southern part of the Serra de S. Macário mountains, about 1.5 km SE of the village of Drave. The surface consists of low scrub. Going E and SE from the mast trees become more abundant and from a distance of 4-5 km the surface is covered by coniferous forest. There are no houses or other obstacles close to the mast.

On the map below, the height contour interval is 50 m and 10 m, respectively, and tick marks are shown for every kilometer.

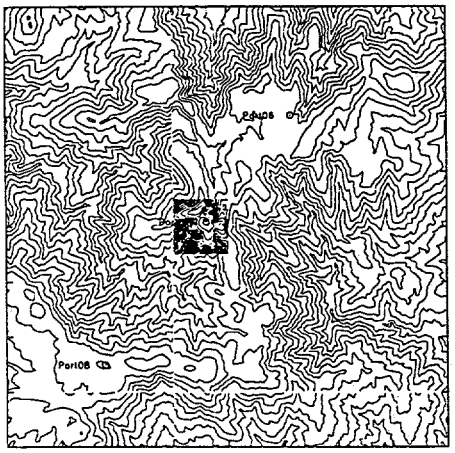

Sector	Input		Obstacles		Roughness		Orography		z_{0m}
0	0.0	0.0	0.0	0.0	0.0	0.0	61.5	1.6	0.0300
30	0.0	0.0	0.0	0.0	0.0	0.0	75.8	6.1	0.0300
60	0.0	0.0	0.0	0.0	0.0	0.0	95.3	4.4	0.0300
90	0.0	0.0	0.0	0.0	0.0	0.0	101.4	-1.3	0.0300
120	0.0	0.0	0.0	0.0	0.0	0.0	87.3	-5.9	0.0300
150	0.0	0.0	0.0	0.0	0.0	0.0	67.9	-4.9	0.0300
180	0.0	0.0	0.0	0.0	0.0	0.0	61.5	1.6	0.0300
210	0.0	0.0	0.0	0.0	0.0	0.0	75.8	6.1	0.0300
240	0.0	0.0	0.0	0.0	0.0	0.0	95.3	4.4	0.0300
270	0.0	0.0	0.0	0.0	0.0	0.0	101.4	-1.3	0.0300
300	0.0	0.0	0.0	0.0	0.0	0.0	87.3	-5.9	0.0300
330	0.0	0.0	0.0	0.0	0.0	0.0	67.9	-4.9	0.0300

Height of anemometer: 10.0 m a.g.l. 199106301535 - 199502161005

Sect	Freq	<1	2	3	4	5	6	7	8	9	11	13	15	17	>17	A	k
0	2.7	49	171	200	161	123	97	70	47	29	37	12	4	1	0	4.4	1.52
30	1.9	71	230	195	155	106	74	51	35	26	32	17	7	2	1	3.9	1.28
60	6.0	20	70	78	86	107	117	115	114	88	125	53	18	6	2	7.3	2.23
90	16.8	9	51	107	135	140	134	107	92	77	99	38	8	2	0	6.5	2.07
120	7.0	21	114	174	168	148	122	85	60	43	46	15	4	0	0	5.1	1.79
150	3.6	32	112	141	137	123	115	94	66	48	74	36	21	2	0	5.8	1.68
180	3.7	10	86	100	128	129	110	95	77	63	103	47	20	4	0	6.4	1.82
210	6.7	17	64	82	101	111	97	81	71	65	109	82	58	35	25	8.0	1.68
240	9.2	17	69	93	125	116	92	88	77	66	101	65	45	24	21	7.4	1.63
270	11.8	16	73	132	190	173	116	76	61	47	56	29	16	8	6	5.4	1.46
300	21.5	7	49	137	242	237	149	80	43	23	21	7	2	1	0	5.0	2.10
330	9.0	14	84	168	208	174	123	85	59	38	31	11	3	2	0	5.0	1.83
Total	100.0	16	74	127	168	160	122	88	67	51	66	32	15	7	4	5.7	1.59

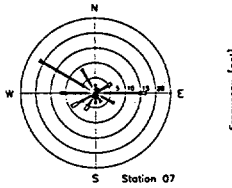

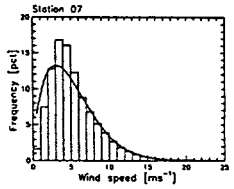

	Jan	Feb	Mar	Apr	May	Jun	Jul	Aug	Sep	Oct	Nov	Dec	Year
0	6.4	6.4	5.2	5.5	5.1	4.6	4.4	4.1	4.4	5.8	5.6	5.9	5.1
1	6.4	6.3	5.4	5.6	5.5	4.9	4.4	4.4	4.4	6.0	5.6	6.1	5.4
2	6.3	6.2	5.5	5.5	5.5	4.9	4.4	4.3	4.4	6.1	5.7	6.0	5.4
3	6.6	5.9	5.6	5.5	5.7	4.7	4.3	4.3	4.7	6.2	5.8	6.2	5.5
4	6.5	5.9	5.5	5.6	5.5	4.8	4.3	4.5	4.9	6.1	6.0	6.3	5.5
5	6.5	6.0	5.3	5.7	5.3	5.1	4.2	4.4	4.9	6.0	5.8	6.1	5.4
6	6.4	6.1	5.2	5.8	5.4	5.0	4.1	4.5	4.8	6.1	5.7	6.3	5.4
7	6.4	6.2	5.3	5.5	5.3	4.9	4.1	4.5	4.8	6.0	5.5	6.1	5.4
8	6.2	5.9	5.2	5.6	5.5	5.1	4.0	4.4	4.7	5.9	5.6	6.3	5.3
9	6.2	6.1	5.2	5.5	5.5	4.9	3.8	4.3	4.4	5.7	5.6	6.1	5.3
10	6.1	6.3	5.1	5.3	5.8	4.6	3.7	4.0	4.3	5.8	5.2	6.0	5.2
11	6.2	6.1	5.1	5.3	5.8	4.5	3.8	4.2	4.5	6.0	5.3	5.9	5.2
12	6.1	6.5	5.0	5.6	6.0	4.5	3.9	4.1	4.5	5.9	5.4	5.9	5.3
13	6.0	6.1	5.0	5.7	6.1	4.5	4.2	4.4	4.7	5.6	5.3	5.9	5.3
14	5.9	6.0	5.1	5.8	6.1	4.8	4.4	4.5	4.9	5.8	5.5	5.8	5.4
15	5.9	5.9	5.1	5.9	6.0	4.8	4.6	4.9	4.9	5.9	5.4	5.8	5.4
16	5.9	5.8	5.1	5.8	5.9	4.7	4.8	5.1	4.9	5.5	5.2	5.6	5.4
17	5.5	5.8	5.3	5.9	5.7	4.9	5.0	5.1	5.0	5.8	5.4	5.7	5.4
18	5.9	5.8	5.4	5.8	5.8	5.0	5.2	5.1	5.1	5.8	5.4	5.8	5.5
19	5.9	5.8	5.4	5.9	5.6	5.0	5.0	5.1	5.1	5.7	5.5	5.9	5.5
20	5.9	6.1	5.5	5.6	5.4	4.8	4.8	4.6	4.8	5.8	5.7	6.0	5.4
21	6.2	6.1	5.2	5.4	5.0	4.7	4.4	4.1	4.6	5.8	5.6	6.0	5.3
22	6.3	6.2	5.4	5.4	5.1	4.7	4.2	4.2	4.5	5.9	5.6	6.1	5.3
23	6.4	6.2	5.4	5.3	5.3	4.6	4.4	4.1	4.4	5.9	5.7	6.1	5.3
Mean	6.2	6.1	5.3	5.6	5.6	4.8	4.4	4.5	4.7	5.9	5.5	6.0	5.4

Wind-climatological fingerprint

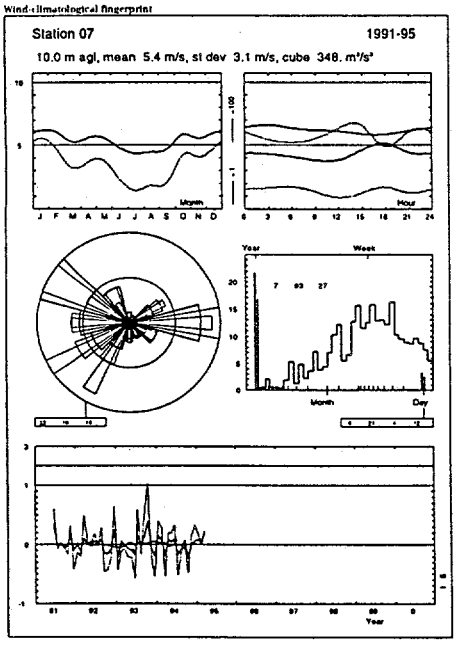

	Jan	Feb	Mar	Apr	May	Jun	Jul	Aug	Sep	Oct	Nov	Dec	Year
1991	–	–	–	–	–	6.4	4.4	4.5	4.4	5.8	6.5	5.4	–
1992	6.1	5.4	5.8	5.6	5.9	5.1	4.4	4.8	4.0	5.0	5.0	7.4	5.4
1993	4.9	6.4	5.2	5.2	5.1	4.0	5.0	4.4	5.3	8.2	5.1	4.9	5.3
1994	7.0	6.4	4.1	6.1	5.9	5.2	3.6	4.1	5.0	4.6	5.6	6.3	5.3
1995	6.7	6.1	6.3	–	–	–	–	–	–	–	–	–	–
Mean	6.2	6.1	5.1	5.6	5.6	4.8	4.4	4.5	4.7	5.9	5.5	6.0	5.4

Roughness Class 0 (z_0 = 0.0002 m)

z	0	30	60	90	120	150	180	210	240	270	300	330	Total
10	4.1	4.2	5.1	4.7	4.3	4.5	5.6	6.4	5.6	4.2	3.9	4.1	4.6
	2.08	1.82	2.49	2.49	2.28	1.99	1.98	1.99	1.90	1.74	2.24	2.27	1.92
25	4.5	4.6	5.6	5.1	4.7	4.9	6.2	7.0	6.1	4.7	4.2	4.5	5.0
	2.15	1.87	2.58	2.56	2.36	2.06	2.05	2.05	1.96	1.79	2.31	2.34	1.98
50	4.9	5.0	6.0	5.5	5.1	5.3	6.6	7.5	6.6	5.0	4.5	4.8	5.4
	2.20	1.92	2.64	2.63	2.42	2.11	2.10	2.11	2.01	1.83	2.37	2.40	2.03
100	5.3	5.4	6.6	6.0	5.5	5.8	7.2	8.1	7.2	5.4	4.9	5.2	5.9
	2.13	1.86	2.56	2.55	2.34	2.05	2.03	2.04	1.95	1.78	2.30	2.33	1.97
200	5.8	5.9	7.3	6.6	6.1	6.4	7.9	9.0	7.9	6.0	5.4	5.8	6.5
	2.02	1.76	2.42	2.41	2.22	1.94	1.92	1.93	1.85	1.60	2.18	2.20	1.87
Freq.	5.9	3.0	5.0	11.8	9.3	5.5	4.8	6.8	8.0	9.3	16.5	14.1	100.0

Roughness Class 1 (z_0 = 0.0300 m)

z	0	30	60	90	120	150	180	210	240	270	300	330	Total
10	2.8	3.0	3.7	3.2	2.9	3.3	4.1	4.4	3.7	2.8	2.7	3.0	3.2
	1.60	1.54	2.17	2.06	1.85	1.67	1.72	1.64	1.59	1.52	2.06	1.91	1.66
25	3.4	3.6	4.4	3.9	3.5	4.0	4.9	5.3	4.5	3.4	3.3	3.6	3.9
	1.73	1.66	2.35	2.22	1.99	1.79	1.86	1.77	1.72	1.65	2.22	2.06	1.78
50	4.0	4.2	5.1	4.4	4.1	4.6	5.7	6.2	5.2	3.9	3.8	4.2	4.5
	1.94	1.87	2.64	2.50	2.24	2.02	2.01	1.99	1.93	1.85	2.50	2.31	1.97
100	4.7	5.1	6.0	5.3	4.8	5.5	6.8	7.3	6.2	4.7	4.5	4.9	5.4
	2.06	1.99	2.81	2.67	2.38	2.15	2.22	2.12	2.05	1.97	2.67	2.46	2.09
200	5.9	6.3	7.5	6.6	6.0	6.8	8.5	9.1	7.7	5.8	5.6	6.1	6.6
	1.97	1.90	2.69	2.55	2.28	2.05	2.12	2.03	1.96	1.88	2.55	2.35	2.01
Freq.	3.5	2.8	5.9	13.8	7.7	4.7	4.8	7.5	8.2	9.8	10.9	12.4	100.0

Roughness Class 2 (z_0 = 0.1000 m)

z	0	30	60	90	120	150	180	210	240	270	300	330	Total
10	2.5	2.8	3.1	2.8	2.6	3.0	3.6	3.8	3.1	2.5	2.4	2.7	2.8
	1.58	1.65	2.14	2.10	1.85	1.67	1.71	1.65	1.56	1.58	2.04	1.97	1.67
25	3.1	3.4	3.8	3.5	3.2	3.7	4.5	4.7	3.9	3.0	3.0	3.3	3.5
	1.69	1.76	2.29	2.25	1.98	1.79	1.83	1.76	1.67	1.69	2.17	2.10	1.78
50	3.6	4.0	4.5	4.1	3.8	4.3	5.3	5.6	4.6	3.6	3.5	3.8	4.1
	1.87	1.95	2.53	2.49	2.19	1.98	2.02	1.95	1.84	1.87	2.40	2.33	1.96
100	4.3	4.8	5.3	4.9	4.5	5.2	6.3	6.7	5.5	4.3	4.1	4.6	4.9
	2.05	2.14	2.79	2.74	2.40	2.18	2.22	2.14	2.02	2.05	2.64	2.56	2.13
200	5.3	5.9	6.6	6.0	5.5	6.4	7.8	8.2	6.7	5.3	5.1	5.7	6.0
	1.97	2.05	2.67	2.62	2.30	2.08	2.13	2.05	1.94	1.97	2.51	2.45	2.04
Freq.	3.4	3.1	6.7	14.2	7.4	4.7	5.1	7.6	8.4	10.7	18.2	11.6	100.0

Roughness Class 3 (z_0 = 0.4000 m)

z	0	30	60	90	120	150	180	210	240	270	300	330	Total
10	2.0	2.3	2.4	2.2	2.1	2.4	2.9	2.9	2.4	1.9	1.9	2.1	2.2
	1.59	1.74	2.07	1.99	1.79	1.68	1.72	1.64	1.52	1.64	1.96	1.84	1.65
25	2.6	3.0	3.1	2.9	2.7	3.2	3.8	3.9	3.1	2.5	2.5	2.7	2.9
	1.68	1.84	2.20	2.11	1.90	1.78	1.82	1.74	1.61	1.74	2.08	1.95	1.75
50	3.2	3.6	3.8	3.5	3.3	3.9	4.6	4.7	3.8	3.1	3.0	3.3	3.5
	1.83	2.00	2.39	2.30	2.06	1.84	1.98	1.89	1.74	1.88	2.26	2.12	1.88
100	3.9	4.3	4.5	4.2	4.0	4.7	5.6	5.7	4.6	3.7	3.7	4.0	4.1
	2.08	2.28	2.72	2.62	2.35	2.20	2.25	2.15	1.98	2.15	2.57	2.41	2.12
200	4.7	5.3	5.6	5.2	4.9	5.7	6.8	7.0	5.6	4.5	4.5	4.8	5.2
	2.00	2.20	2.62	2.52	2.27	2.12	2.17	2.08	1.91	2.07	2.48	2.33	2.05
Freq.	3.3	3.5	7.8	12.4	6.9	4.7	5.4	7.7	8.7	12.0	17.2	10.4	100.0

z	Class 0		Class 1		Class 2		Class 3	
m	ms^{-1}	Wm^{-2}	ms^{-1}	Wm^{-2}	ms^{-1}	Wm^{-2}	ms^{-1}	Wm^{-2}
10	4.1	82	2.9	34	2.5	22	2.0	11
25	4.5	104	3.4	53	3.1	39	2.6	23
50	4.8	126	4.0	74	3.6	57	3.1	38
100	5.2	165	4.7	117	4.3	90	3.8	60
200	5.7	216	5.9	235	5.4	176	4.6	111

Figure 1: Sample four-page station statistics summary (ie two openings) for the Portuguese station Drave [9].

3 MODELLING

An important objective of the measuring campaigns has been to provide wind data which are adequate for the improvement of models for site-specific calculations and for the construction of a model system for regional wind resource assessments. Four regions in four countries with different complex topography and climatic conditions were selected for the measuring campaigns. The regions are depicted in Fig. 2.

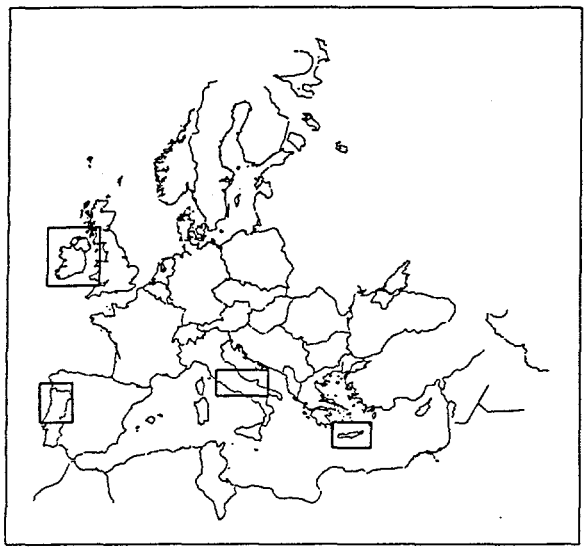

Figure 2: The four regions selected for intensive measurement and modelling campaigns.

The modelling work has thus concentrated on three main themes: 1) Investigating the accuracy and limitations of current wind resource assessment and siting tools – thereby providing data and information for the improvement of these models, 2) Implementing a new concept of nested models for regional wind resource assessment, and 3) Constructing a new model to estimate the turbulent wind conditions in complex terrain.

3.1 Limitations of WAsP

The model used for the European Wind Atlas [8] has a number of characteristics which limits its straightforward use to certain atmospheric and/or topographical conditions:

- Prevailing conditions must be near-neutral
- Orography must be gentle (attached flow)
- Meso-scale effects are not accounted for

The influence of atmospheric stability has been investigated both over land and offshore – examples of the results obtained are given in this volume by Barthelmie et al. [1] and Mortensen and Said [7].

Also in this volume is a report on the achievement on the purpose of improving micro-siting models given by Bowen and Mortensen: Exploring the Limits of WAsP – the Wind Analysis and Application Program [2, 6]. It has especially been attempted to understand the magnitude and variability of the wind resource in mountainous terrain and to quantify the limitations of current micro-siting models in such terrain. Most importantly, a simple indicator of the complexity of a given terrain has been established, which provides some insight into the accuracy of WAsP predictions in mountainous terrain.

3.2 Nested models for resource assessment

The meso-scale effects not accounted for by the current Wind Atlas methodology have been addressed by nesting meso- and micro-scale models in the calculation of the regional wind resources of a region. These results are reported in detail elsewhere in this volume by Frank and Landberg: Modelling the Wind Climate over Ireland [3].

3.3 Turbulence in complex terrain

Finally, the WAsP model [6] has been extended by a module which can predict the turbulence component spectra of (u, v, w) over moderately complex terrain as depicted in Fig. 3. The model builds on the the rapid distortion theory.

4 CONCLUSIONS

The EU-project *Measurements and Modelling in Complex Terrain* (JOUR/0067) has contributed substantially to our knowledge of the European wind resources and to our understanding of the variability and magnitude of these wind resources in mountainous terrain. Concurrently, the models for calculation of wind resources and siting in mountainous terrain have been improved. Specific results and outputs of the project are:

- A database on a CD-ROM containing new high-quality wind data from several complex regions of Europe, ie mean wind speed data, turbulence data, and wind atlas data sets.
- A second volume of the European Wind Atlas [9].
- The limitations of WAsP quantified [2].
- Improved model for siting (WAsP), including a model for turbulence over complex terrain.
- New and improved wind atlas data sets for some mountainous regions of Europe and a model-complex for producing such data: the Karlsruhe Atmospheric Mesoscale Model + WAsP.

ACKNOWLEDGEMENTS

The work by Risø National Laboratory on wind energy resources has—since 1981—been supported by the Commission of the European Union, Directorate-General for Science, Research and Development (DG XII). The present work was supported under contract JOUR–CT90–0067.

REFERENCES

[1] Barthelmie, R.J., N.G. Mortensen, L. Landberg and J. Højstrup (1996). Application of the WAsP model to determine the wind resource in non-neutral conditions in coastal areas. Proceedings of the European Union Wind Energy Conference and Exhibition 1996, Göteborg, Sweden, May 20–24, 1996.

[2] Bowen, A.J. and N.G. Mortensen (1996). Exploring the limits of WAsP: the Wind Atlas Analysis and Application Program. Proceedings of the European Union Wind Energy Conference and Exhibition 1996, Göteborg, Sweden, May 20–24, 1996.

[3] Frank, H.P. and L. Landberg (1996). Modeling the wind climate over Ireland. Proceedings of the European Union Wind Energy Conference and Exhibition 1996, Göteborg, Sweden, May 20–24, 1996.

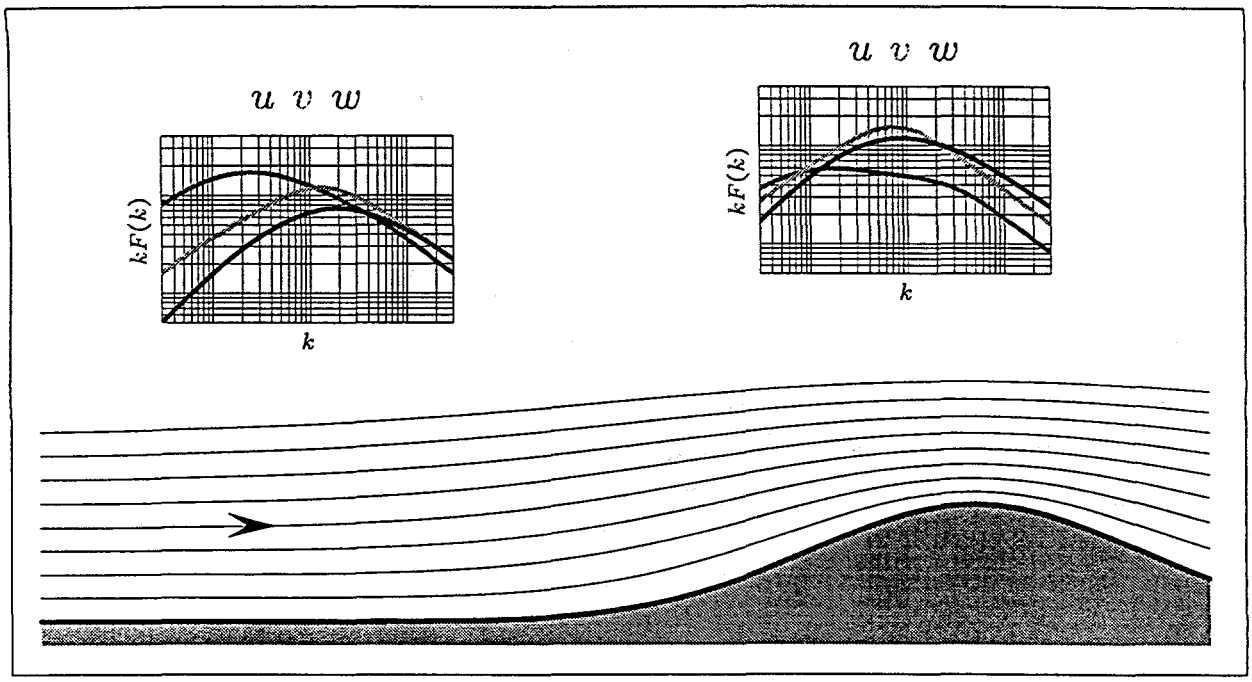

Figure 3: Sketch of wind flow over a hill. The change in the spectra of turbulence can be estimated using rapid distortion theory.

[4] Kristensen, L. (1993). The cup anemometer—and other exciting instruments. Risø–R–615(EN). 82 pp.

[5] Mortensen, N.G. (1994). Wind measurements for wind energy applications—a review. Wind Energy Conversion 1994. Proceedings of the 16th British Wind Energy Association Conference, Stirling, Scotland, June 15–17, 353–360.

[6] Mortensen, N.G., L. Landberg, I. Troen and E.L. Petersen (1993). Wind Atlas Analysis and Application Program (WAsP). Vol. 1: Getting Started, Vol. 2: User's Guide, Vol. 3: Utility Programs. Risø–I–666(EN). Risø National Laboratory, Roskilde. 29 + 133 + 38 pp.

[7] Mortensen, N.G. and Usama Said Said (1996). Wind Atlas for the Gulf of Suez, Arab Republic of Egypt. Measurements and modelling 1991–95. Proceedings of the European Union Wind Energy Conference and Exhibition 1996, Göteborg, Sweden, May 20–24, 1996.

[8] Troen, I. and E.L. Petersen (1989). *European Wind Atlas*. Risø National Laboratory, Roskilde. 656 p. ISBN 87–550–1482–8.

[9] Petersen, E.L., L. Landberg and N.G. Mortensen (1996). *European Wind Atlas. Vol. II: Measurements and modelling in complex terrain.* Risø National Laboratory, Roskilde. To be published.

WIND RESSOURCES IN COMPLEX COASTAL TERRAIN

Jørgen Højstrup
Department of Meteorology and Wind Energy
Risø National Laboratory
DK4000 Roskilde, DENMARK

Bengt Tammelin
Climatology Division
Finnish Met. Institute
P.O.Box 503, 00101 Helsinki, Finland

ABSTRACT: We analyse measurement from a Baltic Sea site, where the atmosphere is very stable for most of the onshore flow situations. The high Richardson numbers encountered makes it dubious to use the ordinarily available methods for calculation of windspeeds at roughness changes and hills. A simple method for calculating the roughness length from maximum and mean values is derived and applied to the problem of computing the aggregated influence on the surface roughness of a mixture of land and sea-surfaces upstream..
Keywords: Coastal Sea Areas: Meteorology: Stratification (Atmospheric): Gust Models

1. INTRODUCTION

The increasing interests in offshore wind energy is caused by both the scarcity of good land sites, but also by the larger wind energy potential offshore. We are here going to illustrate some of the problems that we can encounter at a coastal/island site with 'unusual' climatology.

The problems that we are going to address consist of

- The Baltic Sea has quite cold water for most of the year, and consequently the atmospheric stability will be unusually stable, leading to difficulties when trying to employ the 'normal' relations for *determination of windspeed variations with height.* tical to make measurements for a long time every time we need a new site, some numerical tools that ar where the windprofile shows a maximum at a moderate height.
- How to derive turbulence information from sites with no direct measurements of turbulence and how to use the inferred turbulence to calculate surface roughness lengths.
- How to parameterize the upstream roughness, when we have a number of scattered island upstream.

2. THE KOPPARNÄS SITE

The site is located on the Southern coast of Finland, some 50km West of Helsinki, in very complex terrain, typical for Finnish coastal and archipelago areas. On the Southern side there is practically open sea, to the West and East the wind field is influenced by many wood covered islands, while from the North, the wind comes over very rough vooded landscape (figs. 1 and 2).

The first measurement mast K1 is located on a little island Gåsören, with open sea in from 170° to 20°, and low coniferous trees in the sector from 20° to 170°. The distance from theshoreline to the island is 480m.

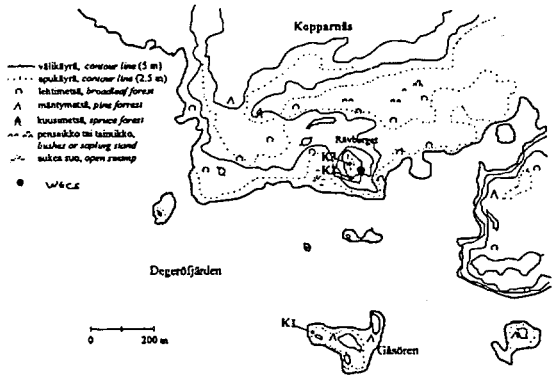

*Figure 1 A 1km*1km map of the Kopparnäs site. The three masts are denoted K1, K2 and K3.*

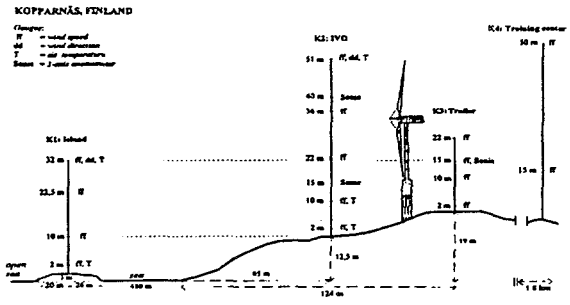

Figure 2

K2 and K3 are placed on an 18m high hill, while K4 is placed 1.8km further inland in a wooded area. K5 is a 300m high TV tower located some 27 km NE from Kopparnäs.

3. ATMOSPHERIC STABILITY

The variation of stability between land and sea varies considerably during the year. In the winter the sea is often

covered by ice, and the whole area will be snow covered. In late autumn, the land will be snow covered while the sea is open. In early spring the sea may still be ice covered while the bare rocks are strongly heated by solar radiation.

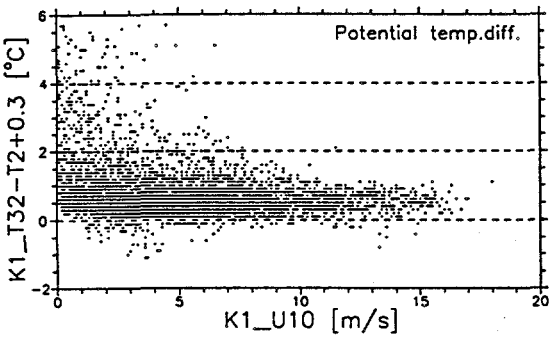

Figure 3 Potential temperature differences for the Gåsören site, mast K1, heights 32m and 2m.

Over the sea, on the average, the atmosphere tends to be stable because the Baltic is colder than the air (fig3). The conditions will in general be stable in winter, going to increasing stability in spring when the air heats up faster than the sea, moving towards less stable conditions in the summer and fall, when the water is slowly heating.up, increasing stability again in winter when the air cools off faster than the sea, see fig.4.

We also note from fig.4 that the stability near the ground is 'normal' in the sense that we see near neutral behaviour in winter, and unstable conditions in summer, meaning that we have a fairly complicated flow situation with typically neutral to unstable stratification near the ground and quite stable conditions further up.

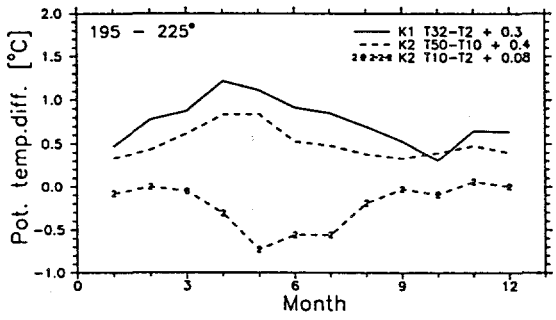

Figure 4 Monthly averages of potential temperature differences at K1 and K2. The K2 data from 50m and 10m were adjusted such that units for the upper level gradient is °C/m (as K1). No adjustments were done on the K2 10m and 2m measurements.

In order to use the stability data in the conventional models for corrections of windprofiles, we calculate the gradient Richardson number

$$Ri = \frac{g \dfrac{\partial \theta}{\partial z}}{T\left(\dfrac{\partial U}{\partial z}\right)^2}$$

We have computed Ri as a function of winddirection and in three windspeed intervals (fig.5). Our problem now is that the conventionally accepted theory says that turbulence only exists for Ri < 0.2, the socalled critical Richardson number, and only if we have turbulence is it possible to use the corrections that are normally applied to the windprofiles to correct for roughness changes and speed-up effects. As we see from fig.5 this is only the case for windspeeds higher than 10m/s, except in the East sector which is for flow over the island towards the mast. So the usual tools cannot be expected to give good results. There is some hope that tools for this situation can be developed [2].

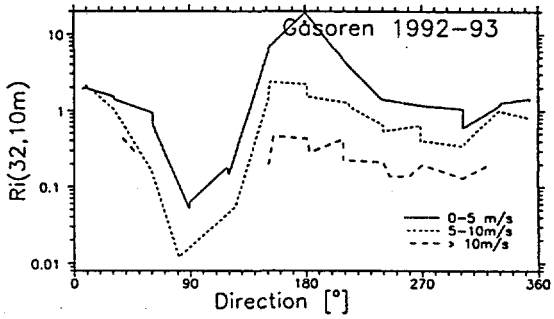

Figure 5 Ri-numbers from the Gåsören mast, 32m and 10m measurements plotted as a function of winddirection. The data were divided into windspeed classes, 0-5m/s, 5-10m/s and larger than 10m/s.

Measurement errors as the cause for the extreme stability conditions that we see here can be ruled out, since masts K1 and K2 provide quite similar results.

4. WINDPROFILES

A set of average windprofiles for a one year data set is shown in fig. 6. We use only directions 196-225°, and windspeeds in the interval 5-10m/s, showing stably curved profiles at masts K1 and K2, acceleration in the upper parts of the profile at mast K3 and deceleration below because of the increased surface roughness. Further inland at masts K4 and K5 we see decreasing windspeeds.

5. TURBULENCE

For this site as well as for many others, we do not always have turbulence measurements directly, but we do often have the maximum windspeed for each averaging interval. It is useful to be able to infer the turbulence levels from these simpler measurements, which we then investigated using three methods:

- Statistical theory assuming gaussianity and well behaved spectral shapes. See [3] for an expression for the gust filtered by a finite response instrument..
- Simulations, using artificial turbulence (Gaussian),

with varying length scales.

- Measurements. At K2 we had both direct turbulence measurements and maxima at four heights for part of the measurement period.

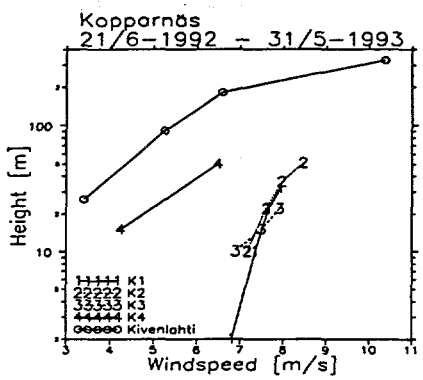

Figure 6 Average windspeed profiles for the five masts for one years data for directions 196°-225° (water fetch for K1, K2)

All three methods give comparable results, the ratio $(U_{max}- U)/\sigma \approx 2.8$ (10minute averaging, 1 second response time). The length scale variation is not very strong from 3.1 at scale 50m to 2.4 at 2000m. The modelled and simulated results are shown in fig.7 and the binaveraged measurements in fig.8.

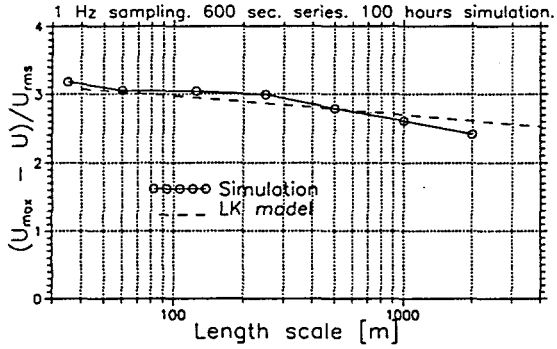

Figure 7 Modelled and simulated values of (U_max-U)/U_rms for different length scales.

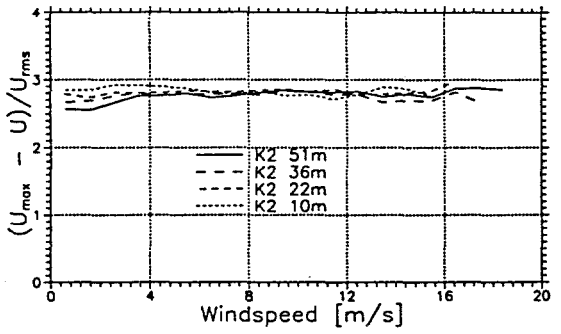

Figure 8 Measured ratios (U_max-U_mean)/U_rms from four heights at mast K2.

6. SURFACE ROUGHNESS OF AN ARCHIPELAGO

The average roughness length when we upstream have an archipelago of many small scattered islands is difficult to derive, we will attempt to get values for the average roughness length to be used for wind energy potential estimation by dividing the upstream area in a number of sectors, determining the percentage of the area that is occupied by islands within a 'footprint' of distances from 10*z to 100*z, thereby assuming that the flow behaviour at height z will be dominated by the area upstream within these distances.

In principle we can derive roughness lengths from the logarithmic windprofile, using windspeed measurements at two heights. In practice it is impossible to derive roughness length from windprofiles, unless the terrain is homogeneous upstream of the measurements. A more indirect method [1] that can be useful for inhomogeneous cases can be derived from an expression for the turbulent intensity:

$$I = \frac{\sigma_U}{U} = \frac{\sigma_U}{u_*}\frac{k}{\ln\left(\frac{z}{z_0}\right)} \approx \frac{1}{\ln\left(\frac{z}{z_0}\right)}$$

where we have used the logarithmic windprofile and the fact that σ/u_* is approximately constant (=2.5). This equation is strictly speaking valid only for neutral conditions, but we will attempt to use it anyway for all stabilities. σ will be derived from the relation $(U_{max}-U)/\sigma=2.8$.

In fig.9 we see the results for the calculated roughness lengths for the island site at two heights together with the K2 mast results. For both masts we see low values as expected for flow from the water, and higher values for other directions, where we have varying amounts of islands covering the upstream surface. The K2 results are somewhat influenced by the land surface also for the Southern sector resulting in higher roughnesses than for the island site.

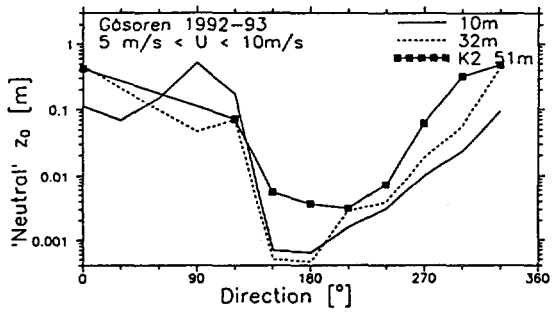

Figure 9 Roughness lengths derived from hourly maximum values from two heights at the island site and one height at mast K2.

The resultant roughness as a function of upstream fractional land cover can be seen in fig.10, where we have used logarithmic averaging of the measured roughnesses in the different categories. Results are shown for four heights at mast K2 (fig.10), where we can see that we get similar results for all heights.

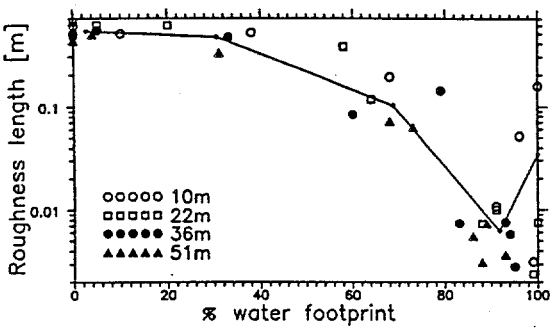

Figure 10 Average roughness lengths as a function of upstream percentage water footprint. The full line shows the bin-averaged values. At 100% the average value seems to increase. This effect was due to near-field influence of the rough surface on the lowest height (10m) on K2.

ACKNOWLEDGEMENT

This project has been supported by the EU (JOU2-CT93-0325).

REFERENCES

[1] Højstrup, J., 1995: Roughness lengths in coastal terrain. 11th symposium on Boundary Layers and Turbulence, Charlotte, USA. Proceedings available from the American Meteorological Society, pp 481-484.

[2] Zilitinkevich, Z and D. Mironov: Wind profiles of a stable stratified atmospheric boundary layer: An engineering model. Paper P13.9 this conference.

[3] Kristensen, L., 1993: The cup anemometer. Risø-R-615(EN), Risø National Laboratory, Roskilde, Denmark.. 82pp. (page 63)

WIND RESOURCE ASSESSMENT AND SITING – A WIDER PERSPECTIVE

Lars Landberg, Niels G. Mortensen and Erik L. Petersen
Meteorology and Wind Energy Department
Risø National Laboratory
DK-4000 Roskilde, Denmark

ABSTRACT: This paper is an attempt to give a broad overview of wind resource assessment and siting around the world. For convenience, the world has been divided into a number of regions according to their wind climate. The characteristics of these regions are described in some detail and so is the ability of state-of-the-art models to predict the wind resources. Where possible, examples of wind resource estimation studies are also given. It is clear that the views and information presented in this paper are biased towards what we ourselves have been working with.
Keywords: wind resource, wind climates, wind atlas methodology

1 INTRODUCTION

The wind resource of a site is e.g. the expected mean wind climate – or the power production of a wind turbine located at that site – over the next 10 to 20 years. If one is interested in the wind resources at one or more sites, like the locations of wind turbines in a wind farm, at least two things are needed: high-quality near-by wind measurements (preferably on site) and a micro-siting model which can estimate the spatial distribution of the wind resource over the entire area. Using only measurements from a near-by mast (e.g. at a meteorological station) will cause the local effects on the flow around that mast to be "transported" to the site in question; this procedure will obviously result in erroneous results. If, for example, the met mast is located near a building – which will reduce the wind speed of the flow coming from that direction – this reduction is almost certainly not found at the site. It can therefore be seen that models have to be used in order to get correct estimates of the wind resource at any site.

Basically, two modelling approaches exist: models based on statistical relations between the two sites and models based on the physical laws governing the wind flow. An example of the first kind of model is the measure-correlate-predict (MCP) method which correlates two sets of measurements – one taken at the site of interest and one taken at a station with a long wind speed and direction record. An example of the physical approach is the WAsP model; however, numerous other models exist as well. For a description of the WAsP model, see Troen and Petersen [8].

2 THE ARCTIC

As wind turbine technology matures, the potential for wind power generation in more marginal areas of the earth – including the arctic and sub-arctic – has been recognised. The exploitation of wind power in these regions has been scarce until now, but this may well be changing. The barriers for wide-spread application of wind energy in the arctic were recently identified (see Lundsager et al, [5]) and comprise both technological, economic, social and institutional barriers. However, many of these barriers are not unique to the arctic – or even particularly severe here.

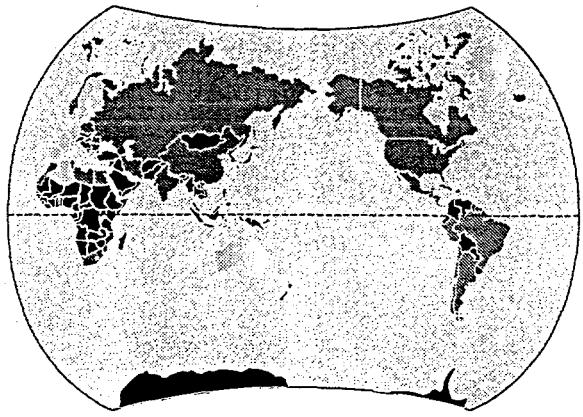

Figure 1: The Wind Atlas methodology has to date been applied in more than 60 countries around the world. National atlases have been published for almost 20 countries (marked in light gray); regional studies and siting of wind turbines have been performed in another 40 or more countries (marked gray).

One important barrier, though, is the lack of adequate knowledge of the wind resources in candidate regions. Apart from the northern parts of Sweden and Finland, little seems to have been done with respect to a systematic mapping of arctic and sub-arctic wind resources. Moreover, it is not clear to what extent the methods developed for wind resource estimation and siting in the temperate climates will apply to these regions.

In general, the density of meteorological stations in the arctic is low; this, however, may not be a problem since measurements are usually taken in or close to the settlements where the power is needed. More importantly, the quality of the wind measurements is often not known and neither is the applicability of current wind resource estimation methods. Snow, ice and sub-zero temperatures not only make it difficult to make reliable wind measurements, it also changes the roughness of the terrain considerably from season to season. Furthermore, the cooling of the lower layers of the atmosphere leads to local wind flows of a limited extent. Consequently, it is often very difficult

to extrapolate the measured wind climate over more than a few kilometers.

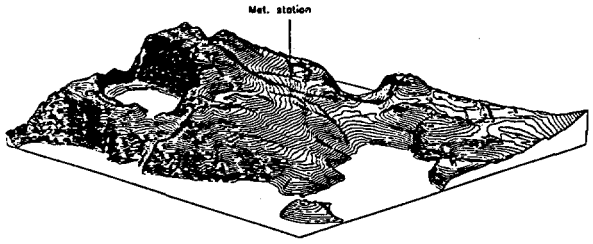

Figure 2: Wind power generation in Greenland and other arctic settings may benefit from the terrain-induced speed up of the wind and also the occurrence of smooth terrain surfaces, like water, snow and ice.

Recent investigations in Greenland suggest that wind power generation may be a viable alternative or supplement to more traditional ways of generating electricity. They also show that the increased costs of constructing and maintaining wind turbines in the arctic may be at least partially offset by the generally higher costs of electricity generation in these areas.

3 TEMPERATE PLAINS AND THE WESTERLIES

The temperate plains are characterised by large-scale low-pressure systems moving over the areas. These systems give rise to powerful storms and – because of the regularity of these systems – a steady wind climate. In wind energy terms this means that the potential and the reliability of predictions of the production can be expected to be high. Another characteristic of at least the European and American parts is, that these areas have the highest growth in the installed capacity of renewables – but also with the highest production of CO_2 and the area with the most intense competition from other sources of energy (coal, gas, nuclear etc.).

The European Wind Atlas methodology was developed with these areas in mind. The method is used to estimate the expected production at a given site using wind data from up to 100 km away. Since, generally speaking, the meteorological network is very dense in these areas, the wind energy potential at virtually any location can be calculated. Furthermore, numerous studies have shown that the method gives very reliable results for these regions. This is fortunate since recently problems with obtaining planning permission have arisen, meaning that accurate siting methods must be used to meet the investor's as well as the planning authorities' wishes and demands.

As a consequence of the above it is possible to estimate the expected wind power potential at almost any location, using either near-by measurements or data from the European Wind Atlas.

In Canada, an atlas similar to the European is being developed and because of the geographical likeness of the two regions, the method is expected to work well here, too. Before the European Wind Atlas was established, the Batelle Laboratories constructed a map of the world-wide wind resources. Although this study provides a good first guess, also of the European resources, it lacks detail over the land areas.

In USA proper, the "wind rush" in California gave a new start to wind energy world wide. The Californian terrain is dominated by local effects, such as seabreeze flows, making the potential very hard to predict. A second "wind rush" in the USA is now taking place in the very windy central states. These areas are in many ways quite similar to the European landscapes, promising much higher reliability in the wind resource estimates.

The European Wind Atlas methodology has also been used in New Zealand, but due to lack of data no firm conclusions can be drawn as of now. Australia has also seen some applications of the methodology and there is a large experience in using the method and good agreement has been found in different parts of the country.

In conclusion, there is no doubt that very reliable estimates of the long-term wind energy potential can be obtained in most of the temperate regions – where the terrain is not too complex.

4 DESERTS AND SEMI-ARID AREAS

From a wind energy point of view these regions have a number of advantages: the "pressure" on the land is often very low, access is easy, and construction work relatively simple. Also, the surface roughness tends to be low and uniform, so siting can be done primarily with optimization of the power production – or minimization of cost – in mind. Such areas could provide space for large-scale utilization of wind energy, provided they are favoured by a healthy wind climate and located not too far from places where power is in demand.

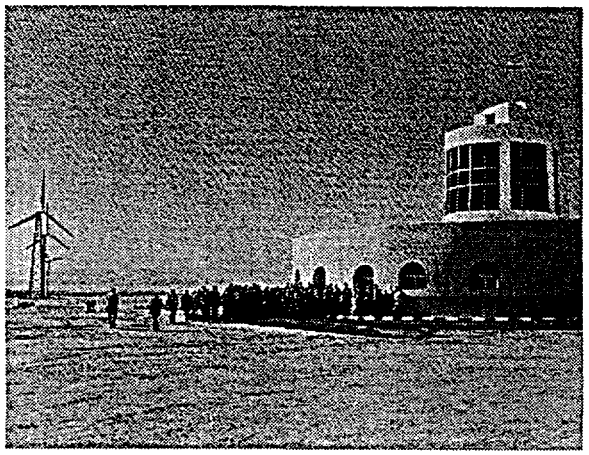

Figure 3: The Hurghada Wind Energy Technology Centre in Egypt.

Unfortunately, like in other sparsely populated regions, the meteorological network is very coarse and the wind climate is therefore not known in great detail at present. The physics of the flows in these dry regions of high solar insolation and little vegetation are also quite different from eg the temperate regions – where most of the models and techniques for wind resource estimation and siting were developed and tested. However, studies carried out in eg Algeria, Libya, Egypt,

Israel, Syria and Jordan should lead to a better understanding of the limits of contemporary models in these regions.

5 THE TROPICS

The tropical regions are dominated by seasonal wind systems, like the monsoon and the trade winds. In many areas the measuring network is dense and dates back many years – giving long records, very useful for wind energy purposes. These regions are also characterised by a high demand for power with many people still without electricity. A very high growth of the population is also found in these areas, resulting in even higher demand for electricity in the near future. Therefore an increasing interest in all kinds of energy – including wind energy – exists.

Because of the aforementioned dense network quite reliable estimates of the expected wind resource can be given for many tropical areas. The task being made slightly difficult by the fact the local thermally driven wind systems can be found in some areas.

Figure 4: The Muppandal wind farm in Tamil Nadu, India.

Studies along the lines laid out in the European Wind Atlas have been carried out in many places. A few examples are: Somalia and India, which are both dominated by monsoonal type flows. Here regional studies have been carried out, and the Wind Atlas method has been verified by comparing the predicted production of wind farms to actual production. India also has a very comprehensive database of meteorological measurements.

On the Cape Verde islands a wind atlas has also been made and again the method has been verified with good results using actual output from wind farms.

6 OPEN SEA

The open sea is in general characterised by a very high wind potential, but a detailed and reliable map of these resources is very hard to produce because of the very sparse measuring network. An overview of the offshore resources is given in the map published by the Batelle Laboratories in the USA (WMO [9]).

There are two sources of information available for estimating the resource: measurements from small islands, which are few and far between, and the so-called COADS data base. COADS is short for the Comprehensive Ocean-Atmosphere Data Set and is a result of a continuing cooperation between several American institutions, see eg Diaz et al. [3]. The data set contains measurements of the wind speed and direction as reported from ships crossing the oceans. This gives a huge, albeit in some areas sparse, data set covering most of the oceans. The data set has been compared to coastal measurements in some areas and the overall agreement seems to be good.

Other sources of information are available for certain limited offshore areas, eg the wind atlas for the North Sea by Børresen [2] . Also, a study covering the Baltic Sea is in progress and a wind atlas will be published within the next year.

7 COASTAL AREAS

Land sites close to the coastline have always been in demand for wind power generation, because of the generally high wind resource compared to (flat) inland sites in the same wind regime. This demand, as well as many other interests in the coastal land area, have led to a decrease in the availability of such sites – and near-coastal offshore sites have therefore become more attractive. Taking "near-coastal offshore" to mean the offshore area where the influence of the land on the wind flow is still present, this zone is of the order of 10 kilometers wide.

Several conflicting constraints must be taken into account in the siting of offshore wind turbines. Evidently, the cost of construction, grid connection and maintenance will increase with increasing distance from the coastline – but so will the available wind resource. Cost can be reduced by erecting the turbines closer to the coastline, but here visual impact and interference with other activities may be (too) high. Because the wind resources (and costs) vary considerably over small horizontal distances, there is an increasing demand for accurate offshore wind resource estimates. In particular, this presents a challenge to the physical models, since offshore wind measurements very rarely exist and would be very costly to perform.

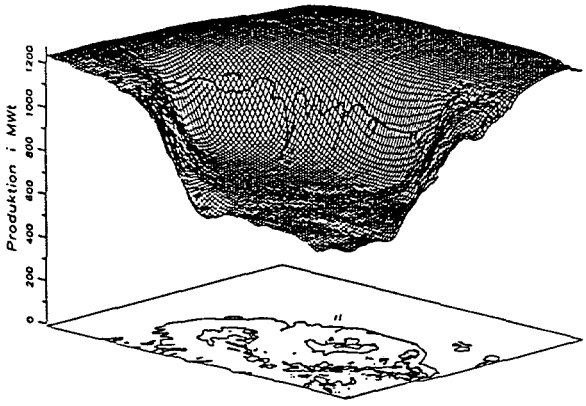

Figure 5: The estimated wind power production in the area of the Vindeby wind farm, Denmark. Here, westerly and southwesterly winds predominate, so the orientation and proximity of the coastline become very important factors in the siting of wind turbines.

The world's first offshore wind farm was constructed in 1990-91 near Vindeby, Denmark (Dyre [4]).

Here, the meteorology of the coastal zone is monitored in great detail from one onshore and two offshore masts (Barthelmie et al [1]). These data will be used to evaluate and further develop models for the prediction of offshore wind climates – leading to improved predictions of the wind power potential of this very promising region.

8 MOUNTAINS

In mountainous regions the topography enhances the existing wind potential, resulting in very high potentials. However, the exact magnitude of this potential is difficult to assess accurately, because mountainous areas are often very sparsely populated and as a consequence have a very sparse wind measuring network. Furthermore, the resources may of course be costly to develop due to the lack of infrastructure.

Because of the very complex nature of the terrain – as well as the fact that the winds are often dominated by local effects, driven by eg local differences in the temperature – it is very difficult to model the wind flow. An EU (European Union) initiative funded under the JOULE programme is addressing this problem by combining micro-siting models with models modelling the flow over a larger area, typically 100's of kilometres. This approach is being tested for Ireland, Northern Portugal, Central Italy and Crete and is indeed showing promising results in these areas [7].

9 CONCLUDING REMARKS

In this paper we have briefly described in wind energy terms most of the areas covering the earth. By examples we have shown that present day state-of-the-art models are indeed able to predict the wind resource in many areas. It has also been indicated that in some areas the potential can still not be satisfactorily estimated. This means that wind energy meteorology today has two main tasks: first, to educate the users in the models currently available – their proper use and known limitations – and, secondly, to conduct research into the fields where knowledge is still missing. Part of this research will be to collect and evaluate the results of the numerous studies that have already been carried out.

ACKNOWLEDGEMENTS

The work by the Risø National Laboratory on wind energy resources has – since 1981 – been supported by the Commission of the European Union, Directorate-General for Science, Research and Development.

REFERENCES

[1] Barthelmie, R.J. et al (1994). The Vindby Project. Risø-R-741(EN), 40pp. Risø National Laboratory, Denmark.

[2] Børresen, J.A. (1987). Wind atlas for the North Sea and the Norwegian Sea. Norwegian University Press and Norwegian Meteorological Institute, Oslo. 183 pp.

[3] Diaz, H.F., K. Wolter and S.D. Woodruff (1992). Proceedings of the International COADS Workshop, Boulder, Colorado, 13–15 January 1992. U.S. Department of Commerce, Boulder, Colorado.

[4] Dyre, K (1992). Vindeby offshore wind farm – the first experiences. In: The Potential of offshore wind farms. EWEA Conference 1992. The Association of Danish Windmill Manufacturers, Herning, Denmark.

[5] Lundsager, P., P. Ahm, B. Madsen and P. Krogsgaard (1993). Wind power in arctic regions. An investigation and a seminar June 3-4, 1993. Risø-I-709(EN), Risø National Laboratory, Roskilde, 251 pp.

[6] Petersen, E.L., N.G. Mortensen and L. Landberg (1994). Wind resource estimation and siting of wind turbines. European Directory of Renewable Energy Suppliers and Services 1994, 181–190.

[7] Petersen, E.L, L. Landberg, N.G. Mortensen (1996). European Wind Atlas part II. Measurements and modelling in complex terrain. Risø National Laboratory.

[8] Troen, I. and E.L. Petersen (1989). European Wind Atlas. ISBN 87-550-1482-8. Risø National Laboratory, Roskilde. 656 pp.

[9] World Meteorological Organization (1981). Meteorological aspects of the utilization of wind as an energy source. WMO Technical Note 175, World Meteorological Organization, Geneva, Switzerland.

EXPLORING THE LIMITS OF WAsP
THE WIND ATLAS ANALYSIS AND APPLICATION PROGRAM

Anthony J. Bowen[1] and Niels G. Mortensen[2]
[1] Mechanical Engineering Dept., University of Canterbury, Christchurch, New Zealand
[2] Meteorology and Wind Energy Dept., Risø National Laboratory, Roskilde, Denmark

ABSTRACT: The influence of rugged terrain on the accuracy of predictions by the Wind Atlas Analysis and Application Program (WAsP) is investigated using a case study of field measurements taken over 3½ years in rugged terrain. The parameters that could cause substantial errors in a prediction are identified and discussed. In particular, the effects from extreme orography are investigated. A suitable performance indicator is developed which predicts the sign and approximate magnitude of such prediction errors. This procedure allows the user to assess the consequences of using WAsP outside its operating envelope and could provide a means of correcting for rugged terrain effects.
Keywords: Resources, complex terrain, models (mathematical), siting.

1. INTRODUCTION

The Wind Atlas Analysis and Application Program (WAsP) has been shown to give accurate climatological predictions over low, smooth hills of small to moderate dimensions with sufficiently gentle slopes to ensure attached flows. WAsP has been used recently to develop the European Wind Atlas [1,2] and for wind-energy assessments in other countries. Out of necessity, WAsP is increasingly used for situations that do not lie within its recommended operational envelope. In particular, the program is being used for the investigation of candidate sites in rugged, complex terrain which may also be subjected to intense solar radiation or stratified atmospheric conditions [3,4].

This paper utilises full-scale wind data from a previous field programme in the rugged hills of northern Portugal to investigate the accuracy of WAsP under such extreme conditions. The goals of this work are to gain a better understanding of the causes and extent of the prediction errors, to develop a practical performance indicator which will enable users to correct for orographic effects if necessary, and to facilitate future improvements to the WAsP program.

2. THE WAsP PROGRAM

WAsP is a PC program used extensively to estimate wind energy resources and is described in detail by [5]. The program can generalise a long-term meteorological data series at a (reference) site which may then be used to estimate conditions at other (predicted) sites. Accurate predictions using the WAsP package may be obtained provided that both the reference and predicted sites are;

a) subject to the same weather regime,
b) the prevailing weather conditions are close to being neutrally stable,
c) the surrounding terrain is sufficiently gentle and smooth to ensure mostly attached flows, and
d) the reference data are reliable.

The orographic model used by WAsP is similar to the MS3DJH family of models and is described in detail by [6]. The linear model is limited to neutrally-stable wind flows over low, smooth hills with attached flows. WAsP predictions over simple isolated hills compare well with the measured field data from the two bench-mark field measurements of Askervein and Blasheval [6,7].

3. FACTORS IN THE PREDICTION PROCESS

The combined WAsP Analysis and Application procedures may be considered as a transfer function model linking the wind speeds at the reference site with those at the predicted site. WAsP assumes that there is a unique speed-up factor between the two sites for each wind direction sector which is determined by the roughness field and local terrain heights at both sites. This speed-up factor is assumed to be independent of climatic conditions.

A significant category of errors are those associated with the terrain surrounding both sites. Such errors are influenced by extensive flow separation, the degree of turning in each sector and the map size. These effects from orography will be discussed later in detail.

Errors in the prediction due to non-standard atmospheric conditions affecting the flow behaviour can also be very significant. Such climatic influences include; atmospheric stability, stratification, diurnal sea breezes, downslope winds, and blocking or channelling in valleys. The cross-correlation coefficient for mean wind speeds between the two sites is assumed by WAsP to be unity, signifying that both sites are subject to the same weather regime. A high correlation between the reference and predicted sites is therefore an essential but not exclusive condition for an accurate prediction by the WAsP model.

A longer averaging time of say, 1 hour, may be more appropriate than the 10 minute averages used here in order to allow a particular wind event to envelope physically the

two sites. However, only a small improvement in the cross correlation coefficients was achieved with 1 hour mean wind speeds. Field observations also indicate that monthly, seasonal and even yearly variations significantly affect the correlation values if the record length is relatively short.

The generalised wind data of the Atlas file is created by forcing the measured data to fit a standard Weibull frequency distribution. The magnitude of any prediction error is affected by the degree of transformation applied by the Analysis procedure in order to create the Atlas file.

The direction rose is often divided into 12 equal direction sectors. Steep, oblique ridges affect the direction of the incident flow and may cause the wind direction at the predicted site to fall into an adjacent direction sector to that occurring at the reference site.

4. ACCUMULATION OF PREDICTION ERRORS

The size of any error by WAsP is therefore dependent on the degree that the operational limits are violated by factors associated with the atmospheric conditions and the terrain. Consider here, only the effects from orography on the accuracy of the WAsP prediction model.

When applied to estimate the mean wind-speeds (U_{Pe}), at the predicted site using measured data at the reference site (U_{Rm}), WAsP first creates a generalised Atlas file by means of its Analysis procedure. The Atlas file represents the distribution of wind-speeds and directions for the whole area around the reference site with all local obstacles, surface roughness and orographic effects either removed or standardised. The effects from local obstacles, roughness and orography are determined for each direction sector using 3 built-in physical models. The Atlas file is assumed to be universal within a region defined by the extent of the wind regime at the reference site. The predicted site is assumed to lie in the same regime so that the same Atlas file may then be used to predict its conditions. The Atlas file generated from measured data at the reference site is then used to estimate the wind-speeds and energy at the predicted site, taking into account the local obstacles, surface roughness and orographic effects at the predicted site, using the WAsP Application procedure.

Consider first the WAsP Application procedure applied using generalised wind-speed data from the Atlas file (U_A) to estimate the sector-wise wind-speeds at a particular (predicted) site (U_{Pe}). The accurate speed-up correction for orographic effects has an accompanying error (E_2). The error will normally have a positive sign in line with the tendency for WAsP to overpredict rugged sites when using a flat reference site. Steep terrain promotes flow separation, particularly on the lee side of a ridge lying at an obtuse angle to the wind flow. When the flow is detached from the ground, the effective terrain is modified to something that is less rugged than the actual terrain. Linear numerical models such as WAsP that assume attached flows, could therefore be expected to overpredict consistently flow speeds over rugged terrain. Supporting evidence for the over-prediction of sites in rugged terrain is available in the literature [4,8].

The tendency for over-prediction of rugged sites should hold equally well for the Analysis and Application procedures as the Atlas file represents a fictitious reference site which is flat and featureless. Thus, for the Application procedure,

$$U_A + (\Delta U_2 + E_2) = U_{Pe}$$

Conversely, when (previously) analysing the reference site measured data (U_{Rm}) to create the corrected speed in the Atlas file (U_A), a further accurate speed-up correction (ΔU_1) with its associated error (E_1) is involved. This Analysis procedure involves the orographic model in the opposite sense such that,

$$U_{Rm} - (\Delta U_1 + E_1) = U_A$$

The overall prediction process utilises both the Analysis and Application procedures in succession. Therefore, combining both equations to eliminate U_A,

$$(U_{Rm} - \Delta U_1 + \Delta U_2) + (E_2 - E_1) = U_{Pe}$$

The estimated speed at the predicted site (U_{Pe}) is made up of the correct (measured) speed (U_{Pm}) and the overall prediction error which has accumulated from the two stages of the prediction process. The measured speed at the predicted site is assumed to involve no errors and is,

$$U_{Pm} = U_{Rm} - \Delta U_1 + \Delta U_2$$

The overall prediction error (U_{Pe}-U_{Pm}) is therefore determined by the difference in the two individual WAsP procedure errors, (E_2-E_1). The magnitudes of the individual procedure errors depend on the degree that each site contravenes the orographic limits of the WAsP prediction model. Both errors as defined, share the same sign as both the reference and predicted sites are invariably more rugged than the featureless site represented by the generalised data in the Atlas file. The sign of the overall prediction error may be positive or negative (signifying over- or under-prediction) depending on the relative magnitudes of the two individual procedure errors. A certain degree of cancellation between the two procedure errors is therefore likely to occur.

The relative sizes of the two procedure errors which may be assumed to be roughly proportional to the individual site ruggedness, thus determine the accuracy and bias of the overall prediction by the WAsP model.

5. CASE STUDY

The wind speed data used here are taken from the Joule programme project [9,10,11] based in Northern Portugal over a period of 3½ years. The results are also used in the European Wind Atlas Vol.2 [2]. The region of interest lies in Northern Portugal just north of latitude 40° N on the coastal ranges of the mountains, some 50km SW of the coastal city of Porto. Site 01 is located on the coastal plain, sites 06, 07, 08 are within 5km of each other on a ridge some 45km away to the east, while sites 09, 10 are situated on an adjacent ridge about 15km to their west. The five hill sites have similar elevations between 932 and 1082m. The terrain is mostly steep with smooth, barren

hillsides leading into a number of deep valleys that run down to the coastal plain. The hill sites clearly lie outside the operational terrain limits for the WAsP program.

The mean wind measurements were taken at 10m a.g.l. as consecutive 10 minute averages, 3s gust speeds and instantaneous wind directions. The data were collected over a period of 3½ years from July 1991 to April 1995. The measured wind-speed statistics and climatologies of the 6 sites were generated by the WAsP Analysis procedure and processed by the Utilities packages.

The prevailing winds blow persistently off the sea from the north-west. The coastal-plain site is frequently in a different wind regime to the high-level hill sites. Wind speeds are higher over the summer months at the coastal site due to the prevailing sea breezes, in contrast to the hill sites which have their peak wind speeds during the winter months. Frequent winter storms occur at the hill-top sites but with significantly weaker winds at the sea-level, coastal plain site. Only the strong wind events are reasonably well correlated between the coastal plain and hill sites.

The instantaneous speed-up ratio of the measured wind-speeds in any direction sector varies widely, especially for the coastal plain-hill site pairs. Significant variations are also evident between the summer and winter owing to the different climatic conditions prevailing during each season. Average cross-correlation coefficients at zero time lag (3m/s threshold) for various site pairs were calculated from the wind-speeds measured throughout the 3½ years of records. The resulting coefficients are not high (61-86%) for any site pair and are lowest (35-45%) for pairs involving the coastal-plain site 01.

Table 1: Score tables for WAsP predictions of site wind-speed and wind energy density from 3½ years of data.

Pred. sites	Ref. sites	01	06	07	08	09	10	Meas-ured
01	U m/s	4.2	3.4	3.3	4.3	4.5	4.5	4.3
	E W/m^2	112	52	53	122	136	126	120
06	U m/s	5.6	4.6	4.4	6	6.1	6.4	4.6
	E W/m^2	254	137	135	358	333	366	134
07	U m/s	6.5	5.5	5.3	7.2	7.3	7.5	5.4
	E W/m^2	387	230	217	615	572	596	214
08	U m/s	6.9	5.2	4.7	6.2	6.7	7	6.2
	E W/m^2	604	214	196	331	440	514	325
09	U m/s	5.7	4.6	4.4	6	6.1	6.4	6.1
	E W/m^2	293	137	144	341	326	380	324
10	U m/s	5.5	4.3	4	5.1	5.5	5.6	5.7
	E W/m^2	256	111	90	194	232	227	225

Predictions by WAsP of the mean wind-speeds and energy densities for all site pair combinations are shown in Table 1. The errors vary in sign and are sometimes large. However, good predictions are obtained between site pairs involving combinations 06-07 and 01-09-10, including all the self-prediction cases. Some sector-wise prediction errors are also large and may exceed those for all-directions. WAsP consistently overpredicts at most hill sites when using the flat, coastal-plain site 01 as reference.

6. PERFORMANCE INDICATORS

6.1 Cross correlations

The cross-correlation coefficient of mean wind-speeds at both sites is a commonly used measure of the sites' suitability for prediction techniques such as WAsP and the *Measure-Correlate-Predict method* (MCP). A high level of cross-correlation in wind speeds will ensure that both sites lie within the same weather regime but does not ensure neutral stability. However, for sites which lie within the WAsP performance envelope for both terrain and atmospheric stability, a high correlation is the only essential pre-requisite for an accurate prediction.

There is no apparent relationship between the size of the prediction error and the cross-correlation coefficient for any of the site pairs considered here. Furthermore, the cross-correlation coefficient is unable to indicate the sign of the prediction error. It can only be assumed that these large prediction errors are due to the fundamental limitations of the orographic model and to a lesser extent, the prevailing atmospheric conditions. It may be concluded that a high level of cross-correlation is not by itself, always a good indication of the potential for WAsP to make an accurate prediction. An additional orographic indicator is also needed for sites situated in rugged terrain.

6.2 Orographic indicator

A practical site parameter is therefore required which quantifies the extent to which the terrain at a particular site exceeds the limits implied in the derivation of the orographic model. Such a parameter should be a measure of site ruggedness and if possible, be derived directly from the site contour data. The ability to predict whether or not the flow will separate is fundamental to the estimation of the performance of the orographic model and other linear numerical models, which assume the presence of attached flows. The fraction of the surrounding terrain which is over a critical slope of say, 0.3 is therefore proposed as a coarse measure of the extent of flow separation [12].

An orographic performance indicator to predict the overall error (E_2-E_1) can now be defined as the difference in these percentage fractions of steep terrain between the predicted and reference sites. The steep-terrain fractions for sites considered here were estimated using a sub-routine which considers the slopes along the centre radius of each of the 12 sectors across each cell in a 250m rectangular grid. The resulting orographic performance indicator (I) provides encouraging results when it is plotted against the percentage WAsP prediction error (E) in Fig. 1. The success of the indicator is insensitive to detailed variations in the method used for estimating its magnitude. In view of the approximate nature of the analysis, a linear relationship between the percentage prediction error and the orographic performance indicator can be made through the origin for the well correlated hill-hill site pairs (solid circles) eg;

$E = k.I$, where $k=3.3$ for $I>0$ and $k=2.3$ for $I<0$.

The systematic trend confirms the strong influence of flow separation in determining the orographic prediction error.

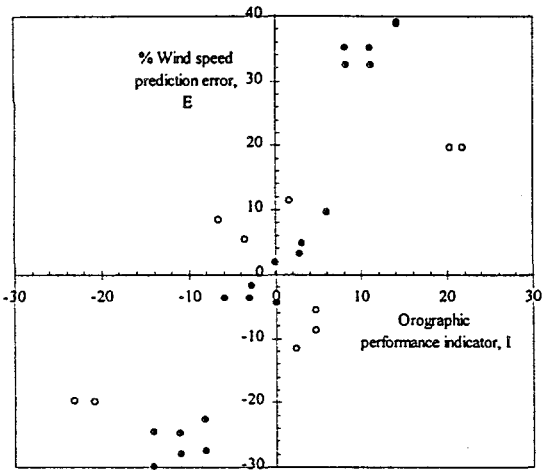

Figure 1: Plot of the WAsP prediction error and the proposed orographic performance indicator. Solid circles are hill-hill site pairs. Open circles are plain-hill site pairs.

Those data points involving the flat coastal-plain site 01 (open circles) are marginalised due to their low correlation caused by the prevailing atmospheric stability. It is proposed that the magnitude of the prediction error for a certain value of the orographic indicator is affected further by the prevailing atmospheric conditions between each site pair. Prevailing stable conditions such as might occur between the coastal plain and hill sites, would reduce the error by a significant amount. Unstable conditions are likely to increase the error by a relatively small amount. These climatic effects would be less prevalent for the hill-hill site pairs which share the same approximate location and elevation.

7. CONCLUSIONS

WAsP prediction errors may be significant if the local climate or terrain lie outside its normal operational envelope. A high level of cross-correlation between wind speeds at the reference and predicted sites is an essential but not exclusive pre-requisite for an accurate prediction. The value of the correlation does not indicate the sign or magnitude of the prediction error.

The sign and approximate magnitude of the prediction error due to orography is proportional to the difference in ruggedness between the predicted and reference sites. An approximate estimate of this error may therefore be made with a performance indicator based on site ruggedness. One suitable indicator developed here is the difference in the fractional extent of the terrain with slopes greater than a critical value between the predicted and reference sites. This indicator also provides a means of defining in quantitative terms, the orographic limits for accurate WAsP predictions and a suitable correction if those limits are exceeded. However further test cases are needed before the reliability of the indicator can be confirmed. The ideas described in this paper are reported in more detail in [13].

8. ACKNOWLEDGEMENTS

The opportunities and financial assistance afforded by the Risø National Laboratory and the University of Canterbury made this project possible and both are gratefully acknowledged.

9. REFERENCES

[1] Troen, I. and Petersen, E.L. European Wind Atlas. Published by Risø National Laboratory, Roskilde, Denmark, ISBN 87-550-1482-8 (1989) 656p.

[2] Petersen, E.L., Landberg, L. and Mortensen, N.G., European Wind Atlas, Vol. II: Measurements and modelling in complex terrain. To be published. Risø National Laboratory, Denmark (1996) 361p.

[3] Botta, G., Castagna, R., Borghetti, M. and Mantegna, D. Wind analysis on complex terrain - The case of Acqua Spruzza. Journal of Wind Engineering and Industrial Aerodynamics 39 (1992) 357-66.

[4] Bowen, A.J. and Saba, T. The evaluation of software for wind turbine siting in hilly terrain. Proc. 9th Int. Conf. on Wind Engineering, New Delhi, India (1995).

[5] Mortensen, N.G., Landberg, L., Troen, I. and Petersen, E.L. Wind Atlas Analysis and Application Program (WAsP), Vol.1: Getting Started. Vol.2: User's Guide. Risø National Laboratory, Roskilde, Denmark (1993) 126p.

[6] Troen, I. A high resolution spectral model for flow in complex terrain. Ninth Symposium on Turbulence and Diffusion. American Meteorological Soc., Risø National Laboratory, Denmark (1990) 417-20.

[7] Walmsley, J.L., Troen, I., Lalas, D.P., and Mason, P.J. Surface-layer flow in complex terrain: Comparison of models and full-scale observations. Boundary-Layer Meteorology 52 (1990) 259-81.

[8] Sandström, S. WAsP - A comparison between model and measurements. Proc. 5th European Wind Energy Association Conf., Thessaloniki-Macedonia, Greece, Vol 3 (1994) 70-4.

[9] Restivo, A. Resource assessment in regions of Portugal with complex terrain. Wind energy technology and implementation. Proc. E.C. Wind Energy Conf., Amsterdam, Holland (1991) 797-801.

[10] Landberg, L. and Mortensen, N.G. A comparison of physical and statistical methods for estimating the wind resource at a site. Proc. 15th BWEA Ann. Wind Energy Conf., York, UK (1993).

[11] Mortensen, N.G., Petersen, E.L. and Landberg, L. Wind resources, Part II: Calculational Methods. Proc. European Community Wind Energy Conf., Lübeck-Travemünde, Germany (1993) 611-4.

[12] Wood, N. The onset of separation in neutral, turbulent flow over hills. Boundary-Layer Meteorology 76 (1995) 137-64.

[13] Bowen, A.J. and Mortensen, N.G. Exploring the limits of WAsP. The Wind Atlas Analysis and Application Program. To be published as an internal report, Risø National Laboratory, Denmark (1996).

APPLICATION OF THE WA^{S}P MODEL TO DETERMINE THE WIND RESOURCE IN NON-NEUTRAL CONDITIONS IN COASTAL AREAS

R.J. Barthelmie*, N.G. Mortensen, L. Landberg and J. Højstrup
Department of Meteorology and Wind Energy, Risø National Laboratory, 4000 Roskilde, Denmark.
*Also affiliated to: Climate and Meteorology Program, Dept. Geography, Indiana University, Bloomington, USA.

ABSTRACT: Differences in stability conditions on- and off-shore mean that the coastal wind field is difficult to predict accurately. Using the default parameters in the WA^{S}P model gives good predictions of mean offshore wind speed profiles at Vindeby offshore wind farm, however, conditions at Vindeby are close to neutral on average. A number of scenarios are evaluated to test whether predictions can be improved in non-neutral conditions.
Keywords: Coastal sea areas, Models (Physical), Off-shore, Meteorology

1. INTRODUCTION

Coastal areas are frequently chosen as wind turbine sites because it is known that offshore wind speeds are typically higher than those onshore. However, accurate assessment of the wind resource in coastal zones is difficult since it depends on the parametrisation of both roughness and stability changes. Both these factors influence the development of the internal boundary layer and hence the wind speed profile moving away from the coast. The modification of atmospheric stability occurs onshore and offshore on different time scales. Diurnal variability is important on land, particularly in spring and summer, while sea surface temperatures change more slowly (Barthelmie et al., 1996). Unfortunately, relatively little is known about the stability climatologies of offshore areas. Stability in the coastal zone depends in part on the air-sea temperature difference and hence on a number of factors such as the orientation of the coastline, the prevailing wind speed and direction, water depth and the latitude influencing the magnitude of seasonal and diurnal changes of net radiation. To date, there have been few measurements in these offshore coastal areas with which models can be developed and evaluated.

In order to predict the wind resource of the Baltic Sea area, a number of approaches have been used which are described in Højstrup et al. (1996). As part of the Baltic Sea Wind Atlas project, stability analyses have been undertaken using data from a number of coastal, island and offshore sites. These show that atmospheric conditions offshore are frequently non-neutral tending towards stable in this area (in agreement with analyses detailed in Joffre, 1985 and Smedman et al., 1996).

2. WA^{S}P

The Wind Atlas Analysis and Application Program (WA^{S}P) (Mortensen et al., 1993) has been used successfully for siting wind turbines both on-shore and offshore. In offshore areas, away from the influence of the coast, it gives good predictions in comparison with observed mean wind speeds and the wind speed profile (Petersen, 1992). However, if conditions offshore are predominantly stable, WA^{S}P will tend to over-predict wind speeds in the near-coastal offshore zone (Barthelmie et al., 1996). This is because the internal boundary layer grows more slowly in stable conditions and, in the range of heights of interest for wind energy (i.e. 30-100m), the increase in wind speed will be smaller than in near-neutral conditions.

Without undertaking a detailed stability analysis for each offshore area, more comprehensive modelling (e.g. using a mesoscale meteorological model) is not possible. However, with a generalised climatology, a number of parameters can be easily changed in WA^{S}P which effectively allows different stability conditions on- and off-shore to be taken into account. Data from the Vindeby offshore wind farm are used to assess how WA^{S}P predicts the modification of wind field moving offshore in different stability conditions.

3. VINDEBY DATA

Meteorological data have been collected at Vindeby wind farm since 1993. The site is shown in Figure 1 and has been described in detail in Barthelmie et al. (1994, 1996). There are three masts - one at the coast LM, and two offshore SMS and SMW at distances of 1400 and 1600m respectively.

Stability conditions at Vindeby have been classified according to the Richardson number (Arya, 1988) and the frequency of different classes are shown for each of the three masts in Table 1. Thus, on average, conditions are shown to be close to neutral, with near-neutral conditions occurring more frequently at LM than at the sea masts.

Table 1. Percentage occurrence of stability classes at Vindeby based on Richardson numbers.

Ri		LM	SMS	SMW
Ri>0.1	Stable	19	26	25
-0.1<Ri<0.1	Near-neutral	66	48	51
Ri<-0.1	Unstable	15	26	24

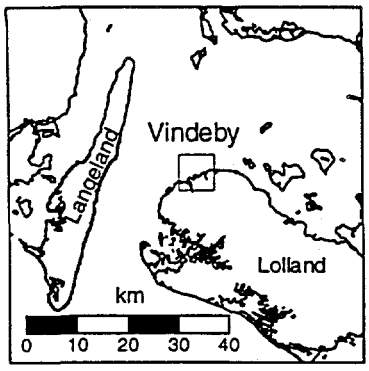

Figure 1. Location of the Vindeby wind farm, Denmark.

4. APPLICATION OF THE WA^{S}P MODEL

4.1 Standard application of WA^{S}P

Wind speed and direction data from 20m height at LM are used to predict wind speed profiles at SMS and SMW using the default parameters of WA^{S}P. Predicted and observed profiles at the three masts are shown in Figure 2. With the exception of the wind speed at 7m at SMS, WA^{S}P predicts the profiles reasonably accurately (within ±0.2m/s or ±3%). The data are then sub-divided according to the stability classes given in Table 1. Data from LM are used to define stability and wind speeds at 20m at LM are used by WA^{S}P to predict wind speed profiles at each mast for each stability class. Note that WA^{S}P uses climatological averages to describe the stability conditions in which conditions over land are slightly unstable and those over sea are slightly stable (see Troen and Petersen, 1989). Wind speed profiles are plotted in Figure 3 as normalised differences (percentages):

$$\textit{Normalised differences (\%)} = \frac{U_{obs} - Upred}{U_{obs}} * 100$$

As shown in Figure 3, in stable conditions WA^{S}P tends to over-predict wind speeds below 20m and underpredict wind speeds above 20m. In near-neutral conditions, wind speeds are slightly underpredicted at all three masts. (Note that differences of up to 2% can be caused solely by rounding errors). In unstable conditions, wind speeds at the sea masts tend to be under-predicted.

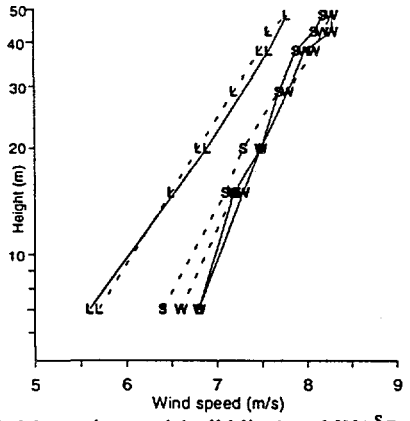

Figure 2. Mean observed (solid line) and WA^{S}P predicted wind speed profiles (dashed line) at the three masts (L=LM,S=SMS,W=SMW).

4.2 Changing WA^{S}P parameters

Within WA^{S}P stability differences between land and water surfaces are incorporated by treating 'stability modifications as small perturbations to a basic neutral state' (Troen and Petersen, 1989). There are 74 parameters in the initial set-up of WA^{S}P, of which 29 can be used to account for deviations of the atmosphere from near-neutral conditions. Since the model is generally shown to model atmospheric responses to roughness changes well (Troen and Petersen, 1989), analyses presented herein concentrate on parameters which deal specifically with changes between land and water surfaces. There are three groups of relevant parameters:

1. Width of the coastal zone.
2. Differences between stability parameters which affect the wind speed profile on- and off-shore.
3. Differences in the heat flux and heat flux variability on- and off-shore.

In order to modify WA^{S}P correctly, it is necessary to calculate appropriate values for each parameter. Data from Vindeby are used below for this purpose. Each set of predictions is based on data from 20m height at LM.

4.3 Changing the width of the coastal zone, *c*

The width of the coastal zone is the distance on either side of a discontinuity over which the discontinuity has an impact on the predicted wind speed. In stable conditions, since the internal boundary layer grows more slowly, it could be assumed that the wind speed reaches the same equilibrium offshore value but over a longer distance from

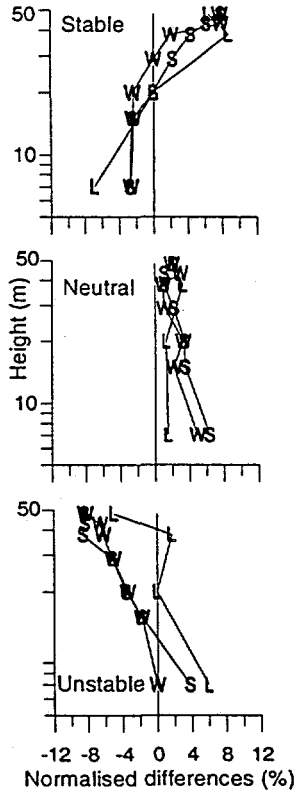

Figure 3. Differences between predicted and observed wind speed profiles at the three masts in different stability conditions (L=LM,S=SMS,W=SMW).

the coast than in near-neutral conditions. The weighting factor, w, is applied to stability corrections where:

$$w=min(x,c)/c$$

and x is the distance from the coast. Reducing c means that close to the coast weighting factors will be larger but applied over a shorter distance (as in unstable conditions), while increasing c means that the factors will be smaller but applied over longer distances. The effect of varying c on the predicted wind speed profile at SMS is shown for different stability conditions in Figure 4. Reducing c gives a better prediction for the wind speed profile in near-neutral conditions, while increasing c improves the predictions below 40m in stable conditions. Differences between the observed and predicted wind speeds appear to arise mainly from the deviation of the observed profile from the near-logarithmic profile predicted by WA^{S}P rather than from variations in the weighting factor.

4.4 Changing the shape of the wind speed profiles

WA^{S}P can apply small changes to the wind speed profile (relative to a logarithmic profile) due to stability effects which are set using three parameters (these are only applied if default parameters are changed). The first is a height parameter, *dy* - 'the height above ground where differences between stable and unstable profiles are smallest' (Mortensen et al., 1993). The default value is 100m. The second is a stability root mean square (r.m.s.) factor which accounts for stability variations in near-surface wind speeds e.g. at 10m. Mortensen et al. (1993) report that this value is close to the r.m.s. of the diurnal variability of wind speeds. The default value is 0.12. The last factor is an offset (the increase in wind speed) due to stability. The default value is 0.11. The equivalent parameters for over water situations can also be changed - these have default values of 50m, 0 and 0 respectively. Values for the first parameter are difficult to determine without measurements to 100m height. However, examination of wind speed profiles in different stability conditions (Figure 3) suggests that *dy* is set correctly. To calculate the second parameter, r.m.s values are determined for the whole Vindeby data set at 20m height at LM and SMS. The data set is then divided into stability classes (as given in Table 1) and the r.m.s value for the near-neutral class calculated. The difference between this r.m.s and the r.m.s. for the whole data set is assumed to be equivalent to the second parameter. For LM this value is 0.29 and for SMS it is 0.33. To determine the offset, the difference between the WA^{S}P predicted profiles at 48m and the observed values are used. For LM and the sea masts the factors are 0.12 and 0.08 respectively (positive in stable conditions, negative in unstable conditions). These are close to the WA^{S}P default. The effect of changing these parameters on the WA^{S}P predicted wind speed profiles is very slight (Figure 5). The improvements in the predictions occur near the top of the wind speed profiles.

4.5 Changing the offshore heat flux

In the standard application of WA^{S}P there are differences between the heat flux, H_0, and heat flux variability over land and sea. The values used are climatological averages with variability introduced by the r.m.s. value, where:

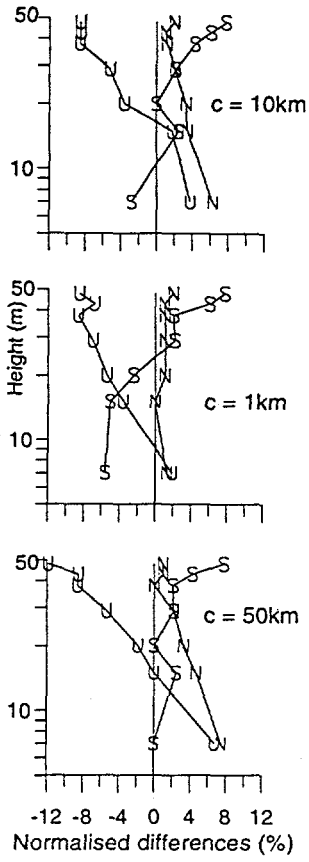

Figure 4. Differences between predicted and observed wind speed profiles at SMS for different values of the width of the coastal zone, c (U=unstable, N=near-neutral, S=stable).

H_0 land -40Wm^{-2} r.m.s H_0 land 100 Wm^{-2}
H_0 sea 15Wm^{-2} r.m.s H_0 sea 30 Wm^{-2}

Analysis of Richardson numbers at Vindeby suggests that stability conditions at SMS are frequently different to those at LM. Here, a number of scenarios are tested in which the default offshore H_0 is varied. The r.m.s. value is unchanged in all cases. The wind speed predictions are improved slightly by setting H_0 to -100 Wm^{-2} in near-neutral conditions, and to +100Wm^{-2} in unstable conditions. Predicted wind speeds are increased at the lower heights if H_0 is negative, and increased at all heights if H_0 is positive. If H_0 is set to -100Wm^{-2} the predictions can be improved at some heights in stable conditions. These results are shown in Figure 6. It should be noted that stability conditions at Vindeby may not be typical of offshore areas due to the low water depths. Further analysis is required to quantify H_0 and r.m.s. H_0 for different offshore areas.

5. DISCUSSION

WA^{S}P is used here to predict wind speed profiles at two offshore masts between 1 and 2km from the coast using data from a land - based mast. In this coastal zone,

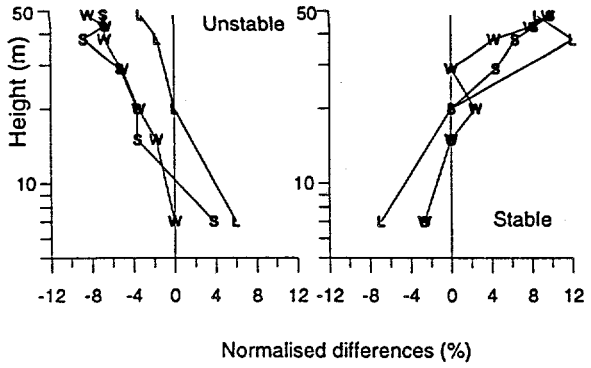

Figure 5. Differences between predicted and observed wind speed profiles for different values of the stability parameters in the wind speed profile on- and off-shore (L=LM,S=SMS,W=SMW).

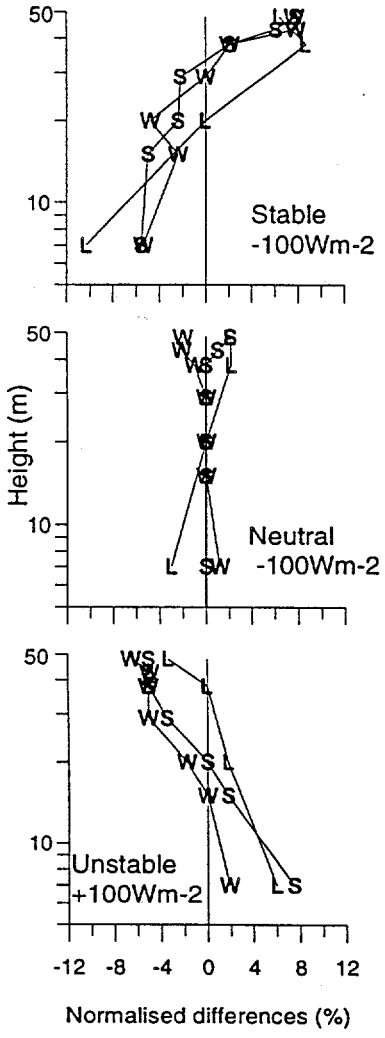

Figure 6. Differences between predicted and observed wind speed profiles for different values of the offshore heat flux (L=LM,S=SMS,W=SMW).

the wind field is modified by changes in both roughness and stability. The standard WA^{S}P application predicts mean wind speed profiles at the sea masts with a good degree of accuracy (within ±0.2m/s or ±3%).

In order to examine WA^{S}P's performance in different stability conditions, the data are subdivided into stability classes. This introduces two errors - those due to stability deviations and the problems of using a small data set. Accurate predictions within WA^{S}P rely on a the fitting of a Weibull distribution which may no longer be valid for short time-series. Even when the data are subdivided by stability class, the maximum difference between observed and predicted wind speeds is ±0.5m/s or ±12%.

WA^{S}P's default parameter settings can be changed to account for different stability conditions. Here three scenarios are evaluated:

1. Width of the coastal zone.
2. Stability parameters in the wind speed profile
3. Heat flux and heat flux variability on- and off-shore.

Predictions of wind speed profiles at the sea masts can be improved slightly by altering these parameters based on data from Vindeby. Further improvement may be obtained by combining changes in the default settings which will allow varying stability conditions to be taken into account more effectively. This requires further investigation, together with detailed examination of stability in different offshore environments. This approach may improve implementation of the WA^{S}P model in offshore areas such as the Baltic where conditions are frequently stable.

ACKNOWLEDGEMENTS

This research was supported by the European Union under contract JOU2-CT93-0325.

REFERENCES

Arya, S. Introduction to micrometeorology. Academic Press Inc., San Diego (1988).

Barthelmie, R.J., Courtney, M.S., Højstrup, J., Sanderhoff, P. *The Vindeby Project: a description.* Risø-R-741(EN). Risø National Laboratory, Denmark (1994).

Barthelmie, R.J., Courtney, M.S., Højstrup, J., Larsen, S.E. Meteorological aspects of offshore wind energy - observations from the Vindeby wind farm. *J. Wind Eng. Ind. Aerodyn. (in review)* (1996).

Højstrup, J., Bumke, K. Adrian, G., Smedman, A.-S. & Tammelin, B. Wind resources in the Baltic Sea. *European Union Wind Energy Conference and Exhibition* (1996).

Joffre, S. *The structure of the marine atmospheric boundary layer.*. Technical Report 29. 119pp. Finnish Meteorological Institute, Helsinki (1985).

Mortensen, N.G., Landberg, L., Troen, I., Petersen, E.L. Wind Atlas Analysis and Application Program Risø-I-666 (EN), Risø National Laboratory, Denmark. (1993)

Petersen, E.L. (1992) Wind resources of Europe (Offshore and coastal resources). EWEA Special Topics Conference '92.

Smedman, A.-S., Bergström, H. and Grisogono, B. (1996) Evolution of stable internal boundary layers over a cold sea. J.Geophys. Res. (in review).

Troen, I. and Petersen, E.L. (1989) European Wind Atlas. Risø National Laboratory, Denmark.

WIND RESSOURCES IN THE BALTIC SEA

Jørgen Højstrup, E.L.Petersen, L.Landberg, B.Barthelmie
Department of Meteorology and Wind Energy
Risø National Laboratory
DK4000 Roskilde, DENMARK

Karl Bumke, U.Karger, L.Hasse
Institut für Meereskunde, University of Kiel
Düsternbrooker Weg 20
D-24105 Kiel, Germany

Ann-Sofi Smedman, Hans Bergström
Department of Meteorology, Uppsala University
Box 516
S-75120 Uppsala, Sweden

Gerhard Adrian, F.Fiedler
Institut für Meteorologie und Klimaforschung
University of Karlsruhe
Kaiserstr. 12, D-76128 Karlsruhe, Germany

Bengt Tammelin
Climatology Division
Finnish Met. Institute
P.O.Box 503, 00101 Helsinki, Finland

ABSTRACT: The wind resource of the Baltic Sea has been investigated, using ship-based measurements and a model to establish the geostrophic wind climatology. Regional climatologies are then generated by meso-scale models, and finally local siting can be performed by the WASP-model. Four different ways of modelling the regional climate have been investigated, three mesoscale models and an empirical approach using near coastal ship-based observations.
Keywords: Coastal Sea Areas: Models (Mathematical): Meteorology: Off-Shore

1. INTRODUCTION

The increasing interests in offshore wind energy is caused by both the scarcity of good land sites, but also by the larger wind energy potential offshore. The available energy potential the EU coastal sea areas were investigated in an earlier JOULE project [1], and the aim of the present project was to extend the investigations to the Baltic Sea, and to provide climate statistics to be used with siting tools for future wind farms in that area, using the methods of the European Wind Atlas [2], supplemented by the use of meso scale numerical models for a good description of the regional climatology in the sometimes quite complex coastal areas.

Thus providing a set of tools for optimizing siting of turbines in coastal areas, where the distance from the coast and the water depth both should be as small as possible because undersea cabling and foundations are expensive, but in the interest of achieving as much energy as possible, it is desireable to be as far away from the coast as possible (away from the influence of the higher roughness of the land surface), where also the deeper water has some effect in diminishing the surface roughness of the water, further increasing the windspeeds.

Aspects of the work and methods used in this JOULEII project is also being reported in a number of other papers in this conference, [I,II,III,IV,V,VI].

2. COASTAL COMPLICATIONS

The knowledge of the wind climate far from the coast in deep water oceans is well established, we have a situation with winddriven waves, having had a long time to develop, and the surface roughness of the sea can be calculated by simplified equations such as the Charnock relation [3]:

$$z_0 = \frac{Au_*^2}{g} \qquad (1)$$

where A is the so-called 'Charnock'-constant. The roughness length is not a constant as it is over land, but it increases significantly with windspeed, but this is only a minor complication. Given the statistics of the geostrophic wind and atmospheric stability, it is now possible to predict the wind energy potential.

Near the coast at a distance where it would be practical to erect windturbines, things get a lot more complicated:

- Internal boundary layers, caused by roughness and thermal differences between land and water (fig.1).

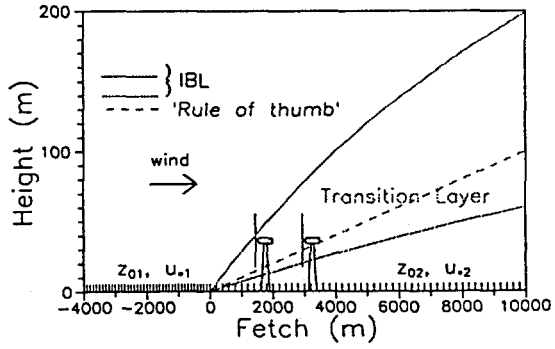

Figure 1 Land-to-sea roughness change for offshore wind. At near-coastal site the turbines are immersed in the transition layer.

For offshore winds the windturbine rotors can be above the shallow equilibrium layer developing offshore close to the sea surface, but still deeply immersed in the layer that has been disturbed by the new surface.

- The sea surface roughness increases, i.e. in eq. 1 ,A is no longer a constant (see fig.2). This phenomenon is still the subject of discussions in the oceanographic community.
- The wind climate will be influenced by secondary circulations (sea breezes), and large scale terrain features on land (cliffs, mountains).
- The Baltic Sea has quite cold water for most of the year, and consequently the atmospheric stability will be unusually stable, leading to difficulties when

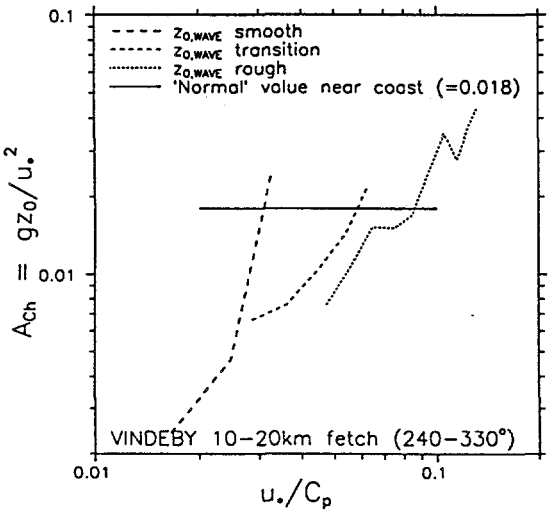

Figure 2 Measured values of the Charnock 'constant' from the RASEX experiment (Vindeby site). The parameter on the abscissa is the inverse wave age, i.e. for constant fetch, the windspeed increases from left to right. C_p is the phase speed of the dominating wave component.

trying to employ the 'normal' relations for determination of windspeed variations with height, including the phenomenon called 'low-level' jet, where the windprofile shows a maximum at a moderate height.

Since obviously, it will not be practical to make measurements for a long time every time we need a new site, some numerical tools that are capable of describing correctly this situation are needed.

3. METHOD

The method employed here can simplified be described in three steps:

- Compute geostrophic wind statistics by using ship observations combined with a numerical model.
- Geostrophic wind statistics is used to generate regional climatologies by combining a large number of runs from meso-scale models, i.e. runs for different winddirection sectors, windspeed intervals and stabilities.
- Use the regional climatologies as input to local-scale siting models giving the wind energy potential at the selected site.

4. GEOSTROPHIC WIND

The data used to derive the geostropic wind statistics consisted of observations from ships and synoptic stations taken four times daily from jan. 1992 to December 1993. About 10300 ship observations were taken. The distribution of their locations are shown in fig. 3.

The analysis followed a scheme developed at the Institut für Meereskunde in Kiel [4,5] using wind and pressure observations. Because of the influence of local orographic features on the flow field, only wind observations from distances larger than 100km from the coast were used. Pressure data were used also from coastal synoptic stations. In brief the method followed these steps in a 1°*1° grid:

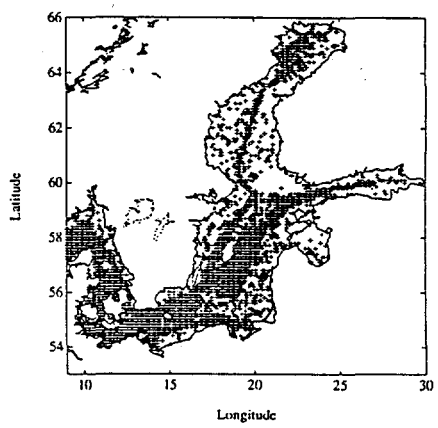

Figure 3 Distribution of wind observations by ships.

- The pressure field p^* was estimated in each measurement point.

$$p^* = a_{00} + a_{10}x + a_{20} + x^2 + a_{11}xy + a_{01}y + a_{02}y^2$$

Where x and y are the distances from the measurement to the grid point.

- The observed windspeeds and winddirections were converted to geostrophic components using a stability dependent approach [6], and were estimated

$$u_g^* = -\frac{a_{01} + 2a_{02}y + a_{11}x}{f\rho}$$

$$v_g^* = -\frac{a_{10} + 2a_{20}x + a_{11}y}{f\rho}$$

where f is the Coriolis parameter and ρ the air density.

- The parameters entering the two formulations above were then computed by minimizing a weighted sum

of the squared differences between estimated and measured values of pressure and geostrophic windspeed.

- The computed parameters now enables us to compute the geostrophic wind components in each gridpoint.

The surface windfields computed from the geostrophic data were finally validated against data from 1994 (8300 observations), see fig. 4 showing a comparison between the predicted wind distribution for all of the Baltic Sea area, compared with observations and compared with the model of the European Area Model of the German Weather Service. We can see that the Kiel model performs well, whereas the German Weather Service Model not does very well.

5. THE MODELS

We have been employing four different models to obtain the results for the regional windclimate:

- The KAMM-model of the University of Karlsruhe [7].
- The University of Uppsala mesoscala model.
- The HIRLAM (HIgh Resolution Limited Area Model) as employed by the Finnish Meteorological Institute.
- An empirical model by University of Kiel, built upon analysis of the near- coastal ship observations.

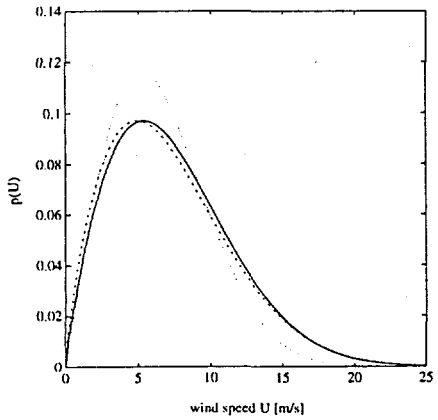

Figure 4 Comparison between Weibull functions fitted to observed (full line), analysed (dash-dot) and German Weatherservice European Model (dotted line).

For the siting model we will use WA^{S}P, taking as input the regional climate statistics from the mesoscale models, with possible non-standard values for some of its adjustable parameters.

The HIRLAM model showed quite discouraging results at an early stage, with quite poor performance for windspeed calculations, but the other three models provide better results. The University of Uppsala model has been plagued with a number of errors, discovered at a late stage, so we can here only show the results from the University of Kiel model (figs. 5,6 and 7) and the KAMM model (fig.8).

We have selected a test-area (around Gotland), where we will compare the performance of the available models, and the very good dataset that exists for this area.

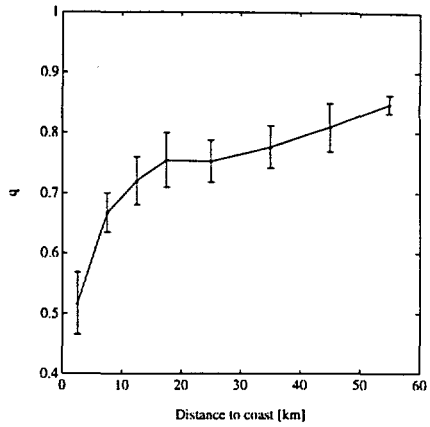

Figure 5 Coefficient q for ratio of analysed geostrophic and observed surface windspeeds for offshore wind directions.

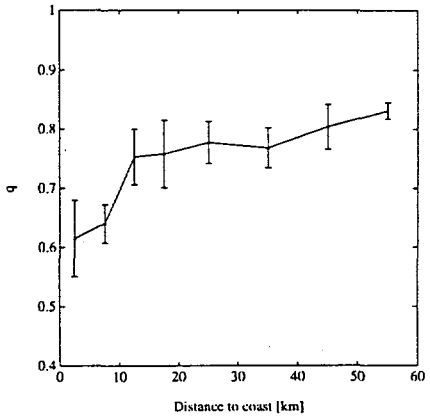

Figure 6 As figure 5, but for onshore wind.

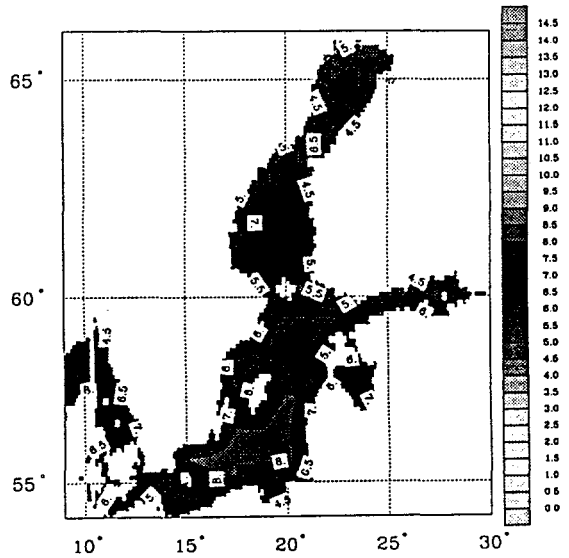

Figure 7 Surface wind speeds in 1993 (Kiel model)

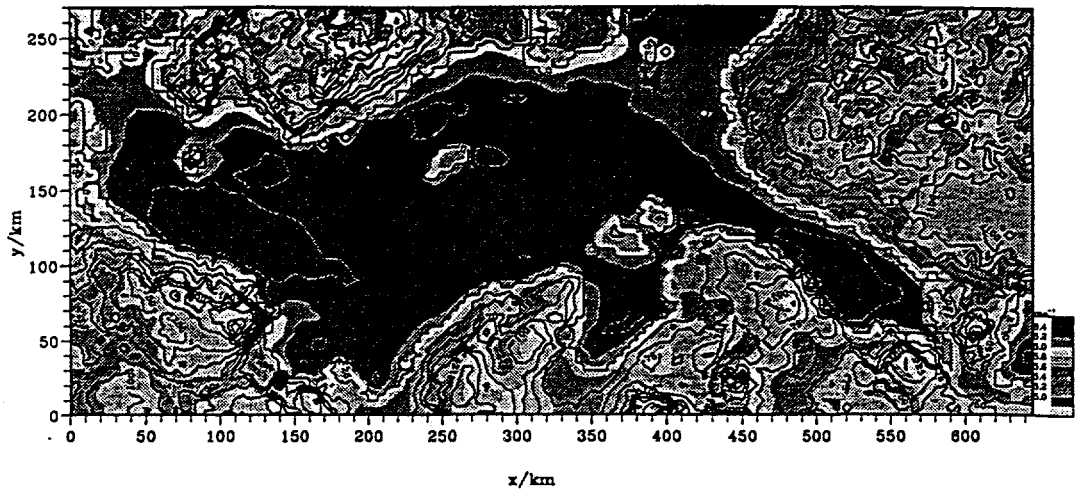

Figure 8 Mean velocity over the Baltic Sea in a height of 40m above the surface (KAMM-model). Note that the figure is tilted such that North is 45°.

6. THE MEASUREMENTS

We have available wind measurements from a number of coastal and offshore(small islands) sites around the Baltic Sea, and for this data we calculate stability information whereever available as well as windspeeds corrected for near surface features (WA^{S}P method) for comparison with the model results.

ACKNOWLEDGEMENT

This project has been supported by the EU (JOU2-CT93-0325), the Danish Research Council (STVF-16-5404-1) and Office of Naval Research (N00014-93-1-0360).

REFERENCES

[1] Matthies, H.G., A.D.Garrad, B.M.Adams, M.Scherweit, T.Siebers: Offshore Wind Energy Potential in the EC. Final report on JOULE I (JOUR 0072), 1993. Germanischer Lloyd and Garrad Hassan and Partners.

[2]Troen, I. and E.L.Petersen: European Wind Atlas, 1989. Published for the CEC, DG for Science Research and Development, Brussels, Belgium.

[3]Charnock, H., 1955: Wind stress on a water surface. Quart. J. Roy. Met. Soc., **81**, 639-640.

[4]Ennenga, U., 1985: Objektive Analyse aktueller Wind- und Druckfelder über dem Nordatlantik, Berichte aus dem Institut für Meereskunde Kiel, **142**, 103p.

[5]Bumke, K. And L.Hasse, 1989: An Analysis Scheme for Determination of true surface winds at sea from ship synoptic wind and pressure observations. Boundary Layer Meteorol., **47**, 295-308.

[6]Luthardt, H. and L.Hasse, 1981: On the relationship between surface and geostrophic wind in the region of the German Bight, Contributions to Atmospheric Physics, **54**, 222-237

[7] Adrian, G. And F.Fiedler, 1991: Simulation of unstationary wind and temperature fields over complex terrain and comparison with observations. Beitr. Phys. Atmosph., **64**, 27-48

[I] Sandström, S.: A climatological study of the wind resources in the Baltic area using a meso-scale model. Paper P13.6 this conference.

[II] Højstrup, J. and B.Tammelin: Wind ressources in complex coastal terrain. Paper p13.8 this conference

[III] Zilitinkevich, Z and D. Mironov: Wind profiles of a stable stratified atmospheric boundary layer: An engineering model. Paper P13.9 this conference.

[IV] Karger, U. and K.Bumke: Coastal influence on the surface wind at the Baltic Sea. Paper P13.14 this conference.

[V] Fiedler, F.: Wind climate estimation by mesoscale meteorological models. Paper OR13.1 this conference.

[VI] Barthelmie, B, N.G.Mortensen, L.Landberg and J.Højstrup: Application of the WASP model to determine the wind resource in non-neutral conditions in coastal areas. Paper P15.9 this conference.

Influence of thermally induced wind systems on the wind climate of the Baltic Sea analysed by numerical simulations

Gerhard Adrian, Nikolai Dotzek, Helmut Frank+
Institut für Meteorologie and Klimaforschung, Universität Karlsruhe, Forschungszentrum Karlsruhe, Kaiserstraße 12, D-76128 Karlsruhe, Germany,
+Risoe National Lab., DK-4800 Roskilde

ABSTRACT: Mesoscale Models have been used to estimate wind statistics with the aid of statistical dynamical regionalisation methods. One major problem of these approaches is the definition of a limited number of episodes to be simulated. A scheme is presented which includes the temperature difference between air and sea surface temperature in addition to the components of the geostrophic wind which are usually taken for choosing the episodes. The temperature field is of special interest in the area of the Baltic Sea because its influence on regional wind systems.
Keywords: Coastal Sites, Forecasting Methods, Meteorology, Navier-Stokes Equations

1. THE STATISTICAL DYNAMICAL APPROACH

For optimum siting of wind turbines spatial distributions of wind statistics with high resolution are required which are usually not available from routine observations. Nearly from the beginning of development of mesoscale models the application of synthetically generated climatology was proposed. One early example of generating wind statistics by using mesoscale models was shown by Wippermann and Groß [1], who restricted the method to wind roses. Adrian [2] applied Wippermann's and Groß's method to construct maps of mean geostrophic drag coefficients. This approach will be extended here.

The method is also called „statistical dynamical approach of regionalisation" of large scale climatology. It is applied to estimate the influence of large scale climate variations on local scales from output of global circulation models used in climate research and weather forecasting.

The method consists on several model assumptions which have to be taken in consideration for discussing the results later. The basic assumption is that the mesoscale state of the atmosphere depend uniquely on few parameters describing the state of the atmosphere in larger, synoptic scales. The synoptic scale flow systems are assumed to be modified by the earth's surface. This modification can be simulated for short episodes with mesoscale models. If regional scale processes are mainly determined by the orography the problem of regionalisation seems to be quite simple which can be proofed by several examples of successful application of the statistical dynamical approach as they can be found in the literature.

The approach consists of the following steps:

1. Definition of „typical episodes" from statistics of parameters classifying the large scale state of the atmosphere.
2. Simulation of the chosen episodes by considering the corresponding values of the large scale parameters.
3. The frequency of occurrence of the specific large scale state is added to the result of simulation.
4. Evaluation of the statistics of the model variables at every grid point by considering the frequencies of every simulated episodes.

In the case of domains like the Baltic Sea internal processes become more dominant. Temperature differences caused by the extreme differences of physical properties between land and sea surface lead to thermally induced circulation systems which have obviously to be considered in such an approach. Hence, an extension of this method is required in those cases as it is proposed in the following by including a stability parameter.

The temperature difference between land surface, sea surface and air vary with an large amplitude during the year caused by totally different time scales between land and sea surface. During winter time the Baltic sea is often partially covered by ice with low surface temperatures. In spring the water is still quite cold while the temperatures of the land surfaces increase. Because of the relatively small extension of the Baltic Sea advection of warm air lead to very stable stratification over the sea inducing small scale circulations. This baroclinicity on regional scales lead to additional phenomena like low level jets.

In autumn and early winter the sea surface is warm in comparison to land surfaces. The stratification is unstable and phenomena like land breezes occur. The occurrence and the intensity of these phenomena depend not only on temperature inhomogeneities but also strongly on the wind velocity which can by described by parameters of dynamical stability.

A scheme of estimating wind climatology has to consider these features of the climate including the seasonal variations.

2. DEFINITION OF EPISODES BY CLUSTER ANALYSIS

As discussed above the definition of „typical

episodes" to be simulated by the mesoscale model must consider wind velocity, wind direction and temperatures of sea surface, land surface and air. To reduce the number of parameters it is assumed here that the air temperature outside the boundary layer over sea is mainly influenced by advection from the surrounding land surfaces. Thereby the boundary layer over sea is expected to be quite thin because of the small roughness. From this assumption follows that the air temperature over the Baltic Sea is correlated with the land surface temperature. Then the only temperature parameter which has to be considered is the difference between air temperature and sea surface temperature ΔT. The absolute value of temperature is of minor importance.

The data required here are therefore the temperature difference ΔT and the components of geostrophic wind u_g and v_g. These values were analysed by Bumke and Hasse [3] from ship observations for two years and to times per day. From these data area averages were calculated. Then a hierarchical cluster analysis with 120 clusters was performed. The result of this cluster analysis is that each observation consisting of the triple (u_g, v_g, ΔT) is sorted into one of 120 clusters as it is shown in figure 1 for 20 clusters as an example.

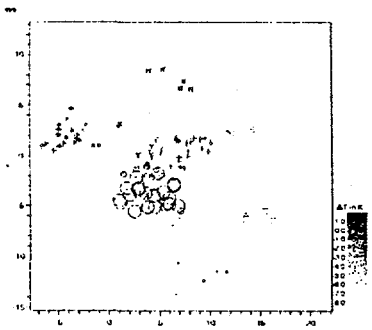

FIGURE 1: The result of the cluster analysis is shown for 20 clusters signed by different symbols. The grey scale displays the temperature difference between air and sea surface, the x-axis the west - east and the y - axis the south north component of the geostrophic wind.

From the members of each cluster the mean values of the geostrophic wind components and of the temperature difference was calculated. These mean values are taken as the definition of the episodes to be simulated by the mesoscale model. Figure 2 shows these mean values for all 120 clusters or episodes. They are taken as external parameters for the mesoscale model.

3. THE KARLSRUHE ATMOSPHERIC MESOSCALE MODEL KAMM

The model applied here is the Karlsruhe Atmospheric Mesoscale Model KAMM [4]. The model is

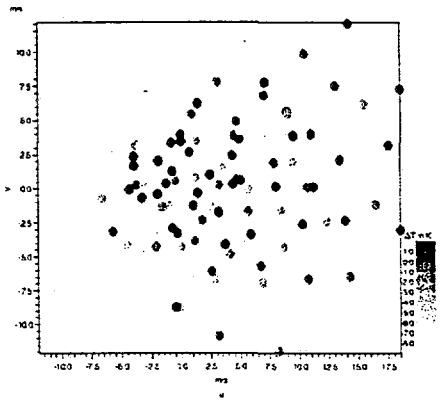

FIGURE 2: Mean values of the west - east (x-axis), of the south-north component (y-axis) of the geostrophic wind and of the temperature difference between air and sea surface (grey code) for all 120 clusters.

a nonhydrostatic model especially designed for the mesoscale γ. In the model the anelastic approximation for shallow convection [5] is applied. A conventional first order closure of the turbulent fluxes is implemented.

Special attention was given to the sea surface by including a parameterisation of the roughness of the sea surface. Although any mean flow or tidal effects have been neglected a drift velocity of the sea surface has been considered to be proportional to the friction velocity u* [6].

The more important parameter is the roughness length z_0 of the sea surface. Two main effects have to be considered, the short capillary waves caused by the surface tension and the long gravity waves. The latter waves become important at higher wind velocities and the corresponding roughness length is parameterised in KAMM by Charnock's formula [7]. The roughness of the sea surface increases with the square of the wind velocity.

At lower wind velocities (< 7 m/s in a height of 10 m above the sea surface) the short capillary waves lead to a different dependence of the roughness of the sea surface on the wind velocity. There the roughness increases with decreasing wind velocity. For this case Wu's model [7] is applied in KAMM. Both parameterisations are matched by taking the maximum roughness length resulting from both formulas.

3.1 The model domain

The model domain covers an area of 1300 km * 540 km between the Danish Islands on one side and the Gulf of Finland on the other side. The domain was turned to the north with an angle of 46,5° to cover most parts of the Baltic Sea at is can be seen in figure 3.

The horizontal grid size was chosen to be 10 km in both horizontal direction. In vertical direction 20 layers are chosen with small grid sizes of 15 m near the surface

and much larger grid sizes at the top of the model domain at 3 km height above sea level.

Because the wind field over the sea surface was of major interest here, only one constant value of 0.1 m for the roughness length over land surfaces was taken as a crude estimate. This was necessary because of lack of data on a unique base.

The surface temperatures were fixed to the values defined by the external parameters coming from the cluster analysis. Because the absolute value of the temperature does not have any influence on the solution of an anelastic filtered model like KAMM the temperature profile of the ICAO standard atmosphere was assumed in all cases. The temperature of land surfaces were fixed to the resulting air temperature and the sea surface temperature was defined then by the external parameter ΔT given by the results of the cluster analysis.

4. EVALUATION OF THE WIND ENERGY POTENTIAL FROM MODEL OUTPUT

For the evaluation of the wind energy potential one additional assumption is made that the simulation results can be described by the two parametric Weibull distribution function. From these two Weibull parameters the moments of the distribution, especially the third moment can be calculated which is proportional to the mean flux of kinetic energy or the wind energy potential. The variation of density of air is neglected here.

These Weibull parameters are determined here by a Maximum Likelihood estimation. From these estimates performed at every grid point of the model the spatial distribution of the energy flux was calculated. Figure 3 shows the result of the method for 50 m height above the ground. For this a vertical interpolation of the model output to the chosen height was necessary.

Most obvious is the difference between the energy fluxes over land and over sea caused by the large differences of the roughness length. At greater heights the picture changes because of different heights of the boundary layer. In heights of about 200 m above the surface orographic effects become more dominant. There the maximum values occur over the Swedish mountains.

In the height of 50 m coastal effects can be recognised in figure 3 like the maximum south of Bornholm or the maximum in the Gulf of Finland. The latter structure is an effect of channelling as it can be observed also in valleys of similar length scales like the upper Rhine valley between Vosgues mountains and the Black forest mountains.

The high values at the other coastal areas are the effect of thermal wind systems which are considered here. The minima over the islands are again caused by the larger roughness of the surfaces of the islands.

5. SUMMARY AND DISCUSSION

A method was proposed to estimate wind statistics from model simulations with mesoscale models including thermal effects like sea breezes. About 100

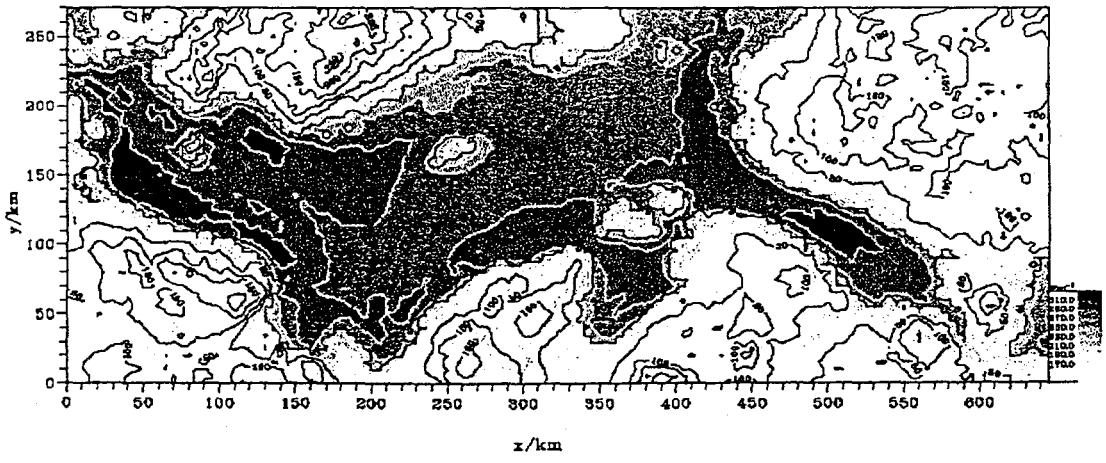

Figure 4: Spatial distribution of the wind energy potential in the area of the Baltic Sea in a height of 50 m above the surface calculated from model simulations

model simulations are required needing about 15 CPU hours on a vector computer (SNI-S600/20 at the Computer Centre of the University of Karlsruhe) all together. This method requires several basic model assumptions like the uniquely dependency of the model results on few external parameters, the definition and the number of episodes to be simulated or the assumption about the frequency distribution of wind velocity. The result at the end of the procedure depends on all these assumptions so that additional tests of the method are necessary. On the other hand the method allows to describe at least qualitatively wind statistics in regions where observations are not available so one gets at least the information where to look for areas of high wind energy potential if the absolute values resulting from the procedure have not the required accuracy.

ACKNOWLEDGEMENTS

This work is part of the project „Wind Resources in the Baltic Sea" funded by the EU, contract no. JOU2-CT93-0325, coordinated by J. Højstrup, Risoe Nat. Lab. Roskilde.

The data of geostrophic wind, sea surface and air temperature were provided by L. Hasse and K. Bumke, Institut für Meereskunde, University of Kiel.

REFERENCES

[1] F. Wippermann, G. Groß,Beitr. Phys. Atmopsh. 54 (1981) 492-501.

[2] G. Adrian, in: K. Grefen, J. Löbel (Ed.), Environmental Meteorology, Kluwer (1988) 387-411.

[3] K. Bumke, L.Hasse, Institut für Meereskunde, Universität Kiel, personal communication.

[4] G. Adrian, F. Fiedler, Beitr. Phys. Atmosph. 64 (1991) 27-48.

[5] J. A. Dutton, G. H. Fichtl, J. Atmosph. Sci. 26 (1969) 241-254

[6] J. Wu, J. Fluid Mech. 68(1975) 49-70.

[7] H. Charnock, Quart. J. Roy. Met. Soc. 81 (1951) 639.

A FEASIBILITY STUDY OF WIND ENERGY ON THE KOLA PENINSULA

E. Peltola, J. Wolff and Y. Rantanen
VTT Energy, P.O.Box 1606, FIN–02044 VTT, Finland

L. Landberg, E.L. Petersen
Risø National Laboratory
Denmark

P. Lundsager
Darup Associates Inc.
Denmark

G. Gerdes
Deutsches Windenergie-Institut
Germany

A. Fragoulis, P. Vionis
Centre for Renewable Energy Sources
Greece

P. Ahm
PA-Energy Ltd
Denmark

B. Tammelin, A. Peltomaa
Finnish Meteorological Institute
Finland

A. Tiilikainen
University of Lapland
Finland

V. Minin, G. Dmitriev
IEN, Kola Science Centre
Russia

S. Islander
SI-Credit Ltd
Finland

ABSTRACT: Within the European Union research programme Joule/Thermie "A Feasibility Study to Develop Local and Regional Use of Wind Energy on the Kola Peninsula, Murmansk Region, Russia (Kola Wind, JOR3–CT95–0036)" is performed. The study reaches its first milestone by June 1996 and outline and the first results are reported in this paper.
Keywords: Integration, Policies, Resources, Feasibility Studies

1. INTRODUCTION

1.1 Background

The Kola Peninsula is located in the most north-western part of Russia, bordering on Finland and Norway and facing the Barents Sea to the north and the White Sea to the south. Almost entirely above the Arctic Circle the climate is generally harsh and snow cover the ground for most of the year. The Gulf stream, however, keeps the Barents Sea coast ice-free throughout winter. Most of the peninsula is taiga or forest-tundra and inland there are several mountainous areas (the highest peak Chasnachos 1191 m a.s.l.). The region is an own administrative unit (Murmansk Oblast) within the Russian Federation.

The wind energy potential on the Kola Peninsula is, by research done at the Kola Science Centre, known to be extremely good, comparable to the best regions in Europe [1]. The technical, political and economical infrastructures are, however, not sufficiently developed to take the necessary steps towards utilising this resource. Therefore international co-operation is needed.

In order to achieve broader international co-operation to develop wind energy on the Kola Peninsula, the University of Lapland arranged the Kola Wind Workshop in Kemi on September 19–21, 1994. During the workshop, which was attended by experts from Denmark, Finland and Russia and sponsored by the Danish Energy Agency and the Finnish Ministry of Trade and Industry, guidelines for the development process were drawn. It was agreed to proceed on an European level within the European Commission R&D programmes of the Fourth Framework.

Subsequently a proposal to the Joule/Thermie programme was submitted in March 1995, which led to a contract being signed in December 1995.

1.2 Partnership

The work is carried out by a broad team of European research institutes and consultants. VTT Energy from Finland is acting as co-ordinator and other EU partners are Risø National Laboratory, Darup Associates and PA-Energy from Denmark, Deutsches Windenergie-Institut from Germany, Centre for Renewable Energy Sources from Greece and the Finnish Meteorological Institute and University of Lapland from Finland. These receive funding from JOULE3.

The Institute of Physical and Technological Problems of Energy in the North of the Kola Science Centre of the Russian Academy of Sciences (KSC-IEN), is the sole formal Russian partner in the project. However, they work in close co-operation with other Russian participants, such as federal, regional and local administrations, other authority bodies, the Kolenergo power company and private firms. KSC-IEN does not receive money from Joule3 and therefore a supplementary proposal has been submitted to EU's INCO-programme for international co-operation. The proposal is under evaluation for the time being.

2 PROJECT DESCRIPTION

2.1 General Outline

The overall objective of the project is to form a basis and to build the necessary tools for an substantial integration of wind energy into the energy supply system of the Kola Peninsula in the Murmansk Region of Russia. Efforts will be put on determining the wind resources, integration and policy issues.

The outline of the project follows what was agreed upon during the Kola Wind Workshop, where this activity was initiated. The aims were described in a Position Paper [2].

that has formed the basis for this project. It was commonly agreed, that the project should be carried out as a four step process, advancing from pre- and feasibility studies via demonstrations to large scale implementation.

The present project cover the two first phases of that context. This phase will, depending to the results, subsequently be followed by a demonstration phase, when the financial resources can be allocated.

Where this feasibility study is co-ordinated and largely carried out by partners within the European Union, the next phases, demonstration and implementation, have to be under Russian co-ordination and be carried out as a part of a general plan for regional development.

2.3 Work Programme

During the first phase preliminary studies on the possibilities for wind energy utilisation on the Kola Peninsula are made. The study focuses on some key-questions, that will be crucial for a successful outcome of the whole project. These questions consider the basic possibilities for wind energy projects, i.e. wind resource, applicability of current technology, general regional political interest. The first phase will also clarify the need of new information, such as e.g. wind measurements at specific sites, and thus one will be able to avoid double work in the second phase.

The information is evaluated and verified, as desk-top studies. Especially the reliability of the information for wind energy purposes is studied. This work thus determines the "starting point" for the following work.

The second phase consists of more clearly defined work packages, which are more detailed and produce models, tools and detailed studies that are necessary when planning large scale utilisation. The work packages contain the following topics:

- *meteorology*
- autonomous sites
- grid connection
- economic issues
- issues supporting regional development.

These detailed studies will as far as possible cover the whole topic of introducing wind energy in a new environment. When the feasibility study is completed most of the necessary preparing work needed for implementing wind energy should have been carried out.

2.4 Work Level Reached

The contract with EU started in January 1996 and the project is approaching the end of its first phase, scheduled to six months after start. In February a first fact finding mission to Murmansk, where the project group made acquaintance with the working environment and met the meteorological office, the administration and the energy supply system and operators of the Kola Peninsula, was held. Visits to sites close to Murmansk and suitable for wind parks and autonomous power stations were scheduled but were cancelled due to bad weather (i.e. snow storms).

During spring visits to the Kolenergo power company, the central office of Murmansk Area Department for Hydrometeorology and Environment Monitoring and the Russian Ministry of Fuel and Energy were made and continuous contacts have been held. Also a meeting with the participation from the Murmansk region administration was held.

Received information has been assessed mainly as desk-top studies. The following chapters briefly present the most significant results from the first phase so far. The final results from the project will be presented at the EWEC-conference in 1997.

3 METEOROLOGY AND WIND RESOURCES

The wind atlas method developed in the European Wind Atlas [3] has been chosen as the method by which the wind atlas for the Kola Peninsula will be made.

A limited number (5 and then another 5 later) of stations have been selected for attempting to give a first raw guess of the wind resource on the peninsula. A list is given in Table I and the location of the stations is given in Figure 1.

TABLE I. *The five selected sites for the first raw estimate of the wind resource. for each station a brief description of the surroundings is given. The mean winds are given at 30 m a.g.l. and taken from [1]. The location of each station is shown in Figure 1.*

Name	Surroundings	Mean Wind [m/s]
Krasnoscele	Village	3.9
Murmansk	Town	6.5
Nikel	Village	4.5
Pjalica	Village	6.0
Teriberka	Coast	9.3

All stations report to the WMO network. The surroundings of each station will be analysed to give a first rough guess of the local effects. The information about the stations is generally rather poor at the moment, with the exception of Murmansk. There are especially difficulties in finding maps good enough to make the necessary descriptions of the environment surroundings of the stations.

The very sparse data material makes it virtually impossible to give any qualified estimates of the wind atlases for the Kola Peninsula. Since it is essential for the other tasks in the project to have some sort of indication, we have come up with a first very coarse guess. This guess is based on three things:

1. The analysis by Minin et al. [1].
2. The analysis of geostrophic winds by Børresen [4].
3. A gut feeling of the distribution of the resource.

The analysis by Minin and Dmitriev seems to indicate a higher resource at the coast with a generally lower resource inland, except for some local extreme in the inland mountainous areas. The highest coastal resource is found at the north coasts (i.e. the Barents Sea coastline) with a smaller resource at the south coast (i.e. the White Sea coastline). The analysis by Børresen indicates that the geostrophic mean wind over the Kola Peninsula will decrease from west to east and also slightly from north to south. Our gut feeling tells us that the resource will decrease as we get further away from the coast and also that the resource at the White Sea coast is smaller then the one at the Barents Sea coast. All this leads to a first tentative map of the wind resource shown in Figure 1.

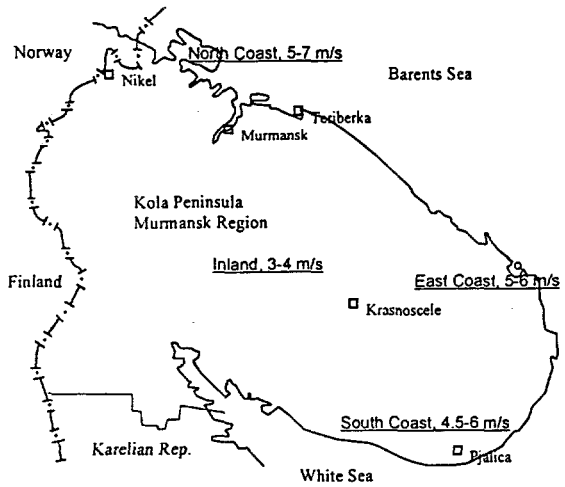

FIGURE 1. *A first tentative map of the wind resource of the Kola Peninsula. Wind atlas values indicated are underlined and refer to 30 m over a flat grass field. Note that actual mean wind speeds at a site might be significantly higher, i.e. up to 9–10 m/s on the north coast. The first met. stations to be analysed are marked with diamonds.*

A final version of the Wind Atlas for the Kola Peninsula is expected ready later this year (1996). It will contain an analysis of raw data from at least 10 meteorological stations. The lay-out will be like the one in the second volume of the European Wind Atlas (to appear in 1996).

In addition, some new measurements will be made, to complete available information especially regarding unconventional locations and complex terrain. The idea has been to use the Nordic Mobile Telephone (NMT) network for the data-transfer.

4. INTEGRATION OF WIND ENERGY

4.1 Power System on Kola Peninsula

The total energy consumption on the Kola Peninsula has during the 90's been 13–17 TWh/year and during 1995 consumption rose for the first time since 1989. The total generating capacity is 3.66 GW, of which 1.6 GW is hydro and 1,8 GW nuclear power. The mostly public owned power company AO Kolenergo handles all sales and distribution and all production, except for the nuclear power plant from which Kolenergo, however, buys the whole production.

68 % of power and 33 % of heat production is used by the industry and respectively 11 and 52 % by communal user.

4.2 Connecting Wind Energy to the Grid

Integration of wind energy is fairly easy on the part of the power system, due to the fair amount of hydro power. The 330 kV and 150 kV transmission lines cover most of the populated parts of the Kola Peninsula (Figure 2) and smaller windfarms (app. 5 MW) may be connected to the 35 kV or 6 kV-networks.

It has not been possible to get full access to detailed information on the electric grid but according to a preliminary study, it should be possible to connect at least 200 MW of wind energy close to the Zerebranskaja and Teriberka hydro power plants east of Murmansk (the area is shown in Figure 2).

Three possible locations have been suggested and taken into preliminary analysis. One site is within the city of Murmansk, one in Teriberka and one in Dalnie Zeletsnyi on the Barents Sea coast. The later are about 100 and 150 km east of Murmansk. All sites have their pros and cons regarding wind resources, terrain and access. Especially the requirements of good connection roads for installation and service may limit the use of some sites. Grid connection possibilities and wind resources seem to bee good enough on all sites but need to be checked. The site within Murmansk would be considered as a visual demonstration, although wind conditions should be reasonably good.

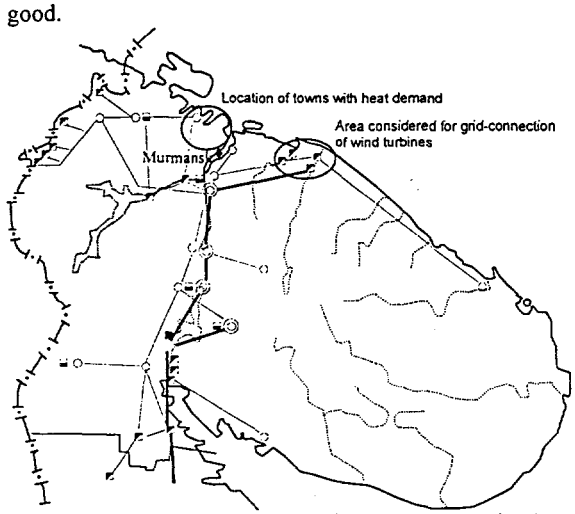

FIGURE 2. *The power grid over the Kola Peninsula. Settlements with autonomous supply are located all along the coast (light houses, met. and border stations) or on the south coast (fishing villages). Towns with a heat demand are north-west of Murmansk and good sites for large wind farms close to the hydro power stations east of Murmansk.*

4.3 Off-Grid Demand

Several settlements, fishing villages, meteorological, radio link, border stations and alike are located far from the electrical grid. Most of them are for the moment powered mainly by diesel generator sets and some small hydro power plants. However, as fuel is getting increasingly scarce wind energy could make a substantial contribution to the power supply in these communities.

Civil settlements are usually built-up around some enterprise or co-operative for fishing, timbering or reindeer farming.

However, all these communities differ from each other, regarding as well function and wind conditions as energy use, supply and load patterns. Thus one has to assess the possibilities for each location separately or in classes of similar characteristics. Table 2 gives a brief comparison of different not grid connected communities.

TABLE 2. *Comparison of different off-grid settlements.*

	Number	Current power supply P [kW]
met. stations	1	8
lighthouses	1	15–50 (base) 10–30 (communal)
frontier guards		50–180
fishing villages		30–360
inland settlements		60–1110

4.4 Wind Energy for Heating

The temporary deliveries and shortage of fuel make wind energy interesting for heating purposes, also in larger grid connected towns with district heating.

Such towns are e.g. are located on the north-western coast of the peninsula. There the grid also is said to be stronger than to the east of Murmansk.

5 POLICY FOR WIND ENERGY

5.1 Federal Policy Supporting Renewable Energy

There exists a concept for a transition towards extended use of regional energy sources within Russia and this development is strongly supported by the Russian Ministry of Fuel and Energy [5]. There will also be a federal programme for renewable energy in the North of Russia, where wind energy will have first priority.

Sources of financing are difficult to find in Russia, although there might be some interest from either federal or regional administration to take part in demonstration projects. An initial assumption, however, is that the first introduction of wind energy will have to be financed largely by foreign capital.

5.2 Energy Prizing

Prizes on power sales in Russia are determined by a prize council with members from the administration and power company. Prizes are set for three months periods after which they usually rise. All consumer groups have their own power tariffs with an energy and a power part. General prizes for electricity is about 3–3.3 US¢/kWh for industrial and ~1 US¢/kWh for domestic consumers (depending on whether they have gas or not). For remote settlements prices for fuel oil are fixed.

It is not yet known what prize an independent power producer could get for sales.

5.3 Regional Development

An important feature of this feasibility study is that it has a broad multi-disciplinary view and takes both social, technical and economical problems into account. It is especially important to involve local Russian enterprises, that can be in charge of a continuous implementation of wind energy in the region.

Wind energy might even stimulate enterprising in remote settlements and thus strengthen local economy and prevent urban drift. Thus the use of wind energy could stimulate the economic life of the whole region and have significant role in the socio-economic development except for the environmental benefit.

Private power plants might be possible and allowing private grid connection will be considered in the federal development programme for renewable energy. However, grid connected wind energy will mostly be operated from within the current energy system. For remote locations small autonomous systems (4–5 kW) could be operated by the owners, medium-sized (10–30 kW) by the local community and large systems (50–100 kW) by private companies (maybe with the participation of ministries).

Except for purely economic development it will be of vital importance to identify the focal points and support structures for introducing wind energy in the region. There will be a need for strengthening the capacity in carrying out both detailed feasibility studies and actual power plant installation. Thus both technical education and efficient information is needed.

6 CONCLUSIONS

The Joule3-project will advance from its pre-feasibility to a feasibility phase during 1996 and end in June 1997. After a first field study the possibilities for both grid integrated and autonomous wind energy installations are good. The main difficulty in developing wind energy on the Kola Peninsula will be financial and international financing institutes will have to be involved.

A reasonable size for wind energy demonstrations could be e.g. one or two wind parks of totalling about 5 MW and wind-based autonomous power stations with a total load of about 1 MW.

ACKNOWLEDGEMENTS

The authors are grateful for the hospitality, interest and help shown by Kolenergo power company, the central office of Murmansk Area Department for Hydrometeorology and Environment Monitoring and the Murmansk region administration. We would especially express our thanks to Dr Pavel Bezroukikh of the Russian Ministry of Fuel and Energy for his devotion and valuable support.

REFERENCES

[1] Minin V. A. et al. Perspectives of Industrial Use of Wind Energy on the Kola Peninsula. In: Stepanov I.R. Murmansk Region Energy Problems – Collected Volume of Scientific Works. Kola Science Centre. Apatity, Russia. 1992. pp. 60–73.

[2] Islander S. et al. Position Paper on Russian-Finnish-Danish Cooperation regarding Wind Energy on the Kola Peninsula. University of Lapland & PA-Energy A/S. November, 1994.

[3] Mortensen, N.G. et al. Wind Atlas Analysis and Application Program (WAsP), User's Guide. Risø National Laboratory, Roskilde, Denmark. 1993. 133 pp.

[4] Børresen, J.A. Wind Atlas for the North Sea and the Norwegian Sea. Norwegian University Press. The Norwegian Meteorological Institute. 1987. 184 pp.

[5] Concept for Development and Use of Small and Non-traditional Sources of Energy in the Energy Balance of Russia. Ministry of Fuel and Energy of the Russian Federation. July 20, 1993.

WIND ATLAS FOR THE GULF OF SUEZ, ARAB REPUBLIC OF EGYPT MEASUREMENTS AND MODELLING 1991–95

Niels G. Mortensen
Meteorology and Wind Energy Dept.
Risø National Laboratory
DK–4000 Roskilde, Denmark

Usama Said Said
Wind Energy Department
New & Renewable Energy Authority
11759 Cairo, Arab Republic of Egypt

ABSTRACT: The results of a comprehensive, 5-year wind resource assessment programme in the Gulf of Suez are presented. The primary purpose has been to establish reliable and accurate wind atlas data sets for this area. With mean wind speeds and energy densities of 9–12 ms^{-1} and 600–1350 Wm^{-2}, respectively, at a height of 25 m over roughness class 0 (water), the wind resources of the Gulf of Suez are comparable to those of the most favourable regions in NW-Europe. The wind atlas methodology has proven very useful in the extreme climatic conditions of the desert. Applied with care, it can provide accurate predictions of the wind climate at candidate sites for wind turbines along the Gulf of Suez.
Keywords: Wind Atlas, Gulf of Suez, Resources, Climatic Conditions.

1 INTRODUCTION

Deserts have a number of characteristics that make them almost ideal for wind energy applications: the pressure on the land is low, access is easy, and construction work relatively simple. Furthermore, the surface roughness tends to be low and uniform, so siting of wind turbines can be done primarily with optimization of the energy production – and minimization of cost – in mind. Desert regions could therefore provide space for large-scale utilization of wind energy, provided they are favoured by a healthy wind climate and situated not too far from places where power is in demand. Unfortunately, the meteorological network is very coarse and the wind climate is therefore not known in any detail at present. In addition, the general circulation and associated wind climates in these dry regions with high solar insolation and little or no vegetation, are quite different from those of eg the temperate regions – where most of the models and techniques for wind resource estimation and siting were developed and tested. Possible wind energy projects thus face a basic lack of knowledge of the wind resource as well as a larger-than-usual uncertainty in the siting process.

Even though the wind resources of the deserts in general are expected not to be extremely favourable for wind energy utilization [9], there exist large desert regions with a very promising wind potential. One such region is the Gulf of Suez and northern Red Sea – between the Eastern Desert and the Sinai peninsula in Egypt, see Fig. 1. The present study is based on measurements of wind speed and direction, taken from 1991 to 1995 at four meteorological stations along a 250-km stretch of the Gulf of Suez and the northern Red Sea. The 25-m masts were erected in 1991 specifically for the wind study, but also provide information on other climate statistics, some of which may be important for the design and implementation of future wind energy projects in this area.

2 PREVIOUS INVESTIGATIONS

It has long been recognized that the wind energy potential along the Gulf of Suez and the Red Sea is

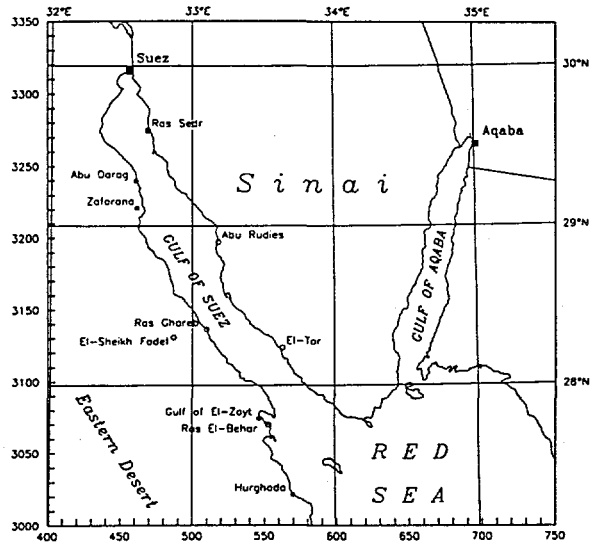

Figure 1: Overview map of the study area with the Gulf of Suez, the northern Red Sea, the Gulf of Aqaba, and the Sinai Peninsula. The four main wind atlas stations (•), as well as several auxiliary stations (○), are shown on both sides of the Gulf of Suez. Cartesian map coordinates are in kilometers, UTM zone 36.

markedly higher than in other parts of Egypt – and most other parts of the North African deserts as well. However, early estimates of the mean wind speed [3] – based on the existing network of meteorological stations in Egypt – range from only about 4 ms^{-1} in the northern part of the Gulf of Suez to about 6 ms^{-1} in the northern Red Sea – values which we today know are far too low.

In the 1970's and 1980's a number of wind resource assessment studies were carried out in Egypt, including the erection of several wind-monitoring stations. These activities were summarized a decade ago by Renne et al. [7] and Elliott et al. [2], who also published a map showing the distribution of seven wind power classes over Egypt. Renne and Elliott [7, 2] rean-

alyzed the existing wind data obtained at stations run by the Egyptian Meteorological Authority and then verified and detailed these resource estimates through additional wind measurements at key locations, in particular along the Gulf of Suez and the Mediterranean coast. They further used climatological data on winds aloft and maps of pressure patterns and air flow, as well as topographical maps, in estimating the wind resources of the data-sparse areas. Their resource estimates were calculated from measured distributions of mean wind speed or, in cases where only average wind speeds were available, by assuming that the wind speeds are distributed according to the Rayleigh distribution. The wind resource estimates were referred to 10 metres a.g.l. over "areas free of local obstructions to the wind and to terrain features that are well exposed to the wind, such as open plains, plateaus, and hilltops" [7].

The mean wind speeds in the Gulf of Suez were found to range from class 3 (5.1-5.6 ms^{-1}) in the northernmost part of the Gulf, to class 6 (6.4-7.0 ms^{-1}), covering the southernmost three quarters of the Gulf. At one station the data even indicated class 7 (7.0-9.4 ms^{-1}), but this was attributed to the location of the station on a well-exposed ridge [7] and may not be representative of the terrain of the region in general.

3 A NEW WIND RESOURCE ASSESSMENT PROGRAMME

The methods for wind resource assessment and siting developed rapidly during the 1980's, and with the publication of the European Wind Atlas [8], many of these techniques and models became widely available. The existing wind data for the Gulf of Suez were therefore reanalyzed in 1990 by the New and Renewable Energy Authority in Egypt and Risø National Laboratory – in the framework of the European Wind Atlas methodology. Based on the findings of this study it was decided to conduct a new wind resource assessment programme with the primary purpose of establishing reliable and accurate wind atlas data sets for the Gulf of Suez and northern Red Sea. Naturally, a secondary purpose was to evaluate the applicability of contemporary wind resource estimation and siting tools – in particular the European Wind Atlas methodology – to the extreme climatic conditions found in the desert.

At the time of writing five-years-worth of wind data have been collected at four meteorological masts along a 250-km stretch of the Gulf of Suez and the northern Red Sea, see Tab. I and Fig. 2.

Table I: Overall summary 1991-95 of wind observations 24.5 m a.g.l. at the four main stations: Weibull A- and k-parameters, mean wind speed ($\overline{U}$), mean energy density ($\overline{E}$), and direction (D_U) and magnitude ($|\overline{U}|$) of the mean wind vector. The occurrence of calms at all four stations is less than 0.1%.

Station	A [ms^{-1}]	k	$\overline{U}$ [ms^{-1}]	$\overline{E}$ [Wm^{-2}]	D_U [deg]	$\lvert\overline{U}\rvert$ [ms^{-1}]
Abu Darag	10.3	3.75	9.0	625	358	7.8
Zafarana	10.3	3.38	9.1	647	000	7.3
G. El-Zayt	11.9	3.67	10.4	965	327	9.7
Hurghada	7.8	2.38	6.9	330	338	5.2

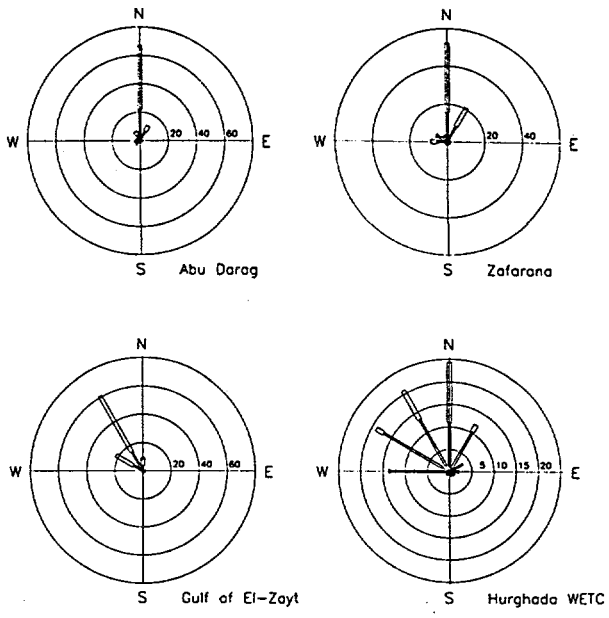

Figure 2: Wind roses for the four stations Abu Darag, Zafarana, Gulf of El-Zayt and Hurghada WETC. Wind direction is shown in twelve 30° sectors (in %) and the distribution of mean wind speeds, U, in each sector is given in four classes: $0 \leq U < 3$, $3 \leq U < 6$, $6 \leq U < 9$, $9 \leq U$ ms^{-1}.

3.1 Data analysis

The wind speed and direction data have further been analyzed using the Wind Atlas Analysis and Application Program (WASP) [5].

The accuracy of the wind speed measurements have been secured by careful calibration of the cup anemometers used; both before and after the period covered by the study.

The roughness of the terrain has been assessed from topographical maps and aerial photographs, as well as during site visits. In addition, the aerodynamic roughness length, z_0, of the desert surfaces have been estimated from wind profile analysis. This analysis shows that the sand surfaces are very smooth indeed – with a roughness length of the order of one mm or less – and also indicates that the roughness is not constant, but proportional to the square of the friction velocity, u_*. This characteristic of 'moving' surfaces like sand, snow and sea is well known [1]; however, for the present wind atlas analysis the roughness is kept constant.

The height variations of the terrain are described in digital terrain models, obtained by digitization of contemporary topographical maps. For the four stations listed in Tab. I, the orographic corrections were found to be negligible.

The analysis finally employs the results of previous investigations [7, 2], as well as satellite imagery obtained from NOAA-11 AVHRR data, in an effort to validate the magnitude and areal distribution of the wind resource.

A report, entitled "Wind Atlas for the Gulf of Suez. Measurements and modelling 1991–95", is in the final stages of preparation and is expected to be published in the summer of 1996. Some preliminary results of this new wind resource assessment programme are given below.

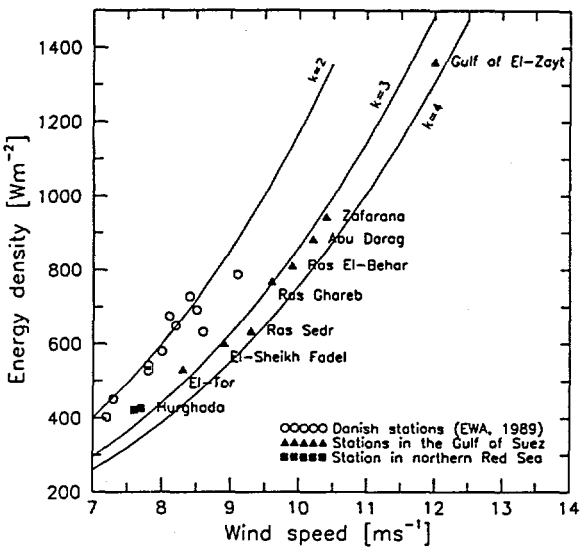

Figure 3: Mean wind speeds and energy densities at a height of 25 m over roughness class 0 (water) for nine stations along the Gulf of Suez and northern Red Sea. For Hurghada, 10-m data for the same period are also shown. The Danish stations of the European Wind Atlas [8] are shown for comparison.

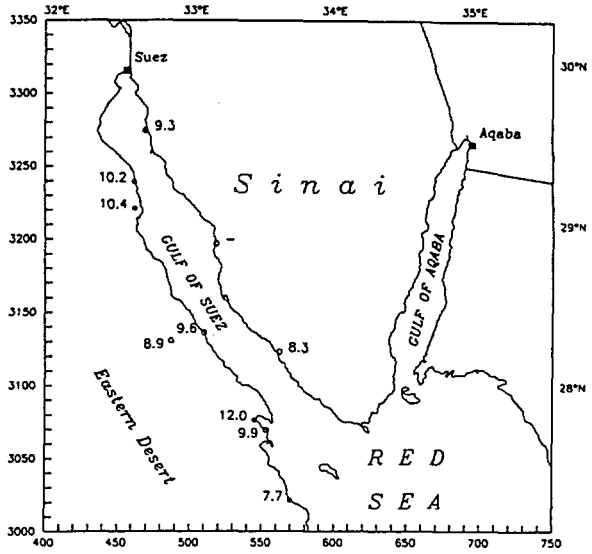

Figure 4: Mean wind speeds in ms^{-1} at a height of 25 m over roughness class 0 at the four main wind atlas stations (•) and five auxiliary stations (○).

4 WIND RESOURCES OF THE GULF OF SUEZ

As might be expected from our knowledge of the general circulation [3, 4], the winds in the Gulf of Suez are predominantly northerly, see Fig. 2 . At Zafarana, the wind blows from north more than half of the time; at Abu Darag this fraction even increases to almost two thirds. This strongly preferred direction, however, is not only due to the general pressure gradient from north to south, but is also caused by channeling of the wind flow between the mountain ranges that border the Gulf of Suez on both sides – reaching heights of 1000 m or more above sea level. The topography is further responsible for the generally high mean wind speeds measured at the three northernmost wind atlas stations. As the flow enters the Red Sea the terrain opens up, the wind looses momentum, and the mean wind speed immediately decreases by about 20 per cent.

Comparing the wind measurements at the four stations listed in Tab. I, it should be borne in mind that these may not be representative of a larger area since the measurements are influenced by the local topography found around the masts. The wind atlas analysis therefore allow us to estimate the wind climates corresponding to certain standard conditions. As an example, Fig. 3 shows corresponding values of mean wind speed and mean energy density for the four stations, as well as from five auxiliary stations, together with similar data for the Danish stations given in the European Wind Atlas [8]. With mean wind speeds and energy densities of 9–12 ms^{-1} and 600–1350 Wm^{-2}, respectively, at a height of 25 m over roughness class 0 (water), the wind resources in the Gulf of Suez are comparable to those of the most favourable regions in NW-Europe.

The geographical distribution of the wind resource is shown in Fig. 4.

5 APPLICATION OF THE WIND ATLAS

Most importantly, the wind atlas methodology makes it possible to predict the wind climate at any site (and height) around the stations, as long as the overall wind climate can be assumed to be basically the same as that of the station(s) used for the prediction [8]. In the case of the Gulf of Suez, this means that most of the near-coastal land areas along the Gulf are now covered by wind atlas data, whereas the predictions become increasingly uncertain with increasing distance to the coastline. In the mountains, and further away, we wouldn't expect the wind atlas and models to give accurate predictions, since the wind climate there most likely is completely different from that along the Gulf.

The wind atlas predictions provide estimates of the sector-wise distribution of the wind direction as well as the distribution of the wind speeds within each sector. Given the power curve of a specific wind turbine we are therefore able to estimate the actual energy production of this turbine at different sites. This is illustrated in Fig. 5, where the yearly energy production of a 450-kW wind turbine is shown as a function of distance to the coastline in the Gulf of Suez. The production is calculated along a 20-km long profile, from 10 km inland to 10 km offshore, using wind atlas data from Zafarana and the actual topography in the modelling. The profile is then roughly perpendicular to the coastline and to the prevailing wind direction. For comparison, calculations for a similar 20-km profile near Vindeby, Denmark, are also shown. The world's first offshore wind farm was constructed here in 1990-91 and the Vindeby profile is also roughly perpendicular to the local coastline and local prevailing wind direction.

The wind resource in the Gulf of Suez becomes even more impressive when seen through the rotor of a wind turbine (Fig. 5). Over sea, the production in the Gulf is estimated to be around 50 per cent higher

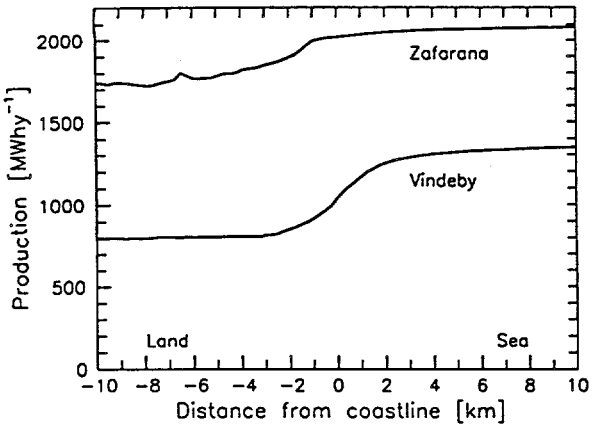

Figure 5: Estimated mean power production of a 450-kW wind turbine in the Gulf of Suez and in Denmark. The power productions are calculated at 250-m intervals along a 20-km profile perpendicular to the coastline. The profiles are situated close to Zafarana and Vindeby, respectively.

than for a similar offshore site in Denmark. Over land, the production in the Gulf decreases to about 80 per cent of the offshore value, whereas the energy production in the Danish example falls to about 60 per cent of the corresponding Danish offshore value. The inland potential in the Gulf of Suez near Zafarana is therefore twice as high as the inland potential close to Vindeby. The different ratios of inland-to-offshore potential are mainly due to the different surface roughnesses of the Egyptian desert and open Danish farmland, respectively; the desert being much smoother to the wind flow.

6 OTHER CLIMATE STATISTICS

In addition to a more reliable and accurate picture of the wind climate and wind resources along the Gulf of Suez, the wind resource assessment programme has also provided valuable information on other climate statistics, some of which may be important for the design and implementation of future wind energy projects in this area. The Wind Atlas for the Gulf of Suez [6] contains information on barometric pressure, air temperature, vertical air temperature gradient, land and sea surface temperatures, atmospheric stability, wind speed profiles, aerodynamic roughness lengths, observed and estimated extreme wind speeds, and gustiness of the wind.

7 CONCLUDING REMARKS

The wind resource assessment programme described above and published in [6] documents in detail the existence of a widespread and large wind resource along the Gulf of Suez – even larger than was hitherto assumed [3, 7, 2]. It further establishes the meteorological basis for utilization of wind energy in this region, and includes the information necessary for the siting of wind turbines and for the estimation of their annual energy production. To what extent this huge wind resource is going to be exploited in the future will of course depend on a number of other factors – related to eg technology, economics and infrastructure – which are beyond the scope of this brief paper.

From a wind-prospecting point of view it is worth noting that the existence of a very healthy wind climate in the Gulf of Suez is only partly resolved by the existing meteorological network; and with much less accuracy and detail than would be required for most wind resource assessment studies. This highlights the need for more detailed analyses – as well as additional wind measurements – in other parts of Egypt; and indeed in many other parts of the world.

The wind atlas methodology, originally developed for wind resource assessment and siting in Europe, has proven very useful in the extreme climatic conditions of the desert. Applied with care, it can provide accurate predictions of the wind climate at candidate sites for wind turbines along the Gulf of Suez; and the experience obtained can be used in other places with a similar climatology.

ACKNOWLEDGEMENTS

The Wind Resource Assessment Programme in the Gulf of Suez is funded by the Danish Ministry of Foreign Affairs through Danida, and by the Egyptian Ministry for Electricity and Energy through the New and Renewable Energy Authority, NREA.

REFERENCES

[1] Chamberlain, A.C. (1983). Roughness length of sea, sand, and snow. *Boundary-Layer Meteorol.* **25**, 405–409.

[2] Elliott, D.L., D.S. Renne and K. Bassyouni (1987). Wind energy resource assessment of Egypt. Proceedings of the Sixth ASME Wind Energy Symposium, Dallas, Texas, 1987, vol. 3, 215–216.

[3] Griffiths, J.F. and H. Soliman (1972). The Northern Desert (Sahara). In: *World Survey of Climatology Volume 10* (The climates of Africa, ed. J.F. Griffiths), 75–132. Elsevier, Amsterdam.

[4] Lockwood, J.G. (1974). *World climatology – an environmental approach.* Edward Arnold, London. 330 p.

[5] Mortensen, N.G., L. Landberg, I. Troen and E.L. Petersen (1993b). Wind Atlas Analysis and Application Program (WASP). Vol. 1: Getting Started, Vol. 2: User's Guide. Risø–I–666(EN). Risø National Laboratory, Roskilde. 133 p.

[6] Mortensen, N.G. and Usama Said Said (1996). *Wind Atlas for the Gulf of Suez. Measurements and modelling 1991-95.* ISBN 87–550–2143–3. Risø National Laboratory, Roskilde, and New and Renewable Energy Authority, Cairo. In press.

[7] Renne, D.S., D.L. Elliot, B.D. Holst and K. El-Bassyouni (1986). Wind energy resource assessment activities in Egypt. European Wind Energy Association Conference and Exhibition, Rome, October 7-9, 299-304.

[8] Troen, I. and E.L. Petersen (1989). *European Wind Atlas.* Risø National Laboratory, Roskilde. 656 p. ISBN 87–550–1482–8.

[9] World Meteorological Organization (1981). Meteorological aspects of the utilization of wind as an energy source. WMO Technical Note 175, World Meteorological Organization, Geneva, Switzerland.

MODELING THE WIND CLIMATE OVER IRELAND

Helmut P. Frank and Lars Landberg
Risø National Laboratory
Meteorology and Wind Energy Department
Roskilde, Denmark

ABSTRACT: The wind climate of Ireland has been calculated using the Karlsruhe Atmospheric Mesoscale Model KAMM. The climatology is represented by 65 frequency classes of geostrophic wind. The results are compared with data from the European Wind Atlas which has been analysed using the Wind Atlas Analysis and Application Program WAsP. The method is presented and the results are discussed.
Keywords: Resources, Wind Field Simulation, KAMM, WAsP.

1 INTRODUCTION

The best method to determine the wind energy potential of some place is to measure the wind on site for several years. However, as this takes a lot of time, one would like to calculate the wind power with atmospheric models. Although this is not as exact as direct measurements it is expected that favorable and unfavorable regions can be distinguished using numerical simulations.

However, the surface wind is a quantity which is specific for each site. The roughness and shape of the terrain, shelters from nearby tree lines or buildings effect most measurements and make it difficult to transfer wind observations to another site.

The Wind Atlas Analysis and Application Program WAsP [5, 7] tries to remove these local influences to obtain corrected data representative for flow over a plane of uniform roughness which can be compared with measurments at other sites. Also, it allows to estimate the wind at a different site by taking into account the local effects at the new site. It can be applied for variations on scales up to 10's of kilometers. However, it can not represent effects on the meso-scale, as the channeling effect of the wind by wide valleys, or thermally induced circulations like sea-breezes, or mountain-valley systems.

These meso-scale and thermal phenomena are calculated using a full atmospheric model, the Karlsruhe Atmospheric Mesoscale Model KAMM [2, 1]. If the large-scale climatological forcing is specified correctly, it can be used to calculate the wind power of a region of several thousand square kilometers. However, this model can not account for local influences on scales below the grid size.

Therefore, a new concept where both models, WAsP and KAMM, are combined has been developed. The paper presents the method to calculate the regional wind climatology for the island of Ireland, as well as a comparison with processed observations from the Irish Wind Atlas.

2 THE DATA

2.1 Wind Atlas data

Data from the old Irish Wind Atlas ([7], p. 40) and from a reanalysis for the new Irish Wind Atlas [4] covering most of the Republic of Ireland have been used. They are from 15 synoptic stations of the Irish Meteorological Service. These measurements have been taken every hour.

Data from most stations in the old Irish Wind Atlas covered 10 years, mostly from 1970-79. For the five newly included stations data from 20 years have been used to make the estimate as climatologically stable as possible. However, at the beginning of the 1980's the mean wind was somewhat higher at most stations. The surroundings of the station might have changed during a period of 20 years, resulting in corrections not optimal for the entire period. Studying the climatological fingerprints of the stations, no trends are found, however, indicating e.g. that the area around the site is getting more and more build up.

The anemometers used are the Dines pressure tubes which consists of a tube with a wind vane attached. The readings are plotted on a drum mounted with a paper chart and at each observation time the observer reads the chart averaging over the last 10 min and reports the reading. The instruments are calibrated yearly by the Irish Meteorological Service. In case of instrument failure the observers have estimated the wind speed and direction, meaning that virtually all observations for all of the period are present.

In some of the expected high wind areas of Ireland three masts have been operated by the University College Dublin and the Electricity Supply Board for three years (1992-94). They are typically equipped with wind speed and direction sensors at 10 and/or 30 meters. The masts collect 10 min averages every hour.

2.2 Geostrophic Wind Climatology

It is assumed that the large-scale geostrophic wind is the primary forcing for surface winds above a certain minimum speed. Therefore, the large-scale climatology is specified only by the frequency distribution of the geostrophic wind. Diurnally varying winds which are thermally forced are neglected.

Two data sets were available. One consisted of two years (1982/83) of geostrophic winds over Ireland from the analysis of the ECMWF given as u_g- and v_g-components . The other data set was the frequency distribution of 10 years of observed winds at 850 hPa at Valentia Observatory in SW Ireland.

Initially a cluster analysis of the geostrophic winds was made and 60 clusters with frequencies between 0.1% and 5.2% were obtained which should represent the frequency distribution. However, the mean and

mean cube of geostrophic wind speed calculated from the clusters were much less than the mean speed and cube of the original data; one reason being that the cluster analysis was done for components u_g, v_g and not for speed and direction. It is not surprising that the simulated mean surface wind and wind power potential were much less than the observed ones.

Another compact representation of the frequency distribution had to be calculated. We used the observed wind at 850 hPa at Valentia because the 10 years from 1970–79 is the same period as most of the data analysed for the old Irish Wind Atlas [7].

To conserve the moments of the original frequency distribution equidistant direction sectors and non-equidistant speed classes are used. The angular resolution is 30° as in the Irish Wind Atlas. The frequency distribution of the wind in one sector is divided into several speed classes of *equal* frequency. This gives higher resolution were the probability density function is greater. The representative wind speed of a class is the third root of the third moment in that class since we want to calculate wind power. A sector is divided into 5 speed classes if its frequency is below 10%. Otherwise it is divided in 6 classes.

The original distribution of winds at 850 hPa at Valentia was given in equidistant speed classes of 1 knot and direction sectors of 45°. It was randomized and resampled in intervals of 0.5 m/s and 30°. Then, the non-equidistant speed classes were calculated. The analysis yielded 65 new frequency classes. The sectors with a westerly wind component, from 210° to 330° have 6, and the other sectors only 5 speed classes. The frequencies of the classes range from 0.75% to 2.54%. The values are shown in Figure 1 together with the 60 cluster centers from the analysis of two years of geostrophic winds over Ireland. The original data sets are different. But, the frequency distributions should be similar as we assume that both represent the same climatology of geostrophic wind. The clusters are concentrated between 5 to 9 m/s. Weak winds and easterly winds are poorly represented. The clusters include cases with higher speed than the 65 classes. However, most of these have only very low frequencies. E.g. the highest westerly wind with 23.36 m/s has a frequency of 2.54% asigned to it. The three cluster values near it have a *combined* frequency of only 0.7%.

Moments of the 65 classes and the cluster representation are listed in Table I. The mean speed of the clusters is over 2 m/s less than the mean speed of the 850 hPa winds at Valentia Observatory, and also over 2 m/s less than the mean speed of the two years of geostrophic winds. The agreement between the 65 classes and the original distribution is very good. The third moment is the same. The mean speed is only 2% too high. Hence, the geostrophic wind climate seems to be well represented by the classes. In contrast, the third moment of the clusters captures only 57% of the mean cubed wind speed at 850 hPa at Valentia.

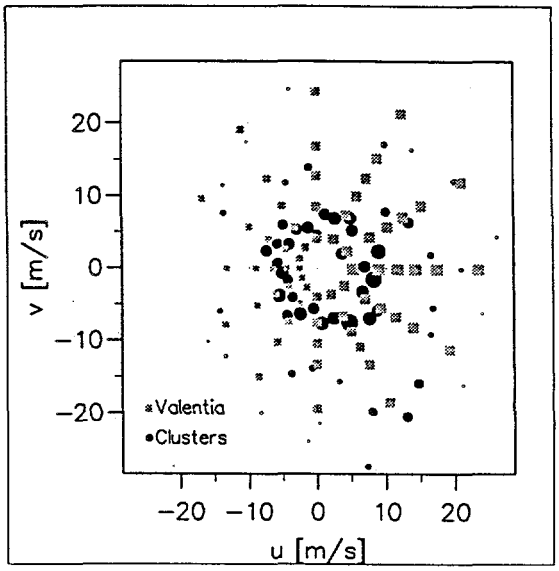

Figure 1: Representative values for the geostrophic wind distribution. The distribution of winds at 850 hPa at Valentia Observatory from 1970-79 is indicated by 65 grey squares. Dots show the 60 cluster centers of 2 years of geostrophic winds over Ireland. The size of the symbols is proportional to the frequency.

Table I: Moments of the original frequency distribution of 850 hPa winds at Valentia Observatory, the 65 non-equidistant classes, and the 60 cluster values. The difference from the distribution at Valentia is given in %. s is wind speed in m/s.

	Val. dist.	65 cla	diff.	60 clu	diff.
$\overline{u}$	4.89	4.76	−2.7	2.46	
$\overline{v}$	1.02	1.00	−2.0	−1.14	
$\overline{s}$	11.79	12.03	2.0	9.50	−19.4
$\overline{s^2}$	179.1	182.2	1.8	115.8	−35.1
$\overline{s^3}$	3196	3199	0.1	1812	−43.3
dir. (°)	258.2	258.1		294.9	36.7

3 THE MODEL

3.1 The Karlsruhe Atmospheric Mesoscale Model – KAMM

KAMM [2, 1] is a three-dimensional, non-hydrostatic atmospheric mesoscale model which assumes non-divergent wind fields to filter sound waves. Subgrid scale fluxes are parameterized using stability dependent turbulent diffusivities. It employs centered differences on an terrain-following coordinate system with variable resolution in the vertical direction. The atmospheric model can be coupled to a soil-vegetation model [6].

The model is initialized with a hydrostatic and geostrophic basic state. This large-scale pressure gradient and the daily cycle of radiation represent the external forcing of the model.

In the simulations for Ireland the model domain consisted of 50 × 60 points in the horizontal with a resolution of 10 km. It covered the whole island plus several grid points over water in each direction. In the vertical direction 30 levels were used from the surface to 5000 m height with the first 2 levels above the surface approximately at 21 m and 53 m. The stratification was stable with a vertical gradient of the potential temperature of 3.5 K/km, and 10°C surface temperature at sea level. KAMM was run without a soil model, i.e. the soil temperature was kept constant at its inital value equal to the inital air temperature. Hence, the soil temperature decreases with height as specified by

the large-scale lapse rate.

The orography was generated from a 1:625,000 scale map (Ordnance Survey, 1972) with height contours with a 300 ft (91 m) resolution. See Landberg and Watson [4] for further details. The roughness has been generated using data from the CORINE land-use database, where each land-use category has been assigned a roughness value and the roughness at each grid point is derived by logarithmically averaging the neighboring roughnesses.

For the 65 cases 6 h real time were simulated. Wind speed, surface stress and surface heat flux were averaged from 3 h to 6 h representing stationary, adapted conditions. The wind climate was constructed from the different simulations by calculating the weighted mean of the simulated wind at each grid point. The weights are the frequencies assigned to the geostrophic wind classes.

3.2 Comparison with Wind Atlas Data

The results are compared with wind data from the Irish Wind Atlas [7, 4]. We think a comparison of simulations to processed observations is better than to real observations because local effects on scales of less than a few kilometers cannot be simulated for such a big area. WASP [5] tries to remove these local effects.

Therefore, the simulations are processed in a similar way as the data. The geostrophic drag law is used to transform the simulated friction velocity u_*, temperature scale θ_*, and local roughness length z_0 to a logarithmic wind profile in a neutrally stratified atmosphere over a given standard roughness z_{0r}. A logarithmic wind profile is used to calculate the transformed wind speed at a specified height.

The simulations are performed for a constant geostrophic wind. However, the strength of the mean geostrophic wind increases approximately by 1 m/s per 400 km from SE- to NW-Ireland. The simulated mean wind and wind power potential are corrected for this variation by an approximate method assuming that deviations from the simulated wind power are proportional to deviations of the cube of the mean geostrophic wind from the mean at Valentia Observatory. For a mean geostrophic speed of 12 m/s changes of the wind power are less than 32 Wm^{-2}, or less than approximately 13%.

The mean wind and wind power from the processed simulations are compared to the wind atlas data at stations on Ireland. The grid values are interpolated to the position of the observations. The values of the four nearest grid points are weighted by $\exp(-r/(0.25\Delta x))$, where r is the distance from the observation station to a grid point and Δx is the grid size of the simulation. Only grid points over land are included in the interpolation because the transformation of wind speed over water to wind speed over a standard land roughness can not correct for the big roughness change at a shore. This would mean that, probably, the Wind Atlas values for the stations near a coast are not correct. Perhaps they could be improved by changing some of the parameters of WASP (Barthelmie et al. [3]).

4 RESULTS

A map of the simulated and processed wind power at 50 m height and roughness length $z_0 = 3$ cm is shown in Figure 2. At each grid point of the model the mean power is shown by a small square. For comparison the values taken from the Irish Wind Atlas [7, 4] are written at the position of the station. The terrain height is indicated by isolines at 100 m intervals.

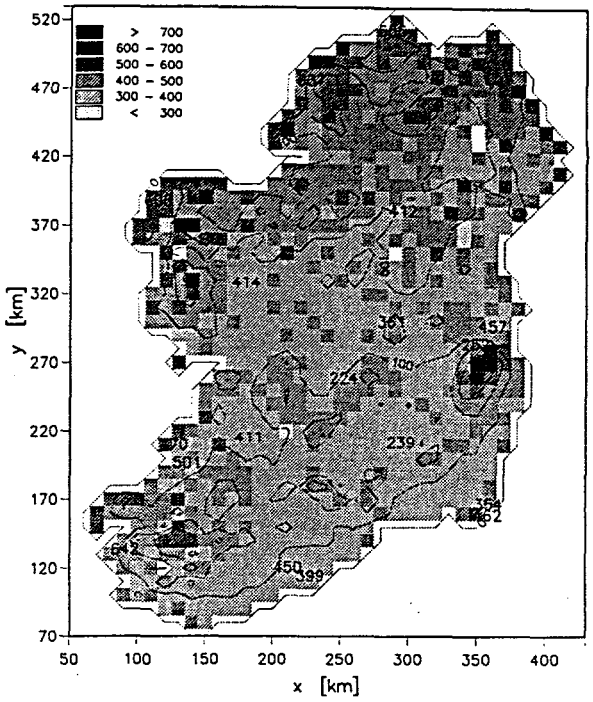

Figure 2: Wind power in Wm^{-2} at a height of 50 m and roughness length $z_0 = 3$ cm over Ireland calculated by KAMM. The values from the old Irish Wind Atlas are written at the position of the stations. A distribution with 65 geostrophic winds was used as input for KAMM. The simulation results have be processed as described in the text.

In Figure 3 the data from the Irish Wind Atlas is compared with the KAMM results interpolated to the position of the stations. The station name and a symbol are plotted at the interpolated value. Data from the old Irish Wind Atlas are indicated by squares, and from the new Irish Wind Atlas by crosses. The range of wind power at the four nearest grid points is show by error bars. This can also be interpreted as a range of uncertainty of a value.

It is noted that the range of values for the KAMM data at these stations is much less than for the Wind Atlas data. However, the range of the KAMM data at all grid points over land goes from 271 Wm^{-2} to 792 Wm^{-2}. I.e. only the stations with low wind power in the wind atlas are outside the range of the numerical simulations.

The strongest disagreement exists comparing the stations Dublin Airport (Dub) and Casement Aerodrome (Cas). They lie only 12.4 km apart. Still, the expected wind power taken from the wind atlas is 457 Wm^{-2} at Dublin and 252 Wm^{-2} at Casement, a difference of 205 Wm^{-2}. The simulations predict 365 Wm^{-2} at Dublin and 545 Wm^{-2} at Casement, a difference of -180 Wm^{-2}. The range of the four neighboring grid points indicates that this is an area with large variations of the wind power potential. We think that a grid size of 10 km still is to large to resolve this

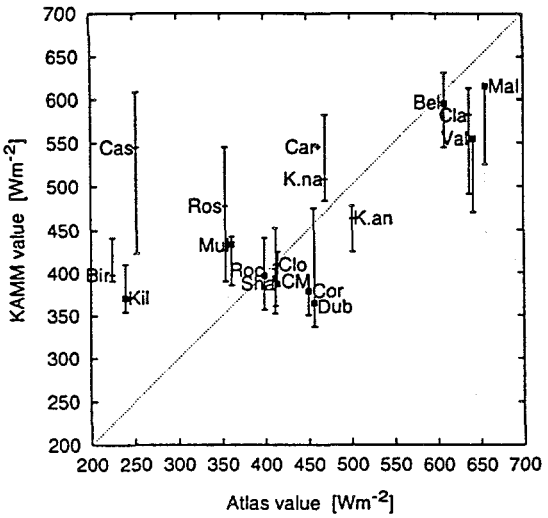

Figure 3: Wind power in Wm^{-2} at $z = 50$ m, $z_0 = 3$ cm at 18 stations in Ireland calculated by KAMM compared to values taken from the old Irish Wind Atlas (■) and from the new Wind Atlas (+). Shown is the range of the 4 grid points nearest to the stations, and the interpolated value with an abbreviation of the name.

appropriately. The overlap with the resolved scales of WAsP is too small. On the 10 km grid Casement lies already on the slope of the Wicklow Mountains to the south whereas in reality it is at the base of the mountains where the flow might be partly blocked. Also it seems that the gradient expected from the Wind Atlas data is too great because the value for Dublin is even higher in the new Irish Wind Atlas.

At Malin Head (Mal) the correct value to choose clearly is the one with the highest value because it represents the most northerly grid point. The station lies on this peninsula directly at the coast. On the gridded map it lies between this grid point and the grid points to the south because of errors in the maps and the averaging to 10 km resolution. Similarly, the representative grid point for Valentia (Val) is on the peninsula west of the station and not just the interpolated value. The calculated wind power at this point is 555 Wm^{-2} which is higher than at any of the four grid points nearest to the station. In the mountainous southwest of Ireland a resolution of 10 km is too big. A smaller grid size would be needed to achieve a better overlap with the scales resolved by WAsP.

At Roches Point (Roc) simulation and wind atlas value agree perfectly. However, the terrain at this station is very complex which requires strong corrections to the measurements in the wind atlas analysis. The new Irish Wind Atlas indicates a much greater wind power potential at this site.

It is not clear why low wind power values are not calculated. The fact that the neighboring grid points to Birr (Bir) and Kilkenny (Kil) are very close together, indicates that the wind atlas values of these two stations might be too low.

5 OUTLOOK

The comparison of the simulation results with the Wind Atlas data is only fair. Several improvements can be made in the future.

Probably, the severest simplification of the simulations is the neglect of different stratification and of thermally forced circulations. This requires many more individual simulations. As pointed out previously (section 2.2), the forcing of the model must be chosen carefully to yield a good representation of the large scale climatology. The model results are very sensitive to this input data.

A smaller grid size with only a few kilometers resolution is expected to yield better agreement with the Wind Atlas data. Then the overlap with the local scales resolved by WAsP is greater.

Additionally, it might be possible to improve the interpolation of the grid point values to a specific site if some information on the terrain is included. Similarly, an interpolation method near the coast should be developed.

Finally, the Wind Atlas data may change if different parameters are chosen in WAsP [3].

REFERENCES

[1] G. Adrian. Zur Dynamik des Windfeldes über orographisch gegliedertem Gelände. Ber. Deutscher Wetterdienst, 188, 1994.

[2] G. Adrian and F. Fiedler. Simulation of unstationary wind and temperature fields over complex terrain and comparison with observations. *Beitr. Phys. Atmosph.*, 64:27–48, 1991.

[3] R. J. Barthelmie, N. G. Mortensen, L. Landberg, and J. Højstrup. Application of the WAsP model to determine the wind resource in non-neutral conditions in coastal areas. In *Proc. EUWEC'96, Göteborg 1996*, 1996.

[4] L. Landberg and R. Watson. The new Irish Wind Resource Atlas. In *Proc. from the European Wind Energy Association Conference and Exhibition, Thessaloniki, Greece*, volume I, pages 233–237. 1994.

[5] N. G. Mortensen, L. Landberg, I. Troen, and E. L. Petersen. *Wind Atlas Analysis and Application Program (WAsP) Vol. 2: User's Guide.* Risø National Laboratory, Roskilde, Jan 1993.

[6] G. Schädler, N. Kalthoff, and F. Fiedler. Validation of a model for heat, mass and momentum exchange over vegetated surfaces using LOTREX-10E/HIBE88 data. *Beitr. Phys. Atmosph.*, 63:85–100, 1990.

[7] I. Troen and E. L. Petersen. *European Wind Atlas.* Risø National Laboratory, Roskilde, 656 p. ISBN 87-550-1482-8, 1989.

ACKNOWLEDGEMENTS

We thank the Irish Meteorological Service for the wind data at the synoptic stations, and the EU for the funding through the JOULE program.

IMPLEMENTING PREDICTION OF POWER FROM WIND FARMS AT UTILITIES

Lars Landberg
Risø National Laboratory
Meteorology and Wind Energy Department
DK-4000 Roskilde, Denmark

ABSTRACT: This paper will describe a project that has as its main task to implement prediction of the power produced by wind farms in the daily planning at a utility. The predictions are generated from forecasts from HIRLAM (HIgh Resolution Limited Area Model) of the Danish Meteorological Institute. These predictions are then made valid at individual sites (wind farms) by applying a matrix generated by the submodels of WAsP (Wind Atlas Application and Analysis Program). In the project 17 wind farms have been selected for study. The farms are located on the Zealand (14) and Bornholm (3) islands and are all controlled by the Danish utility ELKRAFT.
Keywords: Short-term prediction, wind farm power output, HIRLAM, WAsP, MOS

1 INTRODUCTION

To fully benefit from large amounts of wind energy in an electrical grid, it is necessary to know the part of the electricity production generated by the wind. The time frame is up to two days in advance. This will enable the utility to control the conventionally fueled plants in such a way that fossil fuels will in fact be saved. With the abilities of present day numerical weather prediction (NWP) models it is now possible to accomplish the aforementioned task; this has been shown in a now finished CEC-funded JOULE-project [4]. The concept of using NWP model output has also been used in [1]. The economic value of using forecasts has been assessed in [11, 7].

This paper will describe a model based on predictions from HIRLAM run by the Danish Meteorological Institute (DMI) [6]. The WAsP model of Risø National Laboratory [8] has been used to take local phenomena into account. Local phenomena are eg the sheltering of wind breaks, the effect of different roughnesses and the changes in these and the speed-up/down by the orography.

The model which has been implemented at the Danish Meteorological Institute provides forecasts to the utility ELKRAFT and includes 17 wind farms with a total capacity of 35.7 MW, see Figure 1 and Table I. These 17 farms are then linked to the rest of the installed wind power (totalling approximately 100 MW) by a factor varying from hour to hour. The factor depends on the actual number of turbines producing electricity to the grid. The project has three partners: ELKRAFT, The Danish Meteorological Institute, and Risø National Laboratory. It is funded by the Danish Ministry of Energy under the EFP-programme.

2 THE METHOD

The method for predicting the output of a wind farm is outlined in Figure 2. The idea is to use physical models as 'far' as possible, this is done such that the large-scale flow is modeled by a NWP model, here HIRLAM; as we zoom in on the site more and more detail is required, this detail is provided by the WAsP program. To take the shadowing effects of turbines in a wind farm into account the PARK program is used.

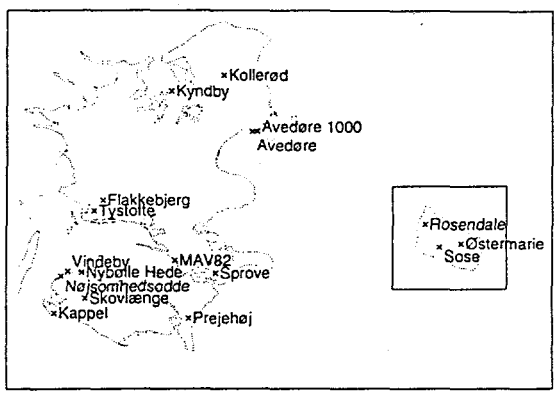

Figure 1: The 17 selected wind farms in the ELKRAFT/Sjællandske Kraftværker area. The farms have a total capacity of 35.7 MW.

Table I: The selected wind farms and their configuration.

Name	ID	Turbines
Avedøre	avd	12 × 300 kW
Avedøre 1000	avv	1 × 1000 kW
Flakkebjerg	fla	1 × 225 kW
Kappel	kap	24 × 400 kW
Kollerød	kol	1 × 500 kW
Kyndby	kvp	21 × 180 kW
MAV82	mav	1 × 750 kW
Nybølle Hede	nyb	2 × 500 kW
Nøjsomhedsodde	noj	23 × 225 kW
Prejehøj	pre	1 × 500 kW
Rosendale	ros	3 × 225 kW
Skovlænge	skv	2 × 150 kW
Sose	sos	2 × 225 kW
Sprove	spr	2 × 150 kW
Tystofte	tys	3 × 450 kW
Vindeby	vin	11 × 450 kW
Østermarie	oem	7 × 225 kW

Finally, to take any effects not modeled by the physical model and general errors of the method into account a model output statistics (MOS) module is used. In the

following each step of the method will be described in more detail.

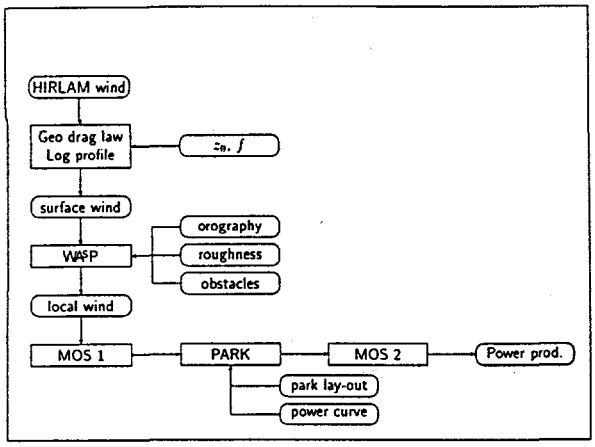

Figure 2: Flow chart.

2.1 HIRLAM

HIRLAM (HIgh Resolution Limited Area Model) has been developed by the Scandinavian meteorological institutes in a cooperation with the Dutch and Irish Met. Services. The HIRLAM version used in this study is the one run operationally by DMI (GRV). The model is run twice a day at 00 UTC and 12 UTC. The forecasts are available about 4 hours after the model has been initialised. The primitive equations form the basis of the model and the model has a number of parameterisations of various physical processes. The model runs in a grid 162 × 136 with 16 horizontal levels and the look-ahead time is 36 hours.

2.2 Surface transformation

The predicted wind from HIRLAM, which is a wind specific to a gridcell of 26 × 26 km^2, is transformed to the surface using the geostrophic drag law

$$G = \frac{u_*}{\kappa}\sqrt{\left[\ln\left(\frac{u_*}{f z_0}\right) - A\right]^2 + B^2} \qquad (1)$$

where G is the geostrophic wind, u_* the friction velocity, κ the Von Kármán constant (=0.4), f the Coriolis parameter, and z_0 the aerodynamic roughness length. A and B are constants set equal to 1.8 and 4.5, respectively, in accordance with [10].

To get a velocity in the surface boundary layer the logarithmic wind profile

$$u(z) = \frac{u_*}{\kappa}\ln\left(\frac{z}{z_0}\right) \qquad (2)$$

is used. Here $u(z)$ is the velocity at height z. Both these equations are in their neutral form. For further details see [5].

2.3 WAsP

The wind calculated so far ($u(z)$ in Eq 2) is still valid for quite a big area and it must now be corrected to take local effects into account. This is done using WAsP (Wind Atlas Analysis and Application Program). WAsP takes the following local effects into account:

- Shelter from obstacles (houses, wind breaks etc).
- Effects of roughness and of changes in roughness.
- Effects of the orography, speed-up/down.

Note, that this list does not include thermally-driven effects as eg sea-breezes and katabatic winds. In most of Northern Europe (including Denmark) these latter effects will not be of any importance, and can thus be left out without loosing any accuracy. If a closer study of the error reveals a yearly variation, the roughness will be made dependent on the season.

After the WAsP-corrections have been applied, we have a prediction of the *local wind*. From the previous study [3, 4] an estimate of the RMSE of the predicted *wind speed* is around 1.5 m/s for a typical station in Northern Europe. The study also showed that implementing simple MOS improved the predictions, and – as a consequence – MOS will also be used in this study.

2.4 MOS 1

Up till this point the method has been based strictly on physical models. These models simulate all the effects that can be described by and implemented in simple models. It is clear, however, that much detail and many physical processes have been left out. To remedy this situation MOS (Model Output Statistics) (cf [2]) is used. MOS will be applied in two places: as a simple scaling of the local wind and as an offset of the production of each wind farm.

It is assumed that the real wind speed (of which we – unfortunately – have no reliable measurement), $\hat{u}$, is connected to the predicted wind speed by the following simple relation:

$$\hat{u} = a(\theta_i)u_{\text{pred}} \qquad (3)$$

where $a(\theta_i)$ is the factor for the i'th sector and u_{pred} is the predicted wind speed.

Folding this back through the power curve, we get:

$$P_{\text{obs}} \simeq P_{\text{pred}} = p(a(\theta_i)u_{\text{pred}})TE \qquad (4)$$

where, P_{obs} and P_{pred} are the observed and predicted power, respectively, of a given wind farm, $p(u)$ is the power a given turbine will produce at speed u, T is the number of turbines operating, and E the efficiency of the wind farm. It is then possible to find the a which for a certain sector gives the smallest value of the absolute error.

After the wind has been corrected, the production of each of the turbines is calculated using their power curve.

2.5 PARK

To take into account the influence of one turbine being in the wake of another, with a reduction of its production as a result, the PARK program [9] has been used. This program creates a park efficiency rose, ie a sectorwise list of the reduction of the output of the turbine caused by wakes from the other turbines in the farm. The PARK program assumes a linear growth of the wake and a -2 decay of the wake with the distance from the turbine.

2.6 MOS 2

To correct for any *bias* another simple MOS model has been chosen to correct the *final* output of the model,

ie the actual production of the park. A simple linear version of MOS is used here

$$P_{\mathrm{MOS}} = P_{model} + b \qquad (5)$$

where P_{MOS} is the MOS-corrected production of a given wind farm (ie the result of the model), P_{model} the production predicted by the physical model, and b the bias. Note that b is not dependent on the sector, since it is assumed that the MOS 1 module took care of any directional variance.

When the model complex depicted in Figure 2 has been applied to the HIRLAM forecast we have calculated the production of the wind farm. To obtain the *total* production this is done for all the selected wind farms.

3 INPUT TO THE MODEL

To be able to predict the power output of a wind farm the following input is needed:

- HIRLAM wind field (Geo. drag law)
- description of orography (WAsP)
- description of roughness (WAsP)
- description of obstacles (WAsP)
- power curve (PARK)
- thrust curve (PARK)
- wind farm lay-out (PARK)
- measurements of actual power production (MOS)

Note that this information, except for the HIRLAM forecast, is needed only for the initial analysis of the wind farm; once the farm is analysed the prediction model uses only the results of the analysis. For an example of the analysis of a wind farm, see [3].

4 OUTPUT FROM THE MODEL

For ease of electronic transfer, the model output is sent as plain ASCII text files. The files contain the 12 forecasts (from +3 to +36 hours ahead) for the total production and for each wind farm. It is imagined that the utility then have a program which displays the forecasts in a user-friendly form. An example of this is given in Figure 3.

5 RESULTS

The model has now run for an entire year and it is possible to draw some firm conclusions as to its performance. Two aspects will be focused on: the ability of the model to predict the power output of a single wind farm and the ability of the model to predict the total wind-farm-produced power.

To get an estimate of the skill of the model the predictions are compared to those of the *persistence* model, which is a very simple model stating that

$$P(t+\ell) = P(t) \qquad (6)$$

where $P(t)$ is the production at time t and ℓ is the look-ahead time. This model could popularly be called the 'what-you-see-is-what-you-get' (WYSIWYG) model!

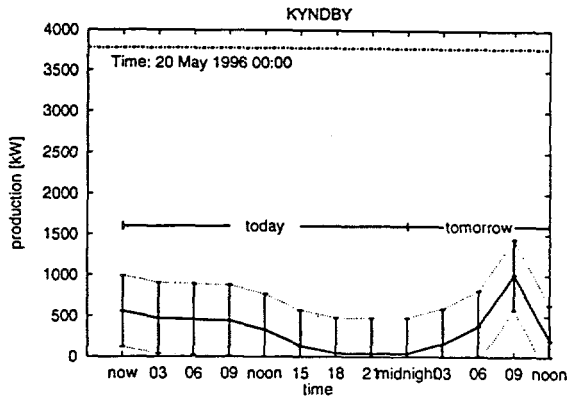

Figure 3: Example of the forecasts as seen at the dispatchers desk. The figure shows: the total rated power (dot-dash line at the top), the prediction (solid line), and the expected error (dotted line on both sides of the prediction). The plot is originally in colour.

A comparison between the predictions for the Kyndby wind farm of the two models is shown in Figure 4. It can be seen from this that in the first four hours the persistence model performs better than the developed model, after that the model is superior. It can also be seen that – as was the case with the model predicting the wind only, cf [5] – that the standard deviation of the error seems to be rising only very slowly.

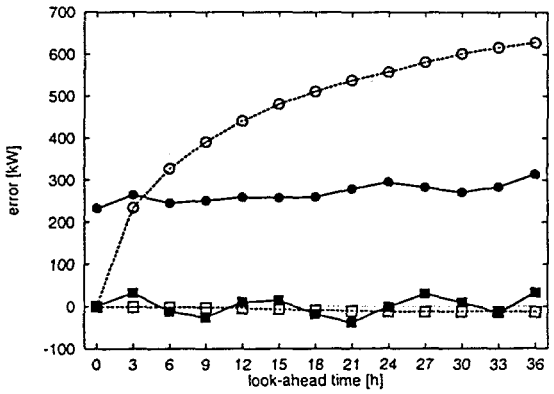

Figure 4: Plot showing the performance of the model described here, compared to the persistence model for the Kyndby wind farm. The rated power of the wind farm is 3780 kW. Filled symbols and solid lines refer to the method and open symbols and dashed lines to persistence. Round symbols are the absolute mean of the error (in kW) and square symbols are the mean error (also in kW). The forecast length (in hours) is along the x-axis.

The qualitative results found for the other wind farms are much like the ones found for Kyndby. There does not seem to be any explanation why some stations perform better and some worse, other than natural variations.

Turning now to the prediction of the *total* power, a subset of the 17 wind farms have been chosen. The

reason for not including all the wind farms is that the number of observations for some of the farms is quite low, due to technical problems with the data acquisition system. The subset consists of 11 wind farms, totalling 24930 kW, (9 on Zealand and 2 on Bornholm) which all have an around 70% data recovery rate.

Comparing the result of the model to that of the persistence model the *skill score*, $1 - \mathrm{MAE}_{\mathrm{model}}/\mathrm{MAE}_{\mathrm{persist}}$, of the prediction of the total together with that of the individual farms are shown in Figure 5. It can be seen from the figure that the skill of the model predicting the total is slightly smaller than that of the well predicted stations, but also that it is not reduced significantly by the not-so-well performing wind farms.

A thorough discussion of the possible error sources is found in [3].

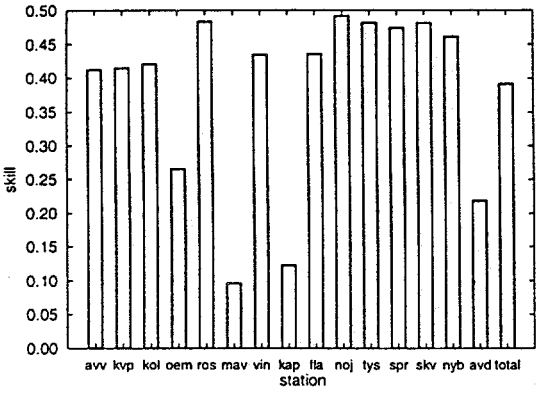

Figure 5: Comparison between the skill of the +12 hour predictions for each of the wind farms and the total.

6 CONTINUATION OF THE PROJECT

The EFP-funded project has now come to an end and the model is in a final stage of development. To try to implement the model on a larger scale a JOULE III project has been initialised where the forecasting model is to be used for predicting the power output from a number of wind farms. These wind farms are located in Denmark (ELSAM and ELKRAFT), Greece (PTT), UK (RES) and USA (Texas). The major partners of the project are: Danish Meteorological Institute (Denmark), Electrical Power Research Institute (USA), ELKRAFT (Denmark), ELSAM (Denmark), Danish Technical University, IMM (Denmark), National Observatory of Athens (Greece), Rutherford Appleton Laboratory (UK) and Risø National Laboratory (Denmark) acting as the coordinator. The project will run over the next 3 years and the expected outcome is an improved prediction model and experience from running the model operationally.

7 SUMMARY

This paper has described a model that predicts the wind power produced energy up to 36 hours ahead for 17 wind farms located on the Danish islands Zealand and Bornholm. The model is based on forecasts from the Danish Meteorological Institute's HIRLAM model. These forecasts are made valid locally by using the WAsP program. The power curve is used to calculate the production and reductions because of wakes from other turbines are calculated using PARK. The model has run for a year generating forecasts to the Danish utility ELKRAFT on a daily basis with good results.

REFERENCES

[1] Barbour, PL and SN Walker, 1995: *Development of wind and energy forecasting for Pacific Northwest utilities.* Paper presented at Windpower 1995, Washington DC.

[2] Glahn, HR and DA Lowry, 1972: *The Use of Model Output Statistics (MOS) in Objective Weather Forecasting.* J. Appl. Met, **11**, 1203–1211.

[3] Landberg, L, 1994: *Implementing Wind Forecasting at a Utility.* In Proceedings from EWEA 94, Thessaloniki, vol I, 357–360.

[4] Landberg, L, SJ Watson, J Halliday, JU Jørgensen, and A Hilden, 1993: *Short-term prediction of local wind conditions.* Report to the Commission of the European Communities, JOULE programme.

[5] Landberg, L and SJ Watson, 1994: *Short-term prediction of local wind conditions.* Boundary-Layer Meteorol., **70**, 171–195.

[6] Machenhauer, B (ed), 1988: *HIRLAM final report.* HIRLAM Technical Report 5, Danish Meteorological Institute, Copenhagen, Denmark.

[7] Milligan MR, AH Miller and F Chapman, 1995: *Estimating the economic value of wind forecasting to utilities.* Paper presented at Windpower 1995, Washington DC.

[8] Mortensen, NG, L Landberg, I Troen and EL Petersen, 1993: *Wind Atlas Analysis and Application Program (WAsP), User's Guide.* Risø-I-666-(EN)(v.2), Risø National Laboratory, Roskilde, Denmark. 133 pp.

[9] Sanderhoff, P, 1993: *PARK - User's Guide. A PC-program for calculation of wind turbine park performance.* Risø-I-668(EN), Risø National Laboratory, Roskilde, Denmark. 8 pp.

[10] Troen, I and EL Petersen, 1989: *The European Wind Atlas.* Published for the CEC by Risø National Laboratory, Roskilde, Denmark. 656 pp.

[11] Watson, SJ, L Landberg, JA Halliday, 1994: *Application of wind speed forecasting to the integration of wind energy into a large scale power system.* IEE Proc.-Gener. Transm. Distrib., **141**, 357–362.

ACKNOWLEDGEMENTS

The project has been funded by the EFP-programme under the Danish Ministry of Energy and the Environment, contract number 1363/94-0005. The JOULE III project is funded by the Commission of the European Communities, contract JOR3-CT95-0008.

A POWER QUALITY FRAMEWORK FOR WIND POWER APPLICATIONS

Per Nørgaard
Risø National Laboratory
P.O.Box 49
DK-4000 Roskilde, Denmark

Per Lundsager
Darup Associates
P.O.Box 30
DK-4000 Roskilde, Denmark

ABSTRACT: The term "power quality" is not well-defined, but covers in principle all aspects of deviations from the ideal power supply. The term "power quality measures" as used in this paper covers the definition and quantification of the power quality property, the requirements to data, the data processing procedures, presentation of the results, methods to compare results from different cases, and proposals for how to specify appropriate criteria.

The present framework was initiated in the Joule project "Power quality of the wind turbine generating systems and their interaction with the grid" (JOU2-CT93-0323). The framework presents the voltage level, the frequency level and the frequency rate of change in terms of their statistical distributions, the wind turbines impact on the voltage flicker by the wind turbines flicker coefficient, the variations of the voltage harmonics components in terms of the standard deviations.

Keywords: Power quality, integration, test methods, standards.

1. INTRODUCTION

Wind turbines (and other equipment) connected to the (public) grid will affect the quality of the power in the grid. Contrary, the wind turbines proper operation will depend on the quality of the power supply.

Several projects have investigated the power quality problems, all with different presentation of the results. Typically, the presentations clearly indicates problems, but without providing the possibility to quantify and compare the problems and the results.

International standards defines different voltage characteristics and specifies requirements to these.

However, it has been useful to supplement the existing standards with dedicated statistical power quality measures related to wind power applications. In general the standards does not specify how to present the data and how to compare results from different measurements.

Prerequisites for more flexible requirements leading to more optimal solutions are the presence of adequate power quality measures to describe and quantify the problems. In specific for the remote power supply systems, the simple maximum deviation criteria are not adequate.

The objectives of the power quality measures presented in the paper are to form a uniform power quality framework for the quantification and presentation of power quality properties related to wind power applications in order to be able to compare results obtained from different installations and to make it possible to specify appropriate criteria.

Nature	Time scale			
Transients		-	100	ms
Fluctuations	0.1	-	10	sec
Variations	0.1	-	10	min

Table 1: The power quality problems classified by their time scales.

2. POWER QUALITY

The term "power quality" is not well-defined, but covers in principle all aspects of deviations from the ideal (3-phase) power supply characterized by three steady and symmetric sinusoidal voltages with constant amplitude and frequency. When discussing power quality it is important to distinguish between

- the description and quantification (the measures),
- the causes to the power quality problems,
- the consequences of a certain power quality level,
- the solution to the problems, and
- the requirements to the power quality.

This paper deals with the selected power quality measures only.

2.1 Time scale classification

It might be useful to classify the power quality problems by their time scales, reflecting the varying causes, problems and solutions. The disturbance may be divided into transient phenomena's, fluctuations of the instant values and variations of the steady state values as indicated in Table 1.

Parameters characterizing transient phenomena are the rise time, the amplitude, the energy, the duration, the frequency spectrum and the repetition rate (IEC Pub 816).

The dynamic properties can be expressed by the standard deviation of a series of data x_i defined by

$$X_{std} = \sqrt{\frac{1}{N}\sum_i (x_i - \overline{X})^2}$$

where $\overline{X}$ is the mean value and N is the number of data points.

The steady state values can be expressed by their RMS values for specified integration time period T:

$$X_{rms} = \sqrt{\frac{1}{T}\int_T (x(t))^2\, dt}$$

Wind turbine characteristics	Power quality properties	Grid characteristics
Power factor	Frequency variations	Inertia
Power fluctuations	Voltage fluctuations	Impedance
Current flicker	Voltage flicker	Topology
Current harmonics	Voltage harmonics	Control
Current asymmetry	Voltage unbalance	

Table 2: Parameters characterizing the wind turbine, the grid and the power quality relevant for the interaction between the wind turbine and the grid

3. POWER SYSTEM CHARACTERISTICS

The power system in question includes

i) the wind turbine(s),
ii) the grid connection and
iii) the power distribution system.

The power quality quantities must correlate to a given testing point in the power system - normally the Point of Common Coupling (PCC, ref IEC 555-1). In general, the power quality will depend on the wind turbine characteristics, the grid characteristics and the "background noise". The wind turbine(s) and the grid should be characterized by the parameters indicated in Table 2.

The power systems may be divided into classes by their stiffness and their size reflecting different typical types of significant power quality problems - see Table 3. In the central part of a large power system both the voltage and the frequency will be relative stiff, while at the end of a feeder the voltage will be more slack. In a small and isolated power system the frequency will be slack as well.

Even though the power quality problems will differ for the different power systems, the same power quality measures can be applied for them all. The power quality criteria, however, must reflect the different requirements.

The grid is simply characterized by its impedance Z and the no-load voltage U_0.

4. POWER QUALITY MEASURES

The term "power quality measures" as used in this paper covers

- the definition and quantification of the power quality property,
- the requirements to data,
- the data processing procedures,
- presentation of the results,
- methods to compare results from different cases,
- proposals for how to specify appropriate criteria.

Where possible, the measures are based on existing standards and definitions, but the measures does *not* include specific criteria or requirements to be met.

The present framework includes the following power quality measures:

- voltage level variations, described in terms of the statistical distribution,
- voltage flicker, expressed by a flicker coefficient characterizing the wind turbine,
- voltage harmonics variations,
- frequency variations and
- frequency rate of change.

The paper will only present proposals to the methods of how to define the measures. The paper will *not* specify the exact parameters necessary for the final uniform definition of the measure. These must be determined by the particular international organizations - e.g. the working group IEC / TC 88 / WG 10[1].

	Large interconnected	Small isolated
Central part (strong)	stiff voltage stiff frequency	(stiff) voltage slack frequency
Feeder (weak)	slack voltage stiff frequency	slack voltage slack frequency

Table 3: Power system classes divided by their stiffness and their size indicating typical power quality characteristics.

4.1 Statistical measures

Most of the proposed measures are of statistical nature, quantified by their discrete probability distributions and presented in terms of histograms, probability curves and duration curves.

The statistical variation of the variable in question (x) is analyzed within a specified range. The range is divided into bins given by their lower and upper limits (x_i and x_{i+1}). The actual probabilities for the value of the variable to be within the range of bin i ($p_i = p\{x_i<x<x_{i+1}\}$) will then form the quantification of the measure in terms of the discrete probability distribution.

In addition to the histogram of the probability distribution, the probability curve given by the summation of the probability distribution is useful:

$$p\{x < x_j\} = \sum_{i=1}^{j} p_i\{x_{i-1} < x < x_i\}$$

The probability curve directly give the answer to the question "how many percent of the time will the variable be below a given value ?"

[1] Working group WG 10 "Power quality requirements for grid connected wind turbines" under the IEC Technical committee TC 88.

Deviation from nominal value

If the variables deviations from the nominal value ($\Delta x = x - x_0$) can be both negative and positive, the negative and positive deviations might have different causes and consequences and should therefore be separated in the analysis and in the presentation of the results. In these cases, one of the bins must include the nominal value (x_0) as the bins center value.

Below and above the nominal value, respectively, the data points for the probability curves are given by

$$p\{\Delta x < \Delta x_j\} = \sum_{i=1}^{j} p\{\Delta x_{i-1} < \Delta x < \Delta x_i\} \quad (\Delta x_j < 0)$$

$$p\{\Delta x > \Delta x_j\} = \sum_{i=j}^{N} p\{\Delta x_i < \Delta x < \Delta x_{i+1}\} \quad (\Delta x_j > 0)$$

Extreme cases of this are the measures with only two defined limits - the lower limit and the upper limit - which should not be exceeded under normal operation. The probability values will then indicate the probabilities for the variable to be either below the lower limit or above the upper limit, and there will be no information of the variables distribution within the allowed range.

As an example, the voltage standard EN 50160 requires the 90 % fractile of the 10-minutes average voltage level to be within a specified range in the one week test period.

Duration curve

Large deviations from the nominal value might be acceptable if they occur only shortly and seldom, while small deviations might be more frequently acceptable.

The analysis of this must be based on time series of the instant values. Again, the variables analysis range is divided into bins, and in addition the time scale must be divided into classes. Each time the variable exceed one of the limits defined for the variable, the time is counted until the variable pass the limit again, and the respective time class for that limit is incremented by one.

Finally, the fractile-values for the specified probability fractile (pf) (e.g. the 90 % fractil) must be calculated for all variable limits.

The results must be given as data sets (Δt_i, Δx_i; @ pf) in tabular form and presented in graphical form as the deviation-duration curve. Thus, the duration curve indicates the probability, that the combination deviation-duration will be below the curve.

Again, if the deviation from nominal can be both negative and positive, the analysis should be split up and carried out and presented for both.

The duration curve as specified here holds no information of the history, but the combination of the histogram and the duration curve gives the probabilities for the combinations deviation-duration-frequency - or how often will the deviation be above a given level for the specified duration - or how often will the duration exceed a given time for the specified deviation.

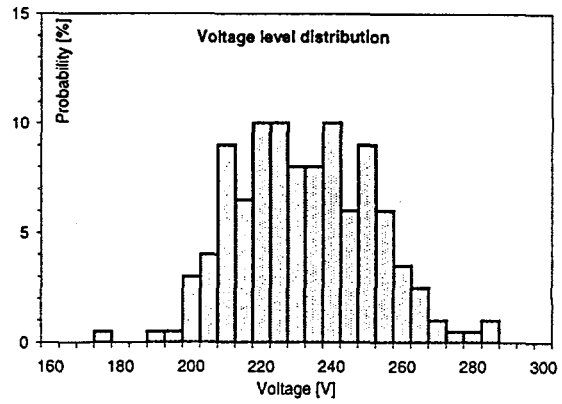

Figure 1: Voltage level distribution presented in histogram form.

4.2 Voltage level

To indicate, if the voltage level can be critical, the discrete statistical distribution of the voltage level for all operation conditions should be determined with the voltage level divided into bins.

The results must be expressed in tabular form, with the following data columns:

i the bin number,
U_i the average voltage level for the bin,
N_i the number of data points within the bin and
p the probability

In addition, the results should be presented in graphical form as illustrated in Figure 1.

4.3 Voltage flicker

The flicker analysis is bases on

- the standard IEC 555-3,
- power (current) and voltage measurements,
- a reference grid.

The flicker level is expressed by the two parameters P_{st} (short term, 10 min) and P_{lt} (long term, 2 hours) and shall be tested over one week.

$$P_{lt} = \sqrt[3]{\frac{\sum_{12} P_{st}^3}{12}}$$

The discrete statistical distribution for both P_{st} and P_{lt} must be determined for the test period, and expressed in tabular and graphical form.

The wind turbines contribution to the flicker level may be expressed by a flicker coefficient characterizing the wind turbine [1]:

$$P_{st} = \left|\cos\varphi_{sc} - 2\tan\varphi_w(W)\sin\varphi_{sc}\right| \frac{S_{wn}}{S_{sc}} I_w f_w(W)$$

4.4 Harmonic analysis

The harmonic analyses are based on the international standards (e.g. IEC 555-2, IEC 1000-3-2 and EN 50160). Interharmonic distortion is not included in the present framework.

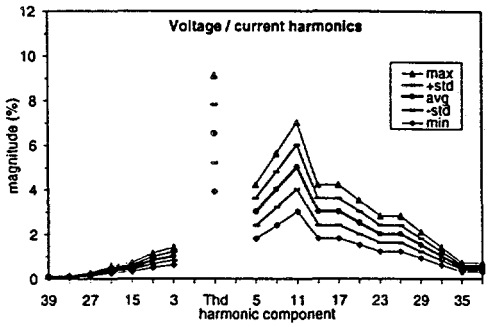

Figure 2: Paradigm for the graphical presentation of the magnitude of the harmonic components.

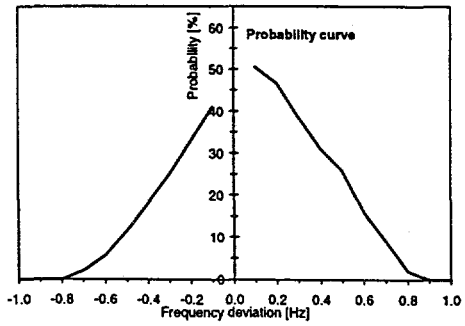

Figure 3: Probability curve for the frequency variations

The magnitude of the harmonic components must be given as relative to the fundamental (the rms value of the harmonic component, U_h, relative to the rms value of the fundamental, U_1, over the specified measuring period):

$$u_h = \frac{U_h}{U_1}$$

The total harmonic distortion, THD, are defined by:

$$Thd_N = \sqrt{\sum_{h=2}^{N} u_h^2}$$

As to prevent aliasing problems, the signals to be sampled must be adequate low-pass filtered and the sample rate must be adequate high.

The harmonic measurements and analysis must be repeated, and the analysis indicate the variations over the test period of each harmonic component.

For each measuring period (few line periods) all the specified harmonic components must be calculated (data set: rms, thd, h_1, h_2, h_3, ... ,h_{40}).

Presentation of results

For the test period (hours) the following must be calculated for each of the harmonic components and the results presented in tabular form with the following data columns (see sample in Table 4):

- the harmonic number,
- the average value of the harmonic component,
- the standard deviation,
- the minimum value recorded,
- the maximum value.

Harm #	% of fundamental component			
	avg	std	min	max
39	0.1	0.02	0.06	0.14
33	0.1	0.02	0.06	0.14
27	0.2	0.04	0.12	0.28
21	0.4	0.08	0.24	0.56
15	0.5	0.1	0.3	0.7
9	0.8	0.16	0.48	1.12
3	1	0.2	0.6	1.4
Thd	6.5	1.3	3.9	9.1
5	3	0.6	1.8	4.2
7	4	0.8	2.4	5.6
11	5	1	3	7
13	3	0.6	1.8	4.2
17	3	0.6	1.8	4.2
19	2.5	0.5	1.5	3.5
23	2	0.4	1.2	2.8
25	2	0.4	1.2	2.8
29	1.5	0.3	0.9	2.1
31	1	0.2	0.6	1.4
35	0.5	0.1	0.3	0.7
37	0.5	0.1	0.3	0.7

Table 4: The variations of the magnitude of the harmonic components specified in tabular form.

In addition, the data should be presented in graphical form as in Figure 2. Only the odd harmonics and the THD are presented. The multiple-of-three components (3, 6, ...) are often relatively low, and therefore separated in the presentation.

4.5 Frequency variations

The statistical distribution of the variation of the steady state frequency level is determined.

The measured steady state frequency data points are divided into equal frequency bins and the average frequency and number of data points in each bin are calculated. The frequency may either be expressed in absolute values or as deviations from the nominal frequency.

The results must be presented in tabular form, in histogram form and as the probability curve (see Figure 3).

4.6 Frequency rate of change

The rate of change of the frequency must be based on time series measurements of the instant frequency, and is defined by

$$\frac{\Delta f}{\Delta t} = \frac{f_{i+1} - f_i}{\Delta t}$$

where Δt is the time step and f_i and f_{i+1} are the frequencies given for step i and i+1 respectively.

The discrete statistical distribution of the frequency rate of change must be calculated, and the results presented in both tabular form and graphical form using the same format as for the frequency variations.

References

[1] Sørensen, P "Methods for calculation of the flicker contributions from wind turbines". Risø-I-939, 1995.

WIND POWER FLUCTUATIONS IMPACT ON CAPACITY CREDIT

John O. Tande and Jens Carsten Hansen
The Test Station for Wind Turbines
Department of Meteorology and Wind Energy
Risø National Laboratory, 4000 Roskilde, Denmark

ABSTRACT: It is generally recognized that at small wind energy penetration levels, the capacity credit of many widely dispersed wind turbines is about equal to their average power output. In systems with few wind turbines, however, wind power fluctuations are not averaging each other out, and the capacity credit must be reduced.

A methodology for estimating the capacity credit taking into consideration the wind power fluctuations is described. The methodology utilizes the commonly applied loss of load expectation index for estimating the capacity credit. Calculations are made and presented for a number of power system configurations and wind power penetration levels. It is concluded that the described methodology gives a consistent approach for determining the capacity credit for small and large systems with a few or many dispersed wind turbines.
KEYWORDS: Capacity credit; Wind farm; Statistical analysis; Performance

1. STATE OF THE ART

The wind power capacity credit or the firm power of a wind farm expresses the substituted amount of conventional capacity still giving the same power supply reliability. For determining the wind power capacity credit, the power supply reliability is commonly expressed by the Loss of Load Expectation (LOLE).

The LOLE is the expected total duration of any power supply shortage within a specific period. A power supply shortage occurs when the available generating capacity $P_{c,i}$ is less than the demand $P_{n,i}$, hence the loss of load expectation in hours per year can be expressed as:

$$LOLE = \sum_{i=1}^{N} T_i \cdot \Pr(P_{c,i} < P_{n,i})$$

Here, N is the number of time periods (e.g. hours), T_i in one year, and $\Pr(P_{c,i} < P_{n,i})$ is the probability that the generating capacity is less than the demand in T_i . The impact of wind power can be found by assuming the demand to be the difference between the consumers load, $P_{l,i}$ and the wind turbines output power, $P_{w,i}$:

$$P_{n,i} = P_{l,i} - P_{w,i}$$

The wind turbines output power is calculated from the wind speed and the wind turbines power curve.

As presented, the method for determining the capacity credit of wind power is quite straight forward, and recent studies of 10 European utility systems conclude that wind power contributes with firm power that can displace conventional capacity investments, Milborrow 1995 [1]. The conclusion of the studies is as generally recognized, that at small wind energy penetration levels, many widely dispersed wind turbines contribute with a capacity credit about equal to the average output.

2. WIND POWER FLUCTUATIONS

Consider a small power system with two diesel generators and one wind turbine supplying a constant load. In case one of the diesel generators are out of operation, the remaining diesel generator and the wind turbine may supply the load as long as the wind power production is above a certain critical level. As the wind power is fluctuating, a reliable supply is achieved only when the average wind power production is well above the critical level. Intuitively, it is seen that the capacity credit of the wind turbine in this case, independent of the wind energy penetration level, must be lower than the average output power due to the impact of the wind power fluctuations.

The capacity credit should obviously be attributed only such output power supplied with a high probability without interruption for periods of sufficient duration.

The output power of a single wind turbine within a 10 minutes period may be fitted reasonably well to

a Gaussian distribution with average power, avg(P_{WT}) and standard deviation, std(P_{WT}). The output power will within a 10 minutes period with 98 % probability be above:

$$P_{WT,\min} = avg(P_{WT}) - 2std(P_{WT})$$

Depending on the wind turbine type, the wind speed and the turbulence intensity, the standard deviation of the output power from a single wind turbine may be significant. Fig. 1 shows the power curve and standard deviation of output power for a fixed speed stall controlled Nordtank (NTK) 300 kW wind turbine measured at the Test Station at Risø.

The output power variations of more wind turbines may be correlated depending on the distance between the wind turbines and the frequency of the variations. A reasonable approximation is to assume that the output power variations from wind turbines are uncorrelated for higher frequencies and weakly correlated within a 10 minutes period depending on the distance between the turbines. Assuming no correlation, the sum output power from N_{WT} of identical wind turbines may be expressed as:

$$avg(P_w) = N_{WT} \cdot avg(P_{WT})$$

and

$$std(P_w) = \sqrt{N_{WT}} \cdot std(P_{WT})$$

Further, the output power will with 98 % probability be above:

$$P_{w,\min} = N_{WT}(avg(P_{WT}) - 2std(P_w) / \sqrt{N_{WT}})$$

From the last equation it is noted that for:

Figure 1 Power curve with indication of standard deviation of output power for NTK 300 kW wind turbine. Measurements from the Test Station at Risø [4].

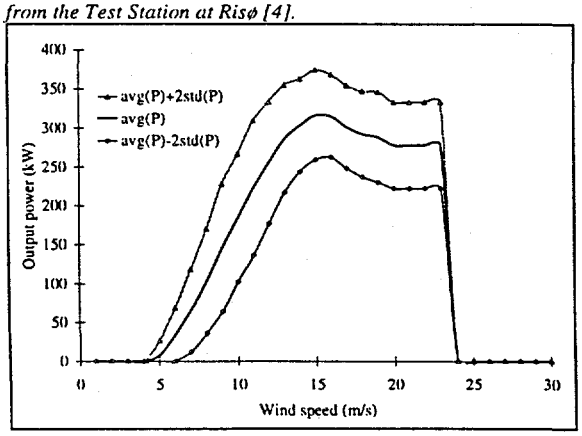

Table 1 Operational statistics - Actual data for Sal, Mindelo and Praia power systems. Jan - Jun 1995.

	Sal	Mindelo	Praia
Available diesel capacity (MW)	3	11	9
Diesel fuel type	gas oil	heavy fuel	gas oil
Installed wind turb. capacity (kW)	600	900	900
Avg. wind speed at hub height (m/s)	7.8	11.6	8.6
Wind energy production (MWh)	893	2655	1596
Wind turbine availability (%)	99	97	99
Total WT availability incl grid (%)	94	92	99
Avg. wind turb. capacity factor (%)	35	68	41
Total power system load (MWh)	3739	14086	14645
Avg. wind energy penetration (%)	24	19	11
Diesel fuel consumption (t)	745	2663	3140
Diesel fuel expenses (MECV)	16.9	40.1	71.1
Estimated fuel savings (MECV)	4.8	8.3	7.8

MECV = millions of Cape Verde escudos
8 000 ECV = 100 US$ = 650 DKK

$N_{WT} \to \infty \Rightarrow P_{w,min} \to P_w$.

Hence, in systems with many wind turbines the wind power fluctuations are evened out.

In order to ensure that the capacity credit calculation takes account for the wind power fluctuations, it is based on the above considerations, suggested to exchange the wind power output determination in the LOLE calculations from using the average power curve to using $P_{w,min} = f(u)$ as determined in the above formula.

3. CASE STUDY

At the Cape Verde islands in the Atlantic Ocean about 600 km west of Africa, electric power has until recently been almost entirely supplied from diesel power stations using gas oil and heavy fuel. This situation changed in 1994 when wind farms with a total capacity of 2.4 MW were installed at the three major island grids as part of a project jointly funded by the Capeverdean and the Danish governments. The wind energy penetration is now approximately 15%.

The wind farms operate together with the diesel power stations. Each of the wind farms consist of a number of standard "Danish type" NTK 300 kW wind turbines and a CMCS (Central Monitoring and Control System) with a remote on-line connection to the diesel power plant control room. This gives the diesel power plant operators immediate information of the wind farms output power, reactive consumption and status as well as the possibility to start or stop the individual wind turbines. Stop of the wind turbines may be a necessity to avoid too low load at the diesel power plant during periods with low load and high wind power production.

Figure 2 Recorded month by month capacity factors of wind farms in Cape Verde.

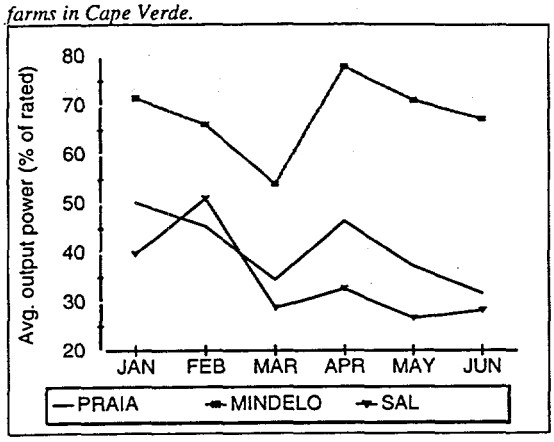

A summary of the production statistics for the period Jan-Jun 1995 is presented in Table 1. More details are found in Delgado et.al. 1995 [2] and Hansen et.al. 1995 [3]. The statistics are based on the 10 minutes average data available from the central monitoring and control systems of the wind farms and on the statistics from the diesel power stations operation.

The period Jan-Jun 1995 has served as a necessary running-in period with training, seminars and adjustments of operational strategies for the power system due the relatively large amount of wind power, especially in Mindelo and Sal. However, the data show high technical availability of the wind farms and may be considered representative for its future performance. Indeed, the recorded operation data show sensationally high productions for Mindelo as seen from Fig. 2.

3.1 Loss of load expectation

The output power of Mindelo wind farm was measured at 1 Hz sampling rate during a two day campaign in November 1994. Fig. 3 shows the recorded data as 5 minutes averages together with standard deviations and maximum and minimum data. It is seen from the plot that output power is rather steady with low power variations. Fig. 4 shows the

Figure 3 Time series plot of measured output power from Mindelo wind farm 4-6 Nov. 94. The curves from top are 1 Hz max. output power, 5 minutes average, 1 Hz min. and standard deviation of 1 Hz output power within 5 minutes.

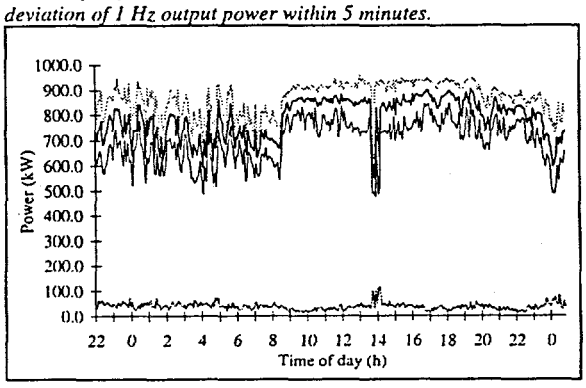

Figure 4 Measured and linear fit of standard deviation vs average output power from Mindelo wind farm 4-6 Nov. 94.

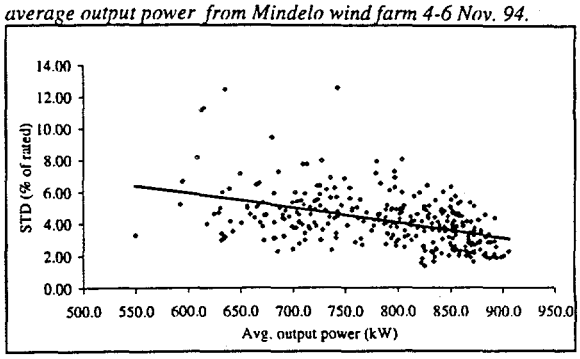

measured standard deviations plotted as a function of the average output power. Assuming no correlation between the output power of the wind turbines within the 5 minutes period and using the measured standard deviations of the wind farm, the standard deviation of the output power for a single wind turbine at the specific turbulence conditions are estimated to be as illustrated in Fig. 5. Comparing Fig. 1 and Fig. 5, it is seen that the standard deviation of the output power is less for the Mindelo wind farm site than for the Test Station site at Risø. This may be explained by the turbulence intensity being approximately 10 % at the Mindelo wind farm site compared to the higher turbulence intencity at the Test Station at Risø.

Assuming power system data as specified in Table 2, and taking account for the wind power fluctuations by assuming the standard deviation in output power as plotted in Fig. 5, the loss of load expectation is calculated for Praia, Mindelo and Sal for 1997 as a function of the installed wind power capacity. The wind energy utilization factor is here assumed to be 1.0 as it is assumed that in case of a loss of load situation, all available wind energy is utilized. The result of the LOLE calculations is shown in Fig. 6. It is seen that the loss of load expectation is reduced due to the installed wind power capacity, roughly a factor of 1.5 reduction is achieved by increasing the installed wind power capacity from 2.4 MW to 6 MW.

Figure 5 Power curve with estimated standard deviation output power for NTK 300 kW wind turbine at Mindelo wind farm site.

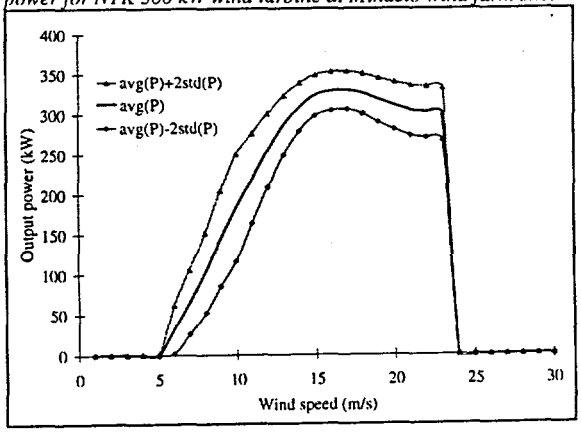

Table 2 Power system specifications assumed for 1997 for calculation of loss of load expectation.

	Praia	Mindelo	Sal
Diesel capacity (kW)	2500	3168	1000
	2650	3168	1000
	2650	2300	1000
	2514	2300	500
	1560		500
Diesel availability	0.9	0.9	0.9
Min load (kW)	2700	2500	1100
Max load (kW)	7000	5000	1700
Wind turbine type		NTK 300 kW	
Weibull scale parameter (m/s)	9.0	11.8	8.4
Weibull shape parameter	3.52	4.05	3.64
Air density (kg/m^3)	1.14	1.17	1.18
Performance factor	0.99	0.99	0.99
Site factor	1.00	1.00	1.00
Technical availability factor	0.95	0.95	0.95
Electric transmission losses factor	0.98	0.98	0.98
Utilization factor	1.00	1.00	1.00

3.2 Wind power capacity credit

As the power system reliability is increased by the introduction of wind power, a fraction of the wind power can be assumed to be firm power, i.e. the wind turbines may be assigned a capacity credit. The wind turbines capacity credit may be estimated by finding the amount of conventional diesel capacity that must be installed instead of the wind turbines as to obtain the same LOLE. Taking this approach, Fig. 7 shows the estimated firm wind power capacity or wind power capacity credit as a function of the installed wind power capacity for the power systems of Praia, Mindelo and Sal of 1997.

There are good prospects for increasing the amount of wind power installed in both Praia, Mindelo and Sal. Assuming a total of nine 300 kW wind turbines at Praia, seven at Mindelo and four at Sal, the firm wind power capacity as can be read from Fig. 7 is 650 kW, 1150 kW and 260 kW. Relative to the installed wind power the corresponding figures are 24, 45 and 21 %.

The difference in capacity credit per installed kW wind power between the three sites is firstly explained by the difference in wind resources as can be seen from Fig. 2. With the assumed wind resources and further specifications as given in Table 2, the annual average capacity factors becomes 31 % for Praia, 58 % for Mindelo and 28 % for Sal giving a ratio between the capacity credit and the average output of 0.75.

4. CONCLUSIONS

In systems with few wind turbines wind power fluctuations have an impact on the capacity credit. A methodology for estimating the capacity credit taking into consideration the wind power fluctuations is described. The methodology utilizes the commonly applied loss of load expectation index (LOLE) for estimating the capacity credit. It is suggested to exchange the wind power output determination in the LOLE calculations from using the average power curve to using a lower "firm power" power curve, e.g. determined as the average minus two times the standard deviation.

The case study shows results from actual operational experience. The average capacity credit is found to be 75 % of the average output power. The capacity credit is seen to be less than the average power typically assumed for large systems with many wind turbines. This reduction is due to the methodology employed taking account for the wind power fluctuations.

It is concluded that the described methodology gives a consistent approach for determining the capacity credit for small and large systems with a few or many dispersed wind turbines.

REFERENCES

1. Milborrow D. (1995) *What happens when the wind stops blowing?* Wind Directions Vol XIV No3 April 1995.
2. Delgado J., J.C.Hansen, J.O.Tande and P.Nørgård (1995) *Running in and economic reassessment of 15 % wind energy penetration in Cape Verde.* Proc. of EWEA'95.
3. Hansen J.C., J.O.Tande and J.Delgado (1995) *High wind energy penetration in Cape Verde: Achievements and perspectives.* Thermie Conf. in Cape Verde, 10-11 Nov 95.
4. Paulsen U.S. (1995) *Measurement Summary No.14.1 May 1995. NTK300/31. Power curve measurement.*

Figure 6 LOLE for 1997 as a function of the installed wind power capacity in Praia, Mindelo and Sal.

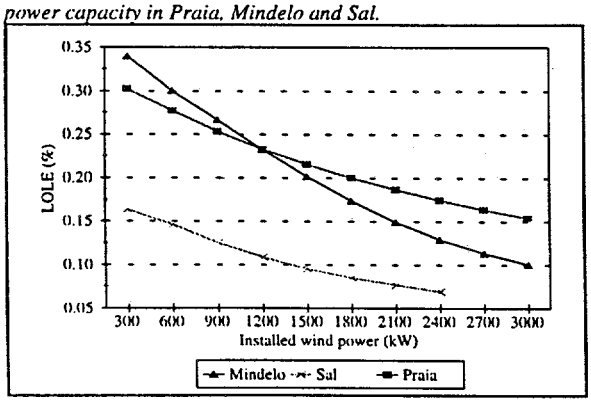

Figure 7 Wind power capacity credit as a function of the installed wind power capacity for Praia, Mindelo and Sal.

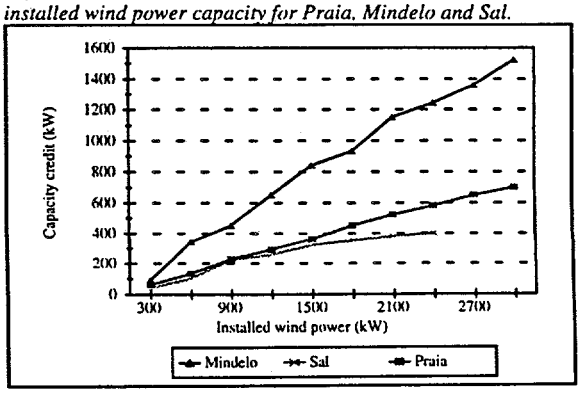

COMBINED WIND DIESEL DESALINATION SYSTEMS: FEASIBILITY STUDIES ON LARGE AND SMALL SYSTEMS

H. Bindner
Risø National Laboratory
P.O.Box 49
DK-4000 Roskilde
Denmark

P. Vionis
CRES
19th km Marathonos Ave.
GR-190 09 Pikermi
Greece

E. Soria Lascorz
CIEMAT
Ave. Complutense 22
ES-28040 Madrid
Spain

P. Lundsager
Darup Ass./CAT
Frederiksborgvej 399
DK-4000 Roskilde
Denmark

ABSTRACT: Combined wind diesel desalination systems applying different desalination technologies are studied. The technical and economic performance of such systems are estimated for two islands from a logistic point of view through the execution of two feasibility studies. The general results show that the combination of wind and desalination increases the amount of wind energy that can be integrated in the power supply system and that a large fraction of the power required by the desalination plant can be supplied by wind turbines. The work presented is part of the work done in an APAS project.
Keywords: Integration, Wind-Diesel Systems, Desalination, Feasibility Studies

1. INTRODUCTION

In the Mediterranean region natural fresh water resources are limited. Lack of water is one of the main reasons that industry and tourism cannot be developed in local communities.

Sea water desalination is one way of getting fresh water. Desalination plants requires energy and depending on the desalination technology applied the energy source is either thermal or electric. Usually the amounts of water required exceeds the amount that can be produced by e.g. waste heat from local diesels.

In order to cover the increased energy demand and to decrease the pollution, renewable energy can be used. The amount of energy required for desalination to cover the water demand of the communities makes wind energy the best suited renewable energy source.

The inclusion of marginal amounts of wind energy in a power supply system is normally no problem. At higher penetration levels care has to be taken in order to ensure that grid stability, power quality and diesel operating conditions are within accepted limits.

The integration of both wind energy and desalination plants may have some advantages in terms of higher penetration levels and lower water production costs.

An APAS project has been executed in which combined wind diesel desalination systems have been studied. The project consisted of two feasibility studies. One of the studies was in Paros, one of the Cyclades in Greece. The other study was on the Balearic island, Menorca, in Spain

The combination wind energy, desalination plants and a diesel powered supply system is studied from a logistic/economic point of view. Various Wind Diesel Desalination (WDD) concepts have been studied and their performance have been evaluated using a logistic model.

Several scenarios are defined and for each scenario the systems performance is simulated. The results, both technical and economic, are then compared.

The principles can be generalized but in each case the assumptions as well as other alternatives have to be investigated.

2. DESALINATION TECHNOLOGY

In the production of fresh water from sea and/or brackish water several different technologies are applied. In the current study three technologies are considered:

- Distillation (Single or Multiple Effect, SED, MED)
- Reverse Osmosis (RO)
- Mechanical Vapor Compression (MVC)

The three different desalination technologies studied may be integrated in a WDD system in different ways e.g. as base load or dump load units.

Distillation uses mainly thermal energy as input, which is not efficient (200-750 kWh/m^3). However, It is well suited for working with variable input power. the desalination unit can therefore be used as dump load.

Reverse osmosis is the most energy efficient desalination technology (8 kWh/m^3). It uses electric energy. It is a membrane technology and is fragile compared to distillation.

Mechanical vapor compression is also a distillation technology but the working principle is to establish a pressure difference with a pump instead of a temperature difference using heat. It is not as efficient (10-12 kWh/m^3) as RO but more robust.

Neither RO nor MVC are at the moment developed to operate with fluctuating input power and they are therefore best suited as base load units.

2.1 Combined Wind Diesel Desalination Systems

There are two main issues in an integrated wind diesel desalination (WDD) system.

The first issue is the integration and control of the wind turbines in order to ensure that operating limits of the diesels are kept and that the power quality is within the standards. The second issue is the integration of the desalination plants in order to optimize the performance of

both the desalination plant and of the wind turbines. The last issue depends on how the first is solved.

The integration of wind turbines in the power supply system is of consequence to the operation of the diesels and on grid stability when a certain penetration level is reached if no extra measures are taken. For the operation of the diesels the main concern is the technical minimum load and the scheduling/spinning reserve.

In systems with a large amount of installed wind turbines, situations with low load and high wind power production can occur. When this occurs the technical minimum load limit of the diesels can be violated. There are several options that can be implemented in order to avoid this:

- Wind turbines can be stopped
- Wind energy can be dumped
- Diesels can be stopped
- Extra load can be connected

Here the impact of using a dump load connected to a desalination plant and using a desalination plant to increase the minimum load on the system is studied.

3. CASE: PAROS

Paros is the object of one of the two feasibility studies in the APAS project.

3.1 Description of Paros

Paros is one of the Cyclades in Greece. Its main source of income is tourism. There is one power station with a total installed capacity of 30.6 MW, while a new unit of 10 MW is expected in service in 1996. The power station also covers the neighbouring island, Naxos. Due to the well developed tourism there is a strong seasonal dependence of both the electric and water demand. All the generating units are diesel gensets. The size range is 2-10 MW.

The water demand is currently covered by ground water. The capacity cannot cover the demand during high season and the average water demand is also above the long term capacity of the fresh water resources of the island.

The main concern of the authorities of the island is fresh water and not power capacity.

For Paros several scenarios are investigated. The scenarios presented here are compared from both an overall point of view in terms of e.g. saved fuel as well as from an investors point of view in terms of e.g. cost of water.

In the latter part the calculations of cost of water and internal rate of return exploits the legal framework existing in Greece regarding the tariffs etc. for renewable energy.

The scenarios presented here are in Table 1. In [1] some of the other scenarios studied are presented. These include the use of waste heat from the diesel units.

Table 1 Paros case scenarios

Scenario	Desalination Plant	Wind Farm Capacity
0	0	0
1	2*1200 m^3/24h MVC	0
2	2*1200 m^3/24h MVC	3000 kW
3	2*1200 m^3/24h MVC	4500 kW
4	0	1800 kW

The size of the wind farm in scenarios 2&4 have been chosen so that the technical minimum load of the diesels is not violated and only approx. 1% of the potential wind energy is dumped.

3.2 Wind Energy Integration

The wind resources of Paros are very favorable. The average wind speed at hub height used in the simulations is 8.2 m/s. The measurements indicate that this is not an optimistic value. The energy production from the model wind turbine (300 kW Nordtank) is 910 MWh/yr. or 103 kW on average.

The key figures on the technical performance of the system is summarized in the table below.

Table 2 Key figures of Paros Scenarios

	Scen 0	Scen 1	Scen 2	Scen 3	Scen 4
Water prod. [m^3/24h]	-	2280	2280	2280	-
Fuel Saved [%]	-	-	10	15	7
Wind Energy Utilized [%]	-	-	99	95	99
Penetration Level [%]	-	-	11.0	15.8	7.3

The main result of the simulations is that the inclusion of a desalination plant increases the allowable wind farm capacity (when the above selection criteria is used). The increase in capacity is more than the load of the desalination plant.

The cost of the wind energy is approx. 0.04 ECU/kWh in all the scenarios. The avoided fuel costs are approx. 0.03 ECU/kWh. Given the new legal framework regarding renewable energy, any of the above scenarios are economically interesting from an investors point of view and it does seem that Greece will be an important market for wind energy development.

3.3 Water Production

The water production is investigated from an investor's point of view. The cost of water is calculated taking the tariffs and possible ownership setup in the legal framework into consideration.

The levelized production costs of water and the IRR for a public owned wind desalination plant is shown in Figure 1 and Figure 2.

The baseline scenario is a grid connected desalination plant and no wind farm.

Different financing options' influence on the costs are also shown in the figures.

The most expensive option is the case without wind energy. The legal framework makes it possible to reduce the cost of water significantly by installing wind turbines.

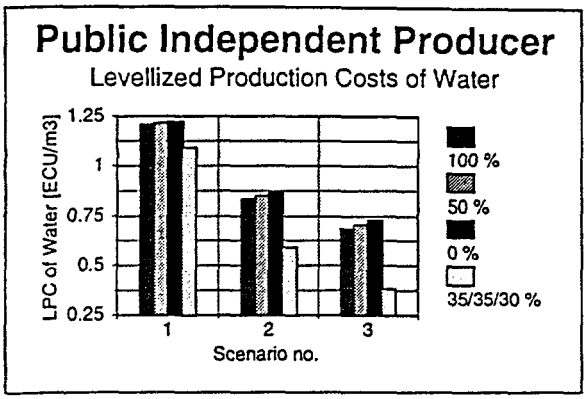

Figure 1 Publicly owned plant (Independent Producer): Internal Rate of Return of the investment for the defined scenarios. Financed by 100 % down payment, 50 % down payment/50 % loan and 100 % loan, 35 % grant/35 % loan/30 % down payment

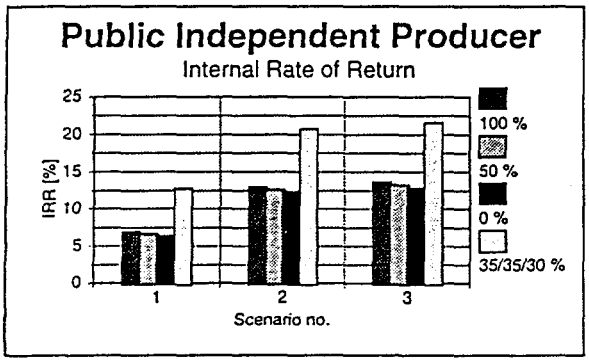

Figure 2 Publicly owned plant (Independent Producer): Internal Rate of Return of the investment for the defined scenarios. Financed by 100 % down payment, 50 % down payment/50 % loan and 100 % loan, 35 % grant/35 % loan/30 % down payment

The most profitable option is the larger wind farm even though 5% of the wind energy is dumped.

4. CASE: MENORCA

Menorca is the other island included in the APAS project.

4.1 Description of Menorca

Menorca is an island in the Balears in the Mediterranean south of the mainland of Spain. The main source of income is tourism but there is also an agricultural sector.

The power system of Menorca is connected to Mallorca through an AC sea cable connection. The power station is situated in Mahon, the principle town of Menorca. The generating capacity consists of 3 15.8 MW diesel units and two gas turbines for peak load coverage. The main generating capacity of Mallorca is coal fired thermal power plants.

The water demand is currently covered by ground water and the capacity is at the moment adequate. However, In the near future there will be a need for water that cannot be covered by ground water. Forecasts estimate that the need for desalinated water will be 5000 m^3/24h in year 2000.

The wind resources of Menorca are not as good as in Paros. For the study a site near Mahon, Cap Negre, is selected.

4.2 Wind Energy Integration

The average wind speed at hub height is 6.5 m/s at the selected site. The energy production from the wind turbine (Nordtank 300 kW) is estimated at 639 MWh/yr. This corresponds to 2130 hours/yr. at rated power or an average production of 24% of rated power.

In Table 3 is the cost of substituted energy from conventional energy production from coal and heavy fuel compared with the cost of wind energy from standard grid connected wind turbines.

Table 3 Cost of energy from coal, heavy fuel and wind turbines (Levelized production costs)

	Coal	Heavy Fuel	Wind
Cost of energy [ECU/MWh]	14	33	60

The figures for coal and heavy fuel are the avoided fuel costs, i.e. the cost of fuel not being used in the conventional power plants when the energy instead is produced by wind turbines. Investment, maintenance and social costs are not included in the figures for coal and heavy fuel.

The cost of energy from wind turbines include investment, installation and operation and maintenance.

In the grid connected case it is assumed that all the produced wind energy is utilized.

The maximum amount of wind capacity in Menorca in the case without the sea cable connection, is 3 MW if the technical minimum load of the diesel units are not violated and no wind energy is dissipated. The high value of the minimum load of the diesels is mainly because the use of heavy fuel.

In the case where the sea cable connection to Mallorca is included in the scenario other operational aspects will determine the maximum limit for installed wind capacity.

4.3 Stand Alone Wind Diesel Desalination System

A stand alone wind diesel desalination system at Cap Negre is evaluated. Different plant sizes are considered, Table 4.

Table 4 Wind diesel desalination system plant sizes

Genset [kW]	500
Wind turbines [kW]	(0-7)*150
Desalination plant [m^3/24h]	1000

In the case of the stand alone wind diesel desalination system the cost of wind energy depends on whether all the potential wind energy is utilized or not. In Table 5 are the key figures for the two of the cases that are studied.

Table 5 Results for stand alone wind diesel desalination systems incl. MVC desalination plant (all figures are levelized)

Wind turbine capacity [kW]	300	600
Cost of wind energy [ECU/MWh]	60	69
Cost of water [ECU/m^3]	1.30	1.43
Penetration level [%]	15	25
Utilized wind energy [%]	100	84

The waste energy from the diesel and surplus energy from the wind turbines can be utilized through the use of a distiller for water production in a common cooling circuit.

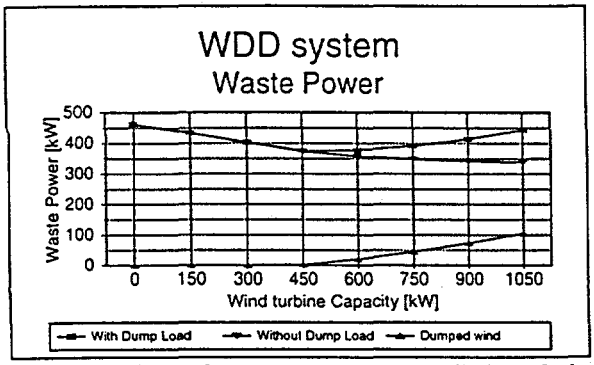

Figure 3 Equivalent average power dissipated in common cooling circuit of stand alone wind diesel desalination system

Figure 3 shows the equivalent average power dissipated in the common cooling system. As the wind turbine capacity increases the power dissipated decreases until the amount of surplus wind power exceeds the decrease in diesel load. It then increases with the wind turbine capacity.

4.4 Water production

The cost of water from a standard grid connected desalination plant depends mainly on the plant investment cost, the operation and maintenance cost and the cost of the energy consumed by the desalination plant.

Several different cases are considered. Together they show the range within which the cost of water lies. The different cases are described in Table 6.

Table 6 Grid connected desalination system cases

Case	Description	COE [ECU/ kWh]
WDD	Wind Diesel Desalination	0.078
GESA, tariff	The COE is the average tariff used by GESA for private customers	0.113
GESA, marg1	The COE is the marginal cost of energy produced by coal	0.014
GESA, marg2	The COE is the average marginal cost of energy in Menorca	0.027
GESA, tot1	The same as above but including O&M and investment in generating capacity	0.063
GESA, tot2	The COE generated in Menorca incl. O&M and investment in generating capacity	0.068

RO plants are considered. The energy consumption used in the calculations are 8 kWh/m^3.

The cost of energy for the different cases are calculated using WINSYS, [2] and are listed in Table 6. The costs of the produced fresh water are in Figure 4. The costs of water from the grid connected plants are compared with that of a WDD plant, see above. In the costs of water from the WDD system the total investment and all O&M of both the wind turbine and the genset are included in the costs.

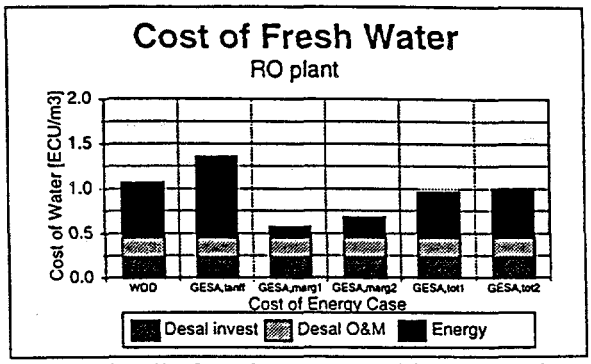

Figure 4 Levelized production costs of fresh water from RO desalination plants for different cost of energy cases

In most of the cases is the cost of the energy more than half the costs of the water.

The real cost of water lies between the cases: (GESA, marg1) and (GESA, tot2). In the first case it is assumed the energy needed by the desalination plant is generated at a coal fired plant in Mallorca at marginal cost. In the latter case it is assumed that the energy needed is generated in Menorca and investment and O&M costs are added to the fuel cost.

In the cases of a RO plant the cost of water from a WDD plant is only marginally more expensive than the cost of water from a grid connected desalination plant when investment and O&M is included.

5. CONCLUSIONS

The paper presents some of the results of the APAS project: *'Feasibility studies on combined wind diesel desalination in Greece and Spain'*.

It has been shown that combining wind energy with desalination has some advantages.

The amount of wind energy that can be installed without dissipating any wind energy production can be increased if a desalination plant is installed due to the increase in minimum load of the system. A large amount of the added load of the desalination plant can be covered by wind energy.

In the Paros case the legal framework regarding renewable energy makes the inclusion of wind energy a very profitable option that can be used to reduce the cost of water. The results of the analysis have shown that it is even profitable to install a larger amount of wind turbines and dump some of the energy that cannot be absorbed by the grid.

In Menorca a combined wind diesel desalination system can produce water at a cost that is not significantly higher than the costs of water from a standard grid connected plant.

REFERENCES

[1] H. Bindner, J.O. Tande, P. Vionis, E. Soria Lascorz. Venice Contractors Meeting, 22-25 Nov 1995, Venice, Italy, (to be published)

[2] J. Delgado, J.C. Hansen, J.O. Tande, P. Nørgård Proc Economics of Wind Energy. EWEA Special Topics Conference, 5-7 Sep, 1995, Helsinki, Finland

Computed 3D Effects on a Rotating Wind Turbine Blade.

M.O.L.Hansen*, J.A.Michelsen* and N.N.Sørensen+
* Dept. of Energy Engineering, Technical University of Denmark
+ Risø National Laboratory

ABSTRACT: Numerical results of 3-D effects on the separated boundary layer on a rotating wind turbine blade is shown. The computations show a spanwise flow from the root to the tip in the separated boundary layer. Further, an increased lift is found close to the hub.
KEYWORDS: Stall Rotation Effects: Navier Stokes Equations: Blade Aerodynamics: Three-Dimensional Flow Effects.

Introduction

Many wind turbines are stall regulated, which means that the shaft torque at high wind speeds is limited by the increasing drag and the decreasing lift, which is present at stall. Stall is obtained by keeping the pitch and the rotational speed of the turbines constant. In high winds this gives high local angles of attack, eventually leading to stall. Since the boundary layers at stall are massively separated one cannot apply an inviscid method to predict the flow past the wings. Stall on rotating blades is a three-dimensional, unsteady and viscous phenomena and in order to investigate this, it is necessary to apply the full three-dimensional Navier-Stokes equations. Such investigations were part of the JOULEII project "Dynamic Stall and 3D Effects" JOU2-CT93-0345. The results shown in this paper have mainly been obtained during this JOULE project.

Numerical Approach

A very practical problem encountered with the numerical methods used to solve the 3-D Navier-Stokes equations is the limited number of gridpoints affordable due to limitations in computer memory and speed. It is therefore impossible both to resolve the largest scales about the size of the wing chord, and the small dissipative scales. The dissipative scales are modelled by an eddy viscosity and the viscous sublayer in the boundary layer is approximated by wall laws. Thus the discretization concerns with resolving the large scales, such as separation bubbles and vortex shedding. The incompressible flowsolver EllipSys is used, see [1],[2]. The SIMPLE algorithm is employed to compute the pressure and to ensure a solenoidal velocity field. Odd-even decoupling of the pressure is avoided by a Rhie-Chow interpolation of the cell face fluxes [3]. To accelerate towards a stationary solution a local timestep found from a local convergence consideration is applied, i.e. a time true solution is not obtained. A second order upwind scheme for the convective terms is used and the standard high Reynolds number k-eps turbulence model [4] with the logarithmic law-of-the-wall is solved to compute the Reynolds stresses. It is well known, see [5], that the k-eps model generally gives to high a level of eddy viscosity and turbulent kinetic energy. The strain rate related to the mean flow is the basis for the turbulent kinetic energy production term, and this strain rate is very strong in the vicinity of the leading edge, where the real flow is almost laminar. Consequently, an excessive turbulent viscosity is predicted at the leading edge suppressing separation. In [6] it is shown that more realistic results are obtained for the 21% thick FFA-W3-211 airfoil if the eddy viscosity is lowered 10%. This airfoil is specially designed for wind turbines. Thus, the eddy viscosity has also been reduced 10% in all results shown in this paper.

Results and discussions

Flow around different blades were computed in the JOULEII project, but the most thorough investigation was made on the non-tapered and non-twisted wing used on the test turbine from Delft University of Technology [7]. The blade is based on a NLF(1)-0416 profile and has a span of 4.417 meters and a chord of 0.5 meters. The turbine is a two bladed upwind machine with a rotor diameter of 10 meters. In the computations only one blade is considered in a C-O mesh. The resolution is 7 blocks of 24*24*24 computational cells. The grid is shown in [8] together with the first preliminary results. Compared to a typical 2-D calculation this is a coarse mesh with only 24 cells in the normal direction to the airfoil and 168 cells in the tangential direction. To assess the expected accuracy of the 3-D computations the 2-D flow was solved on this coarse mesh. Figure 1 shows a comparison between the lift from this computation and wind tunnel measurements for the NLF(1)-0416 profile. The predicted Cl_{max} is sligtly smaller than the measured but results are good in the fully stalled region for this profile. The 3-D effects caused by

rotation is now investigated, where it is known from measurements [9] that the lift coefficient at the root of a rotating blade can grossly exceed the maximum 2-D lift coefficient for the same profile. By varying the tip speed ratio the flow is solved for different angles of attack. For each tip speed ratio the lift coefficient is computed at different spanwise positions r/c and compared to the 2-D computation. In figure 2 it is seen that the computations support the measured observations from [9], i.e. $Cl_{max\text{-}3D}$ is significantly higher than $Cl_{max\text{-}2D}$ close to the rotational axis (small values of r/c). It is noted that the computation is a local simulation in the sense that the computational domain starts 0.5*D upstream of the blade, where D is the rotor diameter. The angle of attack is therefore defined from the geometric angle of attack

$$\alpha(r) = \text{atan}(V_\infty/\Omega r) \qquad (1)$$

where Ω, V_∞, r denote the angular velocity, the free wind speed and the radius from the rotational axis, respectively. To non-dimensionalize the 3-D lift coefficient the helical velocity V_{hel} is used

$$V_{hel} = [V_\infty^2 + (\Omega r)^2]^{1/2} \qquad (2)$$

The centrifugal force causes a flow radially outwards toward the tip in separated boundary layers. It has been suggested by e.g. [10], that the Coriolis force then acts as a favorable pressure gradient that tends to delay separation. This was also tested within the JOULEII project. A 2-D computation was performed at a Reynolds number and at an angle of attack corresponding to a spanwise position close to the rotational axis for the 3-D case. In figure 3 the resulting 2-D and 3-D pressure coefficient -Cp is plotted as a function of x/c for Re=770000, α=19.3. The result from NLR [11] using the quasi 3-D ULTRAN-V code is also shown in the figure. It is seen that both the full 3-D Navier-Stokes results using EllipSys and the quasi 3-D results obtained using ULTRAN-V have a more triangular shaped pressure distribution than the 2-D computation. This indicates that the 3-D flow is less separated than the 2-D case. Plots of the velocity vector close to the airfoil for the 2-D and 3-D case, respectively, are shown in the figures 4 and 5. The figures 4 and 5 clearly show that the 3-D boundary layer at r/c=2.87 is less separated than the 2-D boundary layer for the same Reynolds number and angle of attack, since the size of the separation bubble is smaller and the stagnation point is further back on the profile for the 3-D case. As mentioned earlier the centrifugal acceleration causes a radial flow from the root to the tip in areas with a separated boundary layer. This effect is also seen in the computations and can be used to investigate how the separation evolves at increasing wind speeds. Computations are made for the commercial LM19.1 blade and in figure 6 the velocity vectors in the boundary layer on the suction side of the blade is plottet for increasing wind speeds. The separation zone is recognized as the area with velocity vectors pointing in the radial direction and is marked with a pencil on the figure.

Conclusions

Several blade geometries have been calculated and the expected 3-D effects have been found by the numerical integration of the Reynolds averaged Navier-Stokes equations. These effects have been captured even though it was necessary to use a coarse discretization of approximatively 10^5 gridpoints and wall laws for the viscous sublayer. A drawback of the method, however, is that the local viscous computations around a blade have not been coupled with a global method for the wake, i.e. the axial induced velocities have not been taken into account and the actual windspeed far upstream of the rotor in the computations is therefore not known. To refine results the influence of the wake must be taken into account and a better turbulence model must be applied on a finer grid. The computational time will, however, be so high that for more practical applications the Blade Element Momentum method will still be used. But as a tool for more fundamental investigations of the physics of the boundary layer on a rotating blade at high angles of attack the Navier-Stokes solvers can now be used as a supplement to experiments.

References

[1] Sørensen, N.N., General purpose flow solver applied to flow over hills, Ph.D. dissertation Risø National Laboratory, Risø-R-827(EN), Denmark, 1995.

[2] Michelsen, J.A., Basis3D - a Platform for Development of Multiblock PDE Solvers, Technical note AFM92-05, Dept. of Fluid Mech. DTU, Denmark, 1992.

[3] Rhie, C.M. and Chow, W.L., Numerical Study of the Turbulent Flow Past an Airfoil with Trailing Edge Separation, AIAA Journal 21(11):1525-1532, November 1983.

[4] Launder, B.E. and Spalding, D.B., The numerical computation of turbulent flows, Comp. Meth. Appl. Mech. Eng., 3:269-289, 1974.

[5] Jin, G. and Braza, M., Two-equation turbulence model for unsteady separated flows around airfoils,

AIAA Journal 32(11):2316-2320, 1994.
[6] Hansen, M.O.L., Airfoil Computations using the high Reynolds Number k-eps Model, in 8th IEA-Symposium on Aerodynamics of Wind Turbines, Copenhagen, 1994.
[7] Bruining, A., van Bussel, G.J.W., Corten, G.P. and Timmer, W.A., Pressure distribution from a wind turbine blade; field measurements compared to 2-dimensional wind tunnel data, IW-93065R, Delft University of Technology, Institute for Wind Energy, 1993.
[8] M.O.L.Hansen, J.A.Michelsen and N.N.Sørensen, Navier-Stokes Solver for Rotating Wing. In proceedings of 5'th EUROPEAN WIND ENERGY ASSOCIATION CONFERENCE AND EXIBITION, pages 557-561, 10-14 October 1994, Greece.
[9] Himmelskamp, H., Profile investigations on a rotating airscrew, Ph.D. thesis Gottingen, 1945.
[10] D.Sørensen and J.N.Sørensen, Quasi 3-Dimensional Model for rotating Airfoil. From 13th AIAA Applied Aerodynamics Conference, 19-22 June 1995, U.S.A, AIAA 95-1916.
[11] J.Bosschers, Influence of Blade Rotation on the Sectional Aerodynamics of a Wind Turbine Blade. National Aerospace Laboratory NLR the Netherlands 1995, NLR CR 95290 L.

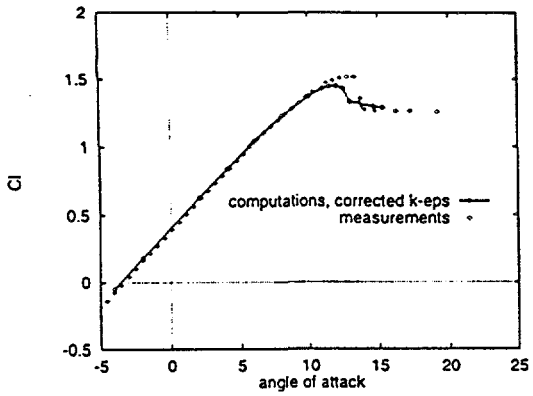

Figure 1: Comparison between measured and computed lift coefficient as a function of the angle of attack for the NLF(1)-0416 profile.

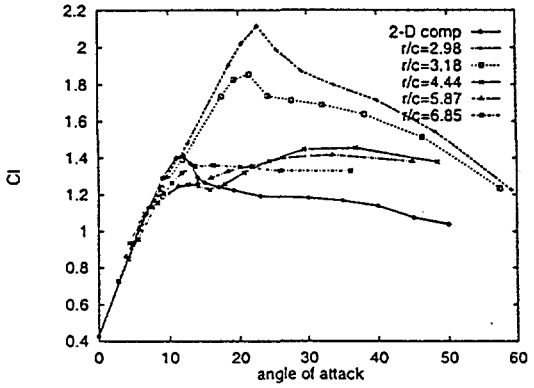

Figure 2: Comparison between local lift coefficient on a rotating blade and 2-D lift coefficient.

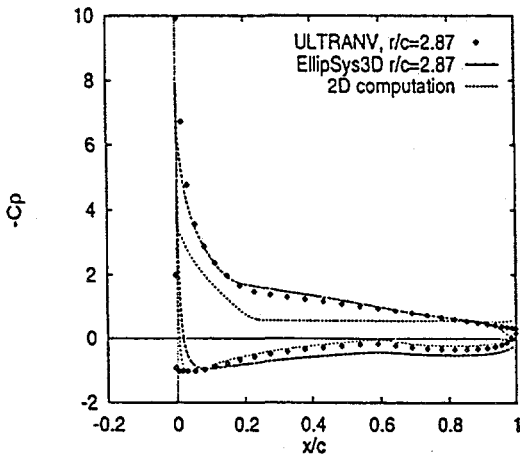

Figure 3: Pressure distribution for 2-D calculations and for calculations with a rotating blade at the same angle of attack.

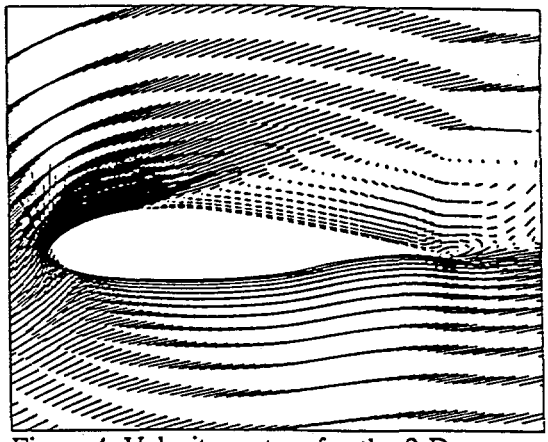

Figure 4: Velocity vectors for the 2-D case, α=19.3 and Re=770.000.

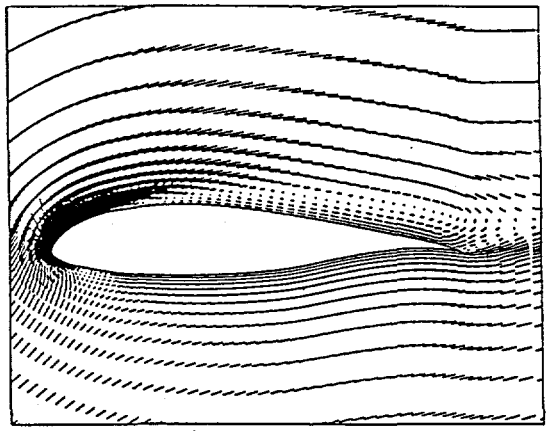

Figure 5: Velocity vectors for the 3-D case, r/c=2.87, α=19.3 and Re=770.000.

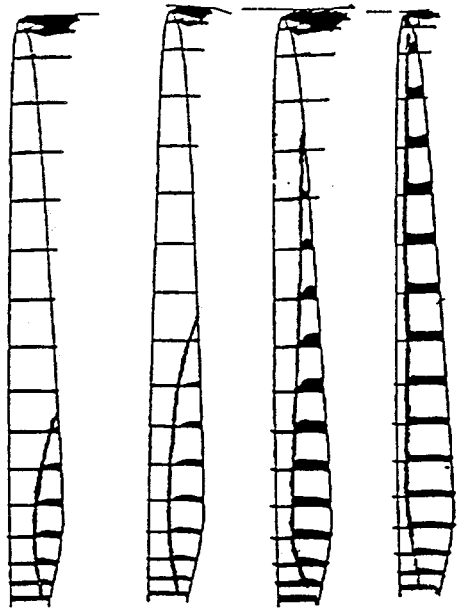

Figure 6: Velocity vectors on the suction side of the blade for increasing wind speeds.

COMPUTATION OF TURBULENT DYNAMIC STALL FLOWFIELDS

John A. Ekaterinaris
Department of Meteorology and Wind Energy
Risø National Laboratory
DK-4000 Roskilde, Denmark

ABSTRACT: Understanding and prediction of two- and three-dimensional dynamic stall flowfields is of interest to wind turbine design and optimization. Calculation of these flowfields requires numerical solutions of the Reynolds-averaged Navier-Stokes equations supplemented with a turbulence model. In this paper the ability of several one- and two-equation turbulence models, widely tested and utilized for steady flow calculations, is tested for the prediction of two-dimensional, fully turbulent, unsteady flows. Solutions computed with one- and two-equation turbulence models are compared with experimental data. For fully turbulent flows with tripped boundary layer most turbulence models predict lift hysteresis reasonably well. Some turbulence models give good qualitative agreement with the measured drag and pitching moment hysteresis loops. Fully turbulent, three-dimensional solutions in the light stall regime over an oscillating are finally presented.

Keywords: Dynamic Stall, Turbulence, Aerodynamics, Three-Dimensional Effects.

1 INTRODUCTION

The prediction of complex separated flows with Navier-Stokes solutions is of great interest and importance to wind turbine aerodynamics. In general, airfoil and turbine blade flows usually evolve under an adverse pressure gradient, which causes rapid transition to turbulence and in many cases leads to flow separation. Simple algebraic and half-equation turbulence models [1-4] are not capable of accurately predicting flow separation and they are responsible for inaccuracies in complex flow predictions. Therefore, incorporation and validation of more sophisticated turbulence [5-9] models into flow solvers is a field of continuous interest. Most turbulence models have been developed and calibrated on simple, steady boundary-layer-type flows. The ability of these turbulence models in predicting two- and three-dimensional unsteady, separated flow must be further investigated.

The standard $k-\epsilon$ [5] and $k-\omega$ [6] two-equation turbulence models as well as the recently developed Baldwin-Barth [7] and Spalart-Allmaras [8] one-equation models, which have been successfully tested for steady attached and separated flows do not suffer from ambiguities related to the determination of characteristic scales, such as the boundary layer thickness, and seem to show promise for more accurate prediction of massively separated unsteady flows. The standard $k-\epsilon$ [5] model without wall functions, because of its stiffness, limits the overall computations to small time steps. Therefore, in the present paper a zonal version of this model is used where the near wall region is computed with the $k-\omega$ formulation which does not suffer from these shortcomings. The standard $k-\omega$ model [6], on the other hand, has a free-stream dependency which can be removed using the suggestions of Ref. 9. The $k-\omega$ model without free stream dependency is referred to as Baseline (BSL) $k-\omega$ model. The BSL $k-\omega$ model can be further improved with the modifications suggested in Ref. 10, where the variation of the shear stress is taken into account in a way similar to the Johnson-King [4] turbulence model. This modified version of the $k-\omega$ model is referred to as the Shear Stress Transport or (SST) $k-\omega$ model. The SST $k-\omega$ turbulence model [10] improved the ability of the model to capture the physics of adverse pressure gradient driven separated flows. In this paper, the ability of one- and two-equation models in predicting massively separated, unsteady, two- and three-dimensional flows over an oscillating blade where dynamic stall occurs and hysteresis effects appear is tested.

The term dynamic stall refers to the unsteady separation and stall of aerodynamic bodies or lifting surfaces that are forced to execute time-dependent motion. It is a complex, fundamental, fluid dynamic phenomenon of practical importance and occurs on helicopter retreating blades, wind turbines, aircraft wings, and in turbomachinery. The majority of work on dynamic stall, summarized in extensive reviews by McCroskey [11], has been devoted to airfoils oscillating with moderate amplitude in a uniform free stream. The main characteristics of dynamic stall are the massive flow separation and development of large-scale vortical structures, when the wing reaches high angles of incidence during the oscillatory cycle, and the large hysteresis in unsteady sepa-

ration and reattachment compared to the static case. Furthermore, values of lift, drag, and pitching moment coefficients are reached which greatly exceed their static counterparts. Testing of simple turbulence models for two-dimensional dynamic stall has been conducted in Refs. 12 and 13. The $k-\epsilon$ model has been compared with the Baldwin-Lomax model in Ref. 14. An extensive evaluation of algebraic and one-equation models for the prediction of dynamic stall was performed in Ref. 12.

2 RESULTS AND DISCUSSION

An upwind-biased numerical scheme [12,15 and 16] used for the numerical solution of the compressible governing equations. The effects of numerical parameters such as grid density and time step on the accuracy of the computed solution were investigated [12,16] in order to exclude influences from numerical artifacts and focus on the effects of the turbulence model and transition alone. The results are presented in the following sequence. First, fully turbulent, two-dimensional solutions for tripped fully turbulent flow obtained with one- and two-equation turbulence models are compared with the experiment of Ref. 17. Three-dimensional effects of fully turbulent flow are shown only for the light stall case.

2.1 Fully turbulent two-dimensional flows

For validation of unsteady, fully turbulent two-dimensional solutions, the experimental measurements of Ref. 17 for a NACA-0015 airfoil are used, because in this experiment, as opposed to that of Ref. 11, the boundary layer was tripped at the leading edge to ensure a fully turbulent boundary layer for attached, light stall and deep stall cases. The free stream Mach number is $M_\infty = 0.3$ and the Reynolds number, based on the airfoil chord length is, $Re_c = 1.9 \times 10^6$. The airfoil oscillates as $\alpha(t) = \alpha_m + \alpha_a sin(\omega t)$ with a reduced frequency $k = 0.1$. The oscillation amplitude remains fixed at $\alpha_a = 4.2^o$ and variation of the mean angle α_m leads to different flow regimes.

The unsteady computations initiate from a computed quasi-steady solution at the lowest angle of the pitch cycle for each of the condition, the airfoil is made to execute pitching oscillations rotating about its quarter-chord point. Two oscillatory cycles are computed for every case and the third cycle is always identical to the second cycle. All computations shown in the following sections are performed with 16000 time steps per cycle which corresponds to a nondimensional time step of $\Delta t = 0.0065$. The computations use a C-type 311 x 71 point grid with 130 points on the suction side and 45 points in the wake having a grid spacing $dz = 0.00001$ chord lengths away from the airfoil surface as baseline grid. Normal spacing of $0.00001c$ yields a $y^+ \approx 2$ for the first grid point above the suction side surface.

The turbulence models are evaluated for three flow regimes, a) attached flow corresponding to $\alpha_m = 4^o$; b) light-stall case corresponding to $\alpha_m = 11^o$; and c) deep-stall case corresponding to $\alpha_m = 15^o$. The performance of all turbulence models is evaluated only for the deep stall case. For the light stall case, solutions are computed only with the B-B, S-A and SST $k-\omega$ turbulence models. The attached unsteady flow case was computed with the B-B and the SST $k-\omega$ models and the computed loads (not shown here) were in very good agreement with the experiment.

2.1.1 Light stall $\alpha(t) = 11^o + 4.2^o sin(t)$

The computed solutions show that this flow is characterized by moderate trailing edge separation which develops at the peak of the cycle. The flow remains separated for a large portion of the downstroke and a recirculatory region of about half a chord length is observed. The hysteresis loops obtained from solutions using the baseline grid with the B-B, the S-A, and SST $k-\omega$ turbulence models are compared with the experimental data in Fig. 1. The B-B model predicts the most separation and yields a lower lift during reattachment but it gives good predictions for drag and pitching moment coefficients. The S-A model predicts the least separation and shows earlier flow reattachment. Similar to the S-A model, the SST $k-\omega$ model, even though it shows closer agreement with the experimental lift during the initial part of the downstroke, predicts more rapid lift recovery.

2.1.2 Deep stall $\alpha(t) = 15^o + 4.2^o sin(t)$

The computed solutions show that this unsteady flowfield is characterized by massive flow separation which develops before the peak angle of incidence. The lift, drag, and pitching moment hysteresis loops obtained from computations with the B-B and S-A one-equation turbulence models are compared with the experiment in Fig. 2. The lift hysteresis is predicted reasonably well by both models. The drag and pitching moment hysteresis loops indicate that both models delay onset of separation. The loads computed with the B-B model show oscillatory behavior at the downstroke. The B-B model predictions are in closer agreement with the experiment. A smaller extent of separated flow is obtained with the S-A model,

resulting in smaller extreme values of drag and pitching moment. A more rapid flow reattachment is also observed.

Predictions of hysteresis loops obtained from solutions with the two–equation turbulence models are compared with the experiment in Fig. 3. The original $k-\epsilon$ and $k-\omega$ models, and the BSL $k-\omega$ did not yield enough separation. As a result, the loads computed with these models significantly deviate from the experimentally measured values. The solution obtained with the SST $k-\omega$ model shows large flow separation and the predictions are in close agreement with the experiment. However, at large angles of incidence and during the downstroke the loads show again oscillatory behavior. Taking into account that the experimental data are averaged over several cycles the load oscillations obtained by a single cycle could be justified.

2.2 Three–Dimensional Blade light stall

Solutions for a three–dimensional, unsteady flowfield over the aspect ratio five blade with rounded tip, oscillating in the same light stall conditions as its two–dimensional counterpart are presented next. This flow is computed with the Baldwin–Barth one–equation model because it showed equally good performance with the SST $k-\omega$ model in predicting separation and reattachment, provides comparable accuracy in unsteady loads prediction, and requires less computing time. A single block $181 \times 51 \times 71$ point C – H type grid along the streamwise, spanwise and normal directions, respectively is used to discretize the flow domain. The distance of the first point from the blade surface is dz = 0.00001 chord lengths.

The computed loads at approximately midspan y/s =47%, where the flow is essentially two dimensional (Fig. 4a) were in very good agreement with the measurements. At the 80% span location where the three–dimensional effects become important the computed solutions are compared with the available experimental data in Fig. 4b. The computed lift hysteresis is in perfect agreement with the experiment throughout the cycle. The computed drag and pitching moment hysteresis loops are also in fairly good agreement with the experiment for this location. At the blade tip location 98% of span, the computed loads (not shown here) follow the experimental trends but do not achieve the same quantitative agreement obtained for the 80% span location. These discrepancies are caused from inadequate grid resolution at the tip region which diffused the tip vortex and deficiencies of the turbulence model.

3 CONCLUSIONS

The ability of one– and two–equation turbulence models in predicting unsteady loads and hysteresis effects of unsteady, fully turbulent, two–dimensional flow over airfoils oscillating in the light and deep stall regimes was evaluated. It was found that all turbulence models tend to suppress separation onset. Reasonably good agreement with the experiment was achieved for solutions computed for the light stall regime. For deep stall, the B–B, S–A and the SST $k-\omega$ turbulence models yield significant improvements over standard two–equation models. The S–A model suppresses separation and predicts early reattachment, in contrast the B–B and SST $k-\omega$ models overpredict separation and for the deep stall case exhibit oscillatory behavior. The trends observed for two–dimensional cases carry over to the three–dimensional light stall computation over an aspect ratio five blade. The numerical solution closely predicted the load variation.

REFERENCES

[1] Cebeci, T., and Smith, A. M., *Analysis of Turbulent Boundary Layers*, Academic Press, NY, 1974.

[2] Baldwin, B. S., and Lomax, H., AIAA Paper 78-257, 1978.

[3] Yakhot, V., and Orzag, S. A., *Jour. of Scientific Computing*, Vol. 1, 1986, 1.

[4] Johnson, D. A., and King, L. S., *AIAA Journal*, Vol. 23, No. 11, 1985, 1684.

[5] Jones, W. P., and Launder B. E., *Int. Jour. of Heat and Mass Transfer*, Vol. 16, 1973, 1119.

[6] Wilcox, D. C., *AIAA Journal*, Vol. 26, No. 11, 1988, 1299.

[7] Baldwin, B. S., and Barth, T. J., NASA TM 102847, 1990.

[8] Spalart P. R., and Allmaras, S. R., AIAA Paper 92-0439, 1992.

[9] Menter, F. R., *AIAA Journal*, Vol. 30, No. 6, 1992, 1657.

[10] Menter, F. R., AIAA Paper 93–2906, 1993.

[11] McCroskey, W.J., NASA TM-81264, 1981.

[12] Ekaterinaris, J. A., Srinivasan, G. R., and McCroskey, J. W., 75th AGARD Meeting, 1994.

[13] Dindar, M., and Kaynak, U., AIAA Paper 92–0027, 1992.

[14] Wu, J.-C., Huff, D. L., and Sankar, L. N., *Journal of Aircraft*, Vol. 27, No. 4, 1990, 382.

[15] Ekaterinaris, J. A., and Platzer, M. F., ASME Paper 94–GT–206.

[16] Ekaterinaris, J. A., *AIAA Journal*, Vol. 33, No. 10, 1995, 1803.

[17] Piziali, R. A., NASA TM 4632 and USAATCOM Technical Report 94–A–011, 1994.

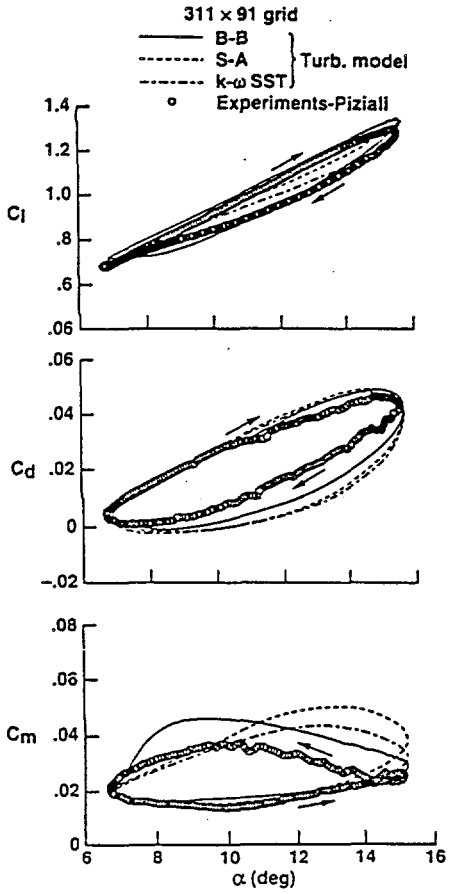

Fig. 1. Performance of one-equation and SST $k-\omega$ models for light stall; $k = 0.1$, $Re_c = 1.9 \times 10^6$.

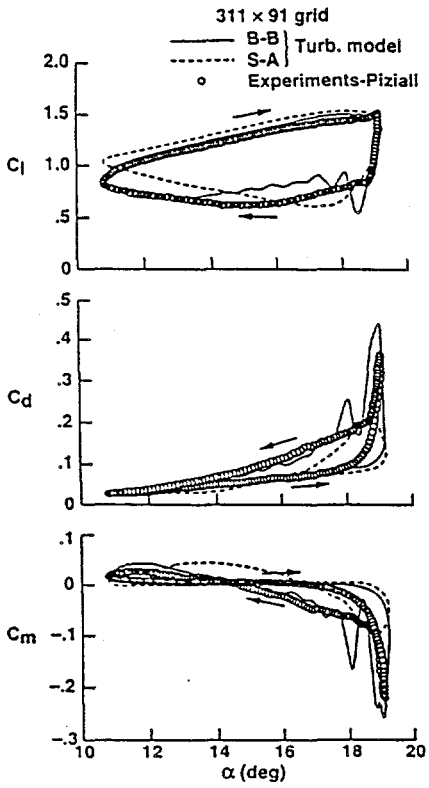

Fig. 2. Performance of the B-B, S-A models for deep stall; $k = 0.1$, $M_\infty = 0.3$, $Re_c = 1.9 \times 10^6$.

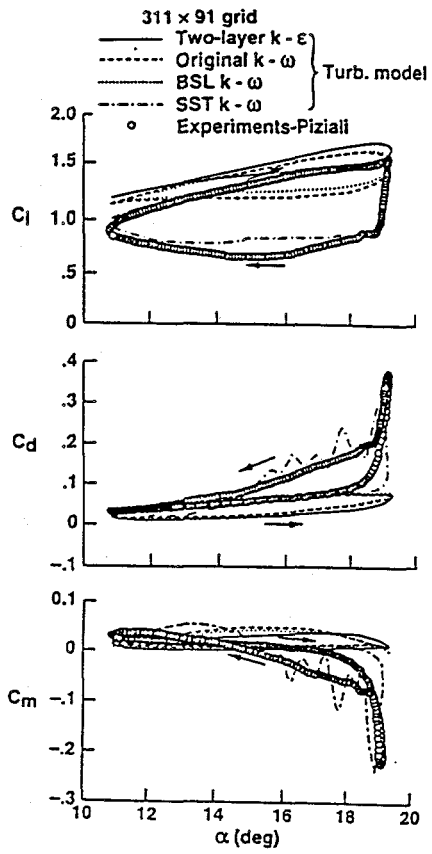

Fig. 3. Performance of two-equation models for deep stall; $k = 0.1$, $M_\infty = 0.3$, $Re_c = 1.9 \times 10^6$.

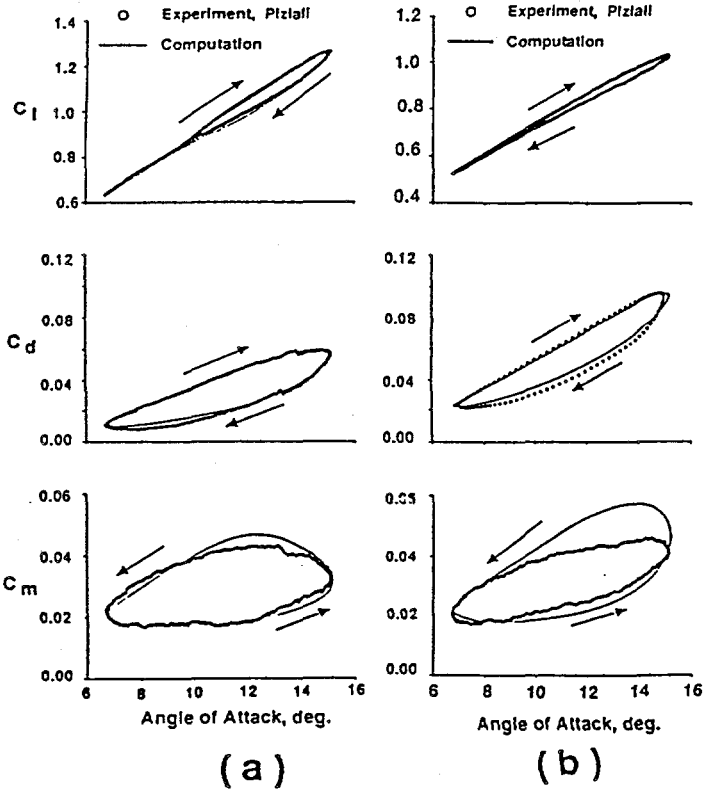

Fig. 4 Load comparison at a) y/s=0.47 and b) y/s = 0.80 span of blade at light stall; $k = 0.1$, $M_\infty = 0.3$, $Re_c = 1.9 \times 10^6$.

WIND TURBINE DESIGN CALCULATIONS
THE STATE OF THE ART

D C Quarton
Garrad Hassan and Partners Ltd
The Coach House, Folleigh Lane, Long Ashton, Bristol BS18 9JB, UK

F Rasmussen
Riso National Laboratory
P.O. Box 49, DK-4000 Roskilde, Denmark

C Nath, K Argyriadis
Germanischer Lloyd
Vorsetzen 32, D-204559 Hamburg, Germany

ABSTRACT: The sophistication of the methods used to carry out wind turbine design calculations has increased enormously over the last two decades. This paper traces the development of ever more sophisticated calculation methods and describes the state of the art. The paper concludes with a discussion of the remaining areas of uncertainty, the prospects for the reduction of those uncertainties and the likely future developments of wind turbine calculation methods.
Keywords: AERODYNAMICS, FLEXIBILITY, TURBULENCE, MODELS

1. INTRODUCTION

There is a common misconception amongst engineers working in other industries that wind turbines are simple devices. Nothing is further from the truth. The behaviour of a modern wind turbine is made up of a complex interaction of components and sub-systems and its design requires the skills of a multi-disciplinary team of engineers with expertise in diverse areas: atmospheric wind flow, rotor aerodynamics, control, mechanical systems, electrical systems and civil engineering. The design problem is particularly complicated since wind turbines have little respect for engineering conventions: the blade aerofoils are often required to operate in stall, the power train components are subject to highly irregular inputs and the number of fatigue cycles experienced by the major structural components can be orders of magnitude greater than for other rotating machines. Understanding the interactive behaviour of the various sub-systems which make up a wind turbine provides the key to reliable design calculations, optimised machine configurations and lower costs for wind generated electricity.

2. A BRIEF HISTORY

The sophistication of the methods used to carry out wind turbine design calculations has increased enormously over the last two decades. The development of ever more sophisticated calculation methods has been driven by a number of factors:

- **A gradual improvement in the understanding of the technology of wind turbine engineering.** This improved understanding has been enabled by the funding and execution of national and international research programmes followed by the dissemination of research results. Research workers have clearly played a vital role in the development and validation of mathematical models which provide reliable representations of both wind turbine behaviour and wind input. Validation of the mathematical models has been and clearly remains a crucial aspect of the wind turbine research programme and has depended on the availability of high quality measurements. A particularly important EU funded research project in this context was the "Wind Turbine Benchmark Exercise on Mechanical Loads" [1], completed in 1991.

- **The trend towards low cost, large scale wind turbines.** The pursuit of lower costs for wind generated electricity has driven manufacturers to less conservative, more optimised machine design at an increasingly large scale. In order to reduce design conservatism without increasing the risk of machine failure, the manufacturers require design calculation methods which are more reliable and less conservative than the simplistic approaches used in the early days of the industry.

- **The increasing power of computers.** Computer processing power and available memory have increased at a phenomenal rate over the twenty years that the modern wind turbine industry has existed. Using standard desk top PC hardware, it is now possible for a designer to make use of calculation methods and design software that would have been impossible using the computer hardware generally available in the early 1980's. The increased power and memory of computers, coupled with the possibilities for extremely user-friendly software environments, allows the wind turbine designer to undertake sophisticated design calculations in a straightforward and convenient manner.

- **Certification rules and design standards.** In northern Europe, particularly in Denmark, Germany and the Netherlands, certification of wind turbines has been required in order for manufacturers to obtain building permits and/or to become eligible for subsidy. The design rules issued by certification agencies have therefore had a direct influence on the methods used by manufacturers for their design calculations and procedures. In the early days of the industry the certification rules were based on simplified methods for calculating design loads. In recent times, as the understanding of wind turbine behaviour has improved and the size of machines has considerably increased, the certification agencies are demanding the use of more sophisticated design calculations.

  The recently developed international wind turbine safety standard IEC 1400-1 [2] specifies a minimum list of physical phenomena which shall be considered in design calculations. Representation of the phenomena specified in the standard requires a sophisticated treatment of wind turbine loading including, for example, realistic modelling of wind turbulence and unsteady aerodynamics. A problem yet to be resolved in the context of certification rules and design standards is that although safety factors are required to be used to account for uncertainty in the design calculations, there is no provision for such factors to be changed depending on the sophistication and reliability of the calculation method.

3. MODELLING OF WIND TURBINES

The behaviour of a wind turbine is made up of a complex interaction of components and sub-systems. The principal elements are the rotor, hub, power train, control system, nacelle structure, tower and foundations.

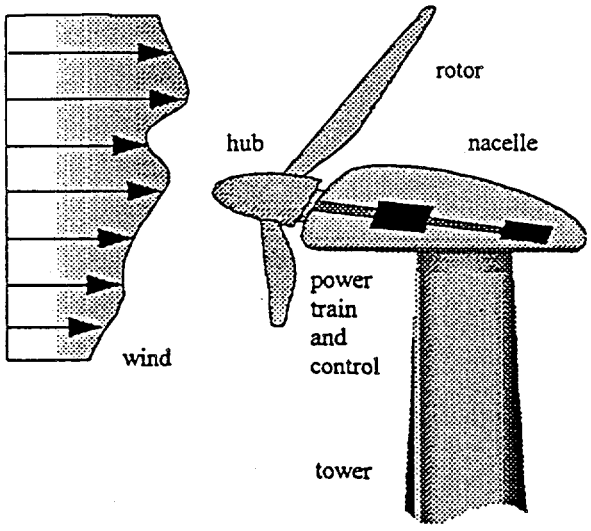

Figure 1: Wind turbine sub-systems

The external forcing is derived mainly from the aerodynamic loading of the rotor due to the incident wind field. Although early design calculations for wind turbines were often based on a highly simplified, quasi-steady treatment of the rotor aerodynamic loading coupled with some rudimentary means of estimating the appropriate dynamic magnification of loads for each machine component, such methods have now largely been discounted. A clear example of the trend away from such simplified calculation methods is provided by the recent amendment by Germanischer Lloyd of their Regulations for the Certification of Wind Energy Conversion Systems [3]. The amendment, issued in July 1995, states that the use of simplified calculations of fatigue load spectra is now acceptable only in the case of the single category of three-bladed rotors of less than 46m diameter.

Current wind turbine design calculation methods are almost invariably based on a rigorous treatment of the aeroelastic nature of the problem with proper account taken of aerodynamic, gravity, inertial, centrifugal and gyroscopic loads and the distributed stiffness properties of the structure. In common with random loading problems in many other fields of engineering, the analysis may, in principle, be carried out using frequency or time domain techniques.

The frequency domain approach to the calculation of structural response to random loading has firm foundations in both wind engineering and the analysis of wave loading of offshore structures. The method becomes complicated for a wind turbine because of the need to deal with the rotation of the rotor blades slicing through the turbulent structure of the incident wind field. This problem was first considered by Rosenbrock in the 1950's [4] and the method was subsequently developed by Madsen et al [5]. Garrad Hassan have more recently extended the frequency domain approach to include the combined effect of wind and wave loading of offshore wind turbines [6].

Although the frequency domain approach has the advantage that it provides for a very rapid analysis of wind turbine loading, it suffers from the major disadvantage that it cannot take account of system non-linearities associated, for example, with the rotor aerodynamics, structural dynamics and/or control system dynamics. For this reason in particular, the frequency domain approach is not currently used as the basis of wind turbine design calculations. The method is, nevertheless, regarded as being of research interest and potentially of some value in the very early stages of wind turbine design for optimisation studies.

The time domain approach to calculating the response of a system subject to some disturbance is termed simulation. Simulation is a widely used method and the techniques involved are well understood. Simulation forms the basis of all current, state of the art wind turbine design

calculations. The main features of the method are described below.

2.1 Wind field representation

Until relatively recently calculations of the loading and behaviour of wind turbines were based on grossly simplified models of the wind. It was common to assume a representation based on a steady wind speed, a constant power or logarithmic law model of wind shear, a constant yaw misalignment and a constant flow inclination. Although such input taken together with some representation of the tower shadow effect enables a satisfactory calculation of the periodic loading, it provides no basis for evaluating the random loads due to turbulence.

The importance of turbulent loading is now universally recognised. A model of the wind field suitable for design loading calculations requires good representation of both the temporal and spatial structure of the turbulence. Early models concentrated on representation of the longitudinal component of turbulence although it is now becoming common practice to base load calculations on a model of the three turbulent velocity components. A number of methods have been developed for the simulation of turbulent wind and a good review is presented by Powell and Connell [7]. All these methods use, as a starting point, auto-spectral and coherence descriptions of the turbulence. There are several such descriptions available with the most common being the von Karman [8] and Kaimal [9] spectral models. A more comprehensive model is that due to Mann [10] based on a representation of the spectral tensor of atmospheric surface layer turbulence.

Although current design standards and certification rules accept the use of standard spectral models of turbulence such as von Karman and Kaimal, see for example IEC 1400-1 [2], considerably more research is required in order to investigate their adequacy for a range of atmospheric stability conditions and for representation of the turbulence associated with flow over complex terrain and within wind farms. Work in this area has recently been carried out under the EU Joule programme [11, 12].

Turbulence models of the form described above are now widely used for the calculation of fatigue loads for design purposes. For calculation of extreme loads, however, it is standard practice to base calculations on deterministic descriptions of extreme wind conditions. Current design standards and certification rules specify extreme events in terms of discrete gusts, wind direction changes and wind shear transients. The form, amplitude and time period specified for these discrete events remain rather arbitrary and largely unvalidated. The development of more reliable methods for the evaluation of extreme design loads, based possibly on the use of probabilistic analysis, requires considerable effort but is crucially important in the context of refining wind turbine design analysis.

2.2 Rotor aerodynamics

The treatment of rotor aerodynamics which forms the basis of all current methods for the calculation of wind turbine design loads is combined blade element and momentum theory [13]. Two major extensions of this theory which have been researched through recent Joule projects include the development of dynamic wake and stall hysteresis models [14, 15]. These models, which attempt to deal with the unsteady nature of wind turbine rotor aerodynamics, are now considered as the state of the art and are generally incorporated in design calculations. In the case of stall hysteresis there are a number of different models available although there is certainly a dearth of reliable validation.

Stall delay on the inboard sections of rotor blades, due to three dimensional and rotational flow effects, has been widely confirmed by studies at both model and full scale, see for example Rasmussen [16]. A number of semi-empirical methods [17, 18] have been developed for correcting two dimensional aerofoil data to account for stall delay and such methods are widely used for the design analysis of stall regulated rotors.

Due to the complexity of the problem and despite the extensive research effort conducted in this area to date, the representation and to some extent the general understanding of aerodynamic stall on a rotating wind turbine blade remain poor, a rather extraordinary situation in view of the importance of stall regulation to the industry. The current uncertainty associated with stall aerodynamics has the effect of limiting the level of confidence that can be placed in design calculations of both steady and dynamic rotor performance and loading. The authors consider that the modelling of stall is the most significant inadequacy of current design calculation methods.

Research funding has been and continues to be used for the development of more sophisticated treatments of rotor aerodynamics. Such work includes the development of vortex methods and Navier Stokes codes. The first complete flow solution for a rotating wind turbine blade has been derived by Hansen and Sorensen [19] using a Navier Stokes code. This work represents a significant step forward providing an improved understanding of aerodynamic stall and offering within the foreseeable future a means of tuning semi-empirical models of the phenomenon.

2.3 Structural dynamics

In the early days of the industry, design loads were evaluated on the basis of quasi-static aerodynamic calculations with the effects of structural dynamics either ignored completely or included through the use of estimated dynamic magnification factors. From the late 1970's research workers began to consider more reliable methods of dynamic analysis and two basic approaches were considered: finite element representations and modal analysis. A review of the development of wind turbine dynamic modelling techniques is given by Garrad [20].

The traditional use of standard, commercial finite element analysis codes for dealing with problems of structural dynamics is problematic in the case of wind turbines. This is because of the gross movement of one component of the structure, the rotor, with respect to another, the tower. Standard finite element packages are only used to consider structures in which motion occurs about a mean undisplaced position although the application to the dynamic stability of periodic soultions of nonlinear systems is discussed in [21]. For this reason the finite element models of wind turbines which have been developed have been specially constructed to deal with the problem.

The form of wind turbine dynamic modelling most commonly used as the basis of design calculations is that involving a modal representation. This approach, borrowed from the helicopter industry, has the disadvantage that the model construction requires considerable algebraic manipulation in order to derive the system equations of motion, but the major advantage that it offers a reliable representation of the dynamics of a wind turbine with relatively few degrees of freedom. The number and type of modal degrees of freedom used to represent the dynamics of a particular wind turbine will clearly depend on the configuration and structural properties of the machine. Current, state of the art methods generally offer representation of blade bending modes in both flatwise and edgewise directions, rotor teeter, drive train torsion, tower bending in two directions, nacelle yaw and/or tower torsion.

At present, largely because of the very extensive computer processing requirements associated with the use of finite element models, the state of the art in the context of wind turbine dynamic modelling for design analysis is based squarely on the use of limited degree of freedom modal models. There are two factors which may change this situation: the trend towards very flexible wind turbine components exhibiting large deflections which cannot be modelled reliably by linear modal theory and the increasing power of computer hardware enabling the use of the finite element approach for design analysis.

In an attempt to determine the extent to which the modal representation of wind turbine dynamics remains valid in the context of a flexible machine design, Garrad Hassan have recently undertaken detailed measurements and computer modelling of the Carter 300 wind turbine. The design concept of the Carter 300 is markedly different from that of other wind turbines on the market incorporating significant structural flexibility in the major components of the machine.

It has been concluded from the work that the modal representation of the structural dynamics provides reliable predictions of the component loading for the operational wind turbine although it is probable that the approach may not be adequate as the basis for calculating the very large bending deflections of the rotor blades parked in very high wind speeds. Example results indicating the benefit of blade flexibility in reducing bending loads are shown below. The figure shows calculations of the blade root flatwise bending moment assuming a rigid unconed blade, a rigid blade with 6 degrees cone angle and a flexible blade. Also shown are measured 10 minute averages of the bending moment plotted against wind speed.

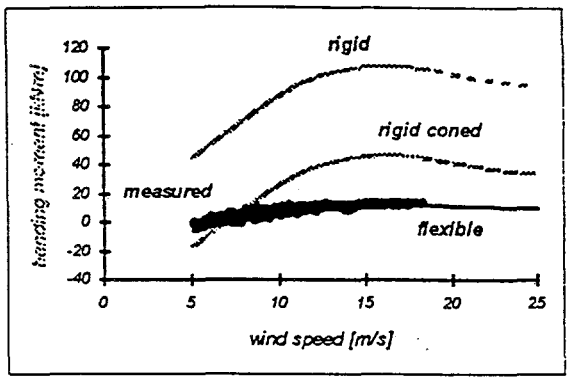

Figure 2: Carter 300 blade flatwise bending loads.

2.4 Power train and control system modelling

One of the most significant advances in the computer modelling of wind turbines for the calculation of design loads has been in the area of power train and control system modelling. Power train and control system designs have become increasingly sophisticated and it is widely understood that both have a major influence on the dynamic loading of major structural components. Current methods for design load calculations will generally take proper account of the power train dynamics and control system behaviour. A state of the art calculation code will include reliable representations of the following:

Transmission

- low speed and high speed shaft flexibility
- flexible mounting of the gearbox or transmission bedplate
- mechanical brake(s)

Electrical system

- induction and synchronous generators
- variable speed power electronics

Closed loop control

- fixed speed or variable speed control algorithms
- active pitch / active stall control algorithms
- transducer and actuator dynamics

Supervisory control

- machine start, stop, standby and safety system strategies

3. FROM RESEARCH CODES TO DESIGN TOOLS

It is evident that over the last twenty years the gradual development and validation of reliable mathematical models of wind turbine behaviour has been conducted largely by research organisations. The sophistication of the calculations carried out by the manufacturing industry has lagged behind these research activities. This state of affairs is quite normal and it is clearly the role of research organisations rather than manufacturers to undertake the fundamental work involved in the development of sophisticated analytical tools. It is, however, very important that the gap between the wind turbine modelling capabilities of the research organisations and the methods being used by manufacturers for machine design should not become too large.

Although the wind turbine designer clearly requires reliable, well validated calculation methods based on the sophisticated models developed by research organisations, he also has a number of other important requirements. For use as a design tool rather than a research code, a computer program for modelling wind turbine behaviour must have the following features:

- User friendly with convenient pre- and post-processing of data
- Capable of rapid design calculations on standard computer hardware
- Produces results of direct use for design and certification
- Well documented

It is a challenge to the research community who have been responsible for developing reliable wind turbine mathematical models that they should now develop software tools which meet these requirements and which are therefore suitable for use by designers. This process is well underway and there are already a number of computer programs which are now being used by manufacturers for design and certification calculations of wind turbines.

4. FUTURE DEVELOPMENTS

There are several aspects of the methods currently used for the design calculation of wind turbine performance and loading which require further research and development effort. The most important problem areas are considered below:

Wind field representation
Further research is required to investigate suitable models of the wind characteristics experienced by wind turbines operating in the following situations:

- In wake flow within wind farms
- On complex terrain sites
- In different conditions of atmospheric stability

A significant body of research has already been conducted in these areas and there is now a need to collate the various results available to develop wind flow models and guidelines appropriate for design purposes. Further measurements and data analysis will undoubtedly be required.

An area of great importance and significant uncertainty is that of the modelling of extreme wind conditions. Current design standards are based on rather arbitrary deterministic descriptions of extreme wind events and there is an urgent need for the validation of this approach or its replacement with alternative, probabilistic methods. At present the lack of measurements of extreme wind conditions is hindering the development of more reliable modelling techniques.

Rotor aerodynamics
Although there has been extensive research in this area, the general understanding of the development of aerodynamic stall on a rotating wind turbine remains poor and the modelling of stall is considered to be the most significant inadequacy of current design calculation methods. The present uncertainty results in poor confidence in the design calculations of performance and loading for stall regulated wind turbines.

Further concerted research effort is required to improve this situation. This effort should involve further analysis of existing measurements from stall regulated wind turbines and new measurements conducted in the wind tunnel and at full scale. The authors believe that the development of models of steady and dynamic stall, reliable across a range of aerofoil sections and rotor configurations, requires the continuation of the major research programme already underway in this area.

There are a number of other aspects of rotor aerodynamics which remain uncertain and which may become more important with the evolution of wind turbine design concepts. Two examples in this context are the aerodynamics of yawed rotors and highly deflected blades. These aspects of aerodynamic modelling will become more important if wind turbines are to incorporate more flexible blade structures and free yaw.

Structural dynamics
A trend towards increasingly lightweight and structurally flexible wind turbine designs will require the development and validation of appropriate dynamic models. The current generation of wind turbine research codes and design tools has received very little validation against measurements from flexible machines. Further research effort will be required in this context leading to design tools which can be used to undertake reliable calculations of the coupled modal properties, aeroelastic stability and loading of wind turbines with flexible components exhibiting large deflections.

5. CONCLUDING REMARKS

Over the last twenty years research workers have played a vital role in the development of mathematical models which can represent the behaviour of wind turbines. This work has involved extensive measurement and model validation activities and has been made possible through funding provided by national and international research programmes.

As confidence in the mathematical models developed by research organisations has grown, there has been increasing interest from wind turbine manufacturers wishing to make use of such models as the basis of their design calculations, replacing the simplistic design approaches of the early days of the industry. It is therefore a challenge to the research community that they should now develop software tools which offer reliable models of wind turbine behaviour but also provide the quality, robustness and ease of use required by the designers. This process is well underway and there are already a number of computer programs which originate from research and consultancy organisations and are now being used by manufacturers for design and certification of wind turbines.

It is anticipated that with the continuation of relevant research programmes and the increasing power of computers, the sophistication and reliability of the design calculations undertaken by wind turbine manufacturers will continue to improve. This trend can only help to reduce unnecessary design conservatism and lead towards lower costs for wind generated electricity.

REFERENCES

1. Van Grol H J at al, Wind turbine benchmark exercise on mechanical loads. Volume 1, part A and B. A state of the art report. ECN-C--91 -031, May 1991.

2. IEC 1400-1, Wind turbine generator systems - Part 1: Safety requirements, First edition, 1994-12.

3. Germanischer Lloyd, Rules and Regulations, IV - Non-Marine Technology, Part 1 - Wind Energy, Regulation for the Certification of Wind Energy Conversion Systems, 1993

4. Rosenbrock H H, Vibration and stability problems in large wind turbines having hinged blades, PhD thesis, ERA, 1955
a
5. Madsen P H et al, Dynamics and fatigue damage of wind turbine rotors during steady operation, Risø-R-512, 1984

6. Garrad A D et al, Study of offshore wind energy in the EC. Final report of Joule project. Contract JOUR-0072.

7. Powell D C and Connell J R, Review of wind simulation methods for horizontal axis wind turbine analysis. PNL-5903, Batelle Pacific Northwest Laboratory, June 1986

8. Engineering Sciences Data Unit, "Characteristics of atmospheric turbulence near the ground. Part II: Single point data for strong winds", ESDU 74031, 1974.

9. Kaimal J C et al, Minimising flow distortion errors in a sonic anemometer. Boundary Layer Meteorology, 53, 103-115.

10. Mann J, Models in micrometeorology, Riso-R-727(EN), March 1994.

11. Tindal A J et al, Dynamic Loads in Wind Farms, Final report on Joule Contract JOUR-0084-C, 1993

12. Adams B A, Dynamic Loads in Wind Farms II, Final report on Joule Contract JOU2-CT92-0094, 1996

13. Prandtl L and Tietjens O G, "Applied Hydro- and Aeromechanics", Dover Publications Inc., 1957.

14. Snel H and Schepers J G, Joint Investigation of Dynamic Inflow Effects and Implementation of an Engineering Method, 1995, ECN-C-94-107, Final Report on Joule Contract JOUR 0083

15. Rasmussen F R, Petersen J T, Winkelaar D and Rawlinson-Smith R I, Response of stall regulated wind turbines- Stall induced vibrations, Riso-R-691(EN), June 1993

16. Rasmussen F R et al, Investigation of the aerodynamics and structural dynamics of the Danwin 180 kW, Riso-M-2727, June 1983

17. Snel H et al, Sectional prediction of 3-D effects for stalled flow on rotating blades and comparison with measurements, ECWEC '93, Travemunde, March 1993

18. Rawlinson-Smith R I, Development of a three dimensional model of dynamic stall, European Union Wind Energy Conference, Gothenberg, May 1996

19. Hansen M O L, Michelsen J A and Sorensen N N, Navier Stokes solver for rotating wing, EWEC '94, Thessaloniki, October 1994.

20. Garrad A D, Dynamics of wind turbines, IEE Proc., Vol. 130, Pt. A, No. 9, December 1983.

21. Matthies H G and Nath Chr., Dynamic stability of periodic solutions of large nonlinear systems, Computer Methods in Applied M and Eng. 48 (1985) 191-202.

RESPONSE PREDICTIONS BY APPLICATION OF A NEW DYNAMIC STALL MODEL

Flemming Rasmussen, Jørgen Thirstrup Petersen, Helge Aagaard Madsen
Risø National Laboratory
Department of Meteorology and Wind Energy
The Test Station for Wind Turbines
4000 Roskilde, Denmark

Abstract
The development of suitable engineering dynamic stall models has been the objective of the JOULE-II project *Dynamic Stall and 3D-effects*. As part of this project, Risø has developed a new dynamic stall model, which is tuned to reproduce the open air blade section measurements performed at Risø as well as wind tunnel measurements. The paper describes the model and the effect on predicted turbine response for different parameter settings by application of the model in aeroelastic calculations. The dynamic stall model takes variations in both angle of attack and flow velocity into account and includes the unsteady aerodynamic effect of vibrations in both blade flapwise and edgewise direction. A parametric study reveals that the characteristics of the dynamic stall model and thus the real dynamic stall characteristics of the blades are very important for the occurrence of stall-induced vibrations.
Keywords: Dynamic Stall: Aeroelastic Stability: Stall Induced Vibrations: Blade Aerodynamics.

1 INTRODUCTION

Response predictions in stall and in particular the prediction of stall-induced vibrations is becoming a major subject with the development towards large, highly optimized wind turbines. It is widely recognized that response predictions in stall is the subject associated with most uncertainty in the wind turbine design process. It is also recognized that the airfoil unsteady aerodynamic characteristics are very important for the occurrence of stall-induced vibrations, and that models for the description of the dynamic stall phenomenon in particular are necessary to include as part of the aeroelastic calculations.

2 DYNAMIC STALL MODEL

The basic assumption is that the dynamic stall phenomina can be given a parametric representation. As described in more detail in [2] it is clear that from the potential flow equations for the unsteady force on a flat plate in simple harmonic motion in a pulsating stream, it follows that for the attached flow condition, the main parameters are the first and second derivatives of the angle of attack and the first derivative of the free stream velocity. From considerations based upon the unsteady *Bernoulli* equation, it follows that also in the separated flow condition the derivatives of the angle of attack and flow velocity are expected to be important parameters, however, with a different phase between independent and dependent parameters, compared to the attached flow condition. The arguments above leads to the assumption that the unsteady lift coefficient can be described in the following way:

$$C_L = C_{L,sta}(\alpha) + f(\alpha)\frac{c}{w}\frac{d\alpha}{dt} + g(\alpha)\left(\frac{c}{w}\right)^2\frac{d^2\alpha}{dt^2} + h(\alpha)\frac{c}{w^2}\frac{dw}{dt} \quad , \quad (1)$$

where f, g and h are functions representing the characteristics of the airfoil and the type of motion. $C_{L,sta}$ is the quasi-static lift coefficient, α is the angle of attack, c is the local chord length and w is the relative velocity. For a given set of data, i.e. variation of angle of attack and flow velocity, the functions are determined as second order polynominals within this interval by application of a systematic numerical optimization algorithm, such that the best fit between measurements and simulations is obtained. Equation (1) is written for C_L, and corresponding equations describe the drag- and pitching moment coefficients.

3 SIMULATION OF DYNAMIC TESTS

The model is intended to work as a reconstructor of unsteady airfoil data obtained from either experiment or in the future from *Navier-Stokes* simulations. However, it represents an efficient analysis tool for measured unsteady airfoil data as well. The functions f, g and h reflect the characteristics af the airfoil, the flow conditions (2-D or 3-D) and the type of motion. In this section the method will be used to analyse and model the measurements by Risø from a blade section of an operating wind turbine blade. Wind tunnel tests of a blade section in both pitch- and plunge motion (3-D) and different airfoils in pitch oscillation will also be analyzed and modelled using this model.

3.1 Open air blade section tests

The HAWT measurements have been performed on a segment of a LM 8.2 m blade of an operating 100 kW Tellus turbine at Risø, which has a rotor diameter of 19.0 m and rotates at 47.9 rpm. The inflow parameters, angle of attack and relative velocity, are measured close to the segment, which is at a radius of 6.475 m and has a chord of 0.734 m. The airfoil section at this point is approximately NACA 63216.

3.1.1 Estimated functions f, g and h

The HAWT measurements represent wind turbine operational conditions in which the angle of attack

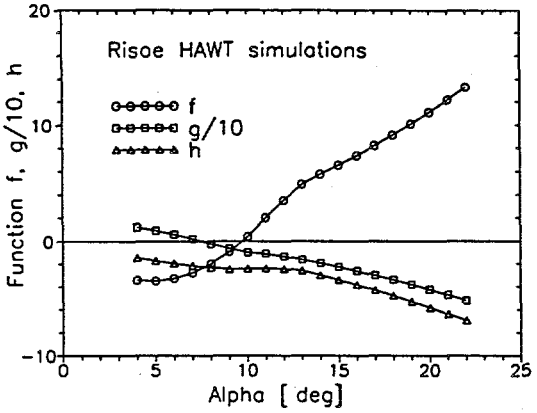

Figure 1: Estimated functions f, g and h.

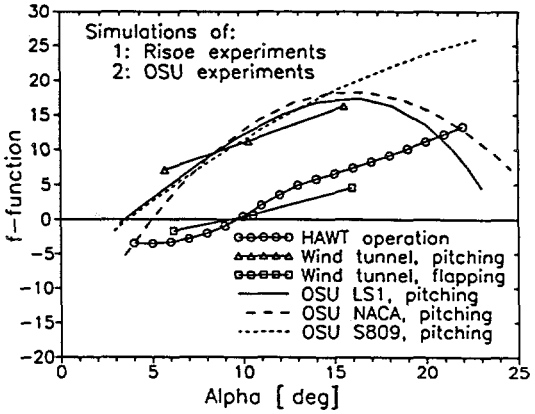

Figure 2: Experimentally estimated f-functions.

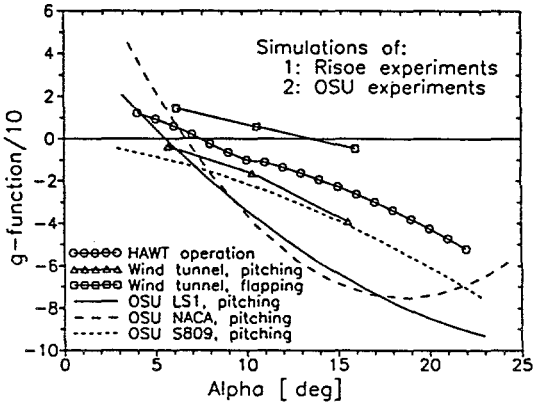

Figure 3: Experimentally estimated g-functions.

and the flow velocity vary. This allows for the determination of all three functions f, g and h by numerical optimization. The resulting functions are illustrated in Figure 1.

The f-function changes sign around 9 degrees corresponding to anti-clockwise hysteresis loops below this angle of attack and clockwise above. The g-function changes sign also around 9 degrees, corresponding to decreased loop slope below and increased above this value. The h-function is always negative and decreases with mean angle of attack.

3.2 Wind tunnel blade section tests

The LM 8.2 m blade has also been tested in wind tunnel for both pitching (around the 25% chord) and flapping (plunging) motion of the blade section.

The actual wind tunnel at Velux has a 4×4 m^2 half open test section. The blade was mounted horizontally and clamped via a roller bearing to a test rig. As the blade passes through the jet, the flow condition is three-dimensional.

Measurements of unsteady aerodynamic characteristics during pitch variations were obtained at nearly constant frequency around 1 and 2 Hz, respectively, and an amplitude around 5 degrees at different mean angles of attack. The tunnel wind speed during the pitch experiment was 29 m/s.

Measurements of unsteady aerodynamic characteristics during plunging motion of the airfoil section was obtained by oscillating the blade in the flapwise direction at the blade natural frequency (2 Hz). The activation was performed by hand at the free tip. The tunnel wind speed during this experiment was 18 m/s.

3.3 OSU wind tunnel tests

Three different wind turbine airfoil sections with a chord of 0.457 m have been tested in a 1.0×1.4 m^2 wind tunnel at Ohio State University [1]. These are LS(1)0421 MOD, NACA 4415 and SERI 809.

The tests were performed in two-dimensional flow in dynamic conditions obtained by pitching the airfoils around the 25% chord position at a mean angle of attack of 14 degrees and an amplitude of 10 degrees. The wind speed was 38 m/s. Dynamic stall events vere recorded at three different oscillation frequencies for each airfoil, approximately 0.6, 1.2 and 1.8 Hz.

Determination of the two functions f and g from the tests at different frequencies reflected that the representation of the frequency dependency by the model is adequate, in the actual frequency range.

3.4 Resulting functions f, g and h

The resulting f- and g-functions for all five pitching and flapping wind tunnel experiments are illustrated in Figures 2 and 3, respectively, together with the corresponding ones from the blade in wind turbine operational conditions.

It is clear that the f-functions for the LS1 and NACA 44 airfoils have the same shape and are rather close and somewhat different from the S809 airfoil. The same is valid for the g-function. This reflects that the measured dynamic stall characteristics of the S809 airfoil are somewhat different from those of the two other airfoils, which have nearly identical characteristics.

It is obvious that the f-functions for the pitching experiments have a mean value quite different from the flapping experiment, which is rather close to the

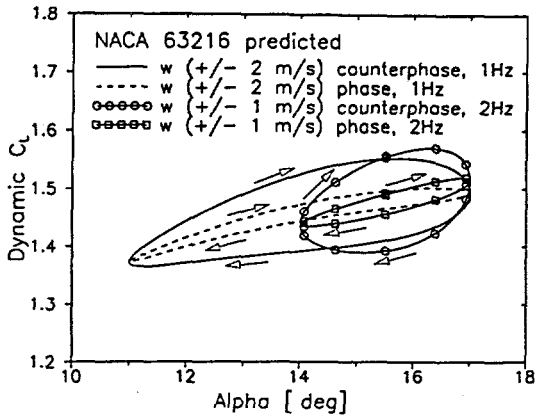

Figure 4: Simulated C_L-α-w loops for harmonic oscillation at 1 and 2 Hz.

results from wind turbine operation. However, the slopes of the three curves are in reasonable agreement. This reflects that there is a difference between pitching and plunging and that wind turbine operational conditions, as expected, correspond mostly to plunging.

The measurements are taken under quite different conditions with respect to e.g. wind speed, *Reynolds Number*, frequency, amplitude and airfoil type and motion, though within the relevant range with respect to wind turbine operation. In spite of this, the model reveals much consistancy in the results, and gives a quite good representation of all measured unsteady airfoil characteristics.

4 MODEL TESTS

For illustration purpose the model is run with a sinusoidal variation in angle of attack and relative velocity with different choices of relative phase. The functions f, g and h are chosen to correspond with those estimated from the wind turbine blade section measurements. The variation of angle of attack α and relative velocity w is described by:

$$\begin{aligned} \alpha &= \overline{\alpha} + \alpha_0 \sin(2\pi\nu t) \text{ and} \\ w &= \overline{w} + w_0 \sin(2\pi\nu t + \varphi) . \end{aligned} \quad (2)$$

Results are shown in Figure 4 for $\overline{w} = 36$ m/s and two different mean values of angle of attack, $\overline{\alpha} = 14$ degrees and $\overline{\alpha} = 15.5$ degrees, respectively. In the first case we have $\nu = 1$ Hz, $\alpha_0 = 3$ degrees and $w_0 = 2$ m/s, and in the second case $\nu = 2$ Hz, $\alpha_0 = 1.5$ degrees and $w_0 = 1$ m/s, corresponding to a doubling of the frequency and a halving of the amplitudes. In each of the two situations, the variations are considered either in phase, $\varphi = 0$, or in counterphase, $\varphi = \pi$.

From the figure it follows that when α and w are in counterphase (as will be the case for a turbine in yaw) the dynamic effect from α and w amplifies to give a large loop (large phase lead). However, when the two are in phase the effects are adverse, which can even result in anti-clockwise loops in the stall region. The higher the frequency, the higher the axis slope and opening of the loop.

Analysis of the effect of the three functions reveals that the f- and h-functions determines the opening of the loop while the g-function determines the change of the axis slope relative to the stationary lift curve slope. The more negative the value of g at a certain mean angle of attack the more the axis slope is increased.

5 AEROELASTIC SIMULATIONS

The fgh dynamic stall model has been implemented in the Risø aeroelastic code *HawC*, and simplified predictions of dynamic response have been performed on a turbine with representative 19 m blades with different parameter settings for the model. In order to investigate the criteria for the aerodynamic characteristics for the occurence of stall-induced vibrations, the focus is on the 2/3 radial station of the blade, which is most important for the blade aerodynamic damping. The structural characteristics of the blade are fully represented, however, aerodynamic loading is only active around the 2/3 radius, and zero elsewhere. This represents a conservative situation, as the aerodynamic damping is positive close to the tip due to the tip effect and at the inner sections of the blade due to the high angles of attack. The structural couplings to the turbine are also neglected.

The airfoil section at 2/3 radius has a chord of 1.08 m and rotates at 40 m/s in a constant wind field. The blade flapwise and edgewise natural frequencies are 2 and 3 Hz, respectively, and the blade is set into flapwise and edgewise vibrations from which the effective aerodynamic damping is calculated as the airfoil characteristics are varied.

An important general finding from this is that concerning the dynamic stall characteristics only the g-function is of importance for the aerodynamic damping. As previously stated the g-function determines the effective slope of the stall-hysteresis loops, while the f- and h-functions in combination determine the opening of the loops. This implies that – concerning the blade response – the g-function determines the vibrational activity at the natural frequencies, while the f- and h-functions determine the aerodynamic forcing.

Assuming steady airfoil characteristics corresponding to those for the NACA 4415 as measured at OSU, the aerodynamic damping in the flapwise and edgewise directions has been predicted at different wind speeds as function of the g-function. From this, the stability boundary has been determined, i.e. the value of g, which is necessary in order to create zero aerodynamic damping. This limit is illustrated in Figure 5, together with the actual g-functions, previously estimated from the dynamic stall measurements.

It is observed that positive aerodynamic damping is obtained for the NACA 4415 airfoil with the g-parameter estimated from the OSU pitching experiment, as this is below the limit for all angles of attack. However, from the previous findings, the g-function for a certain airfoil changes to a higher level, when going from pitching to plunging motion. This implies

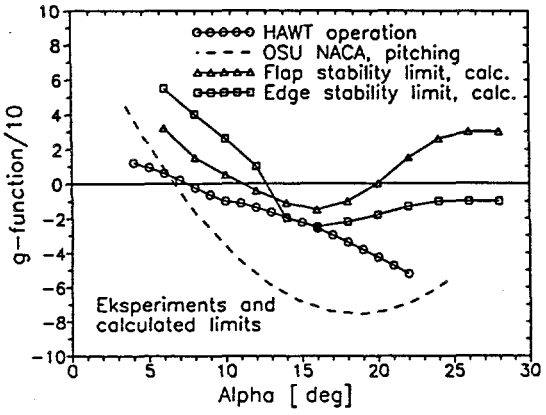

Figure 5: g-function corresponding to stability limit.

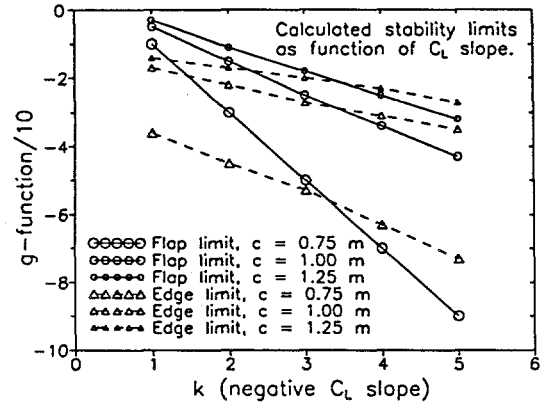

Figure 6: g stability limit for different slopes of quasi-static profile coefficient curves.

that the g-function, or in general the dynamic stall characteristics of an airfoil, should be determined from plunging motion in order to be applicable for the prediction of the occurrence of stall induced vibrations.

Further parametric studies are focused on the relative importance of the chord, the static lift curve slope and the g-function value in stall at a particular operational condition corresponding to 17.5 degrees angle of attack ($\alpha_0 = 0.305$ in Equation (3) below). The lift- and drag coefficients are described by the linear expressions

$$\begin{aligned} C_L &= 1.1 - k(\alpha - \alpha_0) \\ C_D &= 0.12 + (\alpha - \alpha_0)\,. \end{aligned} \qquad (3)$$

The limiting value of the g-function corresponding to zero aerodynamic damping in either edgewise or flapwise direction has been estimated with the lift curve slope (k) and the chord (c) as a parameter. The limiting g-value is shown in Figure 6 as a function of k.

The figure shows that with increasing negative lift curve slope the demand on the value of g – in order to obtain stability – is increasing. Further important is that the aerodynamic stability margin is dependent on the chord squared.

6 EFFECT OF SCALE

It was shown in [3] that for structurally and aerodynamically similar rotors there is no effect of scale on the blade modal damping coefficient, except for second order effects as *Reynolds Number* and 3-D effects. This means that the sensitivity to stall induced vibrations is independent of rotor size. The unsteady aerodynamic damping determined by the g-function from Equation (1) is proportional to $(c/w)^2$ and the blade natural frequency squared. This means that the decreased unsteady aerodynamic damping associated with a development towards higher tip speed and slender blades should be compensated by a corresponding relative increase in blade natural frequencies, assuming similar mode shapes, or airfoils with better aerodynamic damping characteristics, i.e. more negative g-functions.

7 CONCLUSIONS

A new dynamic stall model has been developed and applied for parametric studies of the aerodynamic damping of airfoils. The following conclusions can be drawn:

- The dynamic stall model gives a consistent description of different experiments.
- The flow acceleration parameter is important for the aerodynamic loading of wind turbines.
- Plunging experiments (or pitching around 3/4 chord) should be the basis for determination of parameters for wind turbine simulations.
- Only the g- function is important for the unsteady aerodynamic damping, i.e. the effective slope.
- The sensitivity to stall-induced vibrations is independent of rotor size.
- Development towards high tip speed and slender blades increases sensitivity to stall-induced vibrations.
- It is possible to obtain absolute stability within relevant tip speed limits by application of airfoils with proper damping characteristics.

REFERENCES

[1] Hoffmann, M.J., Ramsay, R.R. and Gregorek, G.M. (1994). *Unsteady Aerodynamic Performance of Wind Turbine Airfoils.* Proceedings of AWEA WindPower '94, Minneapolis, Minnesota.

[2] Rasmussen, F. (1994). *Dynamic Stall of a Wind Turbine Blade Section.* Proceedings of IEA-meeting on Aerodynamics, Technical University of Denmark, Lyngby, Denmark.

[3] Rasmussen, F., Petersen, J.T., Winkelaar, D. and Rawlinson-Smith, R. (1993). *Response of Stall Regulated Wind Turbines - Stall Induced Vibrations.* Risø-R-691(EN). Risø National Laboratory, Roskilde, Denmark.

WIND FIELDS IN WAKES

Gunner C. Larsen, Jørgen Højstrup and Helge Aagaard Madsen
Department of Meteorology and Wind Energy
Risø National Laboratory
DK–4000 Roskilde, Denmark

ABSTRACT: An approximative method is presented for the analysis of the flow field in a *single* wake. The method comprises an analytical description of the *mean velocity wake deficit* (strength, extension) and a cost–efficient numerical procedure for determination of the *turbulence spectrum*. Whereas other simplified wake turbulence descriptions are often based on decaying turbulence generated in the rotor plane, the present model assumes that the dominating part of the turbulence downstream is associated with the shear layer introduced with the wake deficit. The performance of the model is compared with measurements and with the results from a more complex model based on a CFD solution of an actuator disc flow. Finally, a simple empirical *engineering* method, describing the spectrum of the *wake turbulence field*, is introduced. The model predictions are compared with measurements and with the predictions from the numerical method.
Keywords: Wakes; Wind Speed; Turbulence; Numerical Methods

1 INTRODUCTION

An increasing part of the wind turbines will be erected in wind farms in the future due to the diverted reduction in grid costs, the limited number of sites with optimal wind potential, and environmental requirements. Therefore, prediction of both performance and wind induced loads in wind farms is of vital importance, and consequently the wind climate in such farms becomes of interest. The present paper concerns the wind field in the wake of a single wind turbine.

2 SIMPLE WAKE MODEL

The wake description is composed of a closed form solution of the *mean velocity wake deficit* (strength, extension) and a cost–efficient numerical procedure for determination of the *turbulence spectrum* based on the shear layer introduced with the wake deficit.

2.1 Mean Wind Field

Neglecting the blocking effect originating from the ground, the wake behind a wind turbine is considered a free turbulence region. Problems involving free turbulence are often of the same nature as boundary layer problems in the sence that the size of the free turbulence region in the direction perpendicular to the mean flow is considerably smaller than the size in the mean flow direction [3]. The model is thus based on the *presumption* that the wake region can be adequately described by Prandtl's turbulent boundary layer equations (large Reynolds numbers *assumed*). Further, considering wind shear and thermal effects as second order effects, the incompressible and stationary rotational symmetric problem is expressed by [1], [2]

$$\frac{\partial}{\partial x}(u_x r) + \frac{\partial}{\partial r}(u_r r) = 0\,, \tag{1}$$

$$(U_\infty + u_x)\frac{\partial u_x}{\partial x} + u_r \frac{\partial u_x}{\partial r} = \frac{1}{r}\frac{\partial}{\partial r}\left[l^2 r \left(\frac{\partial u_x}{\partial r}\right)^2\right]\,, \tag{2}$$

where the axial and radial directions are denoted by x and r, respectively, and the mean velocities in the wake are $U_\infty + u_x$ and u_r. The Reynolds stresses have been expressed in terms of Prandtl's mixing length theory, where l is the mixing length (which in general vary from point to point). *Assuming* that, for large Reynolds' numbers, the velocities in sections perpendicular to the direction of the undisturbed flow are geometrically and mechanically similar, the local wake radius is proportional to x^n and the velocity deficit is given by

$$u_x \equiv x^m g\left(\frac{r}{kx^n}\right) \equiv x^m f(\frac{r}{x^n})\,, \tag{3}$$

where k is a proportionality constant. *Presuming* u_x to be small compared with U_∞, it can be shown that $n = \frac{1}{3}$ and $m = -\frac{2}{3}$. Introducing this in the equation of motion and retaining only the dominating terms, the local wake radius R_w, and the induced wake velocities u_x and u_r can be determined ([1], [2]) as

$$R_w = \left(\frac{35}{2\pi}\right)^{\frac{1}{5}} (3c_1^2)^{\frac{1}{5}} (c_w A x)^{\frac{1}{3}}\,, \tag{4}$$

$$u_x = -\frac{U_\infty}{9}\left(c_w A x^{-2}\right)^{\frac{1}{3}} \left\{ r^{\frac{3}{2}} (3c_1^2 c_w A x)^{-\frac{1}{2}} - \left(\frac{35}{2\pi}\right)^{\frac{3}{10}} (3c_1^2)^{-\frac{1}{5}} \right\}^2 \tag{5}$$

$$u_r = \frac{U_\infty}{3}(c_w A)^{\frac{1}{3}} x^{-\frac{5}{3}} r \left\{ r^{\frac{3}{2}} (3c_1^2 c_w A x)^{-\frac{1}{2}} - \left(\frac{35}{2\pi}\right)^{\frac{3}{10}} (3c_1^2)^{-\frac{1}{5}} \right\}^2 \tag{6}$$

where A is the rotor area, c_w denotes the rotor drag coefficient, and c_1 is the non–dimensional mixing length defined by

$$c_1 = l(c_w A x)^{-\frac{1}{3}}\,. \tag{7}$$

This expression separates to some degree the rotor specific drag dependance, and c_1 is consequently expected to be relatively insensitive to both the size and the design of the rotor.
For a given rotor, the drag coefficient is obtained either from measurements or from a simple aerodynamic calculation. With c_w determined, the solution contains two parameters which have to be evaluated from boundary conditions – one is the position of the rotor relative to the applied coordinate system, and the second is the non–dimensional mixing length c_1.
The first boundary condition to be satisfied is that the wake radius at the rotor position equals the rotor radius. The second boundary condition is an empirical relationship stating that the wake radius at 9.5 rotor diameters distance from the turbine is determined by $1.08D + 21.7D(I - 0.05); 0.05 \leq I \leq 0.15$, where D and I denotes the rotor diameter and the ambient turbulence intensity, respectively. The empirical relation is based partly on analyses of the Vindeby experiment, where the wake radius showed up to be approximately independent of the undisturbed wind speed, and partly on example calculations in the far field with the Lissaman model [4], showing the wake extension to be primarily related to the *ambient* turbulence level. The *assumed* linear relationship between wake expansion and ambient turbulence intensity is also in accordance with the definition of the wake decay constant in the PARK program [6].

2.2 Turbulence

Downstream of an operating wind turbine we see increased turbulence levels. Away from the near–field of the wake the dominating mechanism will be an augmentation of the shear–produced turbulence originating from the increased windshear.

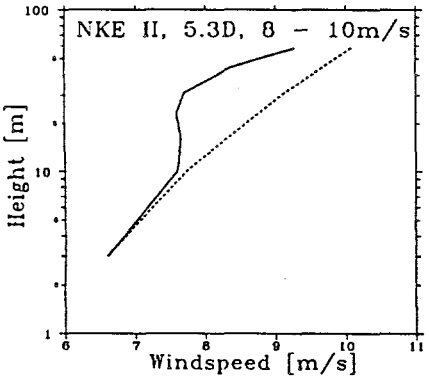

Figure 1: Wind profiles from the Nørrekær Enge wind farm, undisturbed upstream (dashed line) and 5.3 rotor diameters downstream of the windturbine (full line). Wind speeds were selected in the range 8-10 m/s, in a $\pm 5°$ sector around the nominal wake centerline. A total of about 20 hours of data were used.

From Fig. 1 (representing approx. 20 hours of data from the Nørrekær Enge II windfarm [8], [9]) we can see that the windprofile can be described as being in four regimes covering different height ranges:

- Near the ground the wind profile is not influenced by the wake
- From 10–30 m we observe a reduced shear
- Above 30 m (hubheight 31 m) the shear is very much increased
- At some level above the upper measurement point the wind speed will revert to the upstream value. By a rough extrapolation this takes place at 70–80 m

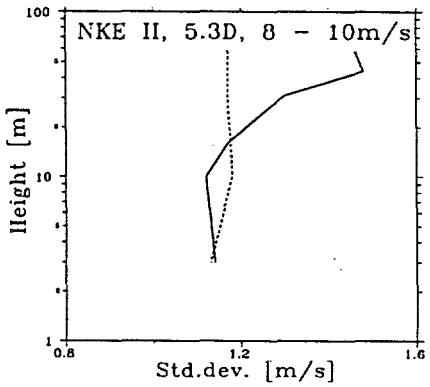

Figure 2: As Fig. 1 but profiles of standard deviations of wind speed fluctuations measured by fast response cup anemometers.

We can clearly see the results of the increased shear in Fig. 2 showing the standard deviations of windspeed fluctuations, in the wake and in the undisturbed upstream flow. The extra turbulence in the wake will be expected to occur at scales comparable to the dimensions of the region affected by the increased shear. As this typically is of the order of the rotor diameter, which is close to the hubheight, we get more turbulence at scales that are considerably smaller than the length scales of the undisturbed turbulence, pushing the resulting length scale of the turbulence in the wake towards shorter scales as can be seen in Fig. 3.

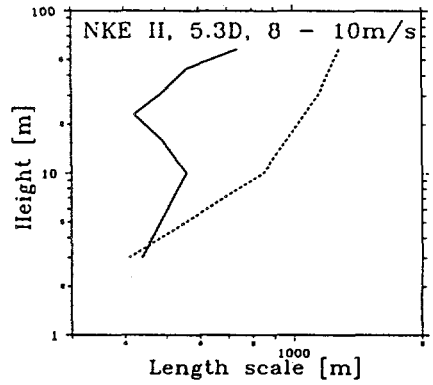

Figure 3: As Fig. 1 but profiles of length scales obtained from velocity spectra.

The turbulence in the wake is not in equilibrium; there are strong crosswind and vertical inhomogeneities in

the flow, and somewhat weaker downstream inhomogeneities, meaning that the usually applied equilibrium expressions connecting the wind shear with the turbulence level, do not apply here. Instead, we have attempted to model the behaviour of the turbulence in the wake in a more *basic* manner.

We observe an air parcel moving up and down over a height range L_i. As the air parcel moves, it will experience changes in windspeed, translating to an average shear for the scale in question. We use the average shear to calculate the contribution to the total spectrum at the length scale L_i (or frequency $f_i = u/L_i$, where u is the average windspeed). For a vertical motion at a different scale, we will see a different average wind shear corresponding to the production of turbulent kinetic energy at that scale. Each scale contributes to the total spectrum in a certain bandwidth, and the total spectrum consists of the sum of all of the individual contributions. The model will reproduce a Kaimal spectrum for the undisturbed logarithmic windprofile. So observing Fig. 1, we see that at hub height, the shear is very small for small scales, and somewhat larger for larger scales. The complete model will be reported elsewhere (see also Fig. 5).

2.3 Model Performance

The basic *model assumptions* for the simplified mean field evaluation are analysed by representing the rotor as an actuator disc and solving the unsteady, incompressible Navier–Stokes (NS) equations in the rotational symmetric situation with the general purpose NS code FIDAP [7]. The pressure term, which was neglected in the simplified formulation, controls the velocity deficit close to the rotor. Therefore, and because of the asymptotic character of the simple model in general, some deviation between the model predictions close to the rotor plane is a priori expected. However, at longer distances the shear stresses dominate the wake development and comparable results should be expected.

In the NS–solution the Reynolds stresses are represented by a k–ϵ model. The ambient turbulence is modelled by specifying the required amount of kinetic turbulent energy at the grid boundary 6 rotor diameters upstream of the rotor plane. The turbulence associated with the wake shear is generated with the formation of the wake mean velocity deficit. Two situations, corresponding to the Vindeby turbines operating at 6 m/s and at 10 m/s (both with an ambient turbulence level equal to 7.5 %), have been analysed with correct thrust distribution along the actuator disc radius coordinate as predicted by a blade element calculation.

We investigated the form of the deficit profiles at different positions downstream from the rotor plane, and found that the *similarity* assumption is a good approximation at down stream distances larger that 10 rotor diameters from the rotor plane. However, as the ambient turbulence in the present NS–formulation decreases with increasing distance to the upstream grid boundary where it is specified, because the mean wind velocity shear is absent within the rotational symmetric formulation, a somewhat slower transition between the pressure dominated region and the shear dominated region is expected compared to experimental conditions. Consequently, the similarity assumption is expected to describe the physical wake even closer to the rotor plane than predicted by the simulation.

Finally, the *decay* of the deficit in the wake center has been investigated, and at distances larger than approximately 10 rotor diameters from the rotor plane good agreement between the NS solution and the $-2/3$–decay in the simple formulation has been found (conservative as with similarity).

The deficit, determined from the closed form solution, is compared with single wake measurements from the Vindeby experiment in Fig. 4. The measurements refer to neutral atmospheric stratification, and the comparison is performed for the (undisturbed) mean wind velocities 6 m/s and 10 m /s, respectively.

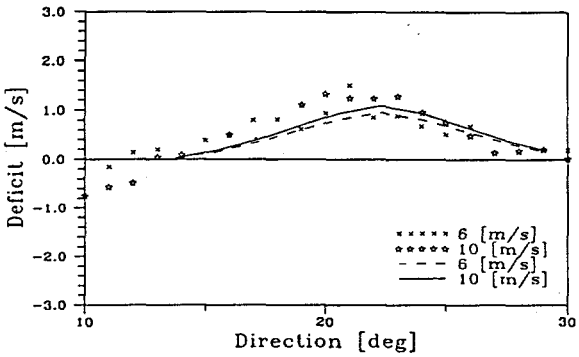

Figure 4: Measured and calculated horizontal deficits at hub height. Measurements are identified by symbols, whereas predictions are represented by lines.

The measurements indicate only a minor difference in the deficit levels corresponding to the investigated undisturbed mean wind velocities. This is also reflected in the predictions. Considering the variability in the measurements, we find the agreement satisfactory, however, with a slight tendency towards underprediction. The measured speed-up effect between directions 10° and 13° originates from flow passage between two neighbouring turbines.

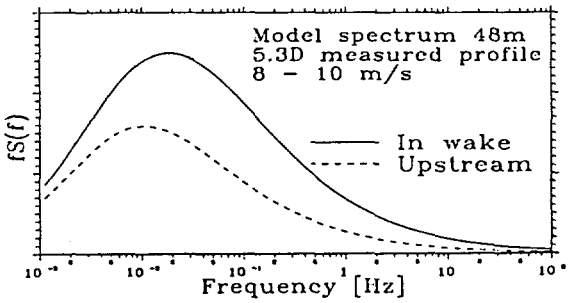

Figure 5: Model spectra for the profile of Fig. 1 at 48 m height.

A preliminary result from the simple model of the tur-

bulence spectrum is shown in Fig. 5, using the wind-profile in Fig. 1.
The modelled velocity spectra reproduces the observed properties – increased turbulence level and a shift towards higher frequencies of the peak of the spectrum. The shift in the frequency peak is of the same order of magnitude as it appears from Fig. 3.

3 ENGINEERING TURBULENCE

The basic *assumptions* of the present empirical approach are that the turbulent wind climate in a wind farm is dominated by the closest upstream wind turbine, and that it is properly described by adjusting the spectrum parameters related to a traditional description of the ambient turbulence in flat homogeneous terrain. Thus, the qualitative characteristics of the turbulence are *presumed* to be preserved, and the wind farm effects are condensed in a suitable modification of only two parameters – turbulence intensity and turbulence length scale.

3.1 Turbulence Intensity

The turbulence field behind a wind turbine rotor originates from different sources – viscous rotor drag, surface shear, and wake shear. The scale of the rotor drag generated turbulence is small compared with the two other contributions, and hence its lifetime is relatively short. Thus, at down stream distances corresponding to traditional spacing in wind farms it is *assumed* that only the surface– and wake shear mechanisms contribute significantly. It is moreover *assumed* that the turbulence fluctuations originating from these two sources are *statistically independent* such that the turbulent energies are additive in the energy sense. Normalizing with respect to the undisturbed mean wind velocity, the total turbulence intensity in the wake, I_{tot}, is expressed as

$$I_{tot} = \sqrt{I_a^2 + I_w^2}\,, \tag{8}$$

where subscripts a and w refer to ambient and wake, respectively. The wake contribution, I_w, depends on both the down wind distance and the undisturbed mean wind velocity. The functional form is *presumed* to be of the form

$$I_w = f(S)g(U_\infty)\,, \tag{9}$$

where S denotes the spacing expressed in rotor diameters, and U_∞ is the undisturbed mean wind velocity. Inspired by a Boussinesq K–model representation [5] of shear generated turbulence, by a Bernoulli representation of an idealised rotor and by the first order wake model presented in section 2, the following functional form is proposed ($S \geq 1$)

$$I_w = K(DS)^{-1/3}\sqrt{1 - \sqrt{1 - \frac{2T}{\rho A U_\infty^2}}}\,, \tag{10}$$

where K is a constant, T is the rotor thrust, ρ is the mass mass density of air, D is the rotor diameter, and A is the rotor area. Calibrating the expression to the Vindeby– and Nørrekær Enge experiments, by a least square fit, we obtained $K = 0.93$.
The proposed model has the correct qualitative– and asymptotic features as I_w increases for increasing T, decreases for increasing U_∞ and S, and tends to zero for S approaching infinity.
The above expression for the turbulence intensity refers to the upper rotor boundary which is usually close to the position where the intensity takes its maximum value. Therefore a simulated turbulence field, specified with this turbulence intensity, will tend to be conservative in terms of fatigue life consumption of a turbine erected in that field.

3.2 Turbulence Length Scale

When the two shear turbulence contributions have scales of comparable orders of magnitude, it is reasonable to expect the resulting spectral shape to be qualitatively invariant. However, the resulting length scale is modified. The modified length scale depends on the rotor thrust coefficient, the spacing distance, the rotor diameter, and the undisturbed turbulence length scale. *Assuming* an approximate linear relationship between thrust coefficient and mean wind speed (for a stall controlled turbine), the following empirical relation is proposed for the length scale inside the wake

$$L_w = L_\infty\left(1 - \frac{12.2\left(1 - \frac{D}{L_\infty}\right)}{U_\infty S_r^{0.6}}\right)\,, \tag{11}$$

where L_∞ is the turbulence length scale in the undisturbed flow, and the reduced spacing, S_r, between the turbines is defines as

$$S_r = 2^{0.8} + (S-2)^{0.8} \qquad \text{for } S \geq 2\,. \tag{12}$$

The undisturbed length scale and the resulting wake length scale refer to hub height. L_w is seen to be monotone in U_∞, L_∞, S_r, and D. However, the dependence on D is not pronounced for the usual size of wind turbines. For large turbine spacings or for large mean wind speeds, L_w tends to approximate L_∞, and the expression thus exhibit the correct asymptotic behaviour.

3.3 Model Performance

In Tabel I, the empirical determined turbulence intensities ($I_{tot,e}$) are compared to measurements from the Vindeby– and the Nørrekær Enge wind farms ($I_{tot,m}$). The measured data reflects different spacing, mean wind velocities, turbines and ambient turbulence intensities.
The agreement between the empirical predictions and the measurements is satisfactory, and comparisons show that the present predictions are marginally less conservative than predictions based on the Danish Recommendation (DR) and, contrary to DR, the present model allows for a distinction between pitch– and stall controlled turbines.

Table I: Comparisons between measured- and empirical determined turbulence intensities. U_∞ and D are given in $[m/s]$ and in $[m]$, respectively.

U_∞	S	D	c_w	I_a	$I_{tot,m}$	$I_{tot,e}$
9.9	2	28	0.67	0.140	0.165	0.211
7.3	5.3	28	0.76	0.119	0.162	0.173
11.5	5.3	28	0.59	0.137	0.175	0.173
11.1	8.5	35	0.52	0.068	0.110	0.103
10.0	9.5	35	0.57	0.072	0.113	0.106

In Tabel II, the empirical determined turbulence length scales (L_{we}) are compared to measurements from the Vindeby- and the Nørrekær Enge wind farms (L_w). The measured data are related to neutral atmospheric conditions and reflect different spacing, mean wind velocities, rotor size, and undisturbed length scales.

Table II: Comparisons between measured- and empirical determined turbulence length scales. U_∞ is given in $[m/s]$, and all the length quantities are given in $[m]$.

U_∞	S	D	L_∞	L_w	L_{we}
9.9	2	28	1070	140	149
7.3	5.3	28	1052	359	343
11.5	5.3	28	1363	788	776
9	8.5	35	940	505	530

Considering the considerable uncertainty related to the determination of length scales in general, and the insensitivity of turbine fatigue loads to *moderate* variations in the length scale in particular, we find the agreement in the present investigation fully satisfactory. Note, that the 8.5 D situation refers to a multi wake situation – however this is not expected to effect the length scale reduction substantially, compared to a single wake situation, as the spacing in the present windfarm is large.
The empirical expression for the wake turbulence length scale is based on analyses of wakes behind stall regulated turbines. However, due to the comparable decrease in thrust for a pitch regulated machine, the model can be applied conservatively to pitch regulated turbines as well.

4 CONCLUSION

A set of simple algorithms has been proposed for a *detailed prediction* of the wind field in a single wake. The mean velocity deficit field as well as the shear generated wake turbulence spectra are provided, and good correlation with available experiments, performed at Vindeby- and at Nørrekær Enge wind farms, has been demonstrated.
Aeroelastic calculations are often based on turbulence simulations from parameterized standard type power density spectra (code requirements). Therefore, based on analyses of data from wind farm experiments, a set of *empirical relations* providing the relevant parameters (turbulence intensity as well as the turbulence length scale) for the turbulence field in a wake is derived. The expressions are applicable for both stall- and pitch regulated turbines – however, the length scale modification related to pitch regulated turbines in the high wind regime is expected to be somewhat conservative.

REFERENCES

[1] Larsen, G.C. (1988) : A Simple Wake Calculation Procedure, Risø–M–2760.

[2] Swain, L.M. (1929). On the Turbulente Wake behind a Body of Revolution. Proc. Roy. Soc. London A 125., p.647–659.

[3] Schlichting, H. (1968). Boundary–Layer Theory. McGraw–Hill Book Company.

[4] Lissaman, P.B.S., Gyatt, G.W., and Zalay, A.D. (1981). Numeric Modeling Sensitivity Analysis of the Performance of Wind Turbine Arrays. Batelle Pacific Northwest Laboratories, Richland, Washington.

[5] Zbigniew, S. (1989). Structure of the Atmospheric Boundary Layer. Prentice Hall Advanced Reference Series.

[6] Sanderhof, P. (1993). PARK – User's Guide. Risø–I–668(EN).

[7] FIDAP 7.0 Theory Manual (1993). Fluid Dynamics International, Inc..

[8] Højstrup, H., Courtney, M.S., and Sanderhof, P. (1991). Measurements of Structural Loads in the Nørrekær Enge Wind Farm. Proceedings of the EWEC '91, Amsterdam, October 1991. Ed. by Van Hulle, F.J.L., Smulders, P.T., and Dragt, J.B.

[9] Højstrup, H., Courtney, M.S., Christensen, C.J., and Sanderhof, P. (1993). Full Scale Measurements in Wind Turbine Arrays. Nørrekær Enge II. CEC/JOULE. Risø–I–684. 58 pp.

DATABASE ON WIND CHARACTERISTICS

Jørgen Højstrup
Department of Meteorology and Wind Energy
Risø National Laboratory
DK4000 Roskilde, DENMARK

Kurt S. Hansen
Department of Energy Engineering
Fluid Mechanics Section
Bld. 404, DTU
DK2800 Lyngby, DENMARK

ABSTRACT: Wind data with high temporal resolution exist from a variety of sites, and have been in demand by windturbine designers and wind engineers. Unfortunately it has always been a problem to gain access to a suitable amount of this data, because they are available from many different sources in different formats and with very different levels of documentation and quality control. We are in the process of gaining access to a large amount of this data, checking the quality of the data and putting the data at the disposition of the windturbine designer community through easy Internet access. Online search will use summary statistics calculated for each series to help in the selection of data. The selected data can then be downloaded directly to the user.
Keywords: Data Bases: Turbulence: Wind Flow Measurements: Load

1. INTRODUCTION

Wind data with high temporal resolution exist from a variety of sites, and have been in demand by windturbine designers and wind engineers to be used as input for load models. Unfortunately it has always been a problem to gain access to a suitable amount of this data, because they are available from many different sources in different formats and with very different levels of documentation and quality control. It was often in the past discussed how to make it possible to use some of the vast amount of data that we all know exist. Now the technical developments in data storage and data transmission have made it possible to achieve this goal within a reasonable price.

We are in the process of gaining access to a large amount of such data, checking the quality of the data and putting the data at the disposition of the windturbine designer community through easy Internet access to a large database. Our aim is to provide online search, using summary statistics calculated for each series to help in the selection of data. The selected data can then be downloaded directly to the user or put on CDROM's and sent by mail in the case of large amounts of data.

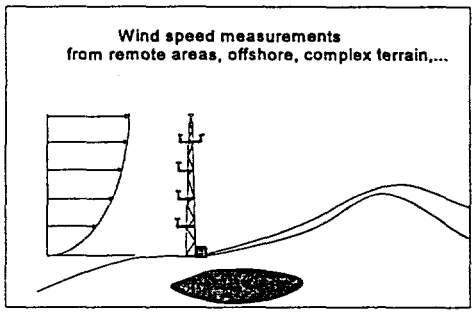

Figure 1 Wind data from many different site types will be included in the database.

2. OBJECTIVES

The objectives of this project are

- to build a database consisting of a large number of timeseries from many different sources. The initial body of data will be composed of data already available, while updating from ongoing and future measurement programs will be carried out on a regular basis to complement the database.
- to make available tools for efficiently searching through the data, to select the cases needed.
- to set up access to this database through Internet for online search and downloading of selected timeseries for use in the models for the design of windturbines (or other structures or buildings)

3. DATA TO INCLUDE IN THE DATABASE

- Existing timeseries of windspeeds, 10 - 60 minutes lengths, sampling at 1-25 Hz (dependent on instrument time- and spatial resolution), from sites in different terrain types: homogeneous, offshore, coastal, mountainous, in windfarms. Measured at heights of interest for windenergy: 15-100m. Data should include 3-D measurements of the windvector where available.
- 1-10 min. statistics, mean, std.dev., extremes, derived from the timeseries, maybe supplemented

with other statistics such as windshear, atmospheric stability and power output of nearby turbines in wake situations. This table also includes information on timeseries availability.
- Accurate site descriptions.
- Climatological descriptions of sites, windspeed distributions, wind roses ....

4. ORGANISATION OF THE DATABASE

The data will be organized in three databases

#1 Database containing the fast sampled timeseries in a common file format.

#2 Database containing relevant statistics for the timeseries data in '1', that can be used for indexing the timeseries data.

#3 Database containing descriptions of the sites, measurement setup and other relevant information about the data.

All three databases will be located on one or several fileservers accessible through the Internet and part of the databases would be available on CD-ROMs.

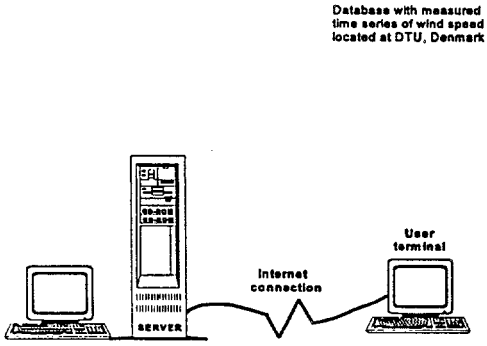

Figure 2

5. USE OF DATABASE

The database will be useful as a supporting tool to identify

- rare meteorological events in terms of occurence, durability, extent, strength and shape
- wind shear
- extreme values
- spatial structure of turbulence
- spacing parametres in wind farms
- other meteorological issues

at different site types [homogeneous, offshore, coastal, mountain, windfarm] around Europe.

The intended main users of the databases are:

- Researchers and/or engineers, defining wind turbine loadcases.
- Designers [manufacturers] performing wind turbine load calculation evaluation for remote sitings with extreme wind conditions.
- Research institutions.
- Meteorologists
- Software developers [for load calculations].
- Researchers and/or engineers, defining loadcases for buildings.

The participants in this project represents both researchers, manufacturers and meteorologists.

6. SITES

We are aiming for receiving data from each member country of the EU from two categories

- Typical sites
- High turbulence sites or other 'unusual' sites, which could be sites exhibiting extreme climatic situations, extreme windprofiles or even very low turbulence sites.

7. CATEGORIES OF DATA

From each site data will be requested for a number of different categories, selected on the basis of windspeed, winddirection and other typical features, i.e. wake/nowake, summer/winter etc. Clearly great care must be taken into defining these categories in the initial phases of the project, such that on the one hand we do not get flooded with data, but on the other hand still get a representative coverage of the possible conditions.

A standardized description of each site will also be stored if available. This includes

- WASP type description of surrounding terrain, possibly supplemented by photographs
- Measured mean wind speeds, wind roses and distributions
- References to other available measured meteorological data

A description of the measurement system setup will also be included :

- Site layout, maps with locations of meteorological masts and wind turbines
- Instrument mounting, boom layout and boom direction
- Instrument descriptions, types, locations
- Instrument calibrations, factory or user calibrated.
- System operational reliability, errors ...
- Reference to available publications based on the measurements

8. SCREENING AND INDEXING OF DATA

We will assume that the data we receive from the participants are good data with no errors in them, but since it is

well-known that the statistics calculated on the basis of these timeseries can be quite sensitive to errors in the data, like spikes, noise or drop-outs, we will set up automatic data-screening procedures before the data is entered into the database.

The procedures when receiving data will be

- Conversion to a standard format
- Screening for errors
- Calculations of the statistics for indexing the timeseries, i.e. mean, std.dev., extremes, length scales ....
- Checking of site descriptions
- Statistics table, other info like stability, windshear, power output of a nearby windturbine, atmospheric pressure, temperature, precipitation, geographic location ... are entered into the index table
- Site descriptions are entered into their respective tables
- Timeseries data are stored

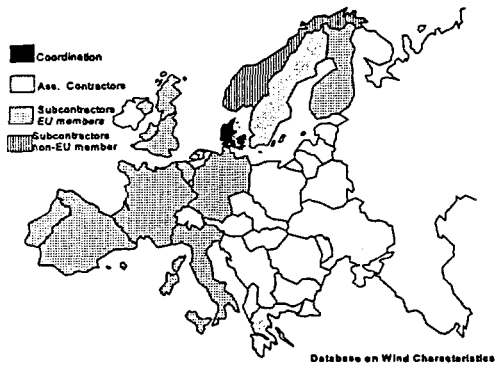

Figure 3 Data is available from nearly all member countries.

9. ACCESS TO DATA

The database will be accessed online by Internet, and the primary access will be through the index database. Using interactive search and selection programs, a list of relevant data can be created.

The user specifies a number of search parameters, i.e.

- Location [World, Europe, USA, ...]
- Site type [homogeneous, offshore, coastal, mountain ...]
- general conditions [normal, instationary, violent events ..]
- specific conditions [windspeed, gust, winddirection, time of year, time of day, temperature, windshear, wake - nowake,.....]
- data types [distributions, averages, timeseries,...]

The utility programs then use the statistics information as index information to search out the cases that are needed, then allowing the user to narrow down the selection/widen the selection depending on the results of the search and finally downloading the selected information to a user specified ftp-site or if large amounts of data are needed, providing the data on some suitable medium for mailing.

Possibilities for plotting of the statistics data will also be available to help the user selecting 'interesting' situations.

After the selection has been finished, the user now has a number of choices

- If the statistics data are sufficient for the present purpose, selected portions of statistics and/or other descriptions are being downloaded to the user's machine.
- The user wants timeseries for his own analysis, and dependent on the amount of data that is needed he can either
  - download the timeseries directly (small amounts of data)
  - request data downloaded to a specified ftp-server, whereupon the data automatically will be downloaded by the server (medium amounts of data)
  - request data sent by mail on some high capacity medium, typically a CD-ROM or the coming high capacity equivalents.

10. SOFTWARE FOR HANDLING OF DATA

The software packages that will be developed/modified consist of

- Graphical user interface for the Internet
- Database software for storage of index data and selection of subsets of data
- Software for retrieval of stored timeseries and automatic downloading of the data or writing to permanent media.
- Software that the user can download to be used for doing simple operations on the data, like transformation to a general format from the (packed) format in which the data will be delivered.
- Programs for simple statistical operations on the data, fourier decomposition, plotting.

11. HARDWARE

The necessary hardware consists of a medium speed workstation with large disk capacity to be used for the development of the system. The final server to be used for interactive access by the end users must be a fast speed workstation with very large harddisk capacity. Both systems also need a suitable selection of large capacity devices for data backup and transfer of data. We estimate a total amount of storage space needed of at least 50 Gbytes.

MORE INFORMATION

Updated information on the database can be found at our WEB-page: **http://www.afm.dtu.dk/wind/database**

ORGANIZATION

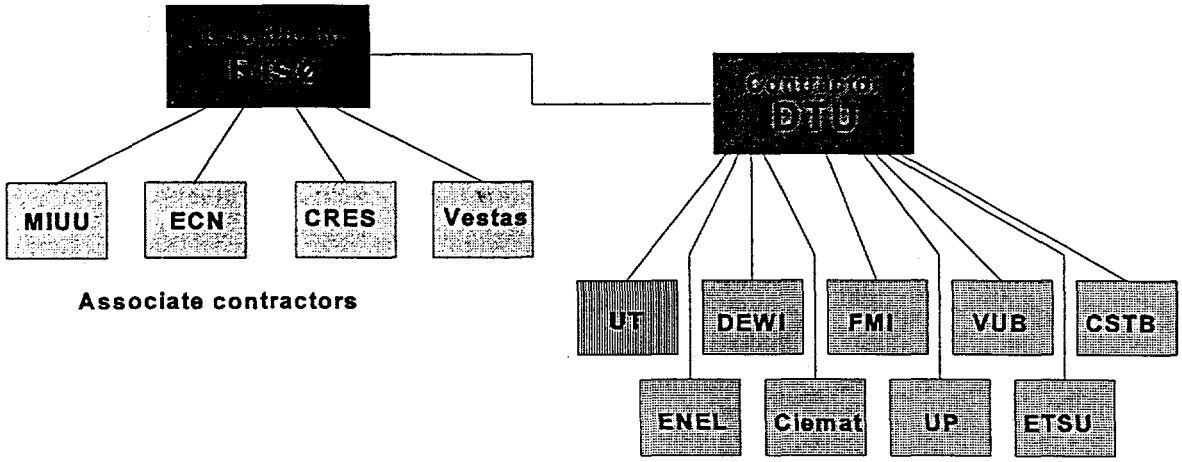

Database on Wind Characteristics

TIME SCHEDULE

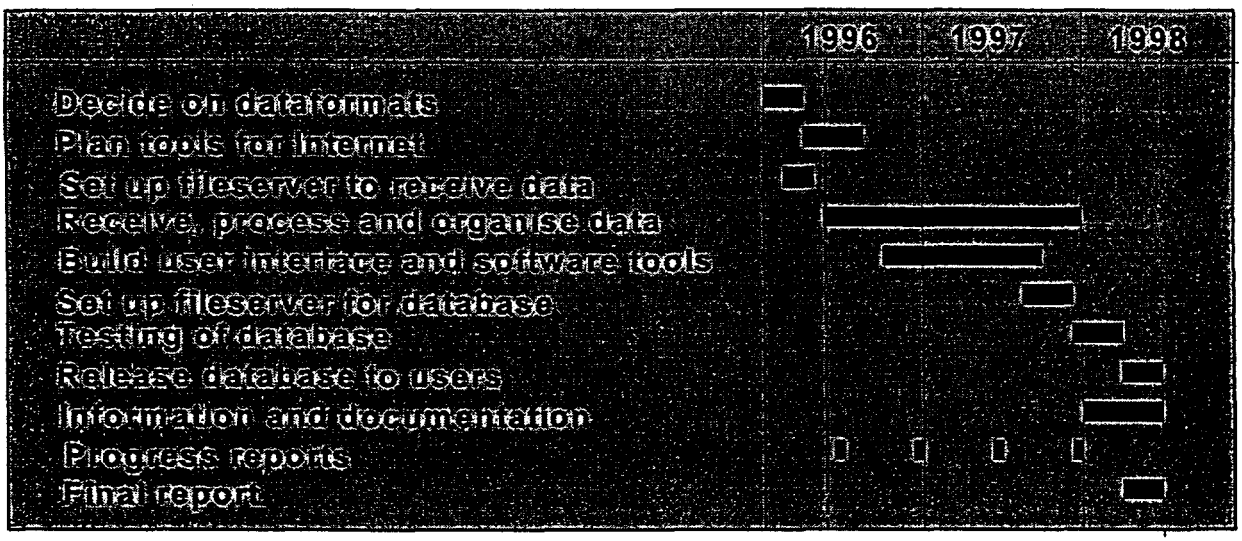

End of project medio 1998

Database on Wind Characteristics

NUMERICAL OPTIMIZATION OF WIND TURBINE ROTORS

Peter Fuglsang, Helge Aagaard Madsen
The Test Station for Wind Turbines
Risø National Laboratory
Roskilde, DK-4000
Denmark

ABSTRACT: This paper presents a newly developed integrated tool for multipoint optimization of rotors for horizontal axis wind turbines. The optimization objective is the cost efficiency, defined as the ratio of the annual energy yield to the cost of the turbine. This includes important loads on, e.g., hub, tower. The method allows multiple constraints on for example extreme and fatigue loads. It includes time domain aeroelastic calculations for estimation of fatigue damage. For optimization purposes, a semi-empirical sensitivity analysis is developed for the life time equivalent fatigue loads. This results in substantial savings in calculation time. Results are shown from the design study of a 1.5 MW stall regulated rotor. Optimization of the blade geometry shows maximum strain on more than 80% of the blade leading to more efficient use of the material. The cost efficiency improves by 3.2% to the same overall blade requirements. The optimum ratio of rated power to swept area is around 460 W/m^2, which is lower compared to today's Danish wind turbines. The optimum $C_{L,max}$ is high over the entire blade.

Keywords: OPTIMIZATION; ROTOR DESIGN; FATIGUE; AERODYNAMICS

1. INTRODUCTION

Today's aerodynamic and structural design of wind turbine rotors for horizontal axis wind turbines (HAWT's) is mainly based on experience and innovation. Recently, numerical optimization procedures was introduced in the design process by Selig et al. [6] and Fuglsang et al. [2]. The latter involves a fully multipoint numerical optimization tool, that enables an inverse design procedure with multiple constraints on, e.g., loads.

It is common practice to aim for either maximum efficiency or maximum energy yield in the aerodynamic design of the rotor. Focus is mainly on the rotor aerodynamics. Hence, there is no or only few constraints on loads. Results are optimum blade shapes and desirable airfoil characteristics, as in Madsen et al. [4]. These eventually form the basis for design of special tailored airfoils [7].

Unconstrained optimization can however result in large loads on important parts of the wind turbine, such as the tower and the blade roots, Fuglsang et al. [3]. Therefore, optimization should not just concern the rotor aerodynamics. Attention should be paid to fatigue damage as well as to extreme loads on the entire turbine. This was in the present work done by the development of a comprehensive optimization tool.

The paper describes the developed design method for HAWT's. Design studies are carried out for the design of a 1.5 MW rotor. These concern the optimum specific power and the optimum desirable airfoil characteristics.

2. DESIGN METHOD

Figure 1 illustrates the design process with numerical optimization. It is divided into three stages: Problem definition, optimization and post processing of results.

In the problem definition stage, the designer specifies an objective function, $f(\boldsymbol{x})$, that depends on a design vector, $\boldsymbol{x}$. f expresses the aim of the optimization, that is being minimized. It is in our case the negative cost efficiency. The cost efficiency is the ratio of the annual energy yield to the total cost. The cost is estimated as the material consumption, based on allowable strains and stresses, and the magnitude of the design giving loads. The cost efficiency is proportional to the kWh-price of energy, when maintenance is neglected.

$\boldsymbol{x}$ contains n design variables. They are any parameter describing the rotor geometry or regulation, such as the chord and twist or the airfoil lift and drag. The minimization of f is subject to the constraints, $\boldsymbol{g}$. The constraints are bounds in the design space. These are component quantities such as blade manufacturing considerations, and overall parameters as for example maximum generator power, noise emission, loads, maximum material stresses and strains. Finally, an initial guess on the rotor, $\boldsymbol{x}_0$, is specified.

In the optimization stage, the optimization algorithm does systematic search for an optimum design by changing $\boldsymbol{x}$ within the bounds of $\boldsymbol{g}$. The change in f is based on the sensitivity, $\nabla f(\boldsymbol{x})$. The sensitivity analysis is a first order Taylor expansion around the present design point. The different calculation models are automatically used to calculate f and $\boldsymbol{g}$.

After convergence, the post processing stage involves the designer doing additional verifying calculations. The optimized result is eventually modified from manufacturing reasons, etc.

The essential advantages by the use of the optimization algorithm are: An inverse design process. A large number of design variables are varied simultaneously. An unlimited number of constraints are automatically taken into account.

A drawback is the iterative procedure, that can involve long calculation time, if the individual calculation models

are time consuming. In addition, high calculation accuracy is often necessary for a reliable sensitivity analysis.

2.1 Calculation sub models

The choice of calculation sub models results as a compromise from limited overall time consumption and calculation accuracy. The degree of detail for each model should allow a relative comparison between some reference rotor and the optimized rotor. The present design tool includes the calculation models, that are normally used at rotor design.

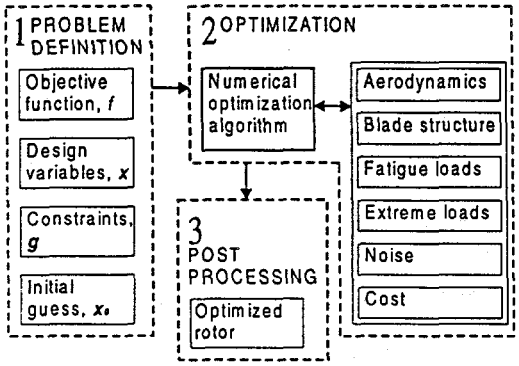

Figure 1: Use of numerical optimization with calculation sub models.

Figure 1 shows the applied calculation models:

The aerodynamic calculation is simple blade element/ momentum theory with a tip loss correction.

The blade structure model for the blade shell is a linear elastic I-beam model. Functions for stiffness and mass are fitted to measurements. This calculates the maximum strain in the shell well.

The fatigue loads are determined by time domain aeroelastic calculations from the "Flex 4" code by Øye [10]. The non linear equations of motion are solved with 20 degrees of freedom. They cover blades, transmission and tower. The applied wind field includes wind shear and tower shadow and a full 3-D turbulence field. A dynamic stall model is used for stall regulation at high wind speeds. The fatigue damage is estimated by Rainflow counting of the load spectra and life time equivalent fatigue loads are determined.

The extreme loads on blade roots, foundation and tower base are calculated from the IEC 1400-1 recommendation and the Danish code of practice for wind turbines.

Calculation of aerodynamic noise from the rotor is based on the semi-empirical approach by Brooks et al. [1].

Calculation of cost is based on Rasmussen et al. [5]. The total cost, C, is calculated as a sum of contributions from the different wind turbine components, C_i. The percentage cost for the i'th component, R_i, is determined from a reference rotor having a total cost on 100%. Each contribution is split into a fixed part, b_i, and a variable part, $1-b_i$. The fixed part contains manufacturing, transport, work up, etc. The variable part depends on the design giving loads. From maximum values of stresses and strains, the material consumption, m_i, is calculated. The weighted percentage component cost is found:

$$C_i = R_i \left(b_i + (1 - b_i) \cdot m_i \right)$$

Two wind turbines of equal size and concept can then be compared on a relative basis by calculating the difference in total cost from the difference in design giving loads.

2.2 Semi-empirical gradient estimation

A major task is the inclusion of time domain aeroelastic calculations, since they are very time consuming. Having n design variables, the numerical sensitivity analysis requires $n+1$ calculations of the life time load spectrum for each iteration. Therefore, a semi empirical gradient calculation method was developed. Thomsen et al. [8] found the following relation between the standard deviation for the power, σ_P, and the standard deviation for the wind speed, σ_W, at wind speeds before rated power:

$$\sigma_P = K_0 \cdot \left[\partial P / \partial W \right]_W \cdot \sigma_W, W < W_R$$

Where $[\partial P/\partial W]_W$ is the slope of the power curve and K_0 is a constant.

For fatigue loads that are dominated by the blade flapwise sampling of turbulence, the life time equivalent load, $R_{eq,l}$, for the load l is related to the standard deviation, σ_l. Furthermore, the slope of the average flapwise blade root moment, $[\partial M_f/\partial W]_W$ is related to $[\partial P/\partial W]_W$.

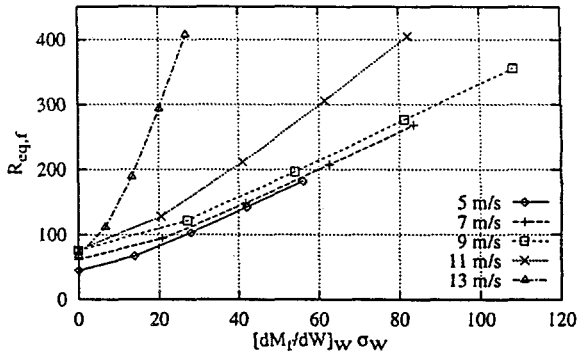

Figure 2: Linear relation between $R_{eq,f}$ and $[\partial M_f/\partial W]_W \cdot \sigma_W$ at wind speeds below rated power (attached flow).

Figure 2 shows the results of aeroelastic calculations for a 1 MW stall regulated rotor at different wind speeds and different turbulence intensities. The life time equivalent flapwise blade root moment, $R_{eq,f}$, is shown versus $[\partial M_f/\partial W]_W \cdot \sigma_W$. It appears, that there is a linear relation between $R_{eq,f}$ and $[\partial M_f/\partial W]_W \cdot \sigma_W$ for wind speeds below rated power. At higher wind speeds stall occurs, and the relation does not exist. However, at higher wind speeds, the average flapwise moment, M_f, can be used instead. In total, the lifetime equivalent fatigue loads for the flapwise dominated loads at both low and high wind speeds are approximated:

$$R_{eq,l} = K_1(W)_l \cdot \left[\partial M_f / \partial W \right]_W \cdot \sigma_W, W < W_R$$

$$R_{eq,l} = K_2(W)_l \cdot M_f(W) \cdot \sigma_W, W \geq W_R$$

Where $K_1(W)_l$ and $K_2(W)_l$ are load and wind dependent constants. Since separation does not occur for pitch regulated rotors, the first relation applies for all wind speeds in this situation.

The edgewise life time equivalent blade root moment, $R_{eq,e}$, is dominated by the variation in the gravitational

moment from the blade weight, ΔM_g. It is easily approximated by the following relation:

$$R_{eq,e} = K_3(W)_{edge} \cdot \Delta M_x$$

After calculation of a full life time spectrum, the semi empirical constants for each load at each wind speed are determined. The sensitivity analysis is based on these constants. Furthermore, it turns out, that a number of optimization iterations can be done before another full time domain calculation. In this way, a full life time spectrum is calculated at each 10 - 15 iterations. Refinement studies show, that the converged result does not rely on the semi empirical approach. At a typical problem size, the time saving is a factor of 1000. This reduces one optimization to around 12 hours on a Pentium PC.

2.3 Optimization algorithm

The important parameters for the choice of the optimization algorithm are: Rate of convergence, time consumption for each iteration and robustness. Two different search methods are applied in combination: Sequential linear programming (SLP) and the method of feasible directions (MFD), both from [9]. SLP is a fast method, that is preferred as long as the actual design vector in the current iteration is feasible, e.g., no constraints are violated. The change in x sometimes results in an infeasible design vector, because of the uncertainty that is related to the semi-empirical gradients. In that case, MFD is used to make x return do the feasible domain. Its lack in rate of convergence and time consumption is counterbalanced by robustness.

2.4 Representation of design variables

The representation of the design variables is very important for the optimization result. Design variables are at the present time: Rotor rpm, tip pitch angle, rotor diameter, chord, twist, relative thickness, shell structure and airfoil lift and drag versus incidence.

Scalars are simply mapped into the design vector. Distributed parameters such as chord and twist are described by descrete points, typical from 3 to 8. They form the basis for either cubic splines or Bezier curves. They have the advantage of global control, so that when one design variable is varied, this changes the entire curve, leading to a better sensitivity analysis.

To ensure reliable results for the airfoil lift and drag coefficients, they have very limited degrees of freedom. Both minimum drag and the lift curve slope are more or less fixed to the airfoil thickness and should not be optimized. Of primary interest is $C_{L,max}$ along the blade. $C_{L,max}$ at a given relative thickness is varied by off-setting the lift curve along the lift curve slope and the drag curve correspondingly along the angle of incidence axis to higher incidence. The relation between $C_{L,max}$ and the increase in pressure drag is then maintained. This simple degree of freedom is preferred instead of a more complex mapping that could lead to nonphysical results.

The total number of design variables is a compromise of sufficient degrees of freedom and calculation time. Typically, around 30 design variables are used.

3. OPTIMUM SPECIFIC POWER

The aim of this investigation is to find the optimum ratio of the generator power to the swept area for a 1.5 MW rotor. Comparisons are done for a reference rotor, following the 3-bladed Danish concept, with the newly developed LM 29.2 blades. The objective function is the negative cost efficiency. Design variables are rotor chord, twist, relative thickness and shell structure along the blades and the tip pitch angle. Rotor rpm and rotor diameter, root chord and tip twist are fixed. The airfoils are fixed to the NACA 634xx series. Constraints are applied to the blade fatigue strain, ε_{fat}, and extreme strain, ε_{ext}, so that the optimized rotor is comparable to the LM 29.2 blade.

An optimization with no constraint on generator power was done. Figure 3 shows the optimized chord and twist distributions compared to LM 29.2. The reduction in chord results in a decrease in the annual energy yield of 5%, because peak power is reduced to 1300 kW and moved to higher wind speeds. The optimized rotor has a specific power on 460 W/m^2, compared to the reference rotor, that has 530 W/m^2 with the LM 29.2 blade. The loss in production is however counterbalanced by a reduction in cost of 8.2%. This is because the life time equivalent fatigue loads are reduced by up to 20% and the extreme loads by up to 15%. Hence, the cost efficiency is increased by 3.2% compared to the LM 29.2 rotor.

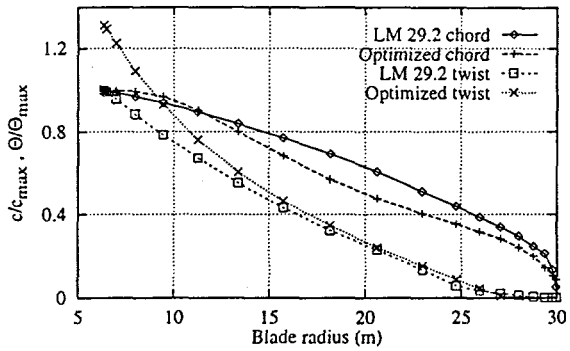

Figure 3: Chord and twist distributions for the LM 29.2 rotor and the optimized rotor.

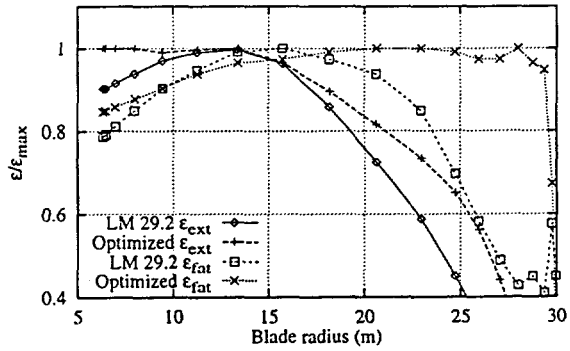

Figure 4: ε_{fat} and ε_{ext} for the LM 29.2 rotor and the optimized rotor.

Figure 4 shows ε_{fat} and ε_{ext} for the optimized rotor and LM 29.2. Towards the root, the extreme loads determine the blade structure, whereas the fatigue loads determine the outer part. The optimized blade has a far better use of the

material, since either ε_{ext} or ε_{fat} are maximum over 80% of the blade, corresponding to a reduction in blade weight on 9%. This shows the effectiveness of the optimization with constraints. Different constraints on the generator maximum power are applied to investigate the variation of the cost efficiency with the specific generator power, Figure 5. Away from 460 W/m^2, the cost efficiency is reduced. The reduction is however small, and the optimum is "flat". The LM 29.2 blade corresponds to 530 W/m^2.

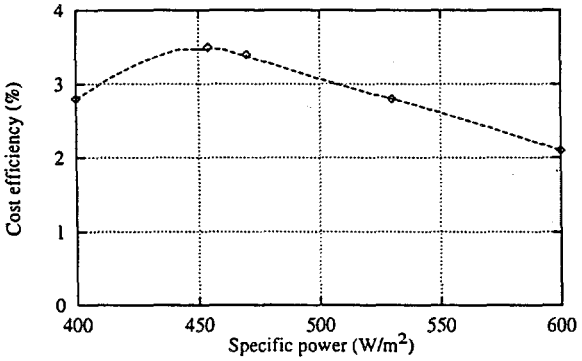

Figure 5: Cost efficiency as function of specific power.

4. OPTIMUM AIRFOIL CHARACTERISTICS

To investigate the optimum airfoil characteristics, the lift and drag coefficients are added as design variables. $C_{L,max}$ is constrained to 1.9. The optimum $C_{L,max}$ distribution is seen in Figure 6.

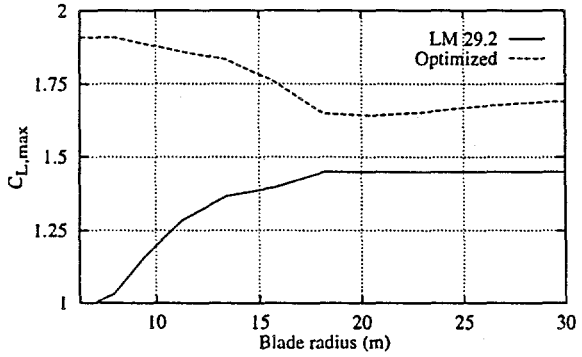

Figure 6: $C_{L,max}$ distribution for the LM 29.2 rotor and the optimized rotor.

Compared to LM 29.2, $C_{L,max}$ is increased on the entire blade. The high $C_{L,max}$ at the root is often seen in optimization studies because of increased production. The relatively high $C_{L,max}$ at the outer part of the blade results as a compromise between reduced blade weight/ reduced extreme loads from a smaller chord and allowable strains.

The improvement in cost efficiency is around 7%. The results are not consistent with the so called low lift airfoils suggested by several authors. However, the inclusion of constraints on loads and the calculation of cost prevent $C_{L,max}$ from being reduced in the tip region. Optimizations with different constraints on $C_{L,max}$ show, that a specific value is less important compared to qualitative requirements such as roughness insensitivity, etc., as long as chord and twist are optimized.

5. CONCLUSIONS

An optimization tool was developed. It includes a semi-empirical gradient method for time domain aeroelastic calculations and the estimation of cost. It is found well suited for optimization studies and parameter investigations.

To the same overall blade requirements, the cost efficiency is improved by 3.2% in the demonstrated example. A reduction in energy yield is counterbalanced by reduced extreme and fatigue loads. Maximum allowable strains are obtained on more than 80% of the blade. The optimum specific power is "flat" around 460 W/m^2, which is lower than Danish wind turbines of today. The optimum $C_{L,max}$ is high towards the root, and around 1.6 - 1.7 at the outer part of the blade. This results in an increase in cost efficiency on 7%. This finding is not consistent with low lift airfoils, but originates from the inclusion of constraints on loads and estimation of cost. Furthermore, it is found that airfoil design should focus on roughness insensitivity and noise instead of on a specific $C_{L,max}$. This can be chosen in a broader region, as long as chord and twist are optimized.

ACKNOWLEDGMENTS

The present work was funded by the Danish Ministry of Energy in the contract, ENS-1363/95-0001.

REFERENCES

[1] Brooks, T.F. et al., 1989, Airfoil Self-Noise and Prediction, NASA 1218, USA.

[2] Fuglsang, P., H.A. Madsen, 1995, Optimization of Stall Regulated Rotors, Proc. 14. ASME Wind Energy Symposium.

[3] Fuglsang, P., H.A. Madsen, 1995, A Design Study of a 1 MW Rotor, Risø-R-799(EN), Risø National Laboratory Denmark.

[4] H.A Madsen, 1994, Afprøvning af en 20 kW - 12.6m Stallreguleret Rotor, In Danish, Risø-I-788(DA), Risø National Laboratory, Denmark

[5] Rasmussen, F., Kretz, A., 1994, Dynamics and potentials for the twobladed teetering rotor concept, Proc. WINDPOWER'94.

[6] Selig M., J. Tangler, 1994, A multipoint inverse design method for horizontal axis wind turbines, Proc. Windpower'94.

[7] Tangler, J., 1987, Status of the Special - purpose Airfoil Families, proc. WINDPOWER'87.

[8] Thomsen, K., Markkilde, S.P., 1992, Experimental Investigation of Gear Box Duration Loadings on Stall and Pitch controlled Wind Turbines, Risø-R-653(EN), Risø National Laboratory, Denmark.

[9] Vanderplaats, G.N., 1984, Numerical optimization techniques for engineering design with applications, MC-GRAW-HILL.

[10] Øye, S., 1992, FLEX4 - Computer code for wind turbine load simulation, Technical University of Denmark.

TERRAIN INDUCED LOADS ON PITCH-REGULATED WIND TURBINES

Kenneth Thomsen
Søren Markkilde Petersen
Jørgen Thirstrup Petersen
Risø National Laboratory,
DK-4000 Roskilde, Denmark

Stig Øye, Technical University of Denmark

Michael Friedrich,
Vestas Wind Systems A/S, Denmark

Abstract
The wind conditions and loads for wind turbines in homogeneous and complex terrain is investigated experimentally and with the use of aeroelastic models. The importance of the differences in wind field parameters for the loads is investigated and we have found that even for complex terrain, the most important load generating parameter is the turbulence intensity. Other differences in wind parameters seem to be of secondary importance for the loads.
Keywords: Aeroelasticity: Fatigue: Mountains/High terrain: Wind field simulation.

1 INTRODUCTION

The loads on wind turbines erected in homogeneous terrain have been investigated thoroughly from both measurements and theoretical considerations, and for this type of terrain the loads are considered well known. This is not the case for wind turbines installed in complex terrain. The effects of the complexity of the terrain on the loadings for a wind turbine are not clearly identified. The design loads for wind turbines erected in complex terrain are often derived from the design rules for wind turbines erected in homogeneous terrain.

The present work (described in detail in [6]) concerns the loads for wind turbines in complex terrain. The objective is to identify the important load-generating mechanisms for wind turbines erected in complex terrain. The investigation is based on both experiments and aeroelastic load predictions.

The experimental part of the investigation is based on measurements on two Vestas V39–500kW wind turbines, one in Denmark and one in the Sky River wind farm in California. The Danish site is very flat terrain, while the terrain in Sky River is very complex, mountainous terrain with many roughness elements. The turbine in Sky River is located in a wind farm, but no measurements from the turbine operating in wake are used in the present analysis.

Due to small differences at the two sites in the wind turbine construction and the wind climate conditions, it is not possible to identify the effects of the terrains in a general way from the experiments alone. The problem is overcome by combining the experiments with load predictions. Using the information gained from the experimental analysis, we identify the assumptions for the load predictions. Afterwards, the load prediction codes are used to generalize the findings and clarify the effects of the different types of terrain on the wind turbine loadings.

2 DESCRIPTION OF THE METHOD

The method can be outlined as follows:

1. Experimental investigation of the wind fields
2. Establishment and validation of aeroelastic modelling
3. Identification of load sensitivity to wind field parameters
4. Prediction of life time loads in different types of terrain

The first step of the investigation is based on experimental work, where wind field parameters and related loads are measured for a wind turbine in homogeneous terrain and in complex terrain. From these experiments, the important wind field parameters for each type of terrain are identified. Due to differences at the two sites in the wind turbine tower construction and in the general wind climate conditions, e.g. air density, it is not possible to compare the measured loads on the two wind turbines directly. The experiments have to be supported by modelling. Thus, the second step of the investigation is to establish an aeroelastic model of the wind turbines and validate this model with the measured loads for the two sites. The third step in the investigation is to use the aeroelastic models to identify the importance of each wind field parameter. The fourth and last step is to combine all wind field parameters and calculate the combined effect on the wind turbine fatigue loads.

2.1 Description of the experiments

The two sites differ significantly in roughness and topography. The Danish site at Lem is a typical Danish very smooth, type of terrain with few trees and fences. The Sky River site is a highly complex mountainous terrain with a high degree of roughness from small trees. The turbine is installed on the top of a ridge.

The wind turbines are in both cases Vestas V39-500kW - a three-bladed, upwind, pitch-regulated turbine with a rotor diameter of 39 m and a rated power of 500 kW. The turbine at Sky River has a lattice tower, and the turbine at Lem has a tubular tower. The blades and nacelle components of the turbines are identical.

The experiments are described thoroughly in [3] and [4].

2.2 Description of the simulations

The load prediction part of the investigation is based on two aeroelastic codes: the *HawC* code developed by Jørgen Thirstrup Petersen [5] and the *FLEX4* code developed by Stig Øye [8].

The HawC model is basically a finite element model developed as a special purpose wind turbine model. The FLEX4 model uses a relatively limited number of degrees of freedom to describe the rigid body motions and elastic deformations of a turbine. Both codes are formulated in the time domain, and the control system for the blade pitching is included in the models.

The wind field is simulated as a deterministic part, i.e. wind shear and tower interference, and a stochastic part simulating the turbulence. In HawC, the turbulence is simulated with the *Mann* model [2], and in FLEX4, the turbulence is simulated with a *Veers* type model, [8]. Both models are three-dimensional and three-component models, but in the Veers model, no cross-correlations between turbulence components are included.

3 RESULTS

From the experiments, the primary results concern the winds conditions from the two sites. Thus, in the first part, we sum up the results from the wind analysis. In the following part, the importance of the wind conditions is summarized, based on calculations with the aeroelastic models.

3.1 Results from the experiments

The wind fields from the two sites have been investigated and compared to models and parameters often used for load predictions for wind turbines. The findings from the wind field analysis are summarized in Table I, and described in the following.

Due to a limited number of meteorological measurements, only three of the parameters in Table I are from the Lem experiments. These are roughness length, turbulence intensity and length scale. For the homogeneous terrain site the turbulence intensity level is 8 - 16 % with a mean value of approximately 12 % for all wind speeds. The spectrum of the turbulence is compared to a Kaimal type spectrum, and length scales of approximately 900 m are found. The roughness length at the homogeneous terrain site is 0.02 m. The rest of the flat terrain values are adopted from an investigation in a similar type of terrain, [1].

Table I: Summary of wind analysis results

	Flat[a]	Complex
Wind shear	logarithmic	Speed-up
Wind vector slope	0^o	7^o
Roughn. length	0.02 m	0.2 m
Mean turb. int.	12 %	14 %
Length sc. L_u	900 m	700 m
L_v/L_u	0.3	0.5
L_w/L_u	0.1	0.3
Coherence (u-u)	12	12
Coherence (v-v)	6	7
Coherence (w-w)	6	5
σ_v/σ_u	0.8	1.0
σ_w/σ_u	0.5	0.8
Distr.	Gaussian	Non-Gaussian

[a]Some values are based on [1]

Several differences in the wind field parameters for the two sites are found. For the complex terrain, the slope of the wind vector follows the slope of the terrain in front of the turbine, approximately 6-8°. The vertical wind speed profile is found to be influenced by the flow over the hill, resulting in a speed-up wind shear. The longitudinal turbulence level is approximately 14% as an average for all wind speeds. The turbulence standard deviations in the transverse directions are higher than expected values in homogeneous terrain. The roughness length is approximately 0.2 m.

The Kaimal spectrum applies well for the complex terrain, using length scales of approximately $L_u = 700\ m$, Figure 1. This is also the case for the transverse turbulence components. Typical values of the length scales for these components are $0.5L_u$ (lateral) and $0.3L_u$ (vertical).

The coherences of the turbulence components are compared to a modified Davenport model, [1], Figure 2. The coherence decay factors are found to be very similar to expected values for homogeneous terrain, $A_{uu} = 12$, $A_{vv} = 7$ and $A_{uu} = 6$. No cross-correlation has been investigated.

The analysis of the wind fields at Sky River has revealed an important characteristic of the wind speed probability distribution function. Many measured wind speed time series are non-Gaussian. The minimum wind speed occurring in the time series is lower than the expected value. The 10 minute minimum values are lower than the expected values ($\approx U - 3 \cdot \sigma_u$), Figure 3. The non-Gaussian phenomenon is only observed for turbulence intensities below 17%.

3.2 Results from the simulations

Using the actual identified wind field parameters, the aeroelastic simulations have been validated for the two turbines. For the Lem turbine a very fine agreement between simulated and measured loads is found using

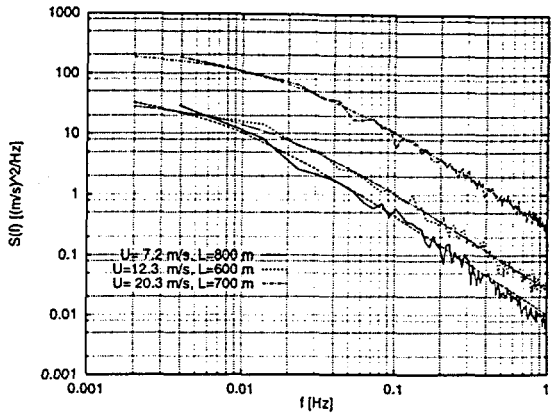

Figure 1: Turbulence spectra of u-component in complex terrain compared to Kaimal spectra

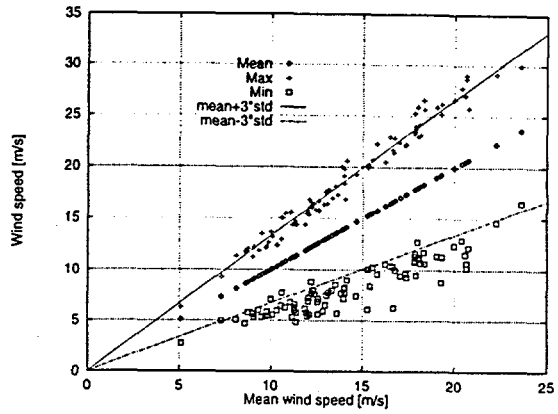

Figure 3: Extreme values of wind speed versus mean wind speed in complex terrain. Turbulence 10-12%

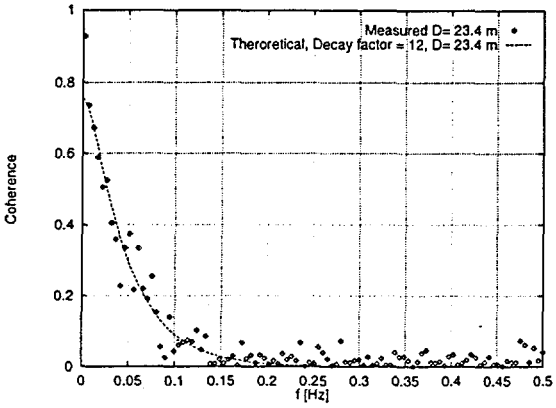

Figure 2: Coherence of u-component in complex terrain compared to Davenport model

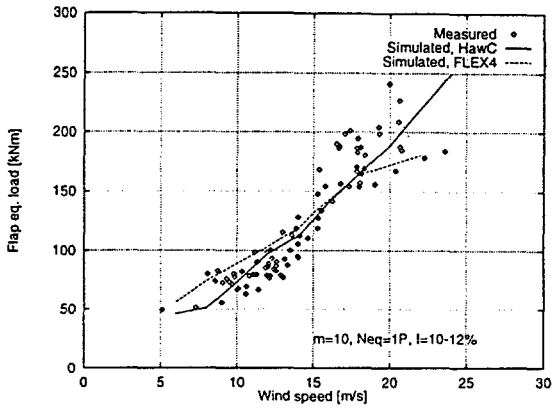

Figure 4: Calculated flapwise fatigue loads for the complex terrain site

the traditional models and parameters for the wind field. To simulate the loads on the turbine at Sky River, it has been necessary to modify the traditional wind models. The most important modification is the so-called gust scaling, a modification which makes it possible to model the non-Gaussian characteristics of the wind speeds. Another modification is the use of a 'speed-up' wind profile. With the modified wind models it is possible to simulate the loads on the Sky River turbine reasonably well, Figure 4.

3.3 Importance of the wind field parameters

The aeroelastic models are also used for examination of the importance of the wind field parameters to the fatigue loads on a wind turbine. One parameter is investigated at a time. The wind speed is 10 ms^{-1} and the turbulence is 10%. We express the sensitivity of the load to the wind field parameter as the difference between the fatigue equivalent load for two load calculations. For the first calculation, the homogeneous terrain parameter is used and in the second calculation the complex terrain parameter is used.

The non-Gaussian wind speed distribution is very important for the loads, the equivalent flapwise blade bending moment is for some situations increased 35%, Table II. Again, it should be mentioned that the phenomenon is observed for $I < 17\%$ only. The other wind field parameters typically result in an increase in the fatigue loads of 3-7% from the Lem turbine to the Sky River turbine. The speed-up wind shear reduces the flapwise fatigue load.

3.4 Prediction of life time loads

We can now use the aeroelastic models to predict the difference in life time fatigue loads between a turbine in complex terrain and in homogeneous terrain. The loads is calculated for several wind speeds, and combined using a Weibull distribution. For both types of terrain we choose the same Weibull parameters, i.e. the annual wind speed distribution is not considered a terrain effect. We use the same wind turbine for the two cases, and wind field parameters as given in Table I for all wind speeds. One parameter is different, though. The turbulence intensity is in general very important for the wind turbine loads, and we have to assume life time values for the two types of terrain. The turbulence intensity is a terrain effect (or more precisely a result of local roughness), but only an indication of the life time turbulence levels can be

Table II: Sensitivity of flapwise equivalent load to wind field parameters ($U = 10\ ms^{-1}$ and $I = 10\%$). Negative sign means reduced load

Speed-up wind shear	-4%
Wind vector slope	3%
Red. length scale	5%
Inc. transverse turbulence	7%
Non-Gaussian distribution	35%

deduced from the measurements. However, we assume the difference in turbulence level in the measurement periods to be representative and choose design turbulence levels as 18% for homogeneous terrain and 20% for complex terrain. Due to the high turbulence level, we do not use the non-Gaussian wind distribution. The results—expressed as increase in complex terrain loads—are given in Table III.

The increase in loads for the complex terrain case is 11-18%, depending on the load. These numbers express the expected increase in wind turbine loads for a complex terrain site compared to a homogeneous terrain site—when these terrain types is close to the ones used for our experiments. A part of the increase is due to the higher turbulence intensity in complex terrain. We have done a similar calculation with the same turbulence intensity, 20%, in both types of terrain. Then the load increase in complex terrain is 2-6% compared to homogeneous terrain. Thus, the important load increasing parameter in complex terrain is the turbulence intensity.

Table III: Increase in complex terrain life time fatigue loads compared to homogeneous terrain. Turbulence intensity is 20% in the complex terrain case and 18% in the homogeneous terrain case

	%-increase
Flap	+13
Tilt	+14
Yaw	+18
Power	+11

4 DISCUSSION

Several differences between complex terrain and homogeneous terrain wind field parameters have been identified. When these differences are accounted for in the wind models used for aeroelastic load calculations, the loads can be simulated reasonably well. Thus, with respect to design loads for wind turbines in complex terrain, we can use the same aeroelastic models as in the case of homogeneous terrain. The uncertainty of the wind field parameters are higher, though.

One of the differences in the wind field characteristics is a non-Gaussian turbulence distribution, which is important for the fatigue loads. However, this phenomenon is observed for relatively low turbulence intensities, and should not be taken into account if the design turbulence intensity is chosen higher than 17%. This can be different for other complex terrain sites.

Other differences in the wind field parameters increase the loads less than 10%. This indicates that even for complex terrain sites, the most important load generating parameter is the turbulence intensity—exactly as in homogeneous terrain. For the present complex terrain site, the observed turbulence intensities are lower than expected, due to the speed-up of the wind speed over the hill top, [7].

When we combine all terrain effects and calculate the life time fatigue loads in complex terrain we find increases of approximately 15% compared to homogeneous terrain. However, this increase is very sensitive to assumed life time wind speed and turbulence distribution. In a design situation, knowledge of these two values is very important, for a given complex terrain site.

REFERENCES

[1] Kretz, A., Madsen, H.A., Petersen, J.T. (1994) Measured and Simulated Turbulence - Compared at a Section of a Rotating Wind Turbine Blade. Risø–R–671(EN). Risø National Laboratory, Roskilde, Denmark.

[2] Mann, J. (1994). Models in Micrometeorology. Risø–R–727(EN). Risø National Laboratory, Roskilde, Denmark, Denmark.

[3] Petersen, S.M. (1994). Wind Turbine Test VESTAS V39 – 500 kW, System Test. Risø–I–807(EN). Risø National Laboratory, Roskilde, Denmark.

[4] Petersen, S.M., K. Thomsen, U.S. Paulsen, T.F. Pedersen. (1994). Load Measurements on Pitch Regulated Wind Turbines in Inhomogeneous Terrain, Sky River – Vestas V39. Risø–I–834(EN). Risø National Laboratory, Roskilde, Denmark.

[5] Thirstrup Petersen, J. (1990). Kinematically Nonlinear Finite Element Model of a Horizontal Axis Wind Turbine. Part 1 and 2. Risø National Laboratory.

[6] Thomsen, K., S.M. Petersen, J.T. Petersen, S. Øye, M. Friedrich (1996). Terrain Induced Loads on Pitch-Regulated Wind Turbines. Risø–R–846(EN). Risø National Laboratory, Roskilde, Denmark.

[7] Vølund, Per (1995). Complex Terrain Induced Wind Turbine Loads. Presented at the BOREAS III, Saariselkä, Finland.

[8] Øye, S. (1994) FLEX4 - Documentation (In Danish).

COMPARISON OF PERFORMANCE AND LOAD CHARACTERISTICS OF TWO V27-225 OPERATING IN DIFFERENT COMPLEX TERRAIN SITES

S.M. Petersen, T.F. Pedersen, U.S. Paulsen
Department of Meteorology and Wind Energy
RISØ National Laboratory, Denmark

E.E. Morfiadakis, M.J. Koulouvari, F. N. Mouzakis
Centre for Renewable Energy Sources, Wind Energy Department,
19th km Marathonos Ave. 19009 Pikermi, Greece

ABSTRACT: In the paper measurement results are compared from two full scale measurement campaigns carried out by Risø and CRES on two Vestas V27-225 kW wind turbines located in different complex terrain sites. Prior to any comparison, differences in both the instrumentation and the analysis tools were identified and corrections were applied where necessary, in order to ensure the compatibility of the results to be compared. Given the resemblance of the basic wind flow properties (i.e wind profiles, turbulence intensity levels, length scales) which are expected to influence the behavior of the machines at the two sites, a fairly good agreement was observed in both performance characteristics and fatigue loading of the two machines. This work is carried out in the framework of the MOUNTURB JOULE-II project co-funded by the European Union.
Keywords: complex terrain, fatigue, loads, power

1. INTRODUCTION

The investigation of the performance and load characteristics of a wind turbine operating in complex terrain sites is very important for the appraisal of the topographical effect on the fatigue loads experienced by the wind turbine and, consequently, for its lifetime.

In this paper the present knowledge about complex terrain interactions with wind turbines is improved. It is attempted through a comparison of the results from two full scale measurement campaigns carried out by RISØ and CRES on two Vestas V27-225 kW wind turbines located in Sky River, California and Andros, Greece, both being complex terrain sites.

The comparison focuses on the wind characteristics at the two sites and the performance characteristics (power curve and load measurements) of the two wind turbines. Differences in both instrumentation and analysis tools were identified and corrections were applied where necessary, in order to ensure the compatibility of the results to be compared. For this purpose the influence of parameters possibly introducing uncertainties in the load calculations, such as the reference wind speed, the air density and the procedure followed for the calibration of the loads are discussed and taken into account.

A description of the sites, the wind turbine characteristics and the instrumentation used at both sites are given. A comparative presentation of the results is provided and discussed.

2. SITE DESCRIPTIONS

Andros is a typically mountainous Greek island with a total area of approximately 400 km^2. It is located in the south Aegean Sea and has sites with annual mean wind speed of 9 m/s at 10 m a.g.l. The wind farm, where the measurement campaign was carried out, is situated on the northern part of the island. The wind farm and the location of the met-masts are shown in Figure1.

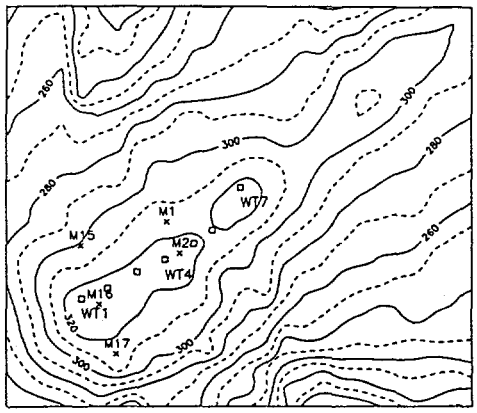

Figure 1: Wind farm and meteorological masts arrangement at the Andros site

The farm consists of seven wind turbines erected on the top of a small ridge. The altitude is 320 to 330 m. Two meteorological masts equipped with cup and vanes at 18m, 31.5m and 40m were placed at 3.9D to the north of WT no. 4 and at 1.6D (43.6m) to the east-northeast (315 °) of WT no. 4.

Data for the three dimensional wind field are provided from a meteorological mast designated M16, positioned on the south-west end of the ridge and equipped with sonic anemometer. The prevailing wind direction is northern and the upwind slope towards this direction is approximately 6°.

The Sky River site is situated in a very complex mountainous terrain about 15 km northeast of Tehachapi Pass, California. The annual wind speed is about 7.7 m/s. The Sky River farm consists of 342 Vestas V27 turbines. The measurement campaign was carried out at the site shown in Figure 2. The measurements were carried out on turbine no 5373. The altitude is about 1525m. The prevailing wind direction is westerly.

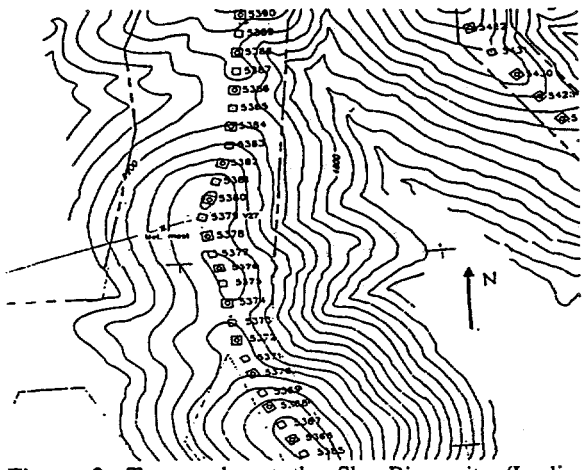

Figure 2: Topography at the Sky River site (Iso-line increment in feet).

The reference met-mast was situated at 1.8D from the instrumented wind turbine in the 254° direction. Cup anemometers were mounted at 10.7m and 28.7m a.g.l. and a sonic was installed at 42.7m. The upwind hill slope towards the prevailing wind direction is approximately 12°. Only undisturbed wind measurements with respect to the wind turbines were analyzed for both cases.

3. DESCRIPTION OF THE WIND TURBINES

Table I provides a brief description of the two Vestas V27 wind turbines. The fundamental resonant frequencies of the wind turbines were found via spectral analysis of campaigns recorded with the machines at standstill and the results are presented in table II.

Table I: The technical data of the wind turbines. For the Andros turbine only differences are outlined.

Parameter	Sky-River	Andros
Rotor diameter	27.0 m	-
Hub height	28.65	31.5
Rotational speed	33 and 44 rpm	
Tilt	4 deg	
Blade length	13.0 m	
Profile	NACA 63-200	
Tower type	Lattice	Tubular
Tower height	27.43	31.0 m
Blade weight	600 kg	
Rotor weight	2900 kg	-
Nacelle weight	7900 kg	-
Tower weight	8900 kg	12000 kg

Table II: Fundamental resonant frequencies

Modal shape	Sky-River	Andros
1. tower bending	1.31 Hz	1.05 Hz
1. shaft torsion. mode	1.88 Hz	1.7 Hz
1. yaw mode	1.72 Hz	2.15 Hz
1. tilt mode	2.06 Hz	2.2 Hz
1.symmetrical flapwise	2.38 Hz	2.6 Hz
1.asymmetrical edgewise	3.41 Hz	3.5 Hz
2. yaw	5.3 Hz	5.9 Hz
2. tilt	5.5 Hz	6.4 Hz

4. DESCRIPTION OF THE INSTRUMENTATION

The two wind turbines have been heavily instrumented underlying the same principles, to enable detailed monitoring of the machine performance and the loading. The following signals have been recorded with a sampling frequency of 32 Hz:

- blade root flapwise and edgewise bending moments
- low speed shaft bending moments
- low speed shaft torque
- nacelle accelerations
- tower top and base bending moments
- tower torsion
- electrical power output
- blade pitch angle

In addition temperature and precipitation sensors have been installed on the met-masts at both sites.

The load measurements were performed using full strain gauge bridges. In the present analysis the comparison of loads is limited to the blade root bending moments and yaw and tilt bending moments calculated from the shaft bending moments. The specific position of the relevant s.g bridges with respect to the hub center (HC) are given in Table III for both wind turbines.

At both machines the strain gauges for the measurement of the blade root bending moments were mounted along two directions perpendicular to each other. At Sky River the directions were chosen to be in the flapwise and edgewise directions, which are out-of-plane and in-plane bending moment for zero pitch. At Andros the s.g. were rotated 45° with respect to the Sky River configuration and the in-plane and out-of-plane bending moments were calculated using the recorded value of the pitch angle.

Table III: Strain gauge location given as the distance from hub center (HC).

Parameter	Position Sky River	Position Andros
Blade root bendings	r=1.05m from HC pitch 0 and 90	r=1.04m from HC pitch -45 and 45
Main shaft bendings	r=0.3 m from HC	r=0.49m from HC

5. WIND FIELD

Both deterministic and stochastic characteristics of the wind field at the two sites in terms of ten minutes averages are investigated in this section, in order to identify similarities and differences. In order to establish a common base for comparison of the various parameters measured at the two sites, a narrow wind direction sector was applied at each site, i.e 234°-274° for Sky River and 335°-20° for Andros. The reason for selecting these sectors is that in both cases the direction of the incoming wind is perpendicular to the orientation of the ridge.

Vertical wind profiles computed for three wind speed intervals, i.e 7-9m/s, 12-14m/s and 16-18m/s are shown for both sites in Figure 4. The profiles are rather uniform exhibiting a slight increase at about hub height.

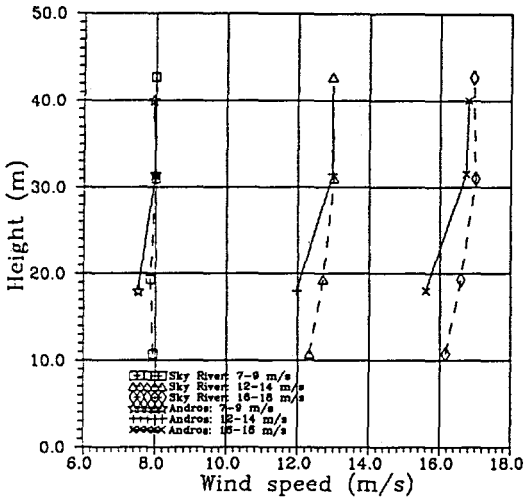

Figure 3: Vertical wind profiles at Sky River and Andros

Mean, maximum and minimum values of the turbulence intensity, computed as the ratio of the standard deviation of the wind speed over the mean wind speed at hub height are shown in Figure 4 for both sites.

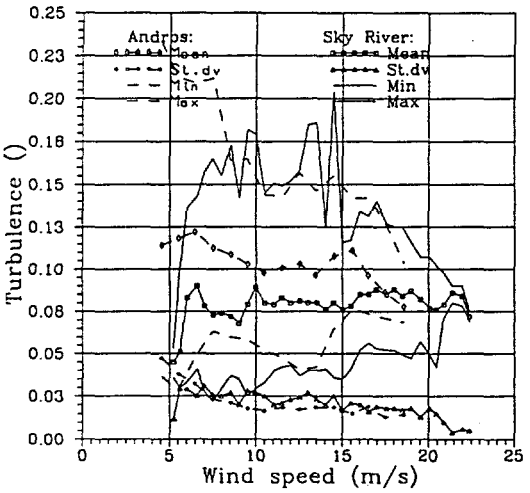

Figure 4: Turbulence intensities at Sky River and Andros.

It is evident that the turbulence intensity values are of the same level, varying in the range from 8% to 10% at both sites. The turbulence intensity values are typical for hill tops and ridge tops with medium slopes [1] and [2].

The ratios of the standard deviations of the turbulence velocity components σ_v/σ_u and σ_w/σ_u were calculated using measurements from the sonic anemometers. The resulting values were found to be similar, in the range, about 1.0 and 0.8 at Sky River and 0.95 and 0.72 at Andros respectively for the two ratios. For flat terrain the corresponding values are lower i.e. 0.8 and 0.5 respectively [3].

The longitudinal length scales were estimated from the cup anemometers for both sites . The relevant calculations were carried out fitting the Von Karman spectrum with the measured data over the frequency range 0.10 Hz to 0.25 Hz. Details can be found in [4]. The lengthscales are shown in Figure 5. The values are lying in the range from 20 to 250 for both sites exhibiting a considerable variation. The lengthscales for the vertical and lateral components were found to $L_v=0.6L_u$ and $L_w=0.24L_u$ at Sky River and to $L_v=0.5L_u$ and $L_w=0.25L_u$ at Andros. At both sites the distribution of the longitudinal wind speed component was found to differ from the Gaussian distribution.

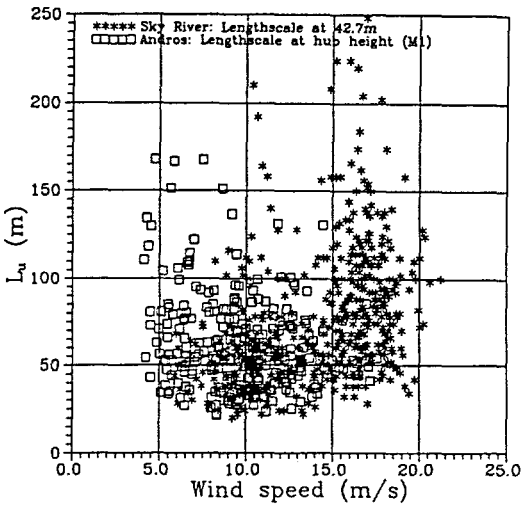

Figure 5: Length scales at Sky River and Andros

6. POWER CURVE MEASUREMENTS

For comparison of the measured power curves, data were normalized to the sea level air density referring to the ISO standard atmosphere (1.225 kg/m^3). In addition data were corrected for mean flow distortion effects which cause the wind speed at the meteorological mast and at the wind turbine location to be different. For the Sky River case the WAsP model was applied for these corrections. For the Andros case a site calibration procedure was implemented, using an anemometer mounted on the top of the nacelle of the wind turbine [5].

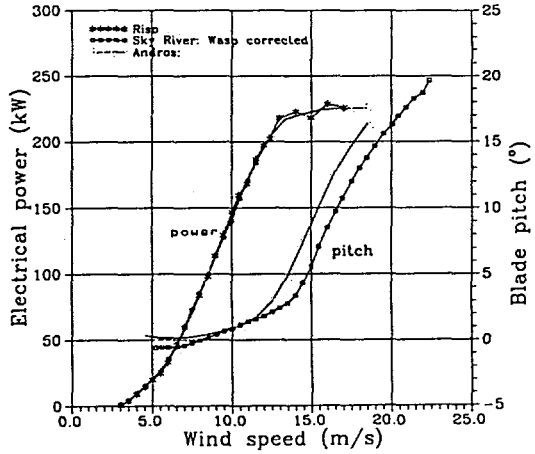

Figure 6: Normalized power curves measured at Sky River, Andros and at Risø (flat terrain)

In Figure 6 the normalized power curves (power normalization for Sky River) referring to the standard air density and to the undisturbed wind speed are presented for both sites along with the power curve measured for the V27 at the Risø test site (homogeneous terrain) [6].

In order to illustrate the behavior of the two machines, the variation of the pitch angle (mostly related to the control strategy of the wind turbine) with wind speed is also presented in Figure 6. As it is expected, the observed differences, are more pronounced in the regulation area, and they are due to the control strategy of the wind turbine. The pitch control system keeps the power at its nominal value at high wind speeds, independently of the air density which is different at the two sites. At Andros the power regulation starts at about 12 m/s and at Sky River it starts about 14m/s. At lower wind speeds the pitch system optimizes the power output by choosing the optimal pitch angle depending on the wind speed.

Concerning the two power curves measured at Sky River and Andros, a good agreement is observed for the entire range of operation. In addition, the observed similarity between the power curves measured in homogeneous and in complex terrain, indicate that the corrections related to the flow distortion were succesfull.

7. LOAD MEASUREMENTS

The fatigue loads for the blade root bending moments, the yaw and tilt bending moments are selected for comparison of the load measurements. The fatigue loads are compared in terms of their damage equivalent load L_{eq}, calculated using the rainflow load spectrum $R_i(n_i)$, by the following equation:

$$L_{eq} = \left((R_i(n_i)^m n_i)/N_{eq} \right)^{-m},$$

where N_{eq} is an equivalent number of load cycles and m is the material SN-curve exponent. N_{eq} equals 1200 for a ten minutes time history corresponding to 1 Hz. The equivalent loads discussed herein, are calculated with m=12 for the blade bending moments and with m=4 for the shaft bending moments. The high value is better suited to plastic material, while the low value corresponds to steel components.

In order to compare the equivalent bending moments it is necessary to ensure similar operational conditions, i.e. yaw misalignment and pitch variation. The above condition is mostly satisfied for wind speeds below the rated power. Above the rated power the turbines are operating at different pitch angels. The flapwise bending moment, the yaw and tilt moment are normalized to the standard air density in the whole wind speed range. The edgewise bending moment is not normalized.

In Figures 7 and 8 the equivalent loads for the blade root flapwise and edgewise bending moment, for both sites, are presented respectively. The fatigue loads for the flapwise bending moment are fully comparable for the two sites. Some high values observed at low wind speeds in the Andros data are due to the change in the rotational speed (33rpm to 44 rpm), similar conditions for the Sky River case have been excluded during data reduction. A fairly good agreement is resulting from the comparison of the edgewise bending moments for wind speeds below 10m/s. The significant discrepancies observed at higher wind speeds should be attributed to the different pitch angles, taking also into account the different coordinate systems used for the calculation of the blade root bending moments. As previously referred, in the Sky River case the bending moments on the blade were measured with reference to the blade coordinate system (flapwise and edgewise blade bending moments). In the Andros case the bending moments were transformed to the hub coordinate system (in-plane and out of plane bending moments). These two coordinate systems coincide only in the case of zero pitch angle.

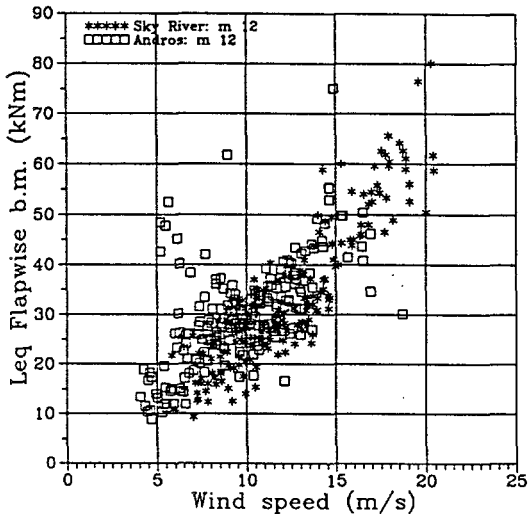

Figure 7 : Equivalent flapwise bending moment (m=12)

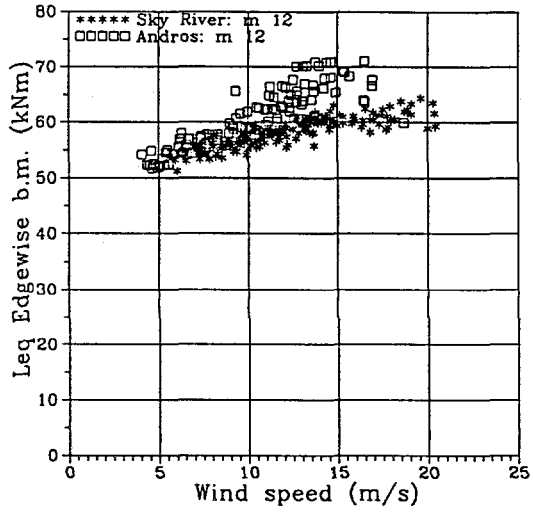

Figure 8 : Equivalent edgewise bending moment (m=12)

The equivalent loads for the yaw and tilt moment, are compared in Figures 9 and 10. The values observed at Sky River at wind speed up to 12 m/s are seen to be slightly lower than the corresponding values observed at Andros. The explanation is probably due to the differences in the yaw and tilt resonant frequencies of the turbines. At higher wind speed comparable values are observed.

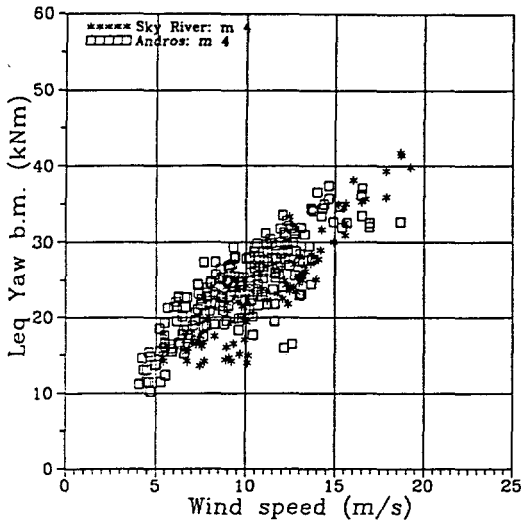

Figure 9 : Equivalent shaft yaw bending moment (m=4)

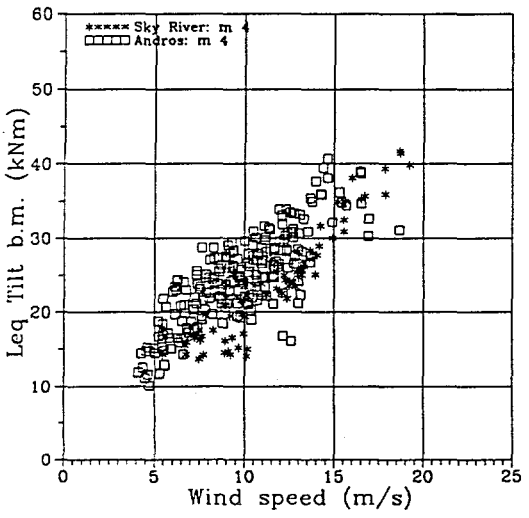

Figure 10 : Equivalent shaft tilt bending moment (m=4)

8. CONCLUSIONS

The basic wind flow properties (i.e wind profiles, turbulence intensity levels, length scales) which are expected to influence the behavior of the machines are investigated for two different complex terrain sites. Next a comparison of the performance and load characteristics of two V27-225 machines operating at the different sites is made.

The inflow wind characteristics at the two sites are found to be comparable. The turbulence level at both sites are very low (8 and 10 %) The lowest turbulence are observed at Sky River where the upwind hill slope is 12°, about twice the slope at the Andros site. The ratios of the standard deviations of the turbulence velocity components σ_w / σ_u and σ_v / σ_u are found to be similar, in the range of 0.95-1.0 and 0.72-0.80 for both sites. For flat terrain the corresponding values are 0.8 and 0.5 respectively. The vertical wind shear profiles were also found to be similar. The profiles were rather uniform exhibiting a slight increase at about hub height.

After normalization of the data to the standard air density and corrections applied to account for the mean flow distortion effects, the measured power curves are found to be in good agreement with each other.

Dynamic loads are computed using their equivalent load ranges. They are found in good agreement in the range where similar operational conditions, i.e. yaw misalignment and pitch variation. In view of the almost identical turbulence characteristics at the two sites, it is impossible to conclude whatever the observed minor differences in the loads are due to the site or due to the fact that the turbines differ slightly with respect to the natural frequencies.

REFERENCES

[1] G.L.Glinou et al. "Wind Measurements in Complex Terrain, the Case of Crete", EWEC'94, Thessaloniki, (1994)

[2] S.M. Petersen et al. "Load Measurements on a Pitch Regulated Wind Turbine in Inhomogeneous Terrain Sky River - Vestas V39", Risø-I-834(EN). Risø National Laboratory, Roskilde, Denmark (1994)

[3] A.Kretz, H.A. Madsen, J.T. Petersen "Measured and Simulated Turbulence - Compared at a Section of a Rotating Wind Turbine Blade", Risø-R-671(EN). Risø National Laboratory, Roskilde, Denmark (1994)

[4] B.M.Adams, "Dynamic Loads in Wind Farms II", Final report of JOU2-CT92-0094, October 1995

[5] E.E.Morfiadakis, G.L.Glinou, N.C.Stefanatos. Power Performance Evaluation of Wind Turbine Operation in a Complex Terrain Wind Farm, CRES

[6] S.Petersen, Wind Turbine Test, Vestas V27-225 kW, Risø-M-2861 (1990)

FATIGUE LOADING ON OFFSHORE WIND POWER STATIONS

Sten Frandsen
Test Station for Wind Turbines, Meteorology and Wind Energy Dept.
Risø National Laboratory
DK-4000 Roskilde, DENMARK

ABSTRACT: The analyses of data from the measurements on the Vindeby Wind Farm are summarized, and wind farm fatigue loads are modelled. The result is that with the configuration of this particular wind farm, the integrated so-called equivalent load is approx. 15% lower offshore. Generalization of the results leads to very simple expressions for an "equivalent turbulence intensity" for wind farm load cases.
Keywords: Wind farm, Coastal sea sites, Fatigue, Turbulence.

1. INTRODUCTION

The objective of the analysis is to quantify the increase or decrease in fatigue loading caused by wind farm effects offshore. The objective is pursued by making a direct comparison of the measurements, and by devising a set of models of turbulence, wake widths etc. to extent the results of the measurements to other wind turbine separations. The analyses are described in details in [1].

Measurements have been conducted for several years on the wind farm at Vindeby 2-3km off to the north-west of the coast of the island of Lolland in the South Baltic Sea. The Vindeby Wind Farm consists of 11 Bonus machines with installed capacities of 450kW, hub height 38m and rotor diameter 35m. The separations of the machines in the rows, see Figure 1, are 300m (8.6*D*), and the distance between the rows is equally 300m. Two machines, 4W and 5E are instrumented for structural measurements; tower base bending, yaw and tilt and edge and flapwise blade root bending moments are measured and statistics for ½hourly consecutive time periods are stored. The statistics include minimum, maximum, mean, standard deviation and the so-called equivalent load widths. The equivalent load width is popularly speaking the amplitude of a sinusoidal load with frequency equal to rotational frequency that would consume the same fatigue life as the actual load sequence.

Wind climate measurements are made at three towers, one placed on the shore, and two, see Figure 1, close to the wind farm. The positions of the sea based tower are so that they match wind turbine positions in an imaginary larger wind farm with the same wind turbine separations. This gives the opportunity to also measure wakes as seen by the wind turbines. In the analyses presented in this paper wind statistics in the height 38m are applied. The analyses apply approx. 13,000 sets of valid ½hour statistics, with the instrumented machines in operation.

2. METHOD OF DATA ANALYSIS

From sensitivity analysis, we know that turbulence is a primary load parameter and it may be argued that from a statistical point of view turbulence can represent other parameters: in the unobstructed flow field in neutrally stratified atmosphere both vertical shear and turbulence are proportional to wind speed, and under wake conditions turbulence and speed deficit (and thus horizontal shear) are proportional to the wind turbine thrust coefficient C_T. While this on the one hand makes it difficult to separate the effects, it does on the other hand imply that a turbulence parameter may correlate well with loads. Thus, we center on the along-wind turbulence component, σ_u, and the free flow mean wind speed at hub height, U, as independent parameters causing fatigue. The analyses to follow aim at verifying simple physical models or empirical expressions for turbulence, mean wind speed and equivalent widths and the inter-connection of these parameters, by means of the data available.

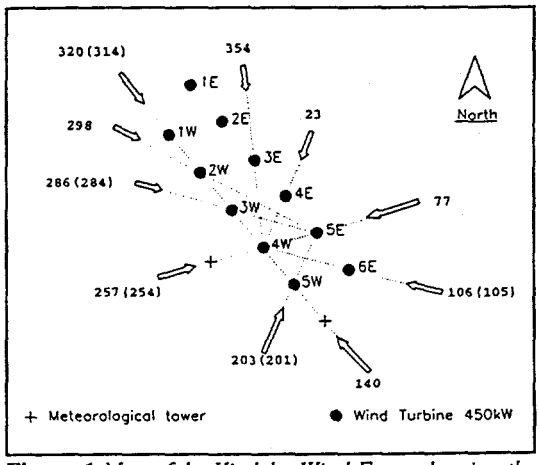

Figure 1 *Map of the Vindeby Wind Farm showing the wind directions, where one or both instrumented wind turbines are in the wake of one of the other machines.*

Seeking simplicity we looked for one structural load, which represents well most turbine loads under most load conditions. The flapwise blade bending moment seems to fulfil that requirement. So when nothing else is stated the equivalent load referred to is the equivalent load of flapwise blade bending of the machines 4W and 5E, Figure 1.

The dynamics - fatigue load spectrum as well

as standard deviation - of the structural components of the wind turbines depend on wind direction as illustrated in Figure 2, where equivalent widths for flapwise bending of blades are shown as function of wind direction. In the figure, the equivalent width, s also denominated *ew* in figure, has been smoothed of 9 ½hour estimates. For westerly wind directions (230° to 300°) the 4W turbine unit, see Figure 1, is exposed to the unobstructed flow, and for easterly directions (340° to 120°) the 5E unit is not in the wake of other wind turbines, and s is basically constant though with some variability. Notably, s increases for both machines from the approximate direction 140° to 220°, for the 5E unit with a wake condition from 5W superimposed.

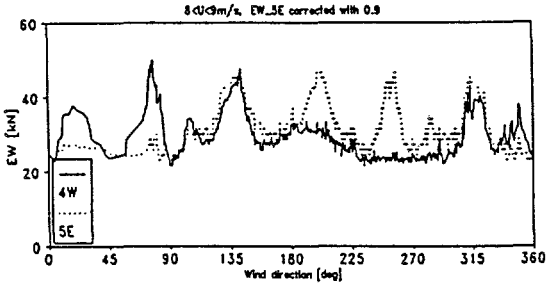

Figure 2 *Equivalent widths of flapwise bending moment of the instrumented units 4W (full line) and 5E.*

In the following we *first* disregard wake effects by choosing load situations without obstructing turbines and investigate how fatigue loads are altered on a stand alone wind turbine when moving from land to offshore. *Secondly*, the turbulence and the equivalent load "wake shapes" - i.e. the change of turbulence and equivalent load across the wake - are analyzed. *Thirdly*, we investigate maximum turbulence levels in the wake. *Fourthly*, we analyze maximum equivalent load under wake conditions. Performing these analyses, we also try to devise more general expressions for the quantities involved, valid for other wind turbine separations and other ambient turbulence. And *finally*, we present an extrapolation of the results to other wind farm configurations (separation and no. of rows) than the one investigated.

2. UNOBSTRUCTED FLOW

The sensitivity analysis, [1], more or less pointed to proportionality between turbulence and dynamic response (standard deviations and equivalent loads). As it was seen in Figure 2, there is a distinct increase in equivalent width s for wind directions from the land side of the wind farm. This could indicate that the smaller turbulence length scale (shorter time scale) from the land side causes a larger s simply by speeding up the process even though the load amplitudes - represented by turbulence intensity - is unchanged. This and other observations, [1], point to an important conclusion, namely that winds from southerly wind directions - despite to 2km distance to shore - represent onshore load conditions with a surface roughness of approx. 0.01m quite well. This is utilized to make reference to onshore load conditions.

In Figure 3 and 4 equivalent widths and σ_u are averaged over 10 ½hour values and plotted against wind speed, for wind from land and water, respectively. It is seen that the equivalent width rather neatly follow a simple curve $a \cdot \sigma_u$, where $a \approx 35$-36.

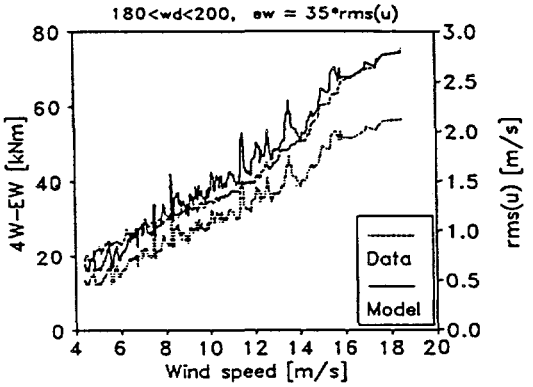

Figure 3 *Equivalent width of 4W from land, with σ_u model.*

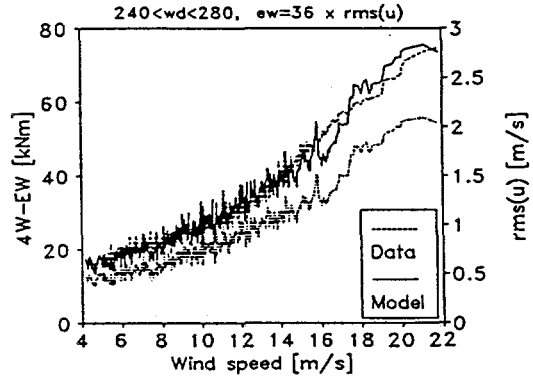

Figure 4 *Equivalent width of 4W with wind from water, with σ_u model fit.*

Also, a regression analyses are performed on azimuthal averaged values of s and σ_u in the transition between land conditions and water conditions, w=180°-224°. This way the following regression expression has been found:

$$s \simeq (24 - 0.25\ U)\ \sigma_u + (0.155U)^3 + 7.6 \qquad (1)$$

Thus, if this expression and the simpler $a \cdot \sigma_u$ are bothvalid we may - indirectly - find the turbulence variation over water as function of wind speed by equalizing the two:

$$\sigma_{u,water} \simeq \frac{(0.155U)^3 + 7.6}{0.25U + 12} \qquad (2)$$

This turns out to be a good approximation of turbulence under free flow conditions over water for wind speeds less than 16-18 m/s under neutral stratification.

Applying [2], it is found that for constant geostrophic wind speed the difference in wind speed at hub height h=38m for terrains with z_o=10^{-4}m and z_o=0.03m (typical Danish farmland), respectively, is

approx. 17%. Thus, comparing fatigue loads in terrains with different surface roughness, also the difference in mean wind speed must be taken into account. The weighted equivalent width, see [1], is calculated as

$$s_e = \left\{ \int_0^\infty s^m(u)\, f_w(u)\, du \right\}^{1/m} \qquad (3)$$

where f_w is the Weibull distribution with shape parameter k=1.8, s=36·σ_u, $\sigma_{u,land}$=0.14·U(=U/ln(h/z_0)) over land, $\sigma_{u,water}$ is found from (2), and m is the exponent of the *SN* curve used to transform the measured fatigue load spectrum to the equivalent load, s. In Table I equivalent loads are given for two different annual mean wind speeds. In the rightmost column the differences in equivalent loads are given. It is seen that for the same annual mean wind speed the difference in equivalent width is 22-25%. The fatigue load-level for pure offshore conditions and for the wind from over land, I=14%, are shaded in the table, showing an approx. 15% lower equivalent width for offshore conditions compared to onshore conditions with the same geostrophic wind speed distribution.

3. WAKE SHAPES AND WIDTHS

Figure 5 shows equivalent widths, s, of flapwise blade bending of unit 5E when more or less in the wakes of units 1W-3W (i.e. multiple wake condition), for wind speed between 9 and 11m/s. Also shown is the model-fit:

$$s = c\,(1 + \alpha \exp(-(\frac{wd - wd_{max}}{\beta})^2)) \qquad (4)$$

where c is base level equivalent load, w and w_{max} is wind direction and wind direction with maximum equivalent load, respectively. The data is seen to fit the "bell" model well. For the selected wind speed range the width parameter is β=8°. This characteristic width is found to fit all wake conditions seen at Vindeby, though it decreases slightly for large wind turbine separations and for high wind speeds. Further, it is found that the wake turbulence (horizontal) profile follows equivalent load closely, [1]. Also indicated in Figure 5 is the "equivalent fatigue wake", i.e. a rectangular wake contributing the same life consumption as the real wake. The derivation of this equivalent wake width is given in [1].

It turns out that horizontal variation of turbulence and equivalent fatigue width for single, double and multiple wake are approximately the same.

4. MAXIMUM WAKE TURBULENCE

Several sets of wake turbulence data selected to represent center line turbulence show that maximum hub height wake turbulence, $\sigma_{u,wake}$ is basically the same whether there is one, two or several wind turbines upstream to of the wake. It is found that the following expression does match measured maximum wake turbulence well:

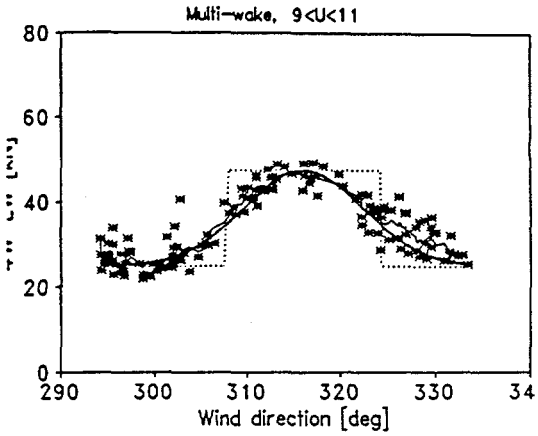

Figure 5 *Multiple wake, raw data, smoothed curve, fit: c=25, α=0.9, β=9°, and equivalent wake.*

$$\frac{\sigma_{u,wake}}{U} = \sqrt{\frac{1.2C_T}{s_t^2} + I_o^2} \qquad (5)$$

where C_T is the (nearest) wake generating wind turbine's thrust coefficient, s_t=x/D the dimensionless turbine separation, and I_o=σ_u/U turbulence intensity of the ambient flow field. Crespo and Hernandez, [3], argue that maximum turbulence in the near wake is 0.36; Højstrup (personal communication) finds - based on experience from various wind farm measurements - that wake turbulence never exceeds 0.25. We apply a maximum limit of (4) of 0.30 for small values of s_t.

5. MAXIMUM EQUIVALENT WIDTH

Figures 6 and 7 give center wake equivalent loads for single and multiple wake conditions. Also free stream turbulence (lowest curve, full line) as well as measured (full line) and modelled wake turbulence (broken line) are plotted in the figures.

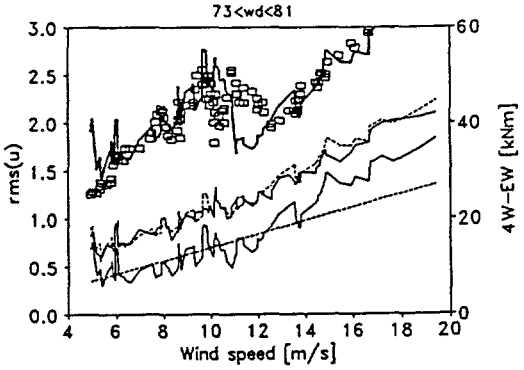

Figure 6 *Single wake on 4W; lowest curve are free-σ_u, wake-σ_u and wake-σ_u-model, respectively; squares are s and thick line s-model.*

First, it is worth noting how well the wake turbulence model, expression (5), works, both for different wind turbine separation, and for single and multiple wake cases. Secondly, it is seen that equivalent loads in the wakes have a more complicated development with wind speed than was found for free stream conditions. At this point we can only offer a qualitative explanation to the phenomena, namely that for low wind speeds, with large C_T/s_t^2, the structure of turbulence including turbulence scale and coherence are dominated by the turbulence generated by the wind turbine, and for higher wind speeds the turbulence structure becomes more identical to free flow turbulence. We offer in [1] a model for maximum equivalent load in the wake.

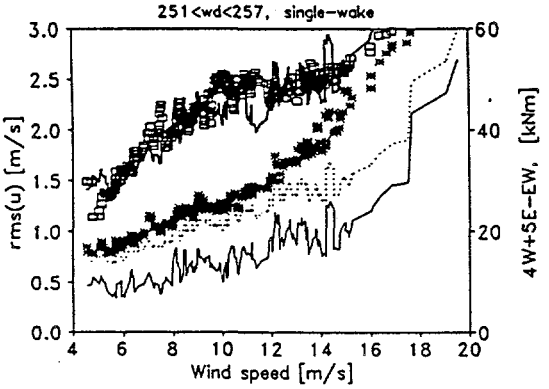

Figure 7 *As last figure; squares are s-5E in wake and crosses s-4W free; only modelled wake-σ_u*

6. THRUST COEFFICIENT, C_T

In pursue of a simple fit of the C_T curve we utilize the observation that the measured wake speed deficit appears constant independent of wind speed at the distance $8.6D$ downstream, $\Delta u(s=8.6)\approx 1$m/s; thus, assuming that Δu is only a function of downstream distance, that Δu=1m/s at the distance s=8.6, and that $max\{C_t\}$=1 lead to the following expression for the thrust coefficient:

$$C_T = \frac{3.5(2U - 3.5)}{U^2} \qquad (6)$$

This expression fits measurements well. It is assumed that the fit to a good approximation can be applied for other machines than the Bonus machine of Vindeby.

7. EXTRAPOLATION OF RESULTS

In order to generalize the results, we use the idealized wind farm layouts illustrated in Figure 8: 1) 1-wake situation, corresponding to two machines close one another (not shown), 2) a single row, 3) 2-rows similar to Vindeby, and 4) "wind farm conditions", case 4) being regarded as one case since we found that the number of layers of wind turbines around the target wind turbine were of little or no consequence to fatigue loading. The number of wakes taken into account is illustrated in Figure 8.

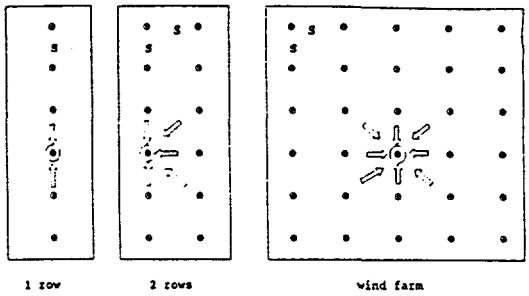

Figure 8 *3 of 4 considered wake configurations; spacings are equal in all directions.*

First, this result is applied to produce a table similar to Table I, but here comparing loads on a machine in a 2-row configuration, offshore and onshore. The result is given in Table II, where it is seen that for the same mean wind speed the equivalent load is 23-29% less offshore, the difference increasing for decreasing annual mean wind speed. If it is taken into account that mean wind speed is higher offshore than onshore for the same geostrophical wind, the difference decreases to 14%.

Next we will apply the setup of models, outlined inhere but described in details in [1], to estimate the total, integrated equivalent load for the four cluster configurations. Figure 9 shows the offshore case for an annual mean wind speed of 8 m/s. For approx s_t>8-10 there are small wind farm effects for all considered cases. For s_t<8-10, the wake effects increase and reach levels up 40% of free stream values for the "farm" case for separations of $4D$ and less than that for the other cases.

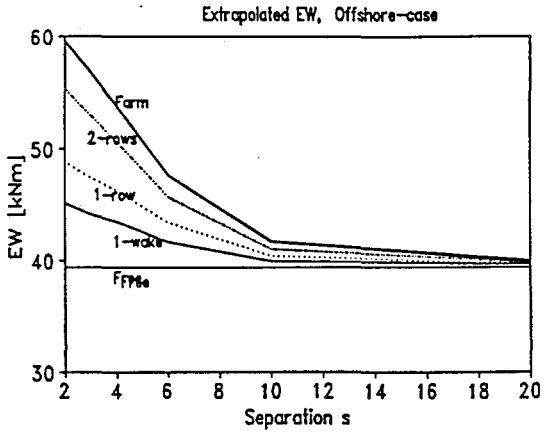

Figure 9 *s as function of wind turbine separation for offshore conditions; 4 machine configurations; Mean wind speed U=8m/s.*

8. CONCLUSIONS

It was found that for the geometry of the Vindeby Wind Farm fatigue loads of equivalent loads are approx. 15% lower offshore than onshore. Calculating an

"effective" turbulence intensity, I_{eff}, to substitute detailed wake calculations it was found that offshore, I_{eff} is not expected to reach - under realistic circumstances - the 0.17 level prescribed in the EIC draft standard as a reference.

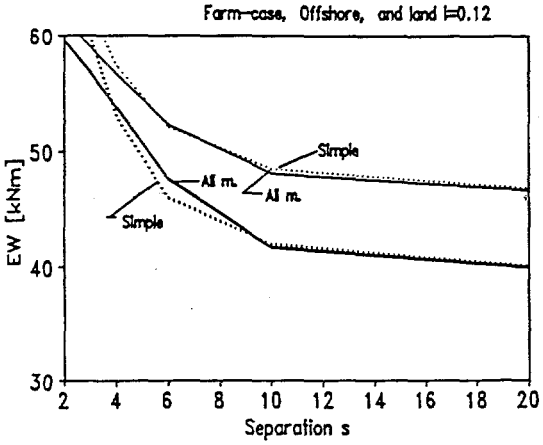

Figure 10 *Comparison of integrated and simple models for farm-case, onshore and offshore; U =8m/s.*

Figure 10 illustrates an attempt to point to future criteria for design of wind turbines for offshore as well as onshore. The figure shows *s* for case 4), the wind "farm" case, for offshore and onshore conditions (full lines), and a very simple model for the effective turbulence intensity to be applied. It is similar to the model applied for wake turbulence, inspired by a model, [4] and [5], which results in expressions for speed deficit and turbulence. Her it has been given an even simpler form:

$$I_{eff} = \sqrt{k_n \frac{0.4 C_T}{s_t^2} + I_o^2} \qquad (7)$$

where k_n is a constant for each of the four machine configurations, being equal to 1 for case 4), and less than 1 for the other cases. The curve fits of Figure 10 have been obtained simply by using an equivalent load of $s=36 \cdot I_{eff} \cdot U$ ($s<75$) and integrating as in (3). As seen the fits are excellent except for the smallest separations.

The modelling outlined is based on data with rather large wind turbine separations, and scarce experimental evidence on dynamic loads for smaller separations. However, while in detail the complex of models are incomplete, we find that the end result is fairly reliable and may be used in future design codes.

Finally it is suggested that some efforts are invested in the near future to a) verify assumptions in more details, b) verify the submodels, and b) to verify and possibly calibrate the models for small wind turbine separations. Also, it should be carefully considered whether - as expected - machines other than the stall regulated concept display basically the same behavior.

9. ACKNOWLEDGEMENT

The work has been co-financed by Danish Government Energy Research Program, the European Commission under contract CT93-0350, and the East-Denmark utility association ELKRAFT.

Table I Equivalent widths for unit 4W, offshore and onshore, no wake effects.

U_y (m/s)	$s_{e,tot}$ offshore (kNm)	$s_{e,tot}$ onshore (kNm)	Difference
8.80	42.9	56.0	-23%
7.38	36.5	51.1	-29%

Table II Equivalent loads, onshore and offshore, 2-row case (3).

U_y (m/s)	$s_{u,tot}$ offshore (kNm)	$s_{u,tot}$ onshore (kNm)	Difference
8.80	44.7	56.9	-21%
7.38	38.8	52.2	-26%

10. REFERENCES

[1] Frandsen, S. (editor), A. Crespo, L. Chacón, R. Gómez-Elvira, J. Hernández, J. Højstrup, F. Manuel, P. Sørensen and K. Thomsen, "Measurements on and modelling of offshore wind farms", Risø Report (1996); to be published.

[2] Petersen, E.L. and I. Troen, "European Windatlas", Risø, (1989).

[3] Crespo A., and J. Hernández, "Analytical correlations for turbulence characteristics in the wakes of wind turbines", Proceedings of ECWEC'93, pp. 436-439. Travemünde, Germany (1993).

[4] Emeis, S. and S. Frandsen, "Reduction of horizontal wind speed in a boundary layer with obstacles", Boundary Layer Meteor., 64, 297-305 (1992).

[5] Frandsen, S., "On the wind speed reduction in the center of large clusters of wind turbines", Journal of Wind Engineering and Industrial Aerodynamics, 39, 251-265 (1992).

DESCRIPTION AND MEASUREMENTS OF THE WIND THAT DRIVES THE POWER PERFORMANCE AND MEAN LOADS OF WIND TURBINES

Troels Friis Pedersen, Søren Markkilde Petersen, Per Vølund
The Test Station for Wind Turbines
Department for Meteorology and Wind Energy
Risø, 4000 Roskilde Denmark

ABSTRACT: The paper analyses the wind input to a cup-anemometer and to a wind turbine to evaluate the definition of the "measured" wind speed relative to the "measured" power and mean loads. The analysis is based on an artificial 3D wind of 8m/s and 0%, 10% and 20% turbulence intensity, respectively, and theoretical models of a cup-anemometer and a wind turbine. A 3D dynamic response code is used to calculate the "measured" wind speed by the cup-anemometer and a 3D aeroelastic code is used to "measure" the power and flapwise root bending moment of one blade on the wind turbine. Flow distorsion effects due to topography, mast, boom, clampts, etc. are not considered, and full correlation between the wind speed at the cup-anemometer and the wind speed at the hub of the wind turbine is assumed. The "measured" data are compared to the well-described artificial wind under different definitions ot the wind speed.

Keywords: Wind speed: anemometers: performance: test methods

1. INTRODUCTION

For the last fdecades, wind speed measurements have been carried out with cup-anemometers positioned at hub height to measure the wind speed and turbulence intensity for power performance and load measurements on wind turbines. Little attention has been payed to the definition of the measurand, i.e. the definition of the "measured" wind speed. The consequence of this is, that the measured wind is not interpreted in a consistent way. It becomes important when high accuracy of the wind speed measurement is required. The question is what the "measured" wind speed of the cup-anemometer is, compared to the definition of the wind speed and the power and loads on the wind turbine.

2. MODELLING THE WIND

The wind that is used for the analysis is an artificial wind for homogenous terrain with wind shear and a wind spectrum corresponding to a Kaimal length scale of about 700m. The model used to generate the artificial 3D wind is the model by Mann, Ref. 1. The wind was decided to have an average u-wind speed component (longitudinal) of 8m/s at the center of the rotor for all wind flows. The wind model derived the wind components u,v,w in a quadratic grid of 24x24 points across the wind turbine rotor. Time series were derived with 32Hz sampling rate for 10 minute data sets.

The wind turbine will be applied the whole wind field throughout the swept area of the rotor, whereas the cup-anemometer will only see the wind flow in the center of the rotor (assuming no induced wind speed on the cup-anemometer from rotor, mast, boom, clamps, topography etc.).

The wind flows that were considered for both the wind turbine and the cup-anemometer are described in the following.

Plane and constant flow

This flow is comparable to a wind tunnel flow. In this case the wind speed (the u-component) is constant all over the swept area of the rotor. The v- and w- components are zero.

Plane Flow (1D flow)

In this case the v- and w-components are zero.
The longitudinal u-component at the cup-anemometer is varying and is the same all over the swept area of the rotor.

Horizontal flow (2D flow)

In this case the vertical w-component is zero, whereas the u- and v-components are varying all over the swept area of the rotor. This flow is based on the assumption that the cup-anemometer only measures the horizontal components of the wind vector and that the wind turbine also only responds to the horizontal components.

Real flow (3D Flow)

This flow represents the real world conditions where the cup-anemometer only sees the varying 3D wind flow in a point and the wind turbine is exposed to the 3D flow field all over the swept area of the rotor.

The following figures describe the main components of the artificial 3D wind speed data used in the analysis.

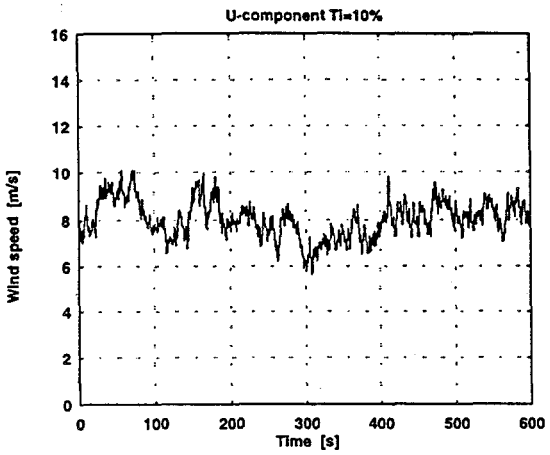

Fig. 1 u-plot of artificial 3D wind speed data at the cup-anemometer with u=8m/s and turbulence intensity 10%

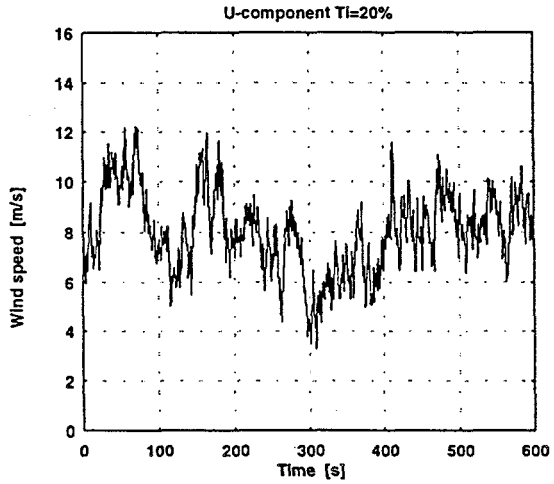

Fig. 2 u-plot of artificial 3D wind speed data at the cup-anemometer with u=8m/s and turbulence intensity 20%

3. THE CUP-ANEMOMETER MODEL

The model of the cup-anemometer is based on the mechanical structure and the aerodynamic response behaviour basically determined by empirical measurements.

The cup-anemometer rotor has a certain moment of inertia I, and the forces on the rotor are the aerodynamic forces from the cups and the frictional forces due to bearings.

Aerodynamic forces

The model of the ideal cup-anemometer is simplified to consider only a constant overall aerodynamic drag coefficient on one cup on each side of the cup-anemometer with the cups positioned always with the cup-arms perpendicular to the wind speed as shown in Fig. 3. The simplification does not consider the detailed aerodynamics of the rotor, but it is justified when the aerodynamic forces are integrated over one third revolution of a rotor with three cups. The aerodynamic torque on the rotor is:

$$M_A = R\frac{1}{2}\rho A((U - R\omega)^2 C_{DH} - (U + R\omega)^2 C_{DL})$$

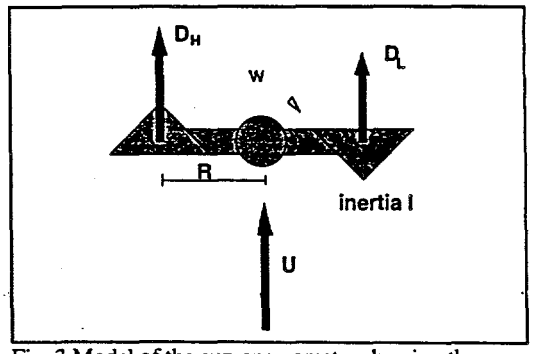

Fig. 3 Model of the cup-anemometer showing the aerodynamic drag forces

Friction

The friction in bearings is the second import force on the cup-anemometer shaft. It has been found that the frictional torque is a second order polynomia to the angular speed. The friction might be quite dependant on the temperature.

$$M_B = B_0 + B_1 \cdot \omega + B_2 \cdot \omega^2$$

The friction coefficient B_0 has the dimension [kg m^2/s^2], B_1 has the dimension [kg m^2/s], and B_2 has the dimension [kg m].

Angular characteristics

The angular characteristics of the cup-anemometer is taken into account as described in the following. The momentaneous wind vector at the cup-anemometer is:

$$\vec{U} = (u, v, w)$$

The momentaneous wind speed (length of the wind vector) is:

$$\left\langle \vec{U} \right\rangle = \sqrt{u^2 + v^2 + w^2}$$

The cup-anemometer responds to the actual flow on the rotor. To take this into account in the model it is assumed that the response at different flow angles is determined relative to the response at a right angle of attack. The angle incident apon the cup rotor is:

$$\alpha = \mathrm{Atan}\frac{w}{\sqrt{u^2 + v^2}}$$

The angular response of the cup-anemometer can then be expressed with the function F_α.

$$U = F_\alpha(\alpha)\left\langle \vec{U} \right\rangle$$

where U is the right angle of attack wind speed that gives the same forces on the rotor as the wind vector inclined to the angle of attack α.

General torque equation with friction

The resulting describing equation of the cup-anemometer is:

$$M = M_A - M_B$$

$$= R\frac{1}{2}\rho A((U - R\omega)^2 C_{DH} \cdot (U + R\omega)^2 C_{DL}))$$

$$-(B_0 + B_1\omega + B_2\omega^2)$$

The equation is valid for speed ratios (Rω/U) higher than zero and lower than one. The general torque equation can be rearranged to:

$$\frac{d\omega}{dt} = \frac{\omega^2}{I}\left(\frac{\rho AR^3}{2}(C_{DH} - C_{DL}) - B_2\right)$$

$$-\frac{\omega}{I}(U\rho AR^2(C_{DH} + C_{DL}) - B_1)$$

$$+\frac{1}{I}\left(\frac{U^2\rho AR}{2}(C_{DH} - C_{DL}) - B_0\right)$$

The solution to the torque equation was found using the Burlish - Stoehr numeric solver to the ordinary differential equation, Ref. 2.

The calibration of the cup-anemometer did in the analysis not follow a straight line, as for usual calibrations, but was based on the static solution to the torque equation, which is almost a straight line:

$$U = \frac{\rho AR^2\,\omega(C_{DH} + C_{DL}) + \sqrt{S_q}}{\rho AR(C_{DH} - C_{DL})}$$

where:

$$S_q = (\rho AR^2\,\omega(C_{DH} + C_{DL}))^2$$

$$-2\rho AR(C_{DH} - C_{DL})\left(\frac{1}{2}\rho AR^2\,\omega^2(C_{DH} - C_{DL})\right.$$

$$-B_0 - B_1\,\omega - B_2\,\omega^2$$

4. CUP-ANEMOMETER DATA

The data for the cup-anemometer used in the analysis are based on the Risø cup-anemometer. The data are considered to have realistic proporties with friction and angular characteristics, though they are collected from different sources and have not been verified in detail. The distance constant derived from the data is 2.8m. Ideal sampling of the angular speed is assumed. Angular characteristics are shown in Fig. 4, from ref. 3.

Table 1 Cup-anemometer data

Cup diameter:	0.07 m
Rotor arm R:	0.093 m
Rotor inertia I:	$1 \cdot 10^{-4}$ kg m^2
High mean cup drag coefficient C_{DH}:	1.2
Low mean cup drag coefficient C_{DL}:	0.16
Static friction coefficient B_0:	$13 \cdot 10^{-6}$ kg m^2/s^2
Dynamic friction coefficient B_1:	$0.7 \cdot 10^{-6}$ kg m^2/s
Parabolic friction coefficient B_2:	$0.001 \cdot 10^{-6}$ kg m^2

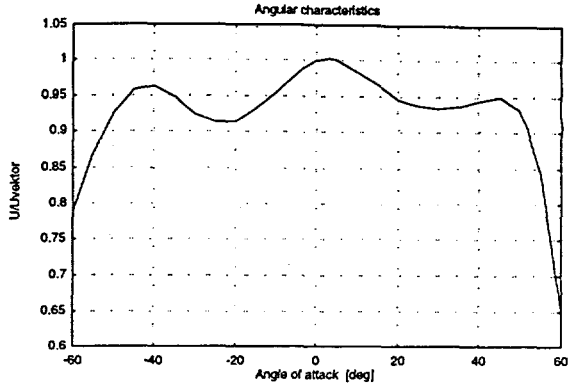

Fig. 4 Angular characteristics of the cup-anemometer, from ref. 3.

5. THE WIND TURBINE MODEL

The aeroelastic code used to calculate the response of the wind turbine is the HawC code, developed by Petersen, Ref. 4. The model uses a full 3D turbulent wind flow input to the rotor. Aerodynamic forces includes tower shadow and dynamic stall modelling. Structural modelling is based on flexibility in blades, rotor and tower. For further information see Ref. 4.

6. WIND TURBINE DATA

The wind turbine data used in the analysis are based on data for the Vestas V27 wind turbine. The average wind speed was 8m/s, and therefore no blade pitching was taken into account in the calculations. The main data of the wind turbine are shown in Table 2.

Table 2 Data for the Vestas V27 wind turbine

Rotor diameter:	27m
Rotational speed:	44 rpm
Tilt:	4deg
Blade length:	13.0 m
Profile:	NACA 63-200

7. RESULTS OF CALCULATIONS

The following tables lists the results of the calculations on the artificial wind, the cup-anemometer and the wind turbine. The results are described by the mean values and the standard deviations, and for the wind also the turbulence intensity. The parameter "anem equi" is the wquivalent horizontal wind speed to the cup-anemometer after correction for angular characteristics.

Table 3 Wind speed (m/s), mean values

10 min. averaged	turbulence 0%	turbulence 10%	turbulence 20%
u	8.0000	8.0000	8.0000
v	0.0	0.0	0.0
w	0.0	0.0	0.0
U_{3D} (vector)	8.0000	8.0361	8.1494
U_{2D} (horiz.)	8.0000	8.0258	8.1060
anem. equi	8.0000	8.0049	8.0600
anem output	8.0000	8.0050	8.0603

Table 4 Electric power (kW), mean values

Flow field	turbulence 0%	turbulence 10%	turbulence 20%
3D	78.195	79.484	82.181
2D	78.195	79.541	82.390
1D	78.195	79.568	82.464

Table 5 Flapwise blade root bending moment (kNm), mean values

Flow field	turbulence 0%	turbulence 10%	turbulence 20%
3D	46.155	46.230	46.228
2D	46.155	46.237	46.244
1D	46.155	46.243	46.252

Table 6 Wind speed (-), turbulence intensity

10 min. averaged	turbulence 0%	turbulence 10%	turbulence 20%
u	0	0.1000	0.2000
v	-	-	-
w	-	-	-
U_{3D} (vector)	0.0	0.0988	0.1911
U_{2D} (horiz.)	0.0	0.0993	0.1946
anem equi	0.0	0.0971	0.1908
anem output	0.0	0.0970	0.1907

Table 7 Electric power (kW), standard deviation

Flow field	turbulence 0%	turbulence 10%	turbulence 20%
3D	3.718	17.278	33.299
2D	3.718	17.766	34.213
1D	3.718	17.761	34.263

Table 8 Flapwise blade root bending moment (kNm), standard deviation

Flow field	turbulence 0%	turbulence 10%	turbulence 20%
3D	2.735	5.749	10.413
2D	2.735	5.832	10.552
1D	2.735	5.791	10.498

8. DISCUSSION

It is seen (Table 3) that there is a difference of 1.9% for 20% turbulence intensity between the mean component-averaged (u-component) and the vector-averaged wind speed. Omitting definition of the wind speed will therefore account for this amount of uncertainty in measurement of the wind speed. For the energy content in the wind or the C_P value of a wind turbine the difference is 5.7%, which is quite significant.

The difference in mean power (Table 4) from 0% to 20% turbulence intensity is seen to be 5.1% for the 3D wind and and 5.5% for the 1D wind. This is quite compatible to the increase in the averaged wind vector cubed, which leads to the assumption, that the power responds to the wind vector. The figures on standard deviation of the power (Table 7) do not give any indications whether or not one definition of the measured wind speed is better than another.

The mean flapwise blade root bending moment (Tabel 5) seems to be quite independent of the turbulence intensity (0.1%) and the dimensions of the flow field. The standard deviation of the flapwise blade root bending moment (Table 8), on the contrary, is very dependant, and is seen to be almost proportional, to the turbulence intensity. The figures, though, give no answer to whether the turbulence intensity is better described by one or the other definition of the wind speed.

The mean equivalent anemometer input (Tabel 3) is seen to be very close to the anemometer output. This indicates that the overspeeding effect due to the unlinear torque characteristic of the anemometer is extremely small. The mean anemometer output seems to be closer to the horizontal wind component than to the wind vector. This is due to the steep slopes at -10° and 10° on the angular characteristics. The most of the vertical angles of attack of the wind are within ±30°. The turbulence of the anemometer output seems to be closer to the vector-averaged turbulence than to the horizontal-averaged turbulence.

9. CONCLUSIONS

From the analysis, the following conclusions can be drawn:

1. Omitting the definition of the wind speed in measurements may account for 1.9% difference at 20% turbulence intensity.
2. For power performance measurements, the vector-averaged wind speed is the best definition of the measured wind speed.
3. The cup-anemometer used in the analysis is closer to the horizontal-averaged wind speed than to the vector-averaged wind speed due to steep angular characteristics.
4. Overspeeding due to unlinear characteristics of the torque curve of the cup-anemometer is extremely small and need no special attention.

10. ACKNOWLEDGEMENTS

This work was part of the development of measurement procedures at The Test Station for Wind Turbines at Risø. The work was sponsored by The Danish Energy Agency.

11. REFERENCES

1. Mann J. "Models in Micrometeorology", Risø-R-727(EN)

2. Press, H.P. et.al. "Numerical Recipes in Fortran", Second Edition, 1992

3. Busch, N.E. et.al. "Meteorological Field Instrumentation", Risø-R-400, 1979

4. Petersen, J.T. "Kinematically Nonlinear Finite Element Model of a Horizontal Axis Wind Turbine", July 11 1990, RISØ, "HawC" model

The ELKRAFT 1MW Wind Turbine: Results from the Test Program

Ioannis Antoniou (1), Søren M. Petersen (1), Stig Øye (2), Carsten Westergaard (3),
Niels Raben (4), Flemming V. Jensen (4)
(1) Risø National Laboratory, P.O. Box 49, 4000 Roskilde, Denmark
(2) Dpt. of Fluid Mechanics, DTU, Building. 404, 2800 Lyngby, Denmark
(3) LM Glasfiber A/S , Rolles Møllevej 1, 6640 Lunderskov, Denmark
(4) SK Power Company, Project Division, Lautruphøj 5, 2750 Ballerup, Denmark

ABSTRACT: The ELKRAFT 1MW wind turbine is the result of a development program carried out by the SK-Power Company on behalf of the ELKRAFT Power pool (the utilities in eastern Denmark). The development costs of the project were covered mainly by ELKRAF while EU (DG17) and the Danish Energy Agency contributed also in the costs with smaller amounts. The turbine has been built as a demonstration project in order to gain experience in the operation of large wind turbines. The turbine was erected and put on line in September 1993 and - after an initial period of adjustments- the measurement program started in October 1994. The turbine will be operated both as stall and pitch regulated. Furthermore it is equipped with two in-line connected generators of 500 kW and an alternative control strategy would include alternative coupling of the two generators as a function of the power produced. The aim of the test program is to verify the design, to evaluate the different operation principles and to improve the long term operation of the turbine. The use of vortex generators improved the turbine's power curve and increased the energy production by around 4%.
Keywords: Large Machines, Demonstration projects, Load, Vortex Generators

1. INTRODUCTION

The ELKRAFT 1MW wind turbine is situated at the Avedøre power station near Copenhagen. It is a typical Danish 3-bladed, constant rpm machine. Among the objectives for the development of this demonstration plant wind turbine, it has been to introduce the stall control concept on MW-size turbines and gain experience from its operation. As this machine is also equipped with pitch bearings, it will - at a later stage - operate with full span pitch control. This will allow the two operation strategies to be compared against each other. The Risø National Laboratory has, under a contract to the SK-power, undertaken the responsibility to carry out a detailed measurement program. For the purpose of discussing and implementing the experience gained from the results of the measurements, a "follow-up" group was also formed. The most important features of the ELKRAFT 1MW are provided in Table I below.

2. THE MEASUREMENT PROGRAM

The setup includes power curve and structural load measurements as well as a number of status and "watch" channels which measure the activity of different turbine components (e.g. number of yaw system activations). The structural loads include measurements on the tower, the main shaft, and the rotor. Strain gauges and accelerometers have been used for this purpose. Fatigue load evaluation through rain flow analysis of the structural data takes place simultaneously with the data acquisition. As a part of the

Table I. Technical specifications ELKRAFT 1MW

Rotor	Power regulation	stall or pitch
	Rotor diameter	50m.
	Hub height	55m.
	Rotor speed	23.13(stall), 25.25(pitch)
	Tilt	3.5°
	Coning	0.0°
	Dir. of rotation(upw.)	clockwise
	Weight	23600kg.
Blades	Material	GRP
	Manufacturer	LM Glasfiber
	Blade length	24m.
	Profiled length	20m.
	Root chord	2.3m.
	Tip chord	0.055m.
	Twist	15°
	Profile	FFA-W3(inner), NACA 634xx(outer)
	Weight	3645kg
Gearbox	Type	Planet-three stage gear
	Exchange ratio	1:65.82(stall), 1:60.30(pitch)
	Effect	1100kw
	Weight	17750kg (without oil)
Generator	Number	two in line on the same shaft
	Voltage	3x690 V
	Current	475A
	Sync. Rotational speed	1500 rpm
	Nominal power	2x500kW
	Nominal slip	1.5%
	Weight	3400kg per generator
Brake	Main	pivotal blade tips
	Main and parking	disk on the main shaft brake with two calipers
	Emergency	disk on the generator shaft with two calipers
Tower	Type	tapered tabular
	Height	53m.
	Weight	95000kg
Hub	Weight	10164kg
Main shaft	Weight	9947kg
Nacelle	Weight	91168kg

program the turbine's natural frequencies were identified at standstill and are given in Table II. The three last eigenfrequencies were measured on one of the blades when mounted in the test rig.

Table II. Measured natural frequencies ELKRAFT 1MW

Mode	Hz
First tower bending mode	0.66
First shaft torsion mode	0.88
First asym. Rotor / tower torsion (yaw)	1.19
First asym. Rotor / tower bending (tilt)	1.25
First sym. Rotor flapwise / tower bending	1.45
First asym. Rotor edgewise	2.44
Sec. Asym. Rotor flapwise / tower torsion (second yaw)	4.05
Sec. Asym. Rotor flapwise / tower bending (second tilt)	3.5
First flapwise (measured in the test rig)	1.45
Second flapwise (measured in the test rig)	4.58
First edgewise (measured in the test rig)	2.65

To the present date the measurement program has been through the following phases:

- 1. Operation of the turbine at a pitch angle of -1.0°
- 2. Operation of the turbine at a pitch angle of 0.5°
- 3. Operation of the turbine at a pitch angle of 0.5° new yaw settings.
- 4. Operation of the turbine with vortex generators installed in the inner part of the blade, pitch angle of 0.5°
- 5. Operation of the turbine with vortex generators installed in the inner part of the blade, pitch angle at -1.0° (still going on).

Shortly after the turbine was set in operation (phase1), it was realized that it could not reach the design rated power. A solution to that was to change to a more positive pitch setting (phase2). The data set from phase2 is the most comprehensive as it includes a considerable

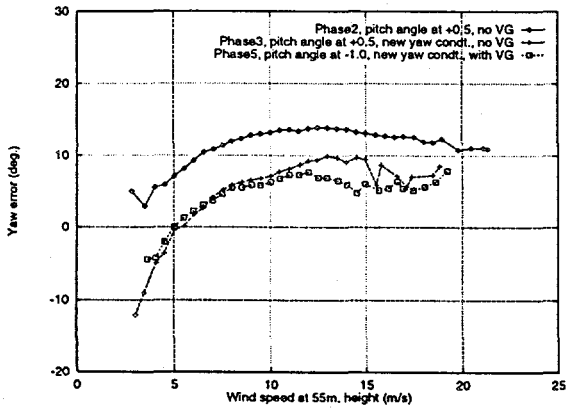

Figure 1. The yaw error for the three power curves

amount of data also at higher wind speeds. Based on the above it was decided to change the turbine yaw settings in order to achieve a smaller yaw error (phase3) and further to install vortex generators in order to improve the turbines power curve (phase4). Initially the pitch angle was kept at +0.5° but as the maximum power was very high, the angle was set at -1.0° (phase5). In what follows results from phase2, phase3 and phase5 will be presented.

3. THE POWER CURVE

In the following the curves presented are the mean binned data values of ten-minutes periods, corrected for temperature and pressure (T=15°C and P=1013.3 hPa). In Fig. 1 the turbine's mean yaw error is shown for the three phases. In order to correct the initial yaw error, the turbine's wind vane was turned 12° in the anti-clockwise direction. This result in a reduction in the yaw error by approximately 7°. The data from phase3 and phase5 follow well each other up to 12m/s after which deviations are observed. It is not clear whether these are due to scatter because of the limited data available or to the modifications of the flow field behind the rotor hub caused by the presence of the vortex generators.

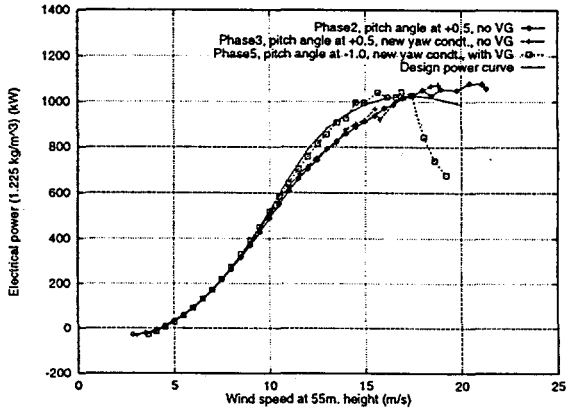

Figure 2. The power curves for the three phases

In Fig. 2 the turbine's power curves, for the three phases, are shown together with the design power curve calculated for a pitch angle equal to -1.0° [1]. The power curves from phase2 and phase3 show good agreement between them up to 7m/s and are in fact slightly better than the design power curve. Between 7m/s and 12m/s the phase3 power curve is better than the phase2 one, which can be attributed to the lower yaw error. At higher wind speeds the two power curves agree well although the phase3 curve shows a higher scatter due to the

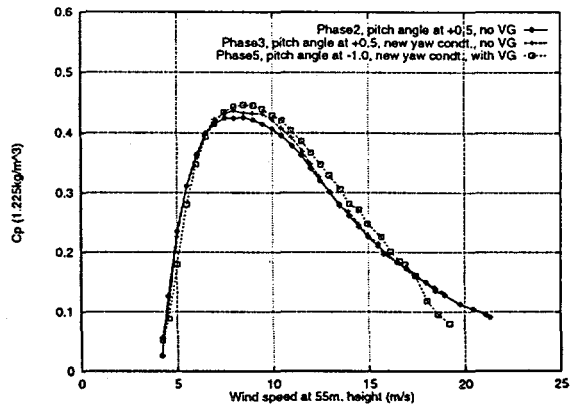

Figure 3. The power coefficient for the three phases

limited amount of data. The two curves are well below the design curve for wind speeds between 8m/s and 17m/s. An explanation of the reduced performance of the rotor under

this configuration is that early separation of the flow occurs in the thick inner sections of the blades. Therefore it was decided to install vortex generators on these parts of the blades. The vortex generators were designed by LM which also decided their positioning on the blades.

Regarding the phase5 curve and the design curve, good agreement exists between them up to 8m/s with the phase5 curve being slightly higher than the design one. At wind speed above 8m/s the two curves follow well each other with the design curve being higher than phase5. Although the number of data points above 17m/s is limited, the existing ones show a strong reduction of the power output, indicating that the rotor operates now in deep stall. The lack of high westerly winds during the autumn of 1995 and the winter of 1996 has hindered the completion of the power curve of this phase.

The power coefficients C_p for the three phases are shown in Fig.3. Below 7m/s the phase5 curve lies lower, while at higher wind speeds it reaches higher values than the two others. In line with the above results from the power curves, it is seen that the phase3 curve is above the phase2 curve between 7m/s and 12m/s.

4. ANNUAL ENERGY PRODUCTION

In order to show how the Annual energy production (a.e.p.) of the turbine has been influenced by the changes in the configuration under the various phases of operation, the Table III is given below. The a.e.p. have been calculated for all three phases and for the corresponding design curve. For each phase two calculations are given for the a.e.p. . For the first (I) calculation, only the positive values of the power curve have been used (first positive value at 4.5m/s), while all negative values are set equal to zero. For the second (II) calculation the first negative value of the power curve (at 4m/s) has also been included. From phase2 to phase5, after the correction of the yaw error and the introduction of the vortex generators, the a.e.p has been increased by approximately 4%. As can be also seen from the Table III, it is important for the a.e.p. that the control strategy does not allow the turbine to be connected to the grid at low wind speeds while the turbine consumes power. Compared to the design curve's a.e.p, the energy produced by the phase5 power curve is on the average less by 2%, for mean wind speeds between 5m/s and 7m/s. At higher wind speeds this difference becomes larger due to the strong reduction of the power output observed in the phase5 power curve.

Table III. Annual energy production of the turbine for different mean wind speeds during the different phases and for different control strategies

Wind speed(m/s)	Phase2 II	Phase2 I	Phase3 II	Phase3 I	Phase5 II	Phase5 I	Design
4	408	415	415	418	410	398	421
5	887	894	905	908	914	904	927
6	1492	1497	1523	1525	1558	1550	1578
7	2156	2160	2197	2199	2254	2247	2291
8	2823	2826	2872	2874	2922	2916	2996
9	3448	3451	3503	3504	3505	3501	3639
10	3995	3998	4054	4055	3974	3970	4188
11	4441	4443	4502	4503	4319	4316	4621

5. STRUCTURAL LOADS

A presentation of the turbines load statistics from phase2 is given in [2]. In order to compare results from the three phases the mean values and the standard deviation of the flap and edge root bending moments is presented for all three phases in Fig. 4 and 5. The phase5 data reach lower wind speeds compared to the ones shown in the power curve (Fig. 2). The reason is that the load measuring part of the data acquisition system was out of function when these wind speeds occurred. In Fig. 4 the three curves follow each other well and only at around 10-12m/s the phase5 curve shows slightly higher values. In Fig. 5 contrary to what is expected the phase5 curve shows lower values than the other two. The influence due to the different yaw condition and the presence of the vortex generators is difficult to detect from the above results. The main reasons is the lack of an adequate number of data sets

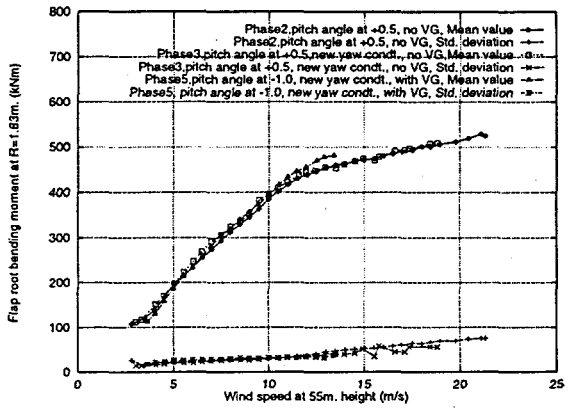

Figure 4. The flap root bending moment for the three phases

and the -even more serious- temperature drift experienced by the strain gauges used for the measurements of the load signals. Therefore in what follows a comparison of the fatigue loads for the flap and the edge root bending moments will be attempted since these quantities are based on the dynamic content of the load signal and therefore not influenced by sensor drift.

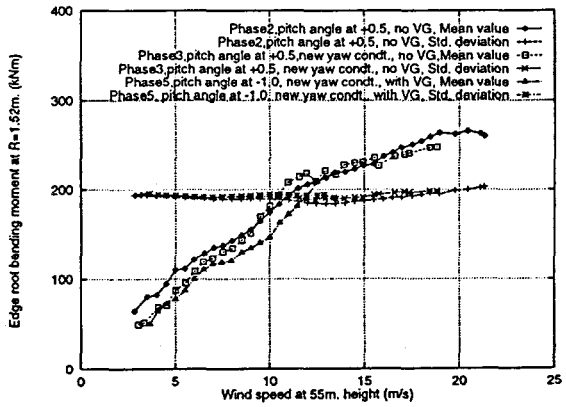

Figure 5. The edge root bending moment for the three phases

The fatigue loads are evaluated using the Rainflow counting method (RFC) described in [3]. The RFC is here performed using 50 range levels between the minimum and

other two phases. The number of data points in the interval is adequate and the behavior is not due to statistical uncertainties. The reason the loads are lower is not obvious. One explanation could be that due to the vortex generators the flow around the blades has become more stable resulting in smaller variations. For the last points of the curve no conclusions can be drawn due to the limited amount of data points.

The damage equivalent edge root bending moment loads for m=10 and for the all three phases are shown in Fig. 9. The phase2 and phase3 curves follow again well each other showing that the change in yaw has not affected the magnitude of the loads. The phase5 curve exhibits clearly higher values than the other two and this in accordance with what it has been expected and seen from the turbine's power curve (Fig. 2). Increased rotor performance due to the higher degree of attached flow on the surface of the blade results in a higher driving moment and thus in higher loads.

6. CONCLUSIONS

The results from the test program show that the performance of the turbine has improved significantly by the installation of vortex generators in the inner part of the blades. The control strategy of the turbine can influence the turbine's energy production by prohibiting power consumption at low speeds. The lack of results at higher wind speeds has to a certain degree prohibited the comparison of the three phases of operation and the drawing of more concrete conclusions regarding the loads.

REFERENCES

[1] S. Øye, "The effect of vortex Generators on the Performance of the Elkraft 1000 kW Turbine" Proceedings 9th IEA Symposium on the Aerodynamics of Wind Turbines, FFA Stockholm, Dec. 11-12, 1995

[2] I. Antoniou, S. M. Petersen, "Wind Turbine Test: Structural Loads ELKRAFT 1MW (Stall Regulated Operation)", Risø-I-865(EN) Report, December 1995

[3] P.H. Madsen, "Recommended Practices for Wind Turbine Testing and Evaluation, 3: Fatigue loads", 2. edition 1990. Executive Committee of the IEA for R&D on Wind Energy Conversion Systems.

the maximum of the signals and a jitter filter size of one level. The fatigue loads are expressed as a damage equivalent load range L_{eq} based on a rainflow spectrum $R_i(n_i)$. The damage equivalent load ranges L_{eq} are calculated from the load signals using an equivalent number of load cycles equal to 1 sec, thus N_{eq}=600 for a 10 minutes time history. The relation between the equivalent load range L_{eq} and the rainflow load spectrum

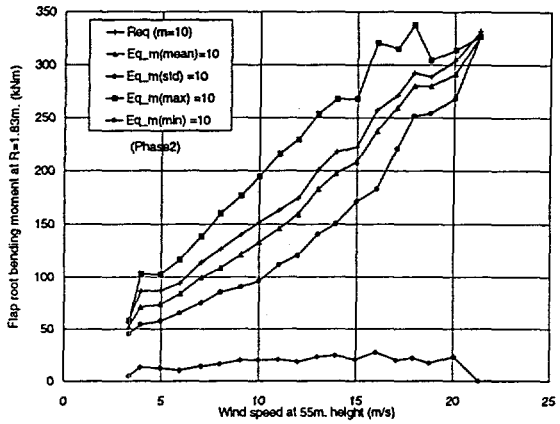

Figure 6. 1Hz Equivalent flap root bending moments.

is $L_{eq}=[(\Sigma R_i^m n_i)/N_{eq}]^{(1/m)}$ where n_i is the number of times a range level appeared and m the material SN curve exponent. Results are shown for m=10 and turbulence intensity between 7%-9%.

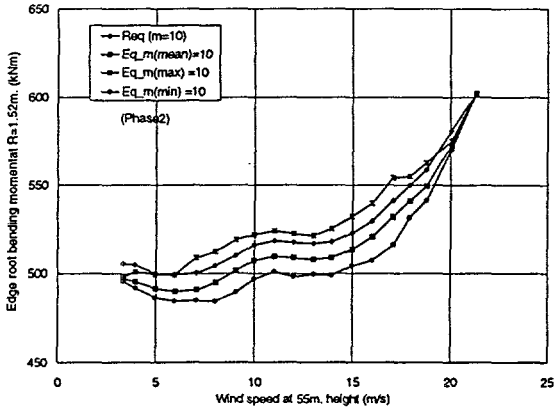

Figure 7. 1Hz Equivalent edge root bending moments.

In Fig. 6 and 7 the 1Hz equivalent flap and edge root bending moments are shown for m=10. The parameter Eq_m(mean) represents the arithmetic mean value of all the damage equivalent load ranges of the 10-minute periods within a speed bin. This value does not represent the mean value of the damage because of the influence of the m exponent and the strong non-linearity associated to it. Therefore we calculate another equivalent load which represents the mean value of the damage. This equivalent load is shown in the Figures as Req.

In Fig. 6 the relatively high scatter of the fatigue loads is of interest to observe since the turbine is situated close to the coastal area (a few meters from the sea) and for the sector chosen the wind blows almost entirely from the sea. Another interesting observation from 7 to 15m/s (where we have a data population from 60 to 120 sets per bin) is the difference between the curves R_{eq} and Eq_m(mean). They are almost parallel and the difference between them is 10-15%. This would mean e.g. that if the turbine was to operate constantly at a wind speed of e.g. 10m/s and the Eq_m parameter was used, then the calculated damage for a specific period would be underestimated by four times.

The same observations can be made for the edge root bending moments (Fig. 7). The differences between Req and Eq_m are of the order of 2%. This is not surprising since the biggest part of the edge loads is due to gravity forces.

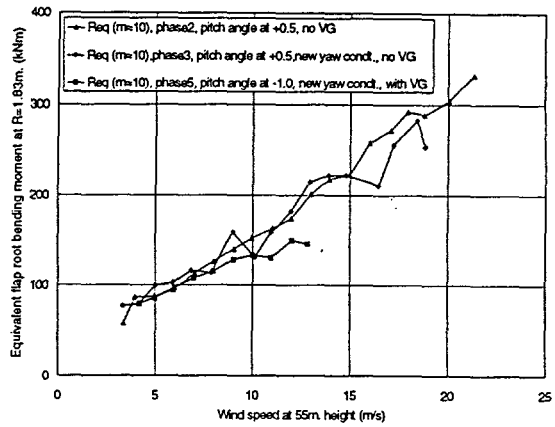

Figure 8. 1Hz Equivalent flap root bending moments for the three phases

The damage equivalent load ranges for the flap root bending moments for m=10 and for all three phases are shown in Fig. 8. The curves from phase2 and phase3 follow well each other and no obvious influence can be seen form the change in yaw conditions. As seen from Fig. 6 the variation at higher wind speeds is higher and this combined with the few data points of the phase3 curve can be the reason for the lower values at higher wind speeds.

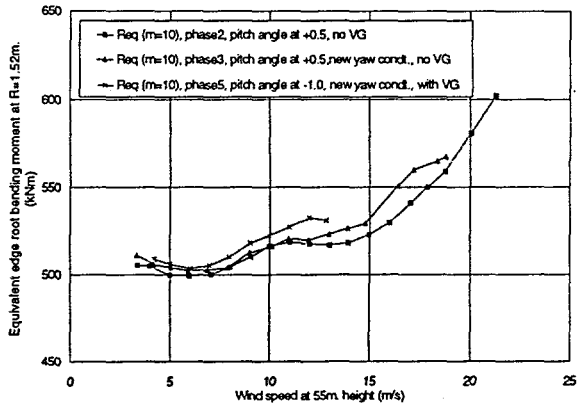

Figure 9. 1Hz Equivalent edge root bending moments for the three phases

The curve from the phase5 shows a tendency for lower values compared to the two others. This up to 7m/s agrees well with the results from the power curve (Fig.2). Different than expected is the behavior between 8-11m/s where we expected the loads to be higher relative to the

Wind Speed Measurements and Anemometer Calibration

D. Westermann, H.Klug
Deutsches Windenergie-Institut, Ebertstrasse 96, 26382 Wilhelmshaven, Germany
Tel.: ++49 4421 480826, Fax: ++49 4421 480843
I. Ravey, R. Hunter, NEL, UK
E. Morfiadakis, CRES, Greece
O. Fabian, T.F. Pedersen, Søren Petersen, RISØ, Denmark
N. van der Borg, ECN, Netherlands

ABSTRACT: Wind speed measurements are of crucial importance for the economics of wind turbine projects. The accuracy of measured power curves is strongly dependant on the wind measurement uncertainty. Harmonisation of wind speed and power curve measurements allows the customer a comparison of different wind turbines and the manufacturer to guarantee a power curve for a series of wind turbines of the same type. European studies have demonstrated that the required accuracy for wind speed measurements is far from being obtained.
The goal of a subproject of the Joule2 project European Wind Turbine Standards (JOU2-CT93-0387, co-financed by European Commission) was to gather information about the existing deviations in anemometer calibrations, work out a calibration procedure for anemometers, to perform comparison measurements and to state the degree of the reached harmonisation.
Keywords: Wind speed, Anemometers, Wind Tunnels, Meteorology

1. INTRODUCTION

Wind speed measurements are of major importance when determining the economics of wind turbine projects. Earlier European studies have demonstrated that the required accuracy for wind speed measurements was far from being obtained.
The first goal of the work described in this report was to develop a calibration procedure for anemometers, to perform comparative measurements and to state the degree of harmonisation reached. During the project the following investigations were carried out:

- Comparison of pressure measurement technique in wind tunnel applications
- Flow field measurements in the wind tunnel
- Reproducibility of anemometer calibrations
- Anemometer calibration comparisons

The work resulted in **Recommendations on the Use and Calibration of Cup Anemometers.** The recommendations are based on the results from a previous CEC programme (87-B-7010-11-7-17). The main modifications incorporated which improve the accuracy of anemometer calibrations are:

- The uncertainty calculation is made consistent with the ISO *Guide to the Expression of Uncertainty*
- A cross calibration of the facility with the low speed tunnel (LST) of NLR in the Netherlands is recommended
- The blockage effect is taken into account
- The influence of humidity on the calibration is introduced
- Traceability is required for all instruments used in the calibration

The deviations between anemometer calibrations in different wind tunnels as a result have been reduced significantly and are now comparable to within 1%.

2. SCOPE AND FIELD OF APPLICATION

The goal was to gather information about the existing differences in anemometer calibrations, work out a calibration procedure for anemometers, to perform comparison measurements and to state the degree of the reached harmonisation.

It was decided that as a base for the recommendation the report Recommendations on the Use of Cup Anemometry at the European Community Wind Turbine Test Stations should be modified. The result of the work are the **Recommendations on the use and calibration of cup anemometers,** describing a standardised and accurate calibration method in wind tunnels. During the project the following investigations were carried out:

- Comparison of pressure measurement technique in wind tunnel applications
- Flow field measurements in the wind tunnel
- Reproducibility of anemometer calibrations
- Anemometer calibration comparisons

2.1 Comparison of pressure measurement technique in wind tunnel applications

A comparison of measurement equipment for pressure measurements was done in the wind tunnel of the university of Oldenburg. This equipment is used to determine the flow speed in a wind tunnel and is therefore responsible for the accuracy of the anemometer calibration.

This examination was done by DEWI, CRES and RISØ was split into two parts.

- comparison of the different Pitot tubes
- comparison of the different pressure transducers

	Reference DEWI 2	P[Pa]	ΔP[Pa]	v[m/s]	Δv[m/s]	% in v
DEWI 2 -DEWI 1	40.00	39.98	- 0.02	8.063	- 0.002	- 0.02
DEWI 2 - CRES	40.00	40.15	+ 0.15	8.080	+ 0.015	+ 0.19
DEWI 2 - RISØ	40.00	40.18	+ 0.18	8.083	+ 0.018	+ 0.22
DEWI 2 - DEWI 1	40.00	40.00	+ 0.00	8.065	+ 0.000	+ 0.00

Table 1: Calibration of different Pitot tubes (pressure 40.00 Pa).

	Reference DEWI 1	P[Pa]	ΔP[Pa]	v[m/s]	Δv[m/s]	% in v
DEWI 1 - CRES	40.00	40.179	+ 0.179	8.083	+ 0.018	+ 0.22
DEWI 1 - RISØ	40.00	40.062	+ 0.062	8.071	+ 0.006	+ 0.07
DEWI 1 - DEWI 2	40.00	40.003	+ 0.003	8.065	+ 0.000	+ 0.00

Table 2: Comparison of different pressure transducers (pressure 40.00 Pa).

2.2 Flow field measurements in the wind tunnel

A detailed examination of the wind tunnel at the university of Oldenburg was carried out. This was done by DEWI using a Laser Doppler Anemometer system. The aim of this examination was to prove that the wind tunnel is suitable for achieving anemometer calibrations with the desired accuracy of better then 0.1 m/s.

2.3 Reproducibility of Anemometer Calibrations

DEWI has calibrated the same anemometer five times. The reproducibility of the calibrations was better than 0.1 %. This was only possible because humidity was measured and corrected for. Table 3 shows the good reproducibility of five calibrations. Since March 1995 DEWI is accredited in the field of anemometer calibration according to EN 45001.

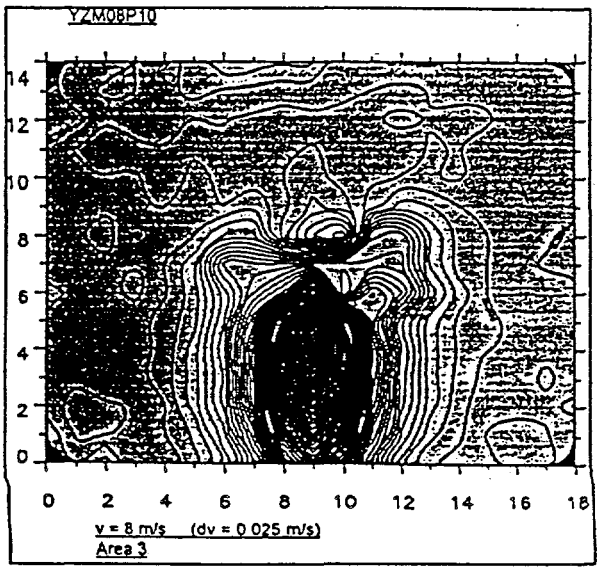

Fig. 1 Flow pattern around the anemometer in the measurement area at 8 m/s wind speed.

Date	a	b	m/s	Δv (m/s)	%
08.07.94	0.0486	0.406	8.188	- 0.007	- 0.08
17.10.94	0.0487	0.401	8.198	+ 0.003	+ 0.04
18.10.94	0.0487	0.388	8.192	- 0.003	- 0.04
15.11.94	0.0489	0.352	8.189	- 0.006	- 0.07
13.12.94	0.0487	0.397	8.197	+ 0.002	+ 0.02

Table 3 Reproducibility of DEWI calibrations
DEWI 100 , a = slope, b = offset, reference: 8.195 m/s

2.4 Anemometer Calibration Comparisons

At the start of the project, the NLR Low Wind Speed Tunnel (LST) in the Netherlands was identified as a suitable anemometer calibration reference facility. All project participants have had at least one anemometer calibrated within the LST. The initial results (given in table 4) indicate that there were differences in the calibration of predefined anemometers in the range of -0.1% to 3.7%.
The results from these initial tests formed the basis for the discussion on the development of anemometer calibration procedures.

The following general areas were investigated:

- absolute calibration of wind tunnels
- the use of an NLR derived 'gross correction factor'
- uncertainty evaluation
- quality of reporting
- anemometer effects
- modification of existing recommendations on the calibration of cup anemometers

Table 4 shows that the deviations between the calibrations in different wind tunnels as a result have been reduced significantly and are now comparable to within 1%.

Date	Institute	Anemometer	slope	offset	r	(≈ 8m/s)	Δv(m/s)	%
26.03.93	DMI (Reference)	Thies-Kombi	0.04812	0.2470		7.946	--	--
19.06.92	DEWI	Thies Kombi	0.04917	0.3200	0.999961	8.187	+ 0.24	+ 3.0
17.02.93	KNMI (Reference)	ECN 0120009	0.06197	0.1204		8.177	--	--
	DEWI	ECN 0120009	0.0621	0.0820	0.999943	8.155	- 0.02	- 0.2
18.02.93	CRES (Reference)	NRG 482	0.74480	0.5567	0.999489	8.005	--	--
06.04.93	DEWI	NRG 482	0.76790	0.4140	0.999907	8.093	+ 0.09	+ 1.1
	WINDTEST (Ref)	DEWI 100	0.04880	0.3500		8.158	--	--
06.04.93	DEWI	DEWI 100	0.04862	0.3730	0.999992	8.152	- 0.01	- 0.1
	RISØ (Reference)	RISØ 217	0.6089	0.1080		8.024	--	--
04.03.93	DEWI	RISØ 217	0.6296	0.1400	0.999994	8.325	+ 0.3	+ 3.7
	NLR	RISØ 217	0.61695	0.17		8.190	+ 0.17	+ 2.1

22.02.94	NLR (Reference)	RISØ 217	0.61695	0.17		8.190	--	--
21.10.94	RISØ	RISØ 217	3. order			8.225	+ 0.04	+ 0.5
25.04.94	NLR (Reference)	DEWI 107	0.04958	0.2960	0.999985	8.229	--	--
18.10.94	DEWI	DEWI 107	0.04943	0.2890	0.999987	8.198	- 0.03	- 0.4
19.12.94	NLR (Reference)	Clima. 3366	0.04703	0.2775	0.999977	8.037	--	--
25.01.95	CRES	Clima. 3366	0.04696	0.3375	0.99992	8.086	+ 0.05	+ 0.6
17.03.94	NLR (Reference)	Vector 3893	0.0495	0.198		8.124	--	--
17.03.94	NEL	Vector 3893	0.04909	0.2682	1.0000	8.118	- 0.01	- 0.1
15.12.94	DEWI (Reference)	DEWI 109	0.04919	0.354	0.999988	8.224	--	--
21.10.94	RISØ	DEWI 109	0.04974	0.2965		8.225	+ 0.00	+ 0.0
17.10.94	DEWI (Reference)	DEWI 129	0.04873	0.377	0.999994	8.174	--	--
25.11.94	CRES	DEWI 129	0.04870	0.3304	0.99996	8.122	- 0.05	- 0.6

Table 4 shows the different calibration results and regression coefficients. The upper part represents calibrations before the project started. The lower part shows comparisons after harmonisation.

2.4.1 Absolute calibration

Adoption of the new procedures with regards the use of a common reference wind tunnel does not remove the need to carry out a full calibration of existing facilities. Indeed, an absolute calibration of wind tunnels is of the upmost importance, and a gross correction factor derived from the NLR or other qualified facility shall only be used when every step has been taken to reduce the uncertainty associated with calibration facilities.

Absolute calibration of a wind tunnel shall include the following:

- calibration of all instruments traceable to National standards
- all pitot tubes to comply with ISO 3966, part 2.1
- a comprehensive calibration of the wind tunnel using two pitot tube measurement systems
- measurement of the flow profile over the working area of the facility

2.4.2 The use of a NLR derived 'gross correction factor'

It may not be possible to fully account for the uncertainty introduced in the calibration of an anemometer due to blockage effects. In the event where the difference in the calibration of the anemometer used as a transfer standard between NLR and the wind tunnel under calibration is greater than 1% then a gross correction factor can be introduced for geometrically identical anemometers.

2.4.3 Uncertainty evaluation

The evaluation of the uncertainty associated with the calibration should be carried out in accordance with the ISO Guide to the Expression of Uncertainty (First edition, ISBN 92-67-10188-9 1993).

2.4.4 Anemometer effects

A number of factors affecting the uncertainty associated with wind speed measurements were investigated (see also Annex A). This included the use of external heating elements, temperature variations (bearings), boom effects and anemometer overspeeding.

2.4.5 Quality of report

It is imperative that anemometer calibration reports should contain the same information for anemometers calibrated at different facilities. It was decided that this shall include

- a summary of the absolute calibration procedure carried out on the facility
- a statement of tracability
- a summary of the calibration procedure
- a statement of uncertainty and repeatability of the facility

2.4.6 Modification of Existing Recommendations Document

The culmination of the project was a document titled Recommendations on the Use and Calibration of Cup Anemometers.

This document is based on a previous set of recommendations which result from a CEC contract (87-B-7010-11-7-17). Although the format of the original document has remained the same, the content has been heavily modified to reflect the discussions and investigations carried out during the project.

The document is intended as a definitive recommendation on the use and calibration of cup anemometers and as such could form the basis for the development of a standard in the future.

3. CONCLUSIONS

The work resulted in **Recommendations on the Use and Calibration of Cup Anemometers** relating to the choice, calibration and use of cup anemometers. Elucidations to the clauses are given and are based on the findings of subsidiary tasks which have been carried out. The deviations between the calibrations in different wind tunnels have been reduced significantly and are now comparable to within 1%.

The recommendations specify both primary and relative calibrations of anemometers of the same type. A field calibration in the open (relative calibration of two anemometers of the same type) is a time consuming process and seems not to diminish calibration costs. Nevertheless in future work such investigations of anemometers in the 'real world' and their behaviour in the turbulent atmosphere (Overspeeding-effect) will be of great importance.

REFERENCES

[1] Raymond S. Hunter 1982 The accuracy of cup anemometer calibration. Wind Engine.. Vol. 14

[2] EG Report 12/1989 Recommendations on the use of cup anemometry. EUEC 25 225/89 National Engineering Laboratory, UK

[3] E.C. Maskell 12/1963 A Theory of the Blockage Effects on Bluff Bodies and Stalled Wings in Closed Wind Tunnel Aeronautical Research Council Ministry of Aviation, R.&M. No. 3400

[4] H.Klug, D.Westermann 1994 Technical Note EWTS-IV 94-10 DEWI 0894 02

CALIBRATION OF PARTIAL SAFETY FACTORS FOR DESIGN OF WIND-TURBINE ROTOR BLADES AGAINST FATIGUE FAILURE IN FLAPWISE BENDING

Knut O. Ronold
Det Norske Veritas
N-1322 Høvik, NORWAY

Jakob Wedel-Heinen
Det Norske Veritas
DK-1051 København K, DENMARK

Carl J. Christensen
The Test Station for Wind Turbines
Risø, DK-4000 Roskilde, DENMARK

ABSTRACT: A probabilistic model for evaluation of the safety of a wind-turbine rotor blade against fatigue failure in flapwise bending is presented. The model accounts for uncertainties in load and resistance. The model is applied in conjunction with a first-order reliability method to perform a reliability analysis of a particular, site-specific wind-turbine. The probability of fatigue failure in flapwise bending of a rotor blade of this wind turbine over a twenty-year design life is calculated. It is demonstrated how reliability analysis results can be used to calibrate partial safety factors for load and resistance for use in conventional deterministic fatigue design.
KEY WORDS: Blades, Fatigue, Reliability, Partial Safety Factors

1. INTRODUCTION

Wind-turbine rotor blades exposed to wind loading are vulnerable to cumulative fatigue damage owing to the cyclic nature of the loading. The wind speed that causes bending of the rotor blades exhibits a natural variability, and the S-N curve that gives the number of stress cycles to failure and represents the resistance of the rotor blade material is encumbered with uncertainty owing to a limited number of test specimens as well as variability from one specimen to another.

Partial safety factors are used in structural design as factors on characteristic values of governing load and resistance quantities to account for variabilities and uncertainties in these quantities.

This paper demonstrates how a structural reliability method can be applied as a rational means to analyze a wind-turbine rotor blade with respect to fatigue in flapwise bending, and to establish partial safety factors for design of such rotor blades against fatigue failure. A site-specific wind turbine of a prescribed make is considered, and probabilistic models for the wind loading and its transfer to bending stresses is established together with a stochastic representation of the material resistance. The event of fatigue failure in flapwise bending is considered as based on a Miner's sum formulation for cumulative damage.

2. THEORY FOR LOAD, RESISTANCE, AND CUMULATIVE DAMAGE

2.1 Wind Climate and Load History for Rotor Blade

The wind climate that governs the loading of a wind turbine and its rotor blades is commonly described by the 10-minute mean wind speed U_{10} at the site in conjunction with the turbulence intensity I_T. The long-term 10-minute mean wind speed distribution can be taken as a Weibull distribution

$$F_{U_{10}}(u) = 1 - \exp(-(\frac{u}{A})^k) \qquad (1)$$

in which k and A are site- and height-dependent coefficients. The turbulence intensity I_T is also site- and height-dependent. It is defined as the standard deviation of the wind speed divided by the mean wind speed U_{10} and represents the gustiness of the wind about this mean. The turbulence intensity I_T is here assumed independent of U_{10}. Detailed information about the distribution of I_T is not available. The mean value can be taken as

$$E[I_T] = \left(\ln \frac{z}{z_0}\right)^{-1} \qquad (2)$$

where z is the height above the ground, i.e., the hub height of the rotor, and z_0 is the roughness parameter for the terrain. A representative value of the coefficient of variation is COV=0.25, and the distribution type can be assumed to be lognormal. The (U_{10},I_T) "space" is discretized into a number of bins ("two-dimensional intervals") of approximately constant values of U_{10} and I_T.

One rotor blade is considered in the following. Let X denote the bending moment range at the blade root in flapwise bending. Hence, X is the double amplitude of the flapwise bending moment response owing to an aerodynamic load cycle that is applied to the rotor blade. One bending moment range is associated with each load cycle, and load cycles are identified by rainflow counting. Observations of the bending moment range X are recorded in 10-minute intervals. Each 10-minute record of X is binned by U_{10} and I_T. For a particular bin (U_{10},I_T) there will be M 10-minute records of X, and they are used to give an estimate of the long-term distribution of X conditioned on (U_{10},I_T), i.e., $X|(U_{10},I_T)$, on discretized form. The number of load cycles n_{10} in each 10-minute interval is also observed and depends on U_{10} and I_T.

Because the distribution of $X|(U_{10},I_T)$ is encumbered with uncertainty owing to limited data for its estimation, it is desirable to parametrize the distribution and represent this uncertainty in reliability analyses as uncertainty in distribution parameters. The distribution of $X|(U_{10},I_T)$ can be parametrized in terms of its statistical moments. These moments are the mean value a_1, the standard deviation a_2, the skewness a_3, and the kurtosis a_4. Their expected values $E[a_i]$, i=1,...4, can be estimated based on the observed discretized version of the conditional distribution of $X|(U_{10},I_T)$. Their standard deviations $D[a_i]$, i=1,...4, and also their correlation matrix ρ can be estimated by a re-

sampling technique such as the jackknife or the bootstrap, see Efron and Tibshirani [2].

It is assumed that the expected values and standard deviations of $a_1,...a_4$ conditioned on U_{10} and I_T are adequately represented by the polynomial surfaces

$$E[a_i] = b_{0i} + b_{1i}U_{10} + b_{2i}U_{10}^2 + b_{3i}I_T + b_{4i}I_T^2 \qquad (3)$$

$$D[a_i] = c_{0i} + c_{1i}U_{10} + c_{2i}U_{10}^2 + c_{3i}I_T + c_{4i}I_T^2 \qquad (4)$$

in which the coefficients b_{ji} and c_{ji}, j=0,...4, i=1,...4, are determined by least-squares regressions of all estimated mean values and standard deviations of $a_1,...a_4$ over the (U_{10},I_T) space.

Based on the central limit theorem and the assumption that the correlation matrix ρ is independent of (U_{10},I_T), the four moments $a_1,...a_4$ can be represented as

$$a_i = E[a_i] + U_i D[a_i], \qquad i = 1,...4 \qquad (5)$$

in which $\mathbf{U}=(U_1,...U_4)^T$ is a four-dimensional normal distribution with zero mean, unit variance, and correlation matrix ρ. Note in this context that U_i is standard notation for a standard normally distributed variable within the field of structural reliability and is not to be confused with any wind speed. Note also that the vector $\mathbf{U}=(U_1,...U_4)^T$ represents the statistical uncertainty in the four moments $a_1,...a_4$ owing to the limited data available for their estimation.

Above, the statistical moments $a_1,...a_4$ of the available measured data for the bending moment range X at the blade root in flapwise bending have been dealt with. However, no statement has so far been made with respect to the distribution of the bending moment amplitudes themselves, neither in the short term, conditional on a particular wind climate (U_{10},I_T), nor in the long term such as over the design life of the rotor blade. A model for the distribution of the bending moment range X is therefore dealt with in the following.

Load response amplitudes are often seen to have marginal distributions which are close to Weibull distributions. The bending moment range is two times such a load response amplitude. Based on the first four moments $a_1,...a_4$ of the distribution of the conditional bending moment range $X|(U_{10},I_T)$, this distribution can be modelled as a cubic expansion of a parent Weibull-distributed variable U_W as follows

$$X = k_0 + k_1U_W + k_2U_W^2 + k_3U_W^3 \qquad (6)$$

in which the parent variable U_W and the coefficients $k_0,...k_3$ are chosen such that the mean a_1 and the standard deviation a_2 are exactly matched and such that the combined error in the skewness a_3 and the kurtosis a_4 is minimized. This choice is accomplished by means of an optimization technique, and quite often it is possible to match also the skewness a_3 and the kurtosis a_4 exactly. Hence, the distribution of the bending moment range X conditioned on (U_{10},I_T) is represented by a generalized distorted Weibull distribution. Reference is made to Winterstein et al. [3]. Note that this generalized Weibull distribution provides a better fit to the data as well as a better representation of the important upper tail of the distribution than the distorted lognormal distribution used by Ronold et al. [4]. The distorted lognormal distribution, obtained by a logarithmic Hermite polynomial expansion of a parent Gaussian distribution, is known to have a heavy upper tail which, as commented by Ronold et al. [4], leads to overprediction of upper quantiles of the bending moment ranges and thereby of the high-range stresses. For future work one could, as an alternative, consider to use the computationally simpler quadratic Weibull model that ignores the cubic term in Eq. (6) and provides exact fits of the mean, standard deviation, and skewness, see Lange and Winterstein [11].

The resistance moment at the rotor blade root is W, and the stress range S corresponding to the moment range X is $S=X/W$. When a discretization of the stress range space is introduced, the above formula can be applied in conjunction with the distribution function of the parent Weibull variable U_W to calculate the probability content of each interval ΔS of this discretization. The corresponding number of cycles within each such interval in a 10-minute period can be determined as this probability content times the total number of cycles $n_{10}(U_{10},I_T)$.

Integrating contributions from all possible 10-minute wind climate bins (U_{10},I_T), weighted according to the quoted Weibull distribution for U_{10} and the lognormal distribution for I_T, this can be used to establish an ordered history of the stress range S over the design life T_L of the rotor blade. This compound lifetime distribution of the stress range S can be expressed in terms of the number of stress cycles n whose associated stress range exceeds a level S during the design life of the rotor blade, see Figure 1. This, in turn, can be used to calculate the number of stress cycles Δn within an interval ΔS of the discretization of the stress range space.

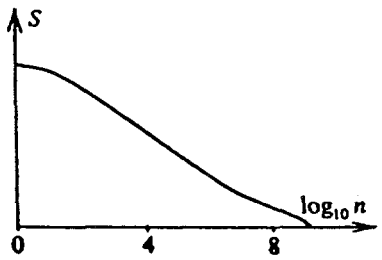

Figure 1 Example of compound stress range distribution over a design life

The number of cycles $n_{10}(U_{10},I_T)$ in a 10-minute interval is also encumbered with uncertainty. However, the coefficient of variation is inversely proportional with the square-root of the interval length, such that when $n_{10}(U_{10},I_T)$ is scaled to give the number of cycles over a long time span such as a 20-year design life, the uncer-

tainty in this number becomes insignificant and can be ignored. In the reliability analysis $n_{10}(U_{10},I_T)$ is therefore left as a deterministic quantity only dependent on U_{10} and I_T.

2.2 Fatigue Strength and *S-N* curve

For a given stress range S, the number of cycles N to failure is generally expressed through an *S-N* curve, $N=BS^{-k}$. However, in tests of composite materials for use in rotor blades, the strain amplitude ε is usually measured rather than the stress range S. Hence, for such materials the number of cycles N to failure is expressed through an ε-*N* curve. On a linear scale, this curve can be repre-sented as

$$\log_{10} N = \log_{10} K - m\log_{10}\varepsilon + e \qquad (7)$$

in which *(K, m)* describe the expected behavior, and e is a zero-mean residual representing local variations from test specimen to test specimen, or from one point of the rotor blade to another. The stress range S that corresponds to the strain amplitude ε can be expressed as $S=2E\varepsilon$, where E denotes the modulus of elasticity of the material in the direction of the loading. The modulus of elasticity is idealized as a constant here, and the possible effect of a non-zero mean stress has been ignored. For other idealizations of the material representation, reference is made to Ronold et al. [4].

2.3 Cumulative Damage and Failure Criterion in Fatigue

According to Miner's rule, fatigue failure in a structural material is defined to occur when the accumulated damage D exceeds 1.0, where D is defined as

$$D = \sum_{i=1}^{k} \frac{\Delta n(S_i)}{N(S_i)} \qquad (8)$$

Here, Δn is the number of load cycles at stress range S in the lifetime of the rotor blade, and N is the number of cycles to failure at this stress range. The sum is over all stress ranges S_i in a sufficiently fine discretization of the stress range space.

3. PROBABILISTIC AND DETERMINISTIC MODELLING

The reliability of a site-specific wind turbine against fatigue failure of one of its rotor blades in flapwise bending is considered. The reliability is computed by a first-order reliability method as described in Madsen et al. [1] and Ronold et al. [4]. The input to the reliability analysis consists of a limit state function, specified in terms of a set of basic variables which consist of stochastic variables as well as deterministic parameters. Furthermore, the statistical distributions of the stochastic variables must be given, and the values of the deterministic parameters must be specified. The following sections describe the stochastic variables, the deterministic parameters, and the limit state function. Separate sections are devoted to make and site of wind turbine, environmental loading, fatigue strength, and limit state function.

3.1 Wind Turbine Characteristics

A 500 kW wind turbine is considered. The hub height is z=35 m, and the resistance moment of the rotor blade at the blade root in flapwise bending is taken as W=0.0015 m^3.

3.2 Environmental Loading

The wind turbine is considered for a location whose wind loading regime is characterized by a scale parameter A=9.1 m/sec, a slope parameter k=1.9, and a terrain roughness z_0=0.05 m, the latter thus implying a mean value of the turbulence intensity of $E[I_T]$=0.153.

A total of 1183 10-minute records of flapwise bending moment ranges X for various wind climate realizations (U_{10},I_T), considered fixed within each 10-minute interval, are available. For each bin (U_{10},I_T), the available M 10-minute moment range records are merged, and the observed moment ranges X are sorted in increasing order. From this, the cumulative distribution function of $X|(U_{10},I_T)$ is derived, and its first four moments, here denoted a_1 through a_4, are estimated. The standard deviations of these four moments are obtained by jackknifing the M 10-minute records. As stated in a previous section, the following model is chosen to represent the coefficients a_1 through a_4

$$a_i = E[a_i] + U_i D[a_i], \qquad i = 1,...4 \qquad (9)$$

in which the mean value $E[a_i]$ and standard deviation $D[a_i]$ of the ith moment a_i are represented as

$$E[a_i] = b_{0i} + b_{1i}U_{10} + b_{2i}U_{10}^2 + b_{3i}I_T + b_{4i}I_T^2 \qquad (10)$$

$$D[a_i] = c_{0i} + c_{1i}U_{10} + c_{2i}U_{10}^2 + c_{3i}I_T + c_{4i}I_T^2 \qquad (11)$$

Table 1 Estimated Coefficients in Polynomial Model for $E[a_i]$

i	b_0	b_1	b_2	b_3	b_4
1	-5.0568	1.5547	-0.0092	244.10	-575.08
2	4.6875	0.7266	0.0101	228.50	-551.22
3	1.6387	0.0249	-0.0035	1.6770	-5.7838
4	2.5245	0.4953	-0.0320	17.458	-37.926

Table 2 Estimated Coefficients in Polynomial Model for $D[a_i]$

i	c_0	c_1	c_2	c_3	c_4
1	2.2512	-0.0863	0.0069	-20.740	72.463
2	2.0024	0.0591	-0.0026	-20.752	64.379
3	0.0822	0.0107	-0.0006	-1.1925	3.4608
4	0.2821	0.0957	-0.0052	-6.3816	19.099

The polynomial coefficients in these expressions are determined by a least-squares regression of the available

data and are presented in Tables 1 and 2. The stochastic variables $\mathbf{U}=(U_1,...U_4)^T$ represent the statistical uncertainties in the bending moment range distributions and follow a four-dimensional normal distribution with mean values 0.0, standard deviations 1.0, and a correlation matrix which is estimated to be

$$\rho=\begin{bmatrix} 1.000 & 0.937 & -0.346 & -0.278 \\ 0.937 & 1.000 & -0.210 & -0.200 \\ -0.346 & -0.210 & 1.000 & 0.923 \\ -0.278 & -0.200 & 0.923 & 1.000 \end{bmatrix} \quad (12)$$

The number of aerodynamic stress cycles n_{10} in a 10-minute interval is represented as a function of (U_{10},I_T) as follows

$$n_{10}=1704-102.8U_{10}+7.027U_{10}^2-10.08I_T+1402I_T^2 \quad (13)$$

in which the coefficients are estimated by a least-squares regression from a total of 1183 records of n_{10}, when U_{10} is quoted in units of m/sec.

As described in a previous section, the conditional distribution of $X|(U_{10},I_T)$, expressed in terms of a parent Weibull distribution, is used in conjunction with the long-term distributions of U_{10} and I_T as well as the number of cycles $n_{10}(U_{10},I_T)$ in 10-minute intervals to establish an ordered lifetime history of the bending moment range X for the considered rotor blade in flapwise bending. The corresponding history of the bending stress range S of interest for prediction of cumulative damage by Miner's sum is easily derived by division by the resistance moment W, hence $S=X/W$.

4.3 Resistance and Stiffness of Composite Laminate

As stated in a previous section, the ε-N curve that gives the number of stress cycles N to failure as a function of the strain amplitude ε is given by the linear relationship

$$\log_{10} N = \log_{10} K - m\log_{10}\varepsilon + e \quad (14)$$

for the rotor blade laminate. Material data as presented in detail by Ronold et al. [4] are used. A regression analysis of these data according to the linear model leads to the following estimates of $\log_{10}K$ and m

$$E[\log_{10}K]=-12.372 \text{ and } E[m]=7.91 \quad (15)$$

when strain amplitudes are quoted as a dimensionless absolute quantity. The uncertainties in $(\log_{10}K, m)$ were shown by Ronold et al. [4] to be insignificant for this particular material, and $\log_{10}K$ and m are therefore represented in the reliability analysis by constants equal to their estimated values as quoted. Note that for other materials, the uncertainties in $(\log_{10}K, m)$ may be significant and may then need to be included in the reliability analysis, see Echtermeyer [5].

The standard deviation of the residual term e is estimated to be $\sigma_e=0.396$. The zero-mean residual term e is represented by a normal distribution with this standard deviation. For details about the tests of the laminates, reference is made to Echtermeyer et al. [6]. A constant modulus of elasticity is used, $E=29.7\cdot10^6$ kPa.

4.4 Limit State Function

The reliability against fatigue failure of the considered rotor blade in flapwise bending is analyzed for the cyclic loading exerted by wind over the design life. For this purpose, a limit state function is defined

$$g(\mathbf{X}) = 1 - D(\mathbf{X}) = 1 - \sum_{i=1}^{k} \frac{\Delta n(S_i)}{N(S_i)} \quad (16)$$

in which D is the cumulative fatigue damage expressed through the Miner's sum as defined in a previous section, and $\mathbf{X}$ denotes the vector of stochastic variables which includes the variables $\mathbf{U}$ that represent the uncertainty in the loading and the variable e that represents the uncertainty in the resistance.

5. RELIABILITY ANALYSES

The reliability is the complement of the failure probability

$$P_F = P[g(\mathbf{X}) \le 0] \quad (17)$$

and may be expressed in terms of the reliability index $\beta=-\Phi^{-1}(P_F)$. The reliability is computed by means of a first-order reliability method as described in Madsen et al. [1] and Ronold et al. [4]. The probabilistic analysis program PROBAN, see Tvedt [7], is used for this purpose. The results of the reliability analysis are presented in Table 3.

Table 3 Results of Reliability Analysis
20-Year Lifetime Fatigue in Flapwise Bending
Rotor Blade, W=0.0015 m^3

Probability of Failure $P_F = 0.52\cdot10^{-4}$
Reliability Index β=3.88

Variable	Distribution	Design point x*	Importance factor α^2
U_1	Normal	0.6008	
U_2	Normal	0.6124	0.026
U_3	Normal	−0.1909	
U_4	Normal	−0.1649	
e	Normal	−1.5170	0.974

By examination of the resulting importance factors reported in the fourth column of Table 3, it appears that the inherent variability in the fatigue life as represented by the uncertainty in the residual e of the ε-N curve is by far the single most important uncertainty source. As much as 97% of the total uncertainty importance is attributed to this resistance variable, while the remainder 3% or less is ascribed to the uncertainty in the load variables $U_1,...U_4$. This represents a significant shift in the uncertainty importance from the fifty-fifty split between load and resis-

tance variables reported by Ronold et al. [4] for a similar wind turbine. This shift in the relative importance between the various uncertainty sources is attributed to the fact that the present study capitalizes on a distorted Weibull distribution for the bending moment ranges, which is believed to provide a good representation of reality, while the study by Ronold et al. [4] is based on a distorted log-normal distribution for these ranges. This distorted log-normal distribution model is in conformance with what was state-of-the-art at the time of that study, but is prone to overestimate the probability content in the upper tail of the distribution of the bending moment ranges with over-prediction of the higher bending stresses (and thereby of the uncertainty importance factor for loads) as the result. The replacement of the distorted log-normal load distribution of the study by Ronold et al. [4] by the distorted Weibull distribution of the present study is considered to represent a significant improvement and is well in conformance with other recent studies, see Lange and Winterstein [12]. On this background, the observed reduction in the uncertainty importance factor for the loads by this replacement is a natural finding, and it emphasizes the importance of a proper representation of the load distribution and in particular its upper tail.

An inspection of the computational results reveals that the major contribution to the cumulative damage is ascribed to the about 10^7 medium-amplitude stress cycles in a couple or more cycle-number decades centered about $\log_{10}N=6$ in the bending moment range distribution. This is a fairly small fraction of the total of about 10^9 stress cycles that occur over the design life of the rotor blade. The fact that such a low fraction of the applied stress cycles vouches for most of the cumulative damage can be ascribed to the value of the slope parameter m of the ε-N curve which is approximately equal to 8 for the composite laminate in the present case. Stress ranges are raised to the mth power for prediction of the number of cycles to failure. This implies that the higher the value of m, the more dominant are the high stress ranges. A comparison can be made with welded steel details whose m values are usually in the range 3-4 and whose major contribution to accumulated fatigue damage is ascribed to the low-amplitude stress cycles that correspond to the lower right part of the stress range distribution in Figure 1. These stress cycles form the majority of the total number of stress cycles over the design life. An interesting consequence of this dependency of the cumulative damage on the value of m is that if epoxy materials are considered for the rotor blade, for which m values of up to 12 or 13 are seen, the fatigue problem may be turned into an extreme value problem as far as the loading goes. Even for the present m value of 8, this indicates how important a proper estimation of the upper tail of the load distribution is.

6. CALIBRATION OF PARTIAL SAFETY FACTORS

6.1 Philosophy

It is of interest to demonstrate how reliability analysis results, obtained as outlined in the previous chapters, play a role in codified practice and design. Calibration of partial safety factors for design is an important application. With the first-order reliability method available, it is possible to determine sets of equivalent partial safety factors which result in rotor blade designs with a prescribed reliability. As a first step, a target reliability index β, must be selected.

The choice for the target reliability index can be derived from a utility-based feasibility assessment in a decision analysis, or by requiring that the safety level as resulting from the design by a reliability analysis shall be the same as that resulting from current deterministic design practice. The latter approach is based on the assumption that current design practice is optimal with respect to safety and economy or, at least, leads to a safety level acceptable by society. A range of target reliability indices will be considered in the following.

In the case of a prescribed reliability level which is different from the one that results from an actually executed reliability analysis of a wind turbine rotor blade, the geometrical quantities of the blade have to be adjusted such that this required reliability level results from a reliabi-lity analysis of the modified blade. The geometrical quantities which can be adjusted to achieve a specified reliability level are sometimes denoted design parameters. It is most practicable to operate on just one such design parameter when adjusting the design in order to reach the specified reliability level. For a rotor blade, the most practicable parameter to adjust is the resistance moment W which is a function of the cross-sectional properties of the blade at the root.

To cover a range of target reliabilities, a series of reliability analyses is carried out for a range of values for the resistance moment W. This gives the reliability index β as a function of the resistance moment W, $\beta=\beta(W)$. In addition, as a byproduct of the reliability analyses, the values of the design point e_d^* of the ε-N curve residual e prove useful in the following and are retained.

6.2 Characteristic Values of Governing Variables

Characteristic values have to be selected for the governing load and resistance variables. A discussion of the philosophy behind and background for the choice of a characteristic load distribution can be found in Ronold et al. [4]. For simplicity, an idealized characteristic moment range distribution is adopted here,

$$X = k_R X_0 (1 - \frac{\log_{10} n}{\log_{10}(3N_r)}) \qquad (18)$$

in which X denotes the moment range which is exceeded in n stress cycles during the design life T_L, $N_r=f_r T_L$ is the number of rotor cycles in this life, f_r denotes the rotor frequency, X_0 is a characteristic bending moment whose derivation is described below, and k_R is a scaling factor. A value of $k_R=2.3$ is applied in the following. This value has been calibrated as the one that will lead to a cumulative damage approximately equal to the median damage

for the true compound moment range distribution derived from the observed conditional moment range distributions as described above.

The characteristic bending moment is defined as

$$X_0 = \frac{\rho}{2} w^2 c C_L \frac{R^2}{3} \tag{19}$$

in which R is the length or radius of the rotor blade measured from the center of the rotor to the tip, c is characteristic chord length at $2R/3$, C_L=1.5 is a lift coefficient at $2R/3$, ρ=1.28 kg/m^3 is the density of air, and w is a reference wind speed defined by

$$w^2 = (\frac{4\pi}{3} f_r R)^2 + v_0^2 \tag{20}$$

where f_r is the rotor frequency as before, and v_0 is the 10-minute mean wind speed at stalling of the entire rotor blade. For the considered 500 kW wind turbine, the following numbers apply: T_L=20 years, f_r=0.5033 sec^{-1}, N_r=0.317·10^9 rotations, R=19.5 m, c=1.18 m, and v_0=14.6 m/sec.

For ε-N curves, it is a standard approach to select the characteristic ε-N curve as the curve that results when the estimated ε-N curve is shifted to the left by a distance equal to two times the standard deviation of the residual e, hence

$$\begin{aligned} \log_{10} N &= E[\log_{10} K] - E[m]\log_{10}\varepsilon - 2\sigma_e \\ &= -12.372 - 7.912\log_{10}\varepsilon - 2\cdot 0.396 \\ &= -13.164 - 7.912\log_{10}\varepsilon \end{aligned} \tag{21}$$

when values for the considered rotor blade laminate are substituted. Reference is made to Det Norske Veritas [8] and Dansk Ingeniørforening [9].

6.3 Partial Safety Factors and Design Load and Resistance Properties

Two partial safety factors are introduced. A load factor γ_f greater than 1.0 is applied as a factor on all load values of the characteristic moment range distribution and the relation S=X/W between stress range S and moment range X is substituted such that the design stress range distribution becomes

$$S = \gamma_f k_R \frac{X_0}{W}(1 - \frac{\log_{10} n}{\log_{10}(3N_r)}) \tag{22}$$

Correspondingly, γ_m is a material factor greater than 1.0. For any given number of cycles to failure, the characteristic strength is divided by this number to give the design strength. Recall the relationship S=$2E\varepsilon$ between stress range and strain amplitude. This implies that the design S-N curve becomes

$$\log_{10} N = -13.164 - 7.912\log_{10}(\frac{S}{2E}\gamma_m) \tag{23}$$

6.4 Calibration

For the same series of values of the resistance moment W that was used for the reliability analyses, deterministic structural analyses are carried out. For each value of W, the accumulated damage D is calculated according to Eq.(8) on the basis of values of Δn predicted from the design stress range distribution in conjunction with values of N predicted from the design S-N curve. Pairs of partial safety factors (γ_f, γ_m) are determined in such a way that this accumulated damage becomes exactly equal to the limit value of 1.0 that indicates failure. This is conveniently done by calculating the accumulated damage D for many trial pairs (γ_f, γ_m) and picking those pairs for which D=1.0 results. For each value of W, there will be an infinite number of pairs (γ_f, γ_m) that will lead to D=1.0. This is a result of the form of the limit state function for fatigue failure in flapwise bending and implies an arbitrariness in selecting the partial safety factors (γ_f, γ_m), as the requirement turns out to be on their product. Hence, the result of this exercise performed for many resistance moment values W is a required partial safety factor product $\gamma_f\gamma_m$ as a function of the resistance moment W, $\gamma_f\gamma_m = \gamma_f\gamma_m(W)$.

The result of the structural reliability analyses, β=$\beta(W)$, and the result of the deterministic structural analyses, $\gamma_f\gamma_m = \gamma_f\gamma_m(W)$, are combined by elimination of the resistance moment W to give the reliability index β as a function of the calibrated partial safety factor product $\gamma_f\gamma_m$, β=$\beta(\gamma_f\gamma_m)$, see Figure 2.

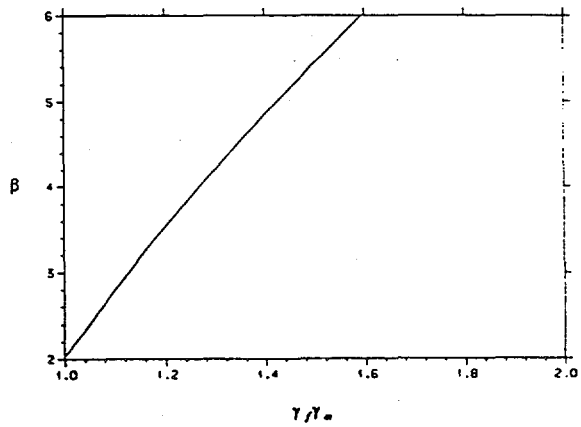

Figure 2 Reliability index β vs. calibrated partial safety factor product $\gamma_f\gamma_m$

As discussed above, an infinite number of possible choices for the set of partial safety factors (γ_f, γ_m) exist for each β value, as the requirement is on their product. A robust choice of partial safety factors is usually a set which leads to design values of stresses and strengths as close as possible to the design point values resulting from the corresponding reliability analysis. This is so because the design point of the reliability analysis represents the most likely outcome of the governing stochastic variables

at failure. In the following, it is outlined how such a particular robust set of partial safety factors can be chosen for the present design problem and thereby remedy the arbitrariness in the result of the calibration.

Based on the characteristic ε-N curve established in Section 6.2 above, the design ε-N curve can be expressed as

$$\log_{10} N = E[\log_{10} K] - E[m]\log_{10}(\varepsilon\gamma_m) - 2\sigma_e \qquad (24)$$

By inspection of the design point of the reliability analysis, the residual e achieves a significant, negative design point value, e_d^*. The ε-N curve in the design point of the reliability analysis can then be represented as

$$\log_{10} N = E[\log_{10} K] - E[m]\log_{10}\varepsilon + e_d^* \qquad (25)$$

and the sought-after particular choice for γ_m is achieved by requiring this design point curve to be equal to the design curve and eliminating N, hence

$$\gamma_m = 10^{-\frac{e_d^* + 2\sigma_e}{E[m]}} = 10^{-\frac{e_d^* + 0.792}{7.912}} \qquad (26)$$

which is a requirement expressed explicitly in terms of the results of the reliability analysis. This particular choice for the material factor γ_m, in conjunction with the requirement to the product $\gamma_f\gamma_m$, is easily seen to suffice for determination of a corresponding particular requirement to the load factor γ_f. The robustness in this particular set of partial safety factors is embedded in the fact that it, by its derivation in compliance with the results of the underlying reliability analysis, truly reflects the uncertainty importance information which is a byproduct of this analysis. Reference is made to Det Norske Veritas [10].

As an example, consider a rotor blade design for high safety and less serious consequence, which would be a reasonable classification for a wind turbine design against fatigue where human life is at negligible risk. According to Nordic Committee on Building Regulations [11], the requirement to the annual failure probability for design under such a classification is 10^{-5}. Under a Poissonian assumption for a rare failure event, this implies that the acceptable failure probability in a 20-year lifetime is $2.0\cdot10^{-4}$, and the corresponding target reliability index is β_t=3.54.

For a target reliability index β_t=3.54, Figure 2 gives a requirement to the product of the partial safety factors

$$\gamma_f\gamma_m = 1.200 \qquad (27)$$

The underlying reliability analysis is performed for a resistance moment W=0.00144 m^3 and yields a design point value e_d^*=−1.384 for the ε-N curve residual e. Hence, the requirement to the material factor becomes

$$\gamma_m = 10^{-\frac{e_d^* + 0.792}{7.912}} = 10^{-\frac{-1.384 + 0.792}{7.912}} = 1.188 \qquad (28)$$

and the requirement to the load factor is then implied as

$$\gamma_f = \frac{\gamma_f\gamma_m}{\gamma_m} = 1.010 \qquad (29)$$

The required load factor is found to be very close to 1.0, which reflects the very small importance attributed to the uncertainty in the loading as assessed by the reliability analysis. The required material factor is correspondingly found to be close to 1.2. This may seem not to be a particularly strict requirement. However, the partial safety factors are much dependent on the choices made for the corresponding characteristic values for load and resistance. In the present case, a lower-tail quantile of the resistance properties is chosen as the characteristic resistance. This implies that the characteristic resistance automatically accounts for part of the uncertainty in the resistance, and the material factor is then only meant to account for the remainder of this uncertainty, thus leaving the safety factor requirement to a mere 1.2.

7. SUMMARY AND CONCLUSIONS

The design of a wind turbine rotor blade against fatigue failure in flapwise bending has been considered. The load history in the design life has been modelled on the basis of observed distributions of bending moments at the blade root of an instrumented prototype rotor blade subjected to wind loads. Statistical uncertainty in the distribution parameters has been estimated and taken into account. The resistance has been modelled in terms of an ε-N curve. Uncertainties in the variables that describe this curve have been estimated and have also been taken into account. The cumulative damage that eventually leads to a fatigue failure has been predicted according to a Miner's sum formulation.

The models for load, resistance, and cumulative damage have been used as a basis for defining a limit state function for fatigue failure, and a first-order reliability analysis of the considered rotor blade against such a failure in flapwise bending has been carried out. The reliability analysis has been interpreted with respect to the probability of failure as well as identification of important uncertainty sources. The inherent variability in the fatigue life as represented by the uncertainty in the residual of the ε-N curve is found to be the single most important uncertainty source.

A reliability-based calibration of partial safety factors for design of the rotor blade against fatigue in flapwise bending has been carried out. A load factor γ_f has been applied to all stresses, and all strengths have been divided by a material factor γ_m. A target lifetime reliability corresponding to an acceptable annual probability of failure of 10^{-5} has been applied for the calibration. Based on a specific choice of characteristic values for load and resistance, a requirement to the product of load factor and material factor $\gamma_f\gamma_m$=1.2 has come out. Based on the importance information of the underlying reliability analy-

sis, a particular robust set of partial safety factors that fulfill this requirement has been determined, hence γ_f=1.010 and γ_m=1.188.

It is emphasized that the reliability-based safety factor calibration presented herein is site and wind-turbine specific and only applicable to flapwise bending of rotor blades. Different safety factors may result for different sites and different wind turbines. Similar calibrations can be carried out for such different wind turbines at various sites, and a common set of partial safety factors for a class of wind turbines and sites can be optimized in dependence of the expected demand for each individual combination of wind turbine and site within the class. Future work is suggested to be devoted to investigations of a series of wind turbines for different sites with the ultimate goal of developing a reliability-based optimal design code. Such a code is not to be limited to rotor-blade fatigue in flapwise bending alone, as extensions to other design cases such as rotor-blade fatigue in edgewise bending as well as fatigue of other wind-turbine components are foreseen.

8. REFERENCES

[1] Madsen, H.O., S. Krenk, and N.C. Lind, *Methods of Structural Safety*, Prentice-Hall Inc., Englewood Cliffs, N.J. (1986).

[2] Efron, B. and R. Tibshirani, *An Introduction to the Bootstrap*, Chapman and Hall, New York, N.Y. (1993).

[3] Winterstein, S.R., C.H. Lange, and S. Kumar, "FITTING: A subroutine to fit four-moment probability distributions to data", Reliability of Marine Structures Report No. 14, Stanford Univ., Stanford, Cal. (1994).

[4] Ronold, K.O., J. Wedel-Heinen, C.J. Christensen, and E. Jorgensen, "Reliability-Based Calibration of Partial Safety Factors for Design of Wind-Turbine Rotor Blades against Fatigue", *Proceedings*, European Wind Energy Conference, Thessaloniki, Greece, Vol. II (1994) 927-933.

[5] Echtermeyer, A.T., "Fatigue of Glass Reinforced Composites Described by One Standard Fatigue Lifetime Curve", *Proceedings*, European Wind Energy Conference, Thessaloniki, Greece, Vol. I (1994) 391-396.

[6] Echtermeyer, A.T., B. Engh, and L. Buene, "Fatigue of Composite Structures - Influence of Matrix and Fabric", Det Norske Veritas, Report No. 92-2067 (1993).

[7] Tvedt, L., "PROBAN Version 2, Theory Manual", Veritas Research, Report No. 89-2023 (1989).

[8] Det Norske Veritas, *Fatigue Strength Analysis for Mobile Offshore Units*, Classification Note No. 30.2, Høvik, Norway (1984).

[9] Dansk Ingeniorforening, *Code of Practice for Loads and Safety of Wind Turbine Structures*, DS472, Copenhagen, Denmark (1992).

[10] Det Norske Veritas, *Structural Reliability Analysis of Marine Structures*, Classification Note No. 30.6, Høvik, Norway (1992).

[11] Nordic Committee on Building Regulations, "Recommendations for Loading and Safety Regulations for Structural Design", *NKB Report*, No. 36, Copenhagen, Denmark (1978).

[12] Lange, C.H., and S.R. Winterstein, "Fatigue Design of Wind Turbine Blades: Load and Resistance Factors from Limited Data", *Proceedings*, 15th ASME Wind Energy Symposium, Houston, Texas (1996).

DEVELOPMENTS IN THE IEC WIND TURBINE SAFETY STANDARD - VERIFICATIONS AND REDUCING ARBITRARINESS

Carl Jørgen Christensen and Peter Hauge Madsen,
Department for Meteorology and Wind Energy.
Risø National Laboratory,
Roskilde,
Denmark

ABSTRACT: In the Joule II Project, European Wind Turbine Standards, the problem of partial coefficients to be used in wind turbine design, an implicit but central point of the definition of safety, has been looked into. Other topics were probabilistic analyses of safety, in particular as determined by the design of the control system of the turbine and the determination of design load spectra. The results are utilised in international standardisation. Presently, the IEC/TC88 has a working group (WG7) revising the 1400-1, Wind Turbine Systems - Safety Requirements, and a CENELEC Task force on wind turbine standards will shortly have to decide on an EU-standard to complete the technical harmonisation going on within the internal market. The IEC/WG7 has now developed an improved draft revision for the current Wind Turbine standard IEC 1400-1. The working group has analysed a number of datasets and various experiences with the standard in order to assess the standard and revise and improve it. The paper presents the major proposed changes. In addition, the different elements of arbitrariness will be described and discussed in order to illustrate the concepts of safety, target safety level and the impact of critical design assumptions.
Keywords: Standards, safety, reliability, Wind turbines.

1. INTRODUCTION

Already when the IEC 1400-1, *Wind Turbine Generator Systems* - Part 1: *Safety requirements*, [1] is being finalised, it was realised by the committee, that further work on the verification of load calculations were needed. Also the safety requirements were felt to be too arbitrary. As a consequence, a revision working group (TC88/WG7) was started prime 1995.

A recent Joule-2 Project, European Wind Turbine Standards has been helpful in pointing to shortcomings and possible improvements. Finally, the European part of the standardisation efforts has to be as precise as possible in defining precise safety requirements in order to comply with the European directives in the field. There efforts have contributed to the IEC revision where the working group has recently finished an improved draft standard to be presented and discussed in the technical committee TC88 of IEC. This paper discusses the most important changes suggested and various elements of arbitrariness in the verification of safety of a wind turbine design.

2. SAFETY CALIBRATION

Modern safety verification calculations usually prescribe the use of the partial safety factor method. This means, that in the simplest cases, a structure is checked by means of a criterion as the following:

$$F_d = F_k / \gamma_m \geq f_k \cdot \gamma_f = f_d \qquad (1)$$

which examines, whether the design resistance (= characteristic resistance divided by a materials partial safety factor) is larger than the design load (= characteristic load multiplied by a load partial safety factor).

This condition has its root in a code format that is designed to keep the probability of failure for the structure acceptably low, not that the structure will never fail. The level of safety built into a code could in principle simplest be expressed in terms of the target maximum failure probability accepted. This is, however, usually not done, because the code format has been simplified to avoid the concept of probability.

If the target failure probability for a code is not prescribed, the only way to assess the safety level is to examine the definitions of all four factors in equation 1.

In equation 1, the characteristic values are not absolute extreme values, but fractiles. Therefore, with a certain probability, worse values can occur and failure can occur. The partial coefficients serves to ensure that the design equation aims at the desired target failure probability. Calibration of safety means calculating what partial coefficients have to be used with the fractiles selected for load and resistance description in order to design for the failure probability prescribed.

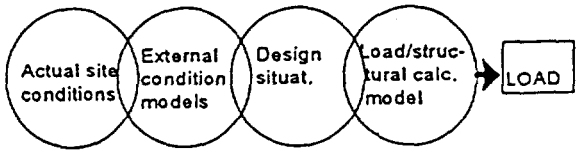

Figure 1. Load chain for determination of f_k

This, however, requires an assessment of not only the material strength but also of the elements in the load chain in fig. 1 above.

Clearly, the assumptions made and the methods used for each element introduces a certain degree of arbitrariness in the resulting safety of the wind turbine; an arbitrariness the standard seeks to minimise.

3. EXTERNAL CONDITIONS

An important task for the working group has been to assess the external conditions given in the standard, both with regard to whether the wind turbine classes given are representative for most potential wind turbine applications and with regard to the consequences for the wind turbine design.

With extensive help from several groups who have supplied wind data of various kind, the working group drafting this new version of the standard has been able to check the old wind condition definitions against real data, both in the case of homogeneous coastal terrain and complex terrain. The comparison, qualitative or quantitative, and the experience shared in the group have resulted in quite a few changes in the section on external conditions.

As turbulence is a primary driver for the wind turbine design and as the wind models are scaled with the turbulence intensity, it was concluded that the wind turbine classes should be extended with turbulence subclasses A and B, showing turbulence behaviour related to complex and homogenous terrain.

Table 1: Turbulence subclass parameters

Turbulence classes	I_{15}	a
A	0.18	2
B	0.16	3

I_{15} is the turbulence level at 15 m/s wind speed. (a), which is found from the same table, decides the slope of wind speed dependence. The formula gives the (mean plus standard deviation) characteristic value. Inserting the parameters in table 1 in equation (2) results in the variation with wind speed of the turbulence intensity shown in figure 2.

$$\sigma_1 = I_{15} \cdot (15\,m/s + a \cdot V_{hub}) / (a - 1) \quad (2)$$

Note that the slope of the gust has nearly doubled. The amplitude parameter was changed to

$$V_{gust50} = 6.4 \cdot \sigma_1 \quad (3)$$

Similarly, based on analysis of the available data, the gust models associated with extreme directions changes and extreme wind shear were modified slightly.

The gust situation, extreme coherent gust with direction change, in the first edition of IEC 1400-1 has been found to lead to extensive loads on some wind turbines. As the justification was weak, the gust situation has been modified leading to less change in direction at higher wind speeds.

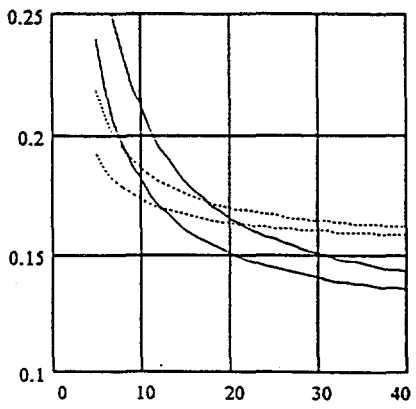

Figure 2: Turbulence conditions, dotted curves: class 0 (upper) and 3 of old IEC-1400-1, full drawn curves: new draft, subclasses A(upper) and B.

Note that the new turbulence specifications give lower levels at wind speeds higher than V_{rated}, i.e. the wind speeds where turbulence affects the fatigue life.

The extreme operating gust has been checked against data and was found to need improvements. First, the gust size was modified. Secondly, it was found that gusts in the data tended to started going negative before raising, and secondly to have a sharper front. Therefore the shape was changed as shown in Figure 3.

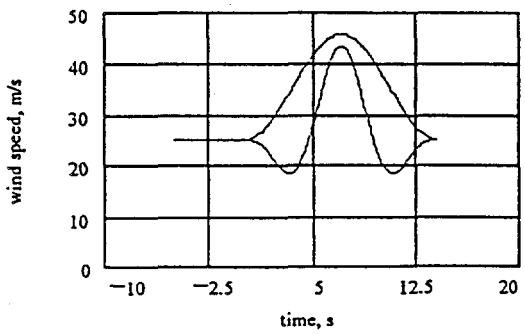

Figure 3: Extreme gust shape wind speed (m/s) vs. time (s). Simple bell: old gust, sharper rise; new gust.

As with most extreme events verification from measurements is difficult. Available data, however, corroborates the proposed gust models.

4. ASSESSMENT OF EXTERNAL CONDITIONS

The use of the IEC 1400-1 wind turbine classification for the choice of external conditions for design verification lead to a standard of reference, but not necessarily to a well defined safety of the wind turbine in a specific application. Referring to figure 1 the missing link is the reference to the actual site conditions

in the form of a comparison between the design assumptions and the site conditions. If the actual site conditions are more benign than the design external conditions the assumed safety level in IEC 1400-1 can be said to have been obtained.

In order to emphasise the need to assess the external conditions at the site, a new section on assessment of the external conditions, i.e. wind conditions, other environmental conditions, electrical network conditions and soil conditions has been added.

As a minimum requirement the wind conditions at the site shall be assessed according to the basic parameters in the wind turbine classification, namely the reference wind speed V_{ref}, the annual average wind speed V_{ave} and the characteristic (mean plus standard deviation) turbulence intensity at 15 m/s I_{15}. In general the assessment can be made from measurements at the site, long term records or from local codes or standards. Requirements to the monitoring period and the measurements are given.. In order to reduce the arbitrariness of safety it is important that the estimate of I_{15} from measurements shall be made for data for wind speeds greater than 10 m/s, as the primary damaging load effect from turbulence takes place at high wind speeds.

For complex terrain no generally accepted models for the detailed wind conditions exist. Assessment of the site must therefore be based on measurements at the site with consideration of local effects for each turbine in the Project. Similarly, wake effects in wind farms must be considered.

5. STRUCTURAL DESIGN

This chapter is, of course, central to the draft standard by defining the safety verification method to be used. The method prescribed is the partial safety factor method as outlined in the basic ISO 2394: General principles on reliability of structures.

Design Situations. It should be remarked that some concepts are not defined exactly as in the ISO document. This is presumably due to the traditions and thinking in the machinery industry being different from those in the building industry, where the roots of the ISO document lies. One important difference is in the classification of design situations. The following table shows the rough equivalence between the ISO design situations and ours.

Table 2 - Comparison of design situations

ISO 2394 design situation	*IEC1400 design situation*
Persistent	Power production
	Parked (standing still or idling)
Transient	Start up
	Normal shut down (braking)
	Transport, assembly, maintenance, repair
Fault	Power production with fault
	Emergency shut down
	Parked with fault

In this connection many more essentially different design situation needs examination for a wind turbine. Each design situation needs its own safety evaluation because of differences in, e.g., structural systems involved, reliability requirements, design values, environmental conditions, or faults involved.

The essential improvements in this chapter in the new draft is in the use of partial coefficients.

Which Safety factors to use. As a principle, the standard assumes the use of one safety factor load and one factor on materials. But furthermore a 'consequences of failure' - factor is retained. This factor has some semblance to the concept 'safety class' used in some countries. It reflects mainly how important a failure in the structural component or system under study could be. The prescription of only one safety factor on loads plus one on materials is, however, not to be taken too literally. For materials, several factors may have to be used for deriving the factor to be used. For loads, the factors prescribed are given with minimum values. Furthermore the designer is requested to present evidence for the validity of calculation methods used or demonstrate verifications. This could be interpreted, that if the evidence is not convincing, one may have to increase the load factor above the ones given.

The most essential problem when writing international safety standards is the lack of suitable international materials standards. This problem was (partly) solved in the old IEC code by allowing the use of national standards for materials. This possibility has been retained. However, the restrictions on how to use such codes have been tightened.

It should be remembered that the safety level of a set of codes (for loads and materials) is only fixed if characteristic values and partial coefficients both for loads and for materials are defined together. This is presumably done in most national code sets. There is, however, a certain *arbitrariness as to how the partial coefficients can be distributed* between the loads and the materials. Therefore one can not be sure, that a load code from one set fits with a materials code from another set. In our code, the treatment of loads is fixed. This means that the resulting safety level may depend on the details of the materials codes of a chosen code set. Therefore already the existing IEC code has some restrictions on how materials codes may be used. These restrictions have been tightened in the new draft as the old one was too weak

The lowest partial coefficient being allowed was just one number (1.15). This *lowest allowed safety factor is now a variable limit* depending on the percentile for the material characteristic value and on the coefficient of variation for the material. This reflects the very different partial coefficients needed for different materials better. See Figure 4.

Some materials codes contain several partial coefficients to be multiplied together as a result of a special factorisation used in the code. Some codes also prescribe the use of reduction factors on the characteristic value to account for some uncertainties concerning the material. The new IEC code now specifies that *all safety and reduction factors have to be*

taken into account when deriving the one materials factor, that our code uses.

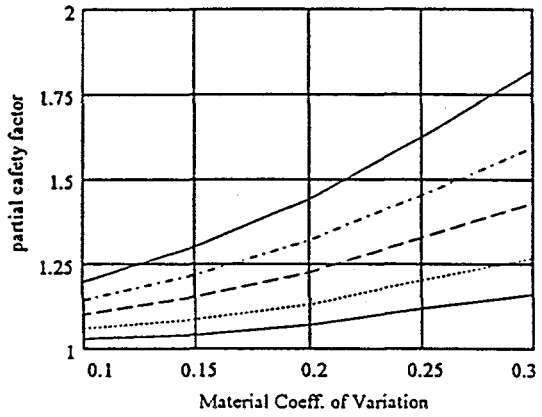

Figure 4: Variation of partial safety factor as a function of the coefficient-of-variation of the material. Fractile for resistance as parameter, values: 99% (lowest), 98%, 95%, 90%, 80% survivability

Finally the designer has to check, whether the *factorisation and the distribution of safety factors on loads and materials* in the national codes to be used corresponds to *the one of ISO 2394*. Otherwise one may have to move a safety factor from loads to materials or vice versa in order to maintain the logic in the safety level definition.

The partial coefficients prescribed (for loads and for the above-mentioned lower limit) have been adjusted so as to *approach the values in general use in the emerging Eurocodes*. This does prepare the way for adopting the standard also as a European (EN-) code.

As a speciality the new draft requires *special attention to be paid to tip deflection*, which should not cause the blade to hit tower. The idea is, that the critical tip deflection is now clearly counted as en ultimate rather than a serviceability state. This reflects the need to evaluate tip deflection as a serious limit state to be evaluated with the necessary higher level of safety of an ultimate state.

6. OTHER REVISIONS

The section on electrical systems in the first edition of IEC 1400-1 was characterised by including good engineering considerations and practices. In the revisions a number of paragraphs have been replaced by references to IEC standards, notably IEC 364, IEC 1000 and IEC 1024-1.

Similarly, the sections on installation, maintenance and erection as well as commissioning, operation and maintenance has been tightened to focus on requirements rather than good practices.

7. CONCLUDING REMARKS

A paper of this length can hardly pay justice to the subject of safety of wind turbines and the work of all the experts that participated in IEC working group TC88/WG7. It does however highlight some conclusions that at present can be included in a wind turbine safety standard. It is believed that the new draft contains significant improvements which will reduce the arbitrariness of wind turbine safety. Further more the work done has had a positive effect on the confidence in the standard.

However, there is ample room for improvements to arrive at a rational and consistent approach to verification of the safety level of a wind turbine at a specific site, taking into account realistic complex site conditions, uncertainties in load, aerodynamic and structural calculation models and their use, pertinent extreme events, how to include measurements in the design verification and characteristics of new materials.

8. ACKNOWLEDGEMENTS

The authors would like to acknowledge the support of the Commission of the European Union for the financial support of the Joule II Project European Wind Turbine Standard which has provided significant input to the IEC TC88/WG7 work reported herein and the support of the Danish Energy Agency to Risø for the participation in international standardisation. Furthermore we wish to thank the permanent members and all contributing experts to the IEC TC88/WG7 as well as Deutcher Wetterdienst and ISET, Germany, Renewable Energy Systems and National Engineering Laboratory, UK, Kvaerner Turbin, Sweden, Yamaha Motor Co. and IHI, Japan, NREL, USA and Risø, Denmark for making data available for the revision of the external conditions section of the standard.

9. REFERENCES

[1] IEC 1400-1: 1994 Wind Turbine Generators - Part 1: Safety Requirements, 1st edition, Dec. 1994.

[2] European Wind Turbine Standards. Vol. 2. Load Spectra for Wind Turbine Design. Vol. 3. Calibration of Partial Coefficients. Vol. 4. Assessment of Wind Turbine safety. Eurec Agency for EU/DGXII Jou2-CT93-0387, Leuwen May 1996.

EXPERIENCES WITH CERTIFICATION OF WIND TURBINES

Carsten Skamris
Risø National Laboratory, PO Box 49 DK-4000 Roskilde, Denmark
Christer Eriksson
DNV, Copenhagen, Nyhavn 16 DK-1051 Copenhagen, Denmark

ABSTRACT: This paper gives a presentation of the experiences gained by DNV and Risø in connection with Type Approval and Certification of Wind Turbines. The paper describes the progress concerning the development of the regulations for wind turbines, the view on the approval system seen from the various interested partners side, the methods used in connection with verification of the wind turbines and various approval systems in other countries. It is concluded that there still is a need for certification of wind turbines.
Keywords: Certification, Type Approval

1. BACKGROUND FOR TYPE APPROVAL IN DENMARK

Type approval of wind turbines in Denmark have been carried out since 1979. In the beginning the contents of the type approval was not so detailed but never the less the assessment of the wind turbine lead to a good understanding of the safety and the quality of the wind turbine for both the manufacturer and the Test Station.

In 1981 the Type Approval System[1] and a subsidy system was linked together, and from that time on most of the wind turbines erected in Denmark was type approved by Risø. The safety and the quality of the wind turbine was assessed on basis of experience and not complex calculations of the strength of the wind turbine.

Written regulations was first issued in 1984 and 2 years later Load Regulations based on measurements on the Gedser Wind Turbine were issued.

In this period many wind turbines was erected in Denmark as well as in California. The design of the wind turbines was based on the environmental conditions in Denmark. The market in California was enormous due to tax benefits and high prices on electricity. The environmental conditions in California showed to be more adverse and the large number of wind turbines manufactured in Denmark lead to a decrease in the quality. The problems forced the manufacturers to ask for a more detailed approval system of their products.

A very comprehensive work in many working groups was started up by The Danish Energy Agency and in 1991 a new system for Type Approval and Certification of Wind Turbines in Denmark[2] was finished. At the same time it became mandatory to have a type approval of the wind turbine if it was erected in Denmark. It has previously only been in connection with subsidies that it was required to have a type approval certificate.

As the wind turbine manufacturer in Denmark after many years with different economical and technical problems was well suited both economical and technical, the type approval system was commercialised in 1994. As a consequence of this, the Danish Energy Agency opened for the possibility for other bodies than Risø, to issue Type Approval Certificates in Denmark.

The commercialisation have been a success. The prices and the time schedule for the services have been fully accepted by the manufacturers and the competition have lead to a clear focus on the manufacturers needs.

The commercialisation have also intensified the co-operation between DNV and Risø. The objectives for DNV and Risø became more even and therefore the situation made it natural for Risø to pay interests in certification of projects and wind turbines in other countries than Denmark. This have actually, in a co-operation between DNV and Risø, lead to implementation of several wind turbine projects in countries outside Denmark on pure commercial basis. DNV had already for some years carried out certification of projects abroad.

2. EXPERIENCES WITH DANISH TYPE APPROVALS

It seems as if the wind turbine manufacturers generally are satisfied with the new type approval system in Denmark. They express that the system insures a high level of quality of the wind turbines and that the manufacturers thereby always keep a good reputation. Furthermore, many of the manufacturers use the type approval system as their quality control of the design. It gives the manufacturer a decreased risk in connection with warranty claims. This situation can be visualised as manufacturers also wants type approval of wind turbines that are mend for projects where there are no requirements for type approval.

In connection with the review of the documentation it is often seen that changes needs to be implemented. The reason has both to do with a too small safety margin or with the quality of the components.

The utility companies makes use of the type approval in two situations. First of all the utility companies have been instructed to check whether a wind turbine is type approved before they connect it to the grid. Secondly the utility companies could rely on the quality of the wind turbines in connection with there own engagement with regard to erection of wind turbines. Previously the Danish utility companies carried out some review of the wind turbines in connection with their own projects. In connection with the new and more comprehensive type approval system from 1991 the utility found that this was not necessary any longer.

3. METHODS FOR DESIGN VERIFICATION/DESIGN APPROVAL

There are several methods of verifying a wind turbine design. The normal methods are:

1. Review of design reports, specifications and drawings
2. Independent analysis
3. Test

As testing is time consuming and expensive, national authorities as well as certification agencies often stipulates requirements with respect to the type and extent of tests. This in order to ensure a more uniform level for the subjected wind turbines. The required extent of testing is in many cases related to the objectives of the national authorities and the certifying agencies.

Independent analysis will normally be used in the case were verification of the strength or load level is difficult due to the use of advanced computer analysis. This is often the case with dynamic analysis and FEM analysis. The criteria for selecting independent analysis as verification tool is normally included in the internal procedures of the approval body.

For serial produced or large wind turbines it may be wise to combine two or all of the listed methods. Again this will normally be decided based on the internal instructions of the approval body.

As there are several ways for verification of a wind turbine design it is important for the users of the final approval/type approval to achieve the details for the verification.

According to the above, the following approval "levels" are suggested.

A. Review of documentation only (independent analyses).
This level should be used during the development of new wind turbine designs i.e. for prototypes.

B. Review of documentation (independent analyses), full scale blade test, test of safety/control system and load measurements.
This level should be used for serial produced wind turbines were there are no requirements with respect to verification of performance.

C. As for B + power curve measurement, noise measurement and electrical quality measurements.
This level should be used for serial produced wind turbines were there are national or purchaser requirements for verification of performance.

4. CERTIFICATION IN VARIOUS COUNTRIES

Type approval schemes have been developed in several different areas where products must conform to a defined set of rules and regulations. The purpose of the type approval is to simplify the approval process for serial produced items like cars, houses, valves, wind turbines etc.. The type approval scheme (i.e. the procedure for the type approval activity) is developed such that the governing rules and regulations are satisfied. The scheme normally includes approval of design documentation, testing, quality control and operation.

For wind turbines and/or wind turbine components, the type approval may as in Germany only apply to the requirements from the building authorities or as in Denmark and the Netherlands apply to the rules and requirements from several authorities as e.g. energy, environmental, labour and building authorities.

Further, it is possible to tailor a set of requirements and establish a type approval or a certification scheme based on these tailored requirements. The advantage with such an approach is that aspects not covered by national schemes can be addressed e.g. low temperature operation, earthquake, extreme sun radiation etc..

The codes and standards available for wind turbines are limited and they do not cover all disciplines and components in detail. Hence, the "wind turbine standards" will in the best case refer to one or several codes relevant for the discipline/component. Further, the "wind turbine standards" give in many cases requirements for safety factors etc. to be used in the discipline/component specific standards. Below is a list given with standards available within different disciplines and components (material standards are not considered).

Wind turbine safety philosophy, environmental conditions, loads and load combinations ("Wind Turbine Standards"):
DS 472, GL-Rules, NEN 6096/2, DNV Guidelines, IEC 1400-1

Blades
NEN 6096/2, GL-Rules, DNV-Guidelines

Blade testing
Danish technical criteria, IEC standard is under preparation

Mechanical transmission
DNV Guidelines, GL-Rules

Gear
DIN 3990, AGMA, DNV Class. Note 41.2, ISO 6336-5 standard expected this year

Bolt connections
VDI 2230

Synthetic Wöhler curves
GL Rules

Tubular towers, buckling
DNV Class Note 30.1, DIN 18 800 T4, BS 5500

Lattice towers
National Codes for Steel Construction and Euro Code 3

Foundation, fatigue
DNV Guideline, Danish Technical Criteria

Electrical systems
National Standards together with IEC standards

Power curve measurements
Danish Technical Criteria, IEA, ECN-217, IEC standard expected within short time

Noise measurements
IEA, GL-Rules, IEC standard expected within short time, National regulations

Quality control
ISO 9000, NEN6096/2, GL-Rules, DNV-guideline

There are some significant differences in the various "wind turbine standards" with respect to calculation of extreme loads. As there are several ways of combining the critical events e.g. yaw error, gusts, wind shear, grid failure, turbine failure, ice with the different operational modes. However, there are fortunately some overlaps between the different standards which have limited the possible number of required load combinations, see also the figure below.

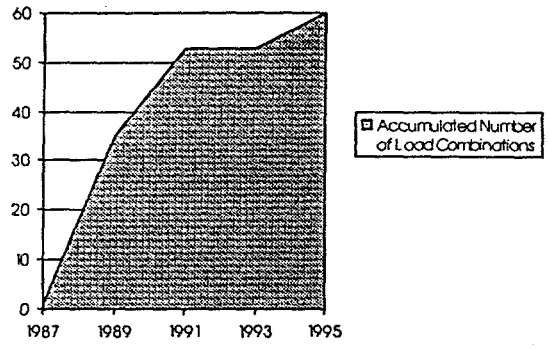

Figure 1.

A comparison between extreme loads in the existing "wind turbine standards" shows that one of the major differences is the definition of accidental load cases. The accidental loads are normally applied without safety factors which result in a reduction in the resulting strength by 40% as compared to "normal" ultimate limit state load cases. Further, the split in the partial safety factors between load and material factors varies. In Denmark 1.3 is applied to extreme wind loads while 1.5 is applied in Germany and the Netherlands. The material safety factors are to some extent compensating for this difference.

For fatigue loads there have been developed various different simplified methods. Today normally advanced aeroelastic dynamic calculation programs are applied. Below are a comparison between different method presented for one wind turbine type. The selected wind turbine type is assumed to have the same tower but not the same rotor dynamics. The comparison is presented as damage equivalent loads i.e. the constant load amplitude that results in the same fatigue damage as the complete spectrum.

The most significant development is that the tower dynamics have been accounted for resulting in a significant reduction in loads. For the other loads it is obvious that the new methods will enable the designer to determine the effect of changes in turbine parameters and wind conditions.

However, without calibration towards tests at representative wind conditions the absolute level is more or less unknown.

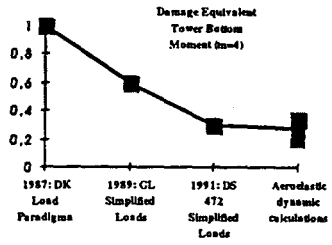

Figure 2

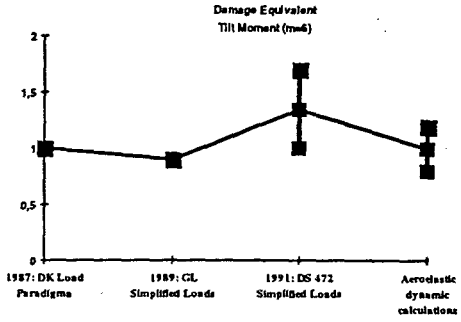

Figure 3

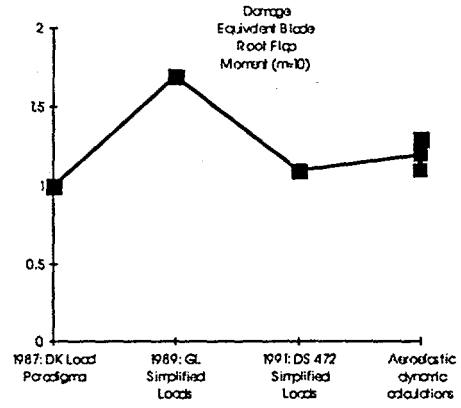

Figur 4.

5. REFERENCES

[1] Regulations for System Approval of Wind Turbines, The Test Station for Wind Turbines, February 8, 1984

[2] Type Approval and Certification of Wind Turbines in Denmark, The Danish Energy Agency, November 1, 1991

Bibliographic Data Sheet **Risø–R–909(EN)**

Title and author(s)

Contributions from the Department of Meteorology and Wind Energy to the EUWEC'96 Conference in Göteborg, Sweden

Edited by Gunner C. Larsen

ISBN	ISSN
87–550–2206–5	0106–2840

Dept. or group	Date
Department of Meteorology and Wind Energy	August 1996

Groups own reg. number(s)	Project/contract No.

Pages	Tables	Illustrations	References
144	49	146	228

Abstract (Max. 2000 char.)

The 5'th European Union Wind Energy Conference and Exhibition – EUWEC'96 – was held in Göteborg, Sweden during the period 20–24 May 1996. 520 delegates, mainly from Europe but also from other parts of the world, attended the conference. The conference contributions included roughly 70 oral presentations and 200 posters.

The Department of Meteorology and Wind Energy contributed with 17 oral presentations and 15 posters with members of the department as authors or co–authors. The present report contains the full set of these papers, covering a wide spectrum of subjects including research strategy, wind resources, power quality, grid connection, wind–diesel systems, aerodynamics, load assessment and reliability, and certification.

Descriptors INIS/EDB

AERODYNAMICS; DYNAMIC LOADS; ELECTRIC GENERATORS; MEETINGS; RISOE NATIONAL LABORATORY; STRUCTURAL MODELS; TURBULENCE; WIND; WIND LOADS; WIND POWER; WIND TURBINES

Available on request from:
Information Service Department, Risø National Laboratory (Afdelingen for Informationsservice, Forskningscenter Risø)
P.O. Box 49, DK–4000 Roskilde, Denmark
Phone (+45) 46 77 46 77, ext. 4004/4005 · Telex 43 116 · Fax (+45) 46 75 56 27